Emittance growth and preservation in a plasma-based linear collider

PhD Thesis

Carl Andreas Lindstrøm

Department of Physics
University of Oslo

January 2019

Series of dissertations submitted to the
Faculty of Mathematics and Natural Sciences, University of Oslo
No. 2067

ISSN 1501-7710

Cover: Hanne Baadsgaard Utigard.
Print production: Reprosentralen, University of Oslo.

Abstract

Particle physics is addressing some of the grandest questions, armed with big science machines: high energy particle colliders. These machines have, however, ballooned in size, and new technologies for accelerating particles are therefore required. Plasma-based acceleration is a promising new concept in this regard, enabling higher-than-ever accelerating fields by surfing particles on plasma waves—or wakefields—promising smaller and potentially cheaper particle accelerators. Nevertheless, many challenges remain before plasma wakefield accelerators (PWFAs) can be used for the next linear electron–positron collider. One particularly important question is whether PWFAs can preserve the required beam quality—or emittance—to produce a sufficient collision rate. This thesis addresses questions about emittance growth in a plasma-based linear collider, specifically for three important aspects of such a machine.

Firstly, staging of several plasma accelerator cells is a method suggested to reach high energies with moderate-energy drivers, but is made difficult by the large chromaticity and emittance growth induced during capture of highly diverging beams. Apochromatic corrective optics—where only linear optics elements are required—is proposed as a (partial) solution to this problem.

Secondly, acceleration of positron beams is not trivial in a plasma accelerator, due to the charge asymmetry of ion–electron plasmas. Hollow channel plasmas have been proposed as a solution to this problem—symmetrizing the electron/positron plasma response. However, strong transverse wakefields in these hollow channels lead to rapid beam breakup, which was measured precisely in an experiment in the FACET facility at SLAC.

Lastly, compact accelerating structures must be matched by similarly compact beam focusing devices. Active plasma lensing is a promising technique in this regard, but can suffer from aberrations and consequently emittance growth due to both nonuniform plasma temperatures and distortive plasma wakefields. This was studied experimentally at the CLEAR User Facility at CERN, where in particular it was found that the nonuniform plasma temperature aberration in an active plasma lens could be suppressed by changing from a light to a heavy gas species. As a consequence, emittance preservation in an active plasma lens was demonstrated for the first time.

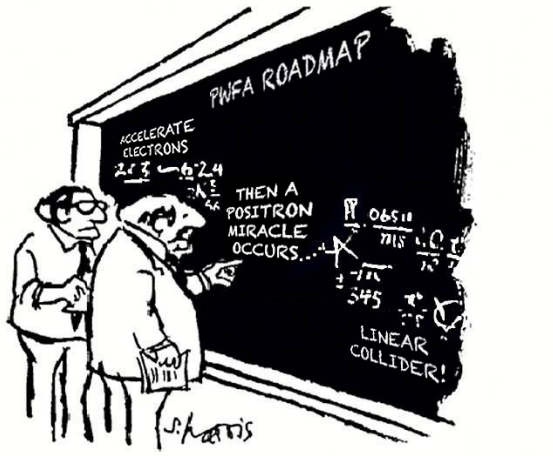

"I think you should be more explicit here in step two."

adapted from © S. Harris

Acknowledgments

It is still somewhat unclear, even to myself, exactly why I chose to start an experiment-based PhD at the University of Oslo. My original plan was to become a theorist, but in hindsight I'm quite happy that didn't happen! I simply could not have foreseen how interesting—and personally developing—it would be to get into experimental physics, as I have got to travel to and work at both SLAC and CERN: two of the biggest high energy physics labs in the world. Working in a small field also allowed me to explore all the different levels of scientific conduct: from tinkering with nuts and bolts in an underground tunnel, to analyzing experimental data, running simulations on supercomputers, publishing papers, giving talks, and all the way to taking part in the planning of future colliders. Most of this can not be learned by reading books: it comes gradually from asking thousands of questions and discussing topics large and small with scientists more clever than I. Overall, I feel extraordinarily lucky to have met so many interesting people over the past four years, without which this document would never have existed.

First and foremost, I want to thank my supervisor Erik Adli, who through countless discussions, emails and late-night experimental shifts has taught me everything he knows (or rather, a small subset of it). He managed the impossible task of balancing between giving strict guidelines, but also the freedom to explore my own ideas. No jedi master can be expected to put this much effort into a padowan, and for that I am extremely grateful.

I also wish to thank my co-supervisor at SLAC, Mark Hogan, who always expressed his belief in me. His ever-present optimism and support kept not only myself motivated, but everyone under his wing. Similarly, my co-supervisor at CERN, Patric Muggli, has always been open for a good, honest discussion of what was the best way forward, whether it be about physics or future endeavors.

Life in the US, where I spent two half years, was a lesson in *big*: big cars, big accelerators, big ambitions! I was thrown into the deep end, suddenly working in one of the most impactful research groups in the field, and I got to know a lot of people at SLAC that I have really come to appreciate and respect: Spencer Gessner showed true companionship and kindly allowed me to take part ownership of his project. Sébastien Corde showed me how to think clearly and how to listen for good ideas. Mike Litos and Brendan O'Shea never tired of my stupid questions, and taught me the ins and outs of the hyper-complicated FACET facility. Navid Vafaei-Najafabadi showed me how to work all night (it involves caffeine), and Ken Marsh imprinted on me that insightfulness and a relaxed attitude can be a deadly combo. Christine Clarke and Selina Green made me appreciate good project coordination.

Antoine Doche, James Allen, Alex Knetsch, Thomas Heinemann, Paul Scherkl, Oliver Karger, Aihua Deng and Rafal Zgadzaj were my fellow soldiers in the darkest hour (i.e., 2 a.m. in the underground tunnel). Chris Clayton showed me the value of original thought, of which he is the unrivaled master. Vitaly Yakimenko impressed on me the importance of firm and thoughtful leadership, as well as just how useful the right amount of skepticism can be. I'd like to direct a special thanks to Chan Joshi for teaching me how to write a good paper, how to identify what is and isn't important, and for entrusting me with publishing a big result. Beyond FACET, I was fortunate enough to discuss theoretical ideas with Alex Chao, who was always encouraging me to develop my own ideas even if they weren't of his caliber. Lastly, thanks to Jean-Pierre Delahaye for many interesting and cheerful discussions.

Unlike many PhD students, I got to familiarize myself with not only one, but *two* big labs. Spending the better part of a year at CERN, I got to try out being in charge of my own experiment. That however, doesn't mean I did it alone! Wilfrid Farabolini helped me with literally everything, accompanied by his never-ending smile and just-do-it attitude: teaching me how to build an experiment from scratch and the meaning of "bricolage". Davide Gamba taught me how an accelerator *really* works and gradually convinced me of the value of not taking shortcuts. Kyrre Sjøbæk unleashed his technical skills and unbridled enthusiasm: I think we made one hell of an experimental team. Reidar Lillestøl took time out of his own project to help with ours: thanks! Finally, Roberto Corsini steered the ship with his pragmatic leadership of the CLEAR facility and showed great interest in the details of our experiment. In fact, there were so many people at CERN that helped out with various aspects of the experiment that I don't have the space to thank them all individually.

Our collaborators at the University of Oxford and DESY were also immensely helpful. Anthony Dyson made me realize the importance and intricacies of electrical engineering, and Simon Hooker truly impressed me with his great insight and even greater kindness. His Oxford group also deserves a shout-out for welcoming me as if I was one of them (thanks Rob, James, Chris and Jakob!). Many good discussions and (too) long experimental shifts were shared with Jan-Hendrick Röckemann, Lucas Schaper and Martin Meisel, all of whom flew in from DESY when extra hands and brains were needed. For that I have to thank Jens Osterhoff and his incredible openness to collaboration, helping us even when we could be seen as direct competitors: teaching by example that while competition may be good, collaboration is even better.

Through it all, I had massive support from friends and family. Thanks to Fredrik, Michael, Saman, Simen, Pernille, Maiken and Morten for good times. Thanks to my sister Christine for having cheered me on since I was little, and walking up the path in front of me. Thanks a million to my parents, Kari Ann and Leiv Åge, for their infinite interest in what I do and for allowing me to follow my interests without reservation. And finally, for walking by my side every step of the way, listening closely even when it wasn't that interesting, supporting me no matter what, and for saying *yes* to the ultimate question: Martine, you are my everything!

Preface

This thesis is submitted for the degree of Philosophiæ Doctor at the Department of Physics, Faculty of Mathematics and Natural Sciences, University of Oslo, Norway.

The introduction and conclusion is written to be accessible to a generally informed reader, whereas the three central chapters are of a more technical nature—written around seven first-authored core publications, listed below and appended at the end (Appendix A).

1. C. A. Lindstrøm, E. Adli, J. Pfingstner, E. Marín and D. Schulte,
   Transverse tolerances of a multi-stage plasma wakefield accelerator,
   Proceedings of IPAC2016, Busan, Korea (JACoW, Geneva, 2016), p. 2561 [1].
2. Carl A. Lindstrøm and Erik Adli,
   Design of general apochromatic drift-quadrupole beam lines,
   Phys. Rev. Accel. Beams **19**, 072001 (2016) [2].
3. C. A. Lindstrøm, E. Adli, J. M. Allen, J. P. Delahaye, M. J. Hogan, C. Joshi, P. Muggli, T. O. Raubenheimer and V. Yakimenko,
   Staging optics considerations for a plasma wakefield acceleration linear collider,
   Nucl. Instrum. Methods Phys. Res. A **829**, 224 (2016) [3].
4. C. A. Lindstrøm, E. Adli, J. M. Allen, W. An, C. Beekman, C. I. Clarke, C. E. Clayton, S. Corde, A. Doche, J. Frederico, S. J. Gessner, S. Z. Green, M. J. Hogan, C. Joshi, M. Litos, W. Lu, K. A. Marsh, W. B. Mori, B. D. O'Shea, N. Vafaei-Najafabadi and V. Yakimenko,
   Measurement of transverse wakefields induced by a misaligned positron bunch in a hollow channel plasma accelerator,
   Phys. Rev. Lett. **120**, 124802 (2018) [4].
5. Carl A. Lindstrøm and Erik Adli,
   Analytic plasma wakefield limits for active plasma lenses,
   submitted to Phys. Rev. Accel. Beams, arXiv:1802.02750 (2018) [5].
6. C. A. Lindstrøm, K. N. Sjobak, E. Adli, J.-H. Röckemann, L. Schaper, J. Osterhoff, A. E. Dyson, S. M. Hooker, W. Farabolini, D. Gamba and R. Corsini,
   Overview of the CLEAR plasma lens experiment,
   Nucl. Instrum. Methods Phys. Res. A **909**, 379 (2018) [6].
7. C. A. Lindstrøm, E. Adli, G. Boyle, R. Corsini, A. E. Dyson, W. Farabolini, S. M. Hooker, M. Meisel, J. Osterhoff, J.-H. Röckemann, L. Schaper and K. N. Sjobak,
   Emittance preservation in an aberration-free active plasma lens,
   Phys. Rev. Lett. **121**, 194801 (2018) [7].

The following coauthored publications are also relevant, but report on work mainly led by others.

8. E. Adli *et al.*, **Transverse oscillations in plasma wakefield experiments at FACET**, Nucl. Instrum. Methods Phys. Res. A **829**, 94 (2016) [8].
9. S. J. Gessner *et al.*, **Demonstration of the hollow channel plasma wakefield accelerator**, Proceedings of IPAC2016, Busan, Korea (JACoW, Geneva, 2016), p. 3202 [9].
10. S. J. Gessner *et al.*, **Demonstration of a positron beam-driven hollow channel plasma wakefield accelerator**, Nat. Commun. **7**, 11785 (2016) [10].
11. A. Doche *et al.*, **Acceleration of a trailing positron bunch in a plasma wakefield accelerator**, Sci. Rep. **7**, 14180 (2017) [11].
12. D. Gamba *et al.*, **The CLEAR User Facility at CERN**, Nucl. Instrum. Methods Phys. Res. A **909**, 480 (2018) [12].
13. R. Corsini *et al.*, **First experiments at the CLEAR User Facility**, Proceedings of IPAC2018, Vancouver, BC, Canada (JACoW, Geneva 2018), p. 4066 [13].

Additional research was also conducted during the PhD period, resulting in several coauthored papers not considered part of the core thesis narrative.

14. P. Muggli *et al.*, **Measuring the Self-modulation Instability of Electron and Positron Bunches in Plasmas**, Proceedings of IPAC2015, Richmond, Virginia, USA (JACoW, Geneva, 2015), p. 2506 [14].
15. E. Adli *et al.*, **Progress of plasma wakefield self-modulation experiments at FACET**, Nucl. Instrum. Methods Phys. Res. A **829**, 334 (2016) [15].
16. J. Pfingstner *et al.*, **Considerations for a drive beam scheme for a plasma wakefield linear collider**, Proceedings of IPAC2016, Busan, Korea (JACoW, Geneva, 2016), p. 2565 [16].
17. E. Adli *et al.*, **Long-range attraction of an ultrarelativistic electron beam by a column of neutral plasma**, New J. Phys. **18**, 103013 (2016) [17].
18. B. Hidding *et al.*, **First measurements of Trojan Horse injection in a plasma wakefield accelerator**, Proceedings of IPAC2017, Copenhagen, Denmark (JACoW, Geneva, 2017), p. 1252 [18].

Contents

List of Figures

List of Tables

Chapter 1

Introduction

Particle accelerators have a wide variety of uses in our society—ranging from consumer products like microwave ovens, and industrial applications such as semiconductor ion implantation, to medical applications such as cancer treatment, and perhaps soon for power production (accelerator-driven nuclear reactors) [19, 20]. However, these are mostly spin-offs of machines that were initially made for fundamental physics research. The scientific success of the particle accelerator is perhaps only rivaled by that of the telescope—both of which have seen a tremendous surge in capability, but also in size and cost over the past century. So what is it about very energetic particles that allow us to discover the inner workings of the universe? How exactly does a particle accelerator work? And finally, what is the future of particle acceleration?

1.1 High energy physics

What we today know as high energy physics started at the turn of the 20th century when J. J. Thomson [21] and E. Rutherford [22] conducted experiments to probe the structure of the atom. Using cathode ray tubes and alpha particle sources—precursors to modern-day accelerators—they revealed that atoms are in fact made from smaller particles they termed "electrons" and "protons". In the following 100 years, a zoo of elementary and composite particles were discovered, facilitated by ever more energetic and intense accelerators. Highlights include the neutron (1932) by J. Chadwick [23]; the positron (1932) by C. D. Anderson [24]; the antiproton (1955) at the Berkeley Bevatron [25]; neutrinos (1956) at Brookhaven [26]; quarks (1968) and the tau lepton (1975) at SLAC [27–29]; the W and Z bosons (1983) in the CERN Super Proton Synchrotron [30,31]; the top quark (1995) at the Fermilab

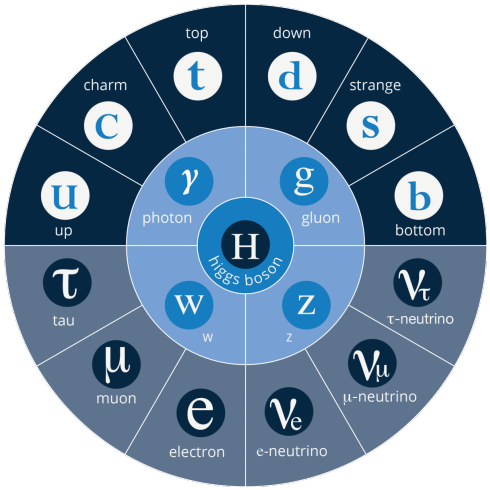

Figure 1.1: The 17 particles of the Standard Model of particle physics—all experimentally verified. Two types of matter particles (fermions) form the outer shell: quarks (upper half) and leptons (lower half). The outer shell is divided into quadrants by charge (+2/3, −1/3, 0 and −1 going clockwise from the upper left quadrant), and then further subdivided by mass in three generations. Force carriers (bosons) form the inner shell, mediating electromagnetism (photon), weak interaction (W and Z) and the strong interaction (gluon). Lastly, the Higgs boson (center) is responsible for giving particles mass. Source: ATLAS Experiment © 2017 CERN.

Tevatron [32]; and most recently the elusive Higgs boson (2012) at the CERN Large Hadron Collider (LHC) [33, 34].

1.1.1 The Standard Model

Throughout this period of discovery, a number of theories were proposed to explain and systematize all the observed particles—sometimes with conflicting predictions. Those that held up to the scrutiny of experimental measurement have since the mid-1970s collectively been known as the "Standard Model of particle physics". It describes three of the four fundamental forces of nature (electromagnetism, the weak and the strong interaction, not including gravity) using a theory of quantum fields [35] that interact with each other and permeate all of space. Packets of bound energy in these fields—like knots on a string—form what we know as particles. The Standard Model has 17 different elementary particles (see Fig. 1.1), organized into matter (fermions) and force carriers (bosons) based on their spin, and further subdivided by how strongly they couple to different fields or what forces they mediate.

The Standard Model is perhaps *the* most abstract description of the universe, but it can be compared to real world experiments in a rather simple way (using a

loose definition of the word "simple"). Although most of the 17 particles do not occur naturally around us, they can be produced by colliding well-known particles such as electrons/positrons, protons or heavier ions. The energy required typically ranges from megaelectronvolts (MeV) and gigaelectronvolts (GeV) to teraelectronvolts (TeV)—supplied not through a large number of particles and their combined rest mass energy, but by concentrating a considerable amount of kinetic energy into single particles. When two counter-propagating particles collide, their combined energy is then converted randomly into any and all available particles, so long as it conserves energy–momentum and various quantum numbers.

Repeating these collisions a large number (sometimes quadrillions) of times therefore provides simultaneous access to all particles and processes, given that enough statistics is gathered. The decay products are observed and characterized in specialized particle detectors, and the measurements are then compared with theoretical predictions. Such predictions are made by calculating so-called *cross sections*, which encapsulate the probability of producing certain outgoing particles given a set of incoming particles. The cross section can be understood by analogy to colliding balls in mid-air: it is much easier to make two basketballs hit each other than two tiny marbles. However, compared to ball-sized cross sectional areas of cm^2–m^2, the typical collisional cross section of particles is ultrasmall at around 10^{-28} m^2 (known as a *barn*), with rare events like Higgs production reaching down to 10^{-43} m^2 (a *femtobarn*) and below.

1.1.2 Unsolved problems

One of the primary goals of the scientific endeavor is to explain and predict natural phenomena. No theory has been more triumphant in this regard than the Standard Model, which among other successes has correctly predicted the electron magnetic dipole moment to better than one part per trillion [36]. Nevertheless, the Standard Model leaves several questions unanswered, including non-zero neutrino masses, baryon asymmetry (why there is more matter than antimatter) and whether it can be unified with general relativity—a quantum theory of gravitation. Related to this is the so-called hierarchy problem, asking how the energy scale of particle physics (1–100 GeV) can be so different from the supposed energy scale of quantum gravity (10^{19} GeV, the Planck scale) without unnatural fine tuning of fundamental constants. Additionally, unsolved mysteries in cosmology and astrophysics have also spurred searches for particle-like dark matter in the hopes that particle accelerators may shed some light on the problem.

With data streaming in from the LHC, early indications are that none of the pop-

ular Beyond the Standard Model theories hold water—like supersymmetry, grand unified theory or sterile neutrinos—although it is too early to write them off completely. The heaviest known particle is still the top quark (179 GeV), and the LHC has so far failed to discover anything heavier (up to a few TeV). Instead, some of the focus is shifting to performing ultrahigh precision measurements of Standard Model processes, which has already provided some intriguing hints of new physics with the apparent breaking of lepton universality [37]. The LHC will continue to run until at least 2035, at which point a new and better machine will hopefully pick up the baton.

1.2 Particle accelerators

Building a state-of-the-art particle collider is no simple feat, as the design of particle accelerators has matured for over a century. However, the general principles are quite simple, and only requires rudimentary knowledge of physics.

1.2.1 Accelerating a charged particle

The only known way for humans to manipulate charged particles is via electromagnetic fields. Electromagnetic particle–field interaction was first described in 1895 by H. Lorentz [38] in his force formula for electrically charged objects

$$\mathbf{F} = q(\mathbf{E} + \mathbf{v} \times \mathbf{B}), \tag{1.1}$$

where $\mathbf{F}$ is the force exerted (bold type denotes a three-vector), $\mathbf{E}$ and $\mathbf{B}$ are the electric and magnetic fields, $\mathbf{v}$ is the velocity, and q is the electric charge of the object. This relation applies universally—for large composite objects as well as elementary particles. One important implication that can be immediately identified, is that magnetic fields can never be used to increase the energy of a particle: this is because the force from a magnetic field will always be perpendicular to the direction of travel (due to the cross product). To accelerate the particle in the direction of travel, and thereby increasing its energy, the only option is to use an electric field.

Relating force to energy using $dE = Fds$, the total energy transferred to a charged particle is therefore

$$\Delta E = q \int_0^L E_z(s)\, ds, \tag{1.2}$$

where, E_z is the longitudinal electric field, s is the coordinate along the accelerator

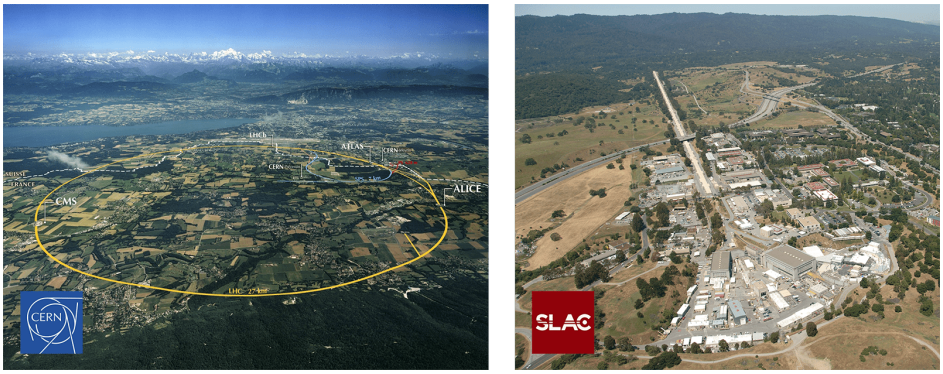

Figure 1.2: Aerial views of (left) the 27 km circular Large Hadron Collider (LHC) at CERN in Geneva, Switzerland, and (right) the 3 km linear accelerator at the Stanford Linear Accelerator Center (SLAC) in California, USA. Both were built primarily for high energy physics, and are currently the world's largest accelerators of their kind (circular and linear, respectively). Sources: (left) Maximilien Brice/CERN and (right) SLAC © 2017.

and L is the total acceleration length. The aim of high energy particle accelerator research is therefore primarily to push the frontiers of (a) higher electric fields and/or (b) acceleration length.

1.2.2 Linear accelerators

The most obvious way to make a strong longitudinal electric field is to set up a large voltage difference across a gap, and let the particle be accelerated from one side to the other. In practice, however, the magnitude of this electric field is limited to a few tens of MV/m by electrical breakdowns (arcs) to earth, even when separated by a vacuum. Fortunately, one can extend the acceleration length over which the force is exerted by varying the electric field synchronously with the passage of the particle. This is often referred to as radio frequency (RF) acceleration and was first proposed by G. Ising [39] in 1924 and experimentally demonstrated by R. Widerøe in 1928 [40]. In principle, there is no limit to the length of such a *linear accelerator* (linac)—apart from what you can afford to build.

The largest linac ever (so far) was built at the Stanford Linear Accelerator Center (SLAC) in California, USA in the late 1960s—accelerating electrons and positrons to 50 GeV using almost 3 km of RF accelerating structures operating at 20 MV/m.

1.2.3 Circular accelerators

A method to overcome the practical problem of very long linacs is to bend the particles back into the same accelerating structure, in order to reuse the device many times over: a concept known as the *circular accelerator*. To make particles travel in a circle, the Lorentz force (Eq. 1.1) shows us that both electric and magnetic fields can be used to apply a force perpendicular to the direction of travel. For relativistic particles ($v \approx c$), however, even a moderate magnetic field is equivalent to a very strong electric field (1 T $\equiv$ 300 MV/m)—which means that in practice magnets are almost always the best choice.

The dipole magnet (a north and south pole magnet separated by a gap) produces a constant magnetic field in both space and time, and is the standard component for bending a particle trajectory. The radius of curvature ρ can be calculated from Eq. 1.1 to be

$$\frac{1}{\rho} = \frac{qB}{p}, \tag{1.3}$$

where p is the particle momentum. The maximum energy in a circular accelerator is therefore limited mainly by the strength of the magnetic field and the circumference of the ring. The highest achievable magnetic field is currently about 2 T in a normal conducting dipole, and about 10 T in a superconducting dipole, although this limit is continuously being pushed [41].

The largest circular accelerator ever built (thus far) is the Large Hadron Collider (LHC) [42]—previously the Large Electron–Positron Collider (LEP) [43]—at the European Organization for Nuclear Research (CERN) in Geneva, Switzerland, which was completed in 2008. It accelerates protons up to 6.5 TeV (and heavy ions up to 2.5 TeV per nucleon) in a 27 km long underground tunnel filled with 8 T superconducting dipoles.

1.2.4 Synchrotron radiation

Clearly, circular accelerators facilitate much higher particle energies, so why are we still interested in high energy linear accelerators? The reason is *synchrotron radiation*: a form of highly directed, wide-spectrum, and often high-power electromagnetic radiation emitted by accelerating relativistic particles. Although there is some radiation emitted during longitudinal acceleration, the total power radiated is negligible compared to the typical energy gained during acceleration. However, when relativistic particles experience transverse acceleration (bending), synchrotron radiation can be very significant.

The power emitted by a particle via synchrotron radiation was first derived by

J. Larmor in 1897 [44] and later generalized for relativistic particles [45] to be

$$P_{\mathrm{SR}} = \frac{e^4}{6\pi\epsilon_0 m^4 c^5} E^2 B^2 = \frac{e^2}{6\pi\epsilon_0 m^4 c^7} \frac{E^4}{\rho^2}, \tag{1.4}$$

where m and E are the mass and energy of the particle in a magnetic field B, e is the electron charge, while ϵ_0 and c are the vacuum permittivity and speed of light, respectively.

Larmor's formula shows that the power scales strongly with energy (quartic) and particle mass (inversely quartic), severely limiting the energies reachable in a circular machine—especially for light particles (electrons/positrons). As an illustration, although LEP occupied the same real estate as LHC does now, it could only accelerate electrons and positrons up to 104.5 GeV (62 times less than for protons in the LHC) due to energy loss from synchrotron radiation. Even the proposed 100 km electron–positron Future Circular Collider (FCC-ee) [46] is only expected to accelerate particles to about 175 GeV. Going beyond this energy for electrons and positrons can only feasibly be done in a linear collider.

1.2.5 Particle colliders

Circular hadron colliders like the LHC reach high energies, good for discovering new particles, but they also produce inherently messy collisions. This is because hadrons are composite particles, consisting of quarks and gluons with an unknown internal distribution of energy and momentum. Lepton machines on the other hand, while typically reaching lower energies, collide elementary particles that have no (known) internal structure—making it easier to perform precision measurements. The two collider types are therefore often referred to as *discovery machines* and *precision machines*, filling complementary scientific roles.

The history of circular colliders is rich and made up of numerous machines continuously stepping up the energy: starting with the lepton machines AdA (1961), VEP-1 (1963) and the Princeton–Stanford collider (1965) [47], and later with hadron machines including the Intersecting Storage Rings (1971), the Tevatron (1983), and today's LHC. The history of linear colliders, however, is comparatively barren: the Stanford Linear Collider at SLAC was completed in 1987 and remains the only linear collider ever constructed. That may change in the near future, as two large and technologically mature proposals are on the table.

First, the International Linear Collider (ILC) [48] is a proposed 20–50 km long 0.25–1 TeV electron–positron collider based on superconducting niobium accelerating cavities operating at 31.5 MV/m (see Fig. 1.3). Second, the CERN-based Com-

pact Linear Collider (CLIC) [49,50] is a proposed 11–50 km long 0.38–3 TeV collider using miniaturized normal conducting copper cavities to accelerate at 100 MV/m with a novel two-beam driver design. Both contenders are the result of decades of research and development. At the time of writing, Japanese authorities have uttered a desire to build the ILC in the Iwate prefecture [51], pending appropriate support from the international community. The price tag for these machines are expected to be ten billion dollars or more.

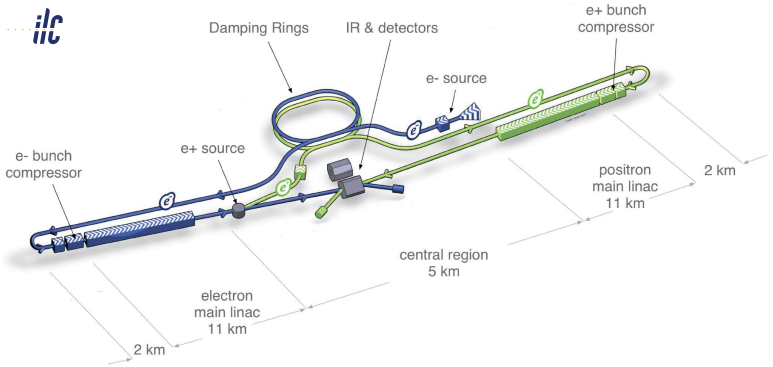

Figure 1.3: The International Linear Collider, as envisioned in the ILC Technical Design Report [48]: a 250 GeV–1 TeV electron–positron collider. Source: ILC © 2013.

1.3 Economics of big science machines

Regardless of what scientists might wish to be the case, economics will always be deeply intertwined with the scientific endeavor. Our ambitions of discovery have grown beyond what a single individual can fund by themselves, so in general funding for big science projects will necessarily be sourced from the broader society. That begs the perhaps philosophical but also very practical question of whether (and if so which) science experiments are worth the tax payer's dime. Cost-effectiveness is consequently an important aspect, especially in particle accelerator physics research—maybe more so than in other fields.

1.3.1 Why so big?

Before we dig into how we can justify spending billions on a science project, it is instructive to look at a very general question: why do these experiments—especially physics experiments—get so big in the first place?

New discoveries in physics are typically made whenever we look at things with new eyes—or increased resolution. The act of *looking* always requires some kind of wave: whether it be electromagnetic radiation, matter particles or more recently the fabric of spacetime itself (gravitational waves [52]). Waves are, however, subject to a fundamental resolution limit, restricting the smallest dimension that can be resolved to

$$\Delta x \approx \Delta s \frac{\lambda}{D}, \tag{1.5}$$

where Δs is the distance from the object to an instrument with an imaging aperture of diameter D, and λ is the wavelength of the wave being imaged. For instance, if you wish to observe a distant galaxy, the distance is fixed and so is the wavelength of the light you are observing: the only variable you can change is the diameter of your telescope. This straight away motivates why telescopes are so large—it is the only way to resolve more distant objects. Currently the largest telescope (Gran Telescopia Canarias [53]) has a 10 m mirror diameter, giving an angular resolution for visible light of about 0.01 arc seconds (or about 5 m on the Moon). Another option is to use an array of smaller telescopes spread over a large area (e.g., in the 8600 km wide Very Long Baseline Array [54]) used to obtain a comparable resolution, but for much larger wavelengths (radio waves).

Observing *small* scales follows a similar trend. Typical light-based microscopes are not that large because they have the added freedom of moving the imaging lens very close to the object. This approach, however, is limited by the manufacture of lenses with very small f-numbers ($\Delta s/D$ in Eq. 1.5), which is hard to make smaller than about 1. The only way forward is then to decrease the wavelength. This is the basis of X-ray crystallography: using short wavelength X-rays to image the nano-structure of crystals, which can be produced by cathode tubes or more recently by synchrotron light sources and free electron lasers (FELs) [55]. An entirely different approach was first outlined by L. de Broglie in his 1924 thesis [56], showing that all matter particles have wavelike properties, and that the wavelength is given by

$$\lambda = \frac{h}{p}, \tag{1.6}$$

where p is the particle momentum and h is the Planck constant. De Broglie's insight is the principle behind the electron microscope, which uses a beam of electrons instead of light to resolve atomic-scale structures.

In many ways, the natural extension of this approach is to build a particle collider, which can be viewed as a microscope for particles themselves. Looking at the very smallest scales can therefore only be done with a high energy accelerator,

because small scales are only accessible with high-momentum, short-wavelength particles. The main difference between a microscope and a particle collider is that in the act of resolving the particles being collided, you also get access to all the other particles existing at that length scale (or equivalently: energy scale).

Unlike for telescopes, where the desired resolution fundamentally dictates the size of your instrument $D = \Delta s\lambda/\Delta x$, the length of a linear accelerator is not directly related to the scale being probed. Instead, it is indirectly related via the longitudinal accelerating field E_z, resulting in a total accelerator length

$$L \approx \frac{1}{\Delta x}\frac{hc}{eE_z}. \tag{1.7}$$

It can be instructive to imagine this as a logarithmic seesaw (see Fig. 1.4), where the desired resolution and the accelerator length is balanced around a "fulcrum" length scale $\sqrt{hc/eE_z}$. By way of example, reaching nuclear scale resolution (10^{-15} m) using accelerating fields of 10 MV/m results in a fulcrum length scale of about 0.3 μm, balanced by an accelerator length of about 100 m. However, if you increase the accelerating field to 1 GV/m, the fulcrum moves to smaller length scales (30 nm) and the accelerator length can be shortened to 1 m and still maintain the same resolution. Alternatively, one can keep the same accelerator length and get an improved resolution of about 10^{-17} m. The continuing quest for increasing the resolving-power with which we look at the Universe is exactly the reason why some particle accelerators have grown so big.

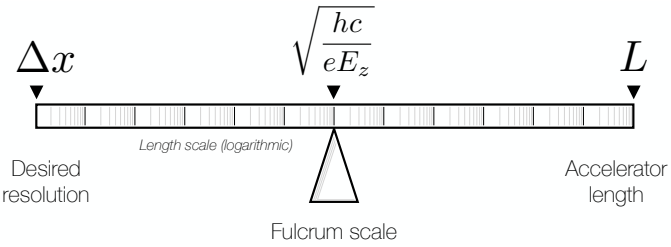

Figure 1.4: Seesaw analogy for the connection between the desired resolution Δx and the length of accelerator L required. The resolution is achieved whenever the logarithmically scaled seesaw is balancing on the fulcrum, which represents the characteristic length scale given by the accelerating field E_z. Increasing the accelerating field moves the fulcrum to the left (smaller scales)—allowing either a shorter accelerator length or a better resolution.

How then, can we afford to pay for this scientific extravaganza? Gradually over the past century or two, science has changed from a gentleman's hobby to big business. The reason that this trend continues, and that fundamental science

can indeed be profitable, is two-fold: large-scale *economic development* and general *technological advancement*. These two, interestingly, also correspond to the two ways of improving the resolution of a linear collider: increasing the length (by building multi-billion dollar facilities), and increasing the accelerating field (driving research and development of novel acceleration methods).

1.3.2 Big Science as a method for economic development

To understand the first of these reasons (economic development) we must do a quick dive into history. World War II (1939–1945) was undoubtedly one of the most destructive events on record, leaving Europe in particular in ruins both physically and economically. However, the same was not true for the United States, which was largely left unscathed. Moreover, the unprecedented American military upscaling—which arguably turned the tide of the war—moved a large fraction of the US work force into industrial production. Even though much of the produced goods were ultimately destroyed in the war or given away to allies, the US subsequently experienced a huge postwar economic boom.

Part of this military upscaling involved the US nuclear weapons research program—the Manhattan Project—which was by far the largest scientific endeavor ever attempted at the time. It cost the equivalent of $22 billion (in 2016 dollars) [57] and employed more than 130,000 people. It was gradually realized that large-scale science projects like this could serve a similar purpose to the more nefarious military operations, and gradually over time more non-military science projects were initiated [58]. The US National Laboratory system is the result of this expansion, currently sustaining 17 national labs doing large-scale science research, often in collaboration with high-tech industry. As more countries have developed increasingly advanced economies, we see this large-scale government spending on science also outside of the US, for instance in Europe with the rise of programs like the European Research Infrastructure [59].

While enabling great scientific progress with big expensive projects like the Stanford Linear Collider at SLAC or the LHC at CERN, this mode of scientific conduct—Big Science—comes with a number of strings attached. Politicians and government officials will typically only agree to pay for a project if a large percentage of the money flows back into their respective economies—the scientific objective takes a back seat. This is one of the reasons why most Big Science projects are so concentrated around physics research: not necessarily because it is more important, but because the equipment required is so big—i.e., the hardware-to-researcher cost ratio is heavily skewed towards hardware. For instance, most of the cost of building

the LHC and its detectors went into the thousands of magnets, pumps, cables, civil engineering, etc., all of which is produced by industries within the CERN member states. In this way, bigger is better, because more of the money goes to hardware instead of project design and management (ideally).

International collaboration is also possible in this Big Science model, but has to be done in a certain way. Instead of transferring cash directly to the host country, contributions must be made *in kind*, i.e., via goods and services. As an example, the US pledged to contribute $531 million [60] to the construction of the LHC by giving superconducting focusing magnets built at Fermi National Accelerator Lab—this way all cash, employment and growth stayed within the US economy, and only the final product was shipped to Switzerland. Another good example is the European Spallation Source (ESS) [61], where about 30% of the total construction cost is supplied in kind.

These considerations are important to large collider proposals such as ILC and CLIC [62]. More generally, we as scientists need to appreciate the advantages and limitations of this type of large-scale government funding, and try to use it for the advancement of our scientific goals.

1.3.3 Science as a long term economic investment

Beyond large-scale economic development, the second way in which science can be profitable is perhaps more widely known: serving as a stable source of new technology. Although most scientific research never finds an application outside of its original scope, viewed statistically, a steady trickle of new technology flows from the sciences into wider society. As mentioned above, even the relatively abstract field of high energy physics has contributed with spin-offs like medical accelerators for cancer therapy [63], the World Wide Web [64], and more recently advancements in artificial intelligence [65].

Viewing science not as an expense but as a long term investment, it is estimated that the return on investment is upwards of 20% per year [66]—vastly outcompeting the stock market on average. However, this investment needs to be sustained over long periods of time, and the return is often not easily identifiable. Nevertheless, many highly developed countries increasingly base their economies on this model. This is especially the case for Israel, Korea, Japan and many Nordic countries, spending between 4.5% and 3% of their gross domestic products (GDP) on research and development [67]. To ensure consistent return on investment, this kind of science spending in general favors smaller scale research to distribute the risk, which also allows more independent and fast-paced research projects—often performed in

university laboratories rather than only in large national labs and institutes.

Research into new ways of improving particle accelerators follows this trend squarely. Many small research groups world-wide are investigating a number of promising concepts on how to produce, accelerate and apply particle beams in cheaper and more compact ways. Much like how computer technology is now used for purposes that would never have been technically or economically viable when a room-sized mainframe was required (e.g., smartphones and smart light bulbs), significantly smaller and cheaper accelerators may not only push the envelope in high energy physics, but also make accelerators more ubiquitous and transformative in society as a whole.

1.4 Advanced accelerator concepts

The physics research field of advanced accelerator concepts (AAC) is as broad as it is new, attempting to improve upon every aspect of particle acceleration. Questions addressed include how to produce high brightness particle beams; how to accelerate and focus them in an energy and space efficient manner; as well as how to improve the corresponding diagnostics needed to observe and optimize such beams. Many of these new advances can be applied in combination with conventional technology, but to reach the overarching goal of making significantly more compact accelerators, all aspects must eventually be improved.

1.4.1 New acceleration mechanisms

The core innovation driver in advanced accelerator research is the hunt for new mechanisms that support high accelerating gradient. Acceleration of particles requires two components: (1) a medium or vessel in which high electric fields can be sustained for the duration of the beam passage, and (2) a driver or energy source able to excite these strong electric fields.

The conventional medium for accelerating charged particles is a normal- or superconducting cavity that can be resonantly driven by 1–3 GHz (L- and S-band) RF electromagnetic fields up to approximately 20 MV/m before breakdowns occur. Newer 12 GHz (X-band) RF cavities developed by CLIC increases this to about 100 MV/m [68]. To go beyond this limit, several different approaches are being investigated—using a combination of new media and new drivers. New media include:

- *Very high frequency, miniature-scale copper cavities*, able to push the formation of breakdowns to somewhat higher electric fields [69], although the

possible gain is limited [70, 71].

- *Dielectric materials*, potentially able to withstand significantly higher electric fields before being damaged, at the level of GV/m or more.
- *Plasmas*, doing away with the concept of breakdowns altogether, as it is already in a fully broken down state. This in principle allows accelerating fields of TV/m and beyond, and is therefore the subject of much attention in AAC research.

Accelerating fields in these media can be driven by:

- *High frequency electromagnetic radiation* in or close to the THz range. Since there are currently not many sources of high-power THz-radiation—also known as "the THz gap"—this is a topic of active research [72, 73].
- *High power lasers* in the terawatt (TW) to petawatt (PW) range, now available due to advances in laser technology over the past decades. Particularly important was the application of chirped pulse amplification (CPA) to lasers by Strickland and Mourou in 1985 [74].
- *High intensity particle beams* reaching particle densities of 10^{14} cm^{-3} or higher, which can drive strong relativistic waves—or wakefields—in dielectric structures and plasmas. Both electron/positron and proton bunches can be used, provided that their bunch length is short (μm-to-mm scale) or that the density is longitudinally modulated with a similarly short wavelength.

The most promising driver–medium combinations thus far are laser-driven plasma wakefield acceleration (LWFA or LPA) [75, 76]; beam-driven plasma wakefield acceleration using electrons/positrons (PWFA) [77] or protons (PD-PWFA) [78]; beam-driven wakefield acceleration in dielectric structures (DWFA or SWFA) [79]; and laser-driven micron-scale dielectric cavity acceleration (DLA) [80].

1.4.2 New particle sources

Conventional sources of particle beams have until recently been based on releasing electrons from a material surface, and making ions by stripping away electrons from atomic gases or vapors. Electron bunches are traditionally made by one of four approaches: through field emission, thermal emission, photo emission or secondary electron emission—the latter of which can also be used to make positrons. Combined with great improvements in lasers, photocathodes have become the modern work horse of high quality electron bunch generation.

However, with the advent of plasma accelerators, a completely new kind of particle source has been discovered. In a plasma there is a virtually limitless supply of free electrons, which can be captured and accelerated [81] in several similar but technically different ways, including:

- *Density down ramp and shock front injection* [82] uses a sharp plasma density change such that plasma electrons are captured and accelerated (more details on plasma wakefields in Sections 1.5 and 2.2). This method is very often used in laser-driven wakefield accelerators.

- *Ionization injection* uses the strong electric field in the plasma wakefields to further field ionize the ions (e.g., from Rb^{+} to Rb^{2+}) and then immediately accelerate these electrons [83].

- *Plasma photocathode injection*—also known as "Trojan Horse" injection—uses an additional gas with a higher ionization potential and an independently controllable laser pulse to release electrons locally inside the plasma wakefield [18, 84].

Additionally, new ways of producing ion beams have been developed, whereby a very intense laser pulse impinges on a thin surface, forms a plasma, and accelerates the ions in the materials to near-relativistic speeds [85–87]. While electron bunch generation from plasmas have already demonstrated good beam quality and charge [88], the same is not yet true for ion acceleration.

Novel, compact positron sources have also yet to be demonstrated, although some ideas have been proposed [89, 90].

1.4.3 New focusing methods

Transverse focusing of particle beams plays an important part in accelerators. This is especially true for miniaturized machines like that of a plasma wakefield accelerator (see Chapter 2). To keep the beam focused between the accelerator modules and to complement their significant reduction in size, it is also necessary to compactify beam focusing devices.

The conventional focusing device—the quadrupole magnet—has seen some improvement in strength and compactness in recent years, with the rise of strong permanent magnetic quadrupoles (PMQs) [91, 92] and micro-scale quadrupole electromagnets [93]—capable of providing field gradients an order of magnitude stronger than usual electromagnet-based quadrupoles. However, in any quadrupole, net focusing is a second-order effect (the beam is focused in one plane and defocused in

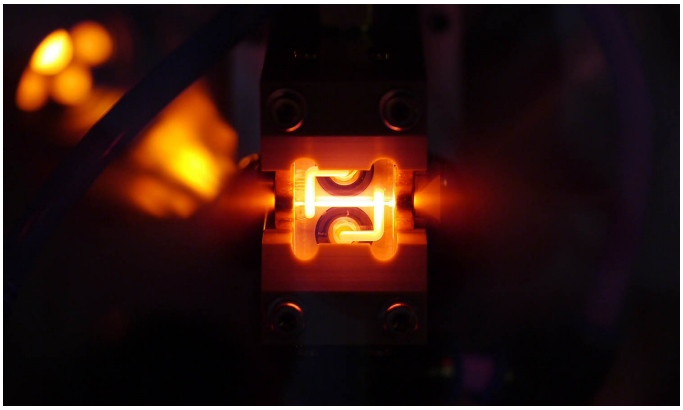

Figure 1.5: Discharge capillary-based active plasma lens for compact focusing of particle beams. During the discharge a large current flows inside a thin sapphire capillary, through which also a beam propagates. The magnetic fields focus the beam particles strongly in both transverse planes. Source: Kyrre N. Sjøbæk, CLEAR User Facility at CERN © 2018.

the other) and can therefore only be achieved using a series of magnets. New alternative methods are actively being investigated, where focusing is a first-order effect (focusing in both planes). Two plasma-based approaches are of particular interest:

- *Active plasma lensing* [94], whereby a column of plasma is used to conduct a large current density parallel to the beam, setting up strong kT/m magnetic field gradients (see Fig. 1.5).
- *Passive plasma lensing* [95], where the ion column exposed in a plasma wakefield accelerator is used primarily for focusing the bunch instead of accelerating it. This method can provide extreme focusing gradients of MT/m, but is also in general dependent on the longitudinal and transverse beam distribution.

See Chapter 4 for more details on active and passive plasma lensing.

1.5 Beam-driven plasma wakefield acceleration

All the novel acceleration methods outlined in Section 1.4.1 can supply large accelerating gradients. However, this is not a sufficient condition for selecting a future linear collider technology, which also requires high energy efficiency and preservation of the transverse beam quality. Beam-driven plasma wakefield acceleration is by many considered to be the most promising alternative for a high energy collider because particle driver beams can be produced and accelerated at a relatively high overall wall-plug-to-beam efficiency of around 60% (based on estimates for CLIC [96]).

Compare this to the energy efficiency of a laser system, which is typically less than 0.1% [97] for state-of-the-art Ti:sapphire lasers [98], although this number may rise considerably with the application of multi-pulse wakefield excitation [99] using thin-disk [100] or fiber lasers [101].

The history of plasma wakefield acceleration is considered to have started in the late 1970s when Tajima and Dawson investigated sending interfering laser pulses through a plasma to excite strong electric fields [102], however the first ideas can be traced back to Soviet scientists Budker [103], Veksler [104] and Fainberg *et al.* [105, 106] who in 1956 proposed to accelerate particles in a "plasma waveguide". Nevertheless, it was not until the mid 1980s that the idea of using intense particle bunches to drive plasma wakefields was picked up by Ruth *et al.* [107] and Chen *et al.* [108]. Table 1.1 presents a historical list of some of the most important milestones in the field of *beam-driven* plasma wakefield acceleration to date—fascinating, personal accounts of which were given by Dawson [109] and Joshi [110, 111].

1.5.1 Plasmas

Plasmas are often termed the fourth state of matter. Heat a solid and it becomes a liquid; heat a liquid and it becomes a gas; continue heating and the electrons will eventually separate from the atoms/ions to form an ionized gas—a plasma. The energy required to ionize a gas is typically large, e.g., about 50 MJ or 14 kWh for a cubic meter of air (at standard pressure and temperature). However, unless the plasma continues to be heated, the electrons will rapidly recombine with the ions and go back to being a gas on a time scale of ns to μs, depending on how hot the plasma is.

Creating a plasma is therefore not easy, as a large amount of energy must be administered to the gas or vapor in a very short amount of time—demanding high peak power. Nevertheless, this is done routinely in laboratories through a number of approaches, including high voltage discharges (also seen in fluorescent lamps and in lightning bolts), high-power TW-class lasers, or helicon sources using RF electromagnetic waves. Unlike for fusion experiments (like JET [141] and ITER [142]) that require the plasma to last for an extended amount of time, plasma wakefield experiments do not require the plasma to last for longer than the passage time of the beam, which is typically only on the order of ps to ns.

Separating electrons and ions in the plasma sets up electric fields, which is the basic premise of plasma wakefield acceleration. How strong these fields can become depends mainly on the single most important plasma parameter: the plasma density n_0. On a sufficiently small scale and short duration, there can be a different electron

Year	Milestone (beam-driven plasma wakefield acceleration)
1956	Early ideas by Budker [103], Veksler [104] and Fainberg [105].
1979	A seminal paper by Tajima and Dawson [102] describes the interaction between intense laser pulses and plasmas, laying the foundations for the field of plasma acceleration—Dawson being an instrumental figure in the development of the field [109, 110].
1985	The laser–plasma idea is extended by Ruth [107] and Chen *et al.* [108] to using intense charged particle bunches to drive wakefields in the plasma.
1986	Beam loading in a plasma wakefield accelerator for reduced energy spread and increased efficiency is described by Katsouleas [112].
1988	First experimental observation of beam-driven plasma wakefields using electrons at Argonne National Lab by Rosenzweig *et al.* [113].
1990	Acceleration using bunch trains at KEK by Nakajima *et al.* [114].
1991	The blowout regime is discovered by Rosenzweig *et al.* [115], providing strong, uniform fields for both acceleration and focusing.
1991	The hosing instability is described by Whittum *et al.* [116], predicting large emittance growth.
1998	Formation of a self-modulation instability in long bunches is described by Lotov [117], allowing proton-driven plasma wakefields.
2000	First acceleration in the blowout regime at Argonne by Barov *et al.* [118].
2003	Positron beams transported and accelerated by plasma wakefields at the FFTB facility at SLAC by Hogan [119] and Blue *et al.* [120].
2004–5	Muggli [121] and Hogan *et al.* [122] demonstrate multi-GeV acceleration and meter-scale transport of electrons in the blowout regime at FFTB.
2006	A nonlinear blowout theory is proposed by Lu *et al.* [123, 124].
2007	Huang *et al.* [125] finds that hosing is less severe than predicted.
2007	Energy doubling of a 42 GeV electron beam by Blumenfeld *et al.* [126, 127] at FFTB demonstrates 52 GV/m accelerating fields.
2008	First two-bunch acceleration in a plasma by Kallos *et al.* [128] at Brookhaven National Lab.
2014	Loaded two-bunch acceleration with high energy efficiency is demonstrated at the FACET facility at SLAC by Litos *et al.* [129].
2015	The nonlinear self-loaded plasma wakefield positron acceleration regime is discovered at FACET by Corde *et al.* [130].
2017	Mehrling *et al.* [131] presents an analytic theory of hosing for beams with energy spread.
2017	The FLASHForward facility [132] at DESY starts operation as a beam-driven PWFA test facility aimed at accelerating high quality beams.
2018	Self-modulation of electrons [133] and high transformer ratios [134] are observed by Gross and Loisch *et al.* at DESY's PITZ facility.
2018	The self-modulation instability [135] and electron acceleration [136] is observed using long, 400 GeV proton bunches in AWAKE [137] at CERN.
(2019)	The FACET-II facility [138] at SLAC will start experiments aiming to demonstrate a working PWFA cell for high energy physics applications.

Table 1.1: Selected milestones in beam-driven PWFA, listed by year of publication. See articles by Hogan [77], Joshi [111, 139] and Esarey [140] for in-depth reviews.

density n_e and ion density n_i, but the resulting electric fields will always move electrons and ions about in such a way as to quickly return to charge neutrality. The characteristic time scale of this movement is given by the electron plasma frequency

$$\omega_p = \sqrt{\frac{n_0 e^2}{\epsilon_0 m_e}}, \tag{1.8}$$

where m_e is the electron mass. This plasma response sets up waves traveling at or close to the speed of light, enabling us to also define a plasma wavenumber

$$k_p = \frac{\omega_p}{c} = \sqrt{\frac{n_0 e^2}{\epsilon_0 m_e c^2}}. \tag{1.9}$$

This quantity can be used to determine the spatial extent $1/k_p$ of a local electron–ion density disturbance. For instance, a typical laboratory plasma with a density 10^{16} cm^{-3} will have a $1/k_p$ of about 50 μm.

1.5.2 Beam–plasma interaction

When a relativistic, charged particle bunch enters a plasma with a particle density comparable to that of the plasma, it will repel plasma electrons away from the axis (using an electron bunch) or attract plasma electrons towards the axis (using a positron/proton bunch). The plasma ions, however, tend to remain stationary on the relevant timescale: this leads to a charge separation and therefore electric fields. If the particle bunch density is much lower than the plasma density ($n_b \ll n_0$) the plasma response is harmonic—the linear regime. If, however, the particle bunch density is close to the plasma density ($n_b \approx n_0$), the plasma response is not harmonic and will behave very differently for electrons and positrons—the nonlinear regime.

For an intense electron bunch, the plasma electrons will be completely "blown out" to form a bare ion column with a surrounding sheath of plasma electrons—forming a plasma cavity (see Fig. 1.6). This is often called the *blowout* regime, and it provides very favorable accelerating conditions compared to the linear regime.

Since the exposed ion column is uniform, beam electrons observe a linear focusing force which implies that the beam quality is preserved (see Chapter 2). This is not the case in the linear regime, where the focusing is increasingly nonlinear away from the axis, and nonuniform in the longitudinal, inevitably leading to beam quality degradation. Another attractive feature of the blowout regime is a uniform accelerating gradient for all radii. While the accelerating gradient is not constant longitudinally, as shown in Fig. 1.6, the blowout regime deviates from the so-called *fundamental theorem of beam loading* [143] which states that the trailing wakefield

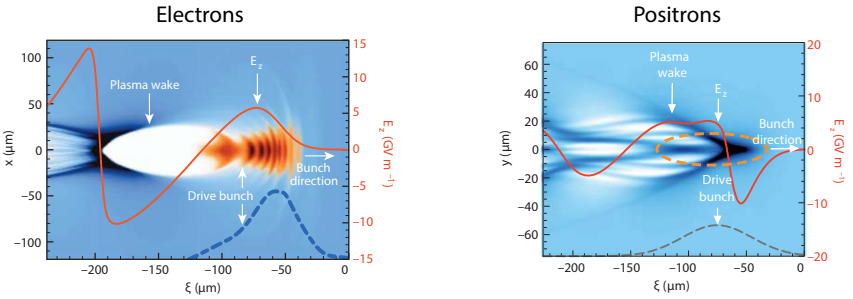

Figure 1.6: Particle-in-cell simulations of plasma wakefields driven by intense electron (left) and positron (right) bunches in the nonlinear regime. The corresponding longitudinal electric (accelerating) fields are also shown, seen to be in the multi-GV/m range. Sources: (left) Litos *et al.*, Nature **515**, 92 (2014) [129] and (right) Corde *et al.*, Nature **524**, 442 (2015) [130].

amplitude cannot be larger than twice that observed by the driving bunch. The linear regime *is* subject to this constraint, but in the blowout regime large ratios of driver decelerating field to trailing accelerating field (formally known as the transformer ratio) can be achieved towards the back of the plasma cavity [134].

Several experiments have demonstrated the combined large acceleration and focusing of the blowout regime, some over meter-scale distances [126, 129, 144].

Positron bunches—vital to an electron–positron collider—are, however, a very different story. The relatively low mass of the plasma electrons compared to that of the ions ensures that the plasma response is intrinsically charge asymmetric. While the quick movement of the plasma electrons is key to the blowout regime, it also implies that plasma electrons are quickly "sucked in" towards an intense positron bunch. Since the distribution of plasma electrons is not uniform, the focusing fields are nonlinear and not beam-quality preserving. Note, however, this does not mean that it is not possible to obtain large accelerating gradients for positrons: experiments at SLAC have demonstrated GeV/m-scale acceleration and even focusing for positrons [11, 130, 145], but never while preserving the beam quality. This positron problem remains one of the biggest unsolved challenges for plasma wakefield acceleration.

See Chapter 2.2 for a more theoretical description of plasma wakefield acceleration.

1.6 The road to a plasma-based linear collider

The advanced accelerator research community owes its booming activity and continued funding not only to its many breakthroughs in recent decades (see Table 1.1), but also to its great potential for improving high energy physics research—in particular with a new generation of linear colliders. This was specifically highlighted in a 2014 report by the US Particle Physics Project Prioritization Panel (P5) [146], which has resulted in the development of several *road maps* [147, 148] defining the direction of research over the next decade or more. These collider road maps identify the most important problems to be solved within each technology, specifically laser- and beam-driven plasma wakefield acceleration, as well as structure-based dielectric wakefield acceleration—represented by three US-based undertakings based at Lawrence Berkeley, SLAC and Argonne National Labs, respectively. In particular, the beam-driven PWFA road map aims to continue basic research until 2025 (dates are approximate), while simultaneously ramping up collider design work with the intent of producing a conceptual design report (CDR) by 2035 and a technical design report (TDR) by 2040, after which construction would start.

More recently, an international effort spearheaded by the International Committee for Future Accelerators (ICFA) [149] is attempting to draw up an *international* road map for an advanced linear collider (ALC) [150, 151]—defined as supporting a 1 GeV/m average acceleration gradient, irrespective of the underlying technology. Four 5-year phases have been proposed, gradually shifting from a proof-of-concept, to high beam quality, then high reliability and lastly to a mature technical design—all largely in line with US based road maps. However, an important short-term goal of this effort is to identify the need for and to propose new experimental facilities required to make rapid progress in this regard.

Whether real progress can follow the ambition of these road maps is left to be seen. In particular, prior experience from fusion research has shown that plasmas do not always conform to ten-year schedules.

1.6.1 Early concepts

Nevertheless, to make headway we must start somewhere. Early attempts at studying the feasibility of advanced linear colliders have already been made, with varying degree of detail:

- A PWFA-based linear collider concept by Adli *et al.* (2013) [152] using 25 GeV drive beams to drive a large number of 3.3 m long plasma wakefield accelerators with a 7.6 GV/m accelerating gradient (see Fig. 1.7). This concept builds on

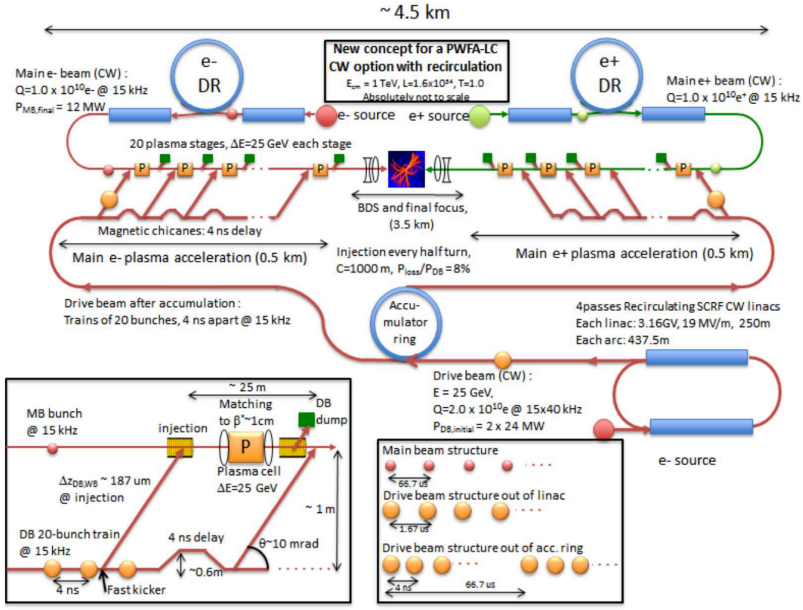

Figure 1.7: Conceptual design of a 1 TeV beam-driven plasma wakefield accelerator-based linear collider using many stages, each with 25 GeV energy gain. The total length is only 4.5 km, where a total of 1 km is taken up by the main linacs. This study assumes that electron and positron acceleration can be treated identically. Source: Adli *et al.*, arXiv:1308.1145 (2013) [152].

earlier work by Rosenzweig *et al.* [153] (1998) and Seryi *et al.* [154] (2009).

- An LPA-based linear collider concept by Schroeder *et al.* (2010) [155], proposing ultrashort 1 μm beams and 5 GeV/m energy gain up to a total collision energy of 1 TeV.

- A DLA-based simple "strawman" linear collider concept by England *et al.* (2014) [156] proposing to use bunches with ultra-small emittances and very low charge per bunch (only 30000 particles), but at a very high repetition rate (20–60 MHz).

- A DWFA-based linear collider concept by Jing *et al.* (2013) [157]—a CLIC-like collider with 30 cm long dielectric structures operating at 270 MV/m (not strictly reaching the 1 GV/m goal, but this could feasibly be improved).

None of these collider concepts are particularly mature, in the sense that they represent a detailed and self-consistent machine design. Instead, they should be seen as a first indication of usable parameters, and as a way to identify the more subtle

problems. Based on these early ideas, it has become apparent that we likely *can* efficiently accelerate particles in a compact space, but that achieving the required collision rate will not be easy.

1.6.2 The luminosity challenge

To probe interesting physics with femtobarn-scale cross sections within a few years of operation, particle colliders must maintain a high collision rate. For instance, the LHC nominally produces 600 million collisions per second [158], equivalent to a so-called *luminosity* of 10^{34} cm^{-2} s^{-1} (10 nb^{-1} s^{-1})—the event rate per cross section. The luminosity of a particle collider is given by

$$\mathcal{L} = H\frac{N^2 f}{4\pi\sigma_x\sigma_y}, \tag{1.10}$$

where N is the number of particles in each bunch, f is the collision frequency, σ_x and σ_y are beam sizes in the horizontal and vertical plane, and H is a small geometrical factor from bunch tilts and pinching effects. Circular colliders can reach high luminosities by colliding at extremely high frequencies (40 MHz for LHC), reusing the same bunches over and over. That is not possible in a linear collider because every bunch is used only once. This can be remedied by colliding much more tightly focused bunches, such that a higher fraction of the particles collide—however, this is not trivial and places tight constraints on the machine.

To better understand these machine constraints, we can recast the luminosity expression by changing to more practical parameters

$$\mathcal{L} = \frac{H_D}{8\pi m_e c^2}\frac{P_{\text{wall}}}{\sqrt{\beta_x\epsilon_{Nx}}N}\frac{\eta}{\sqrt{\beta_y\epsilon_{Ny}}}, \tag{1.11}$$

where P_{wall} is the total wall-plug power consumed, η is the wall-plug-to-beam energy efficiency, ϵ_N is the normalized emittance (or beam quality) and $\beta_{x,y}$ is a measure of how tightly the beam is focused in the horizontal and vertical plane (see Chapter 2.1 for a review of transverse beam dynamics). The total power available is typically limited to a few hundred MW, and due to "beamstrahlung" [159] effects during collisions (proportional to N/σ_x) the horizontal beam size cannot be smaller than a few hundred nm (but can be much smaller in the vertical). The bunch charge is also typically limited to about 10^{10} particles, and the overall efficiency is hard to increase above 10%. Finally, with a state-of-the-art final focusing system, the optics can squeeze β_y down to about 0.1 mm. Overall, if the luminosity requirements are to be met, an extremely small vertical emittance of 10–100 nm rad must be maintained

for the full length of the collider. This presents an immense challenge, and has been an important driver of the design decisions in both CLIC and ILC.

For a plasma-based linear collider, this challenge is set to become a great deal more difficult. Some plasma acceleration techniques—like the blowout regime—does in principle preserve the emittance, but this has not yet been demonstrated to the required level. This is both due to practical difficulties like extremely tight alignment and synchronization tolerances, as well as more fundamental difficulties such as in- and out-coupling of beams (staging). Moreover, for positrons there is currently no known plasma accelerator scheme that preserves emittance while simultaneously maintaining a reasonable bunch charge and efficiency. This sentiment was echoed in the conclusion of the Advanced Accelerator Concepts Research Roadmap Workshop Report [147]: "*the two areas of beam–plasma physics considered most pressing for research in the next decade are emittance preservation and positron acceleration.*"

This thesis investigates three separate approaches attempting to tackle the luminosity challenge for a plasma-based collider. Chapter 2 looks at the various sources of emittance growth in a beam-driven PWFA-based accelerator, with emphasis on the staging aspect, from a theoretical and simulational point of view. Chapter 3 tackles the positron problem using the interesting technique of hollow channel plasma wakefield acceleration and its severe limitation caused by emittance growth from any small misalignment in the channel—investigated for the first time in experiments conducted at SLAC. Lastly, Chapter 4 looks closer at whether the novel beam focusing method of active plasma lensing can feasibly be used as a technology for compact staging, reporting on both theoretical developments and experiments done at CERN.

Chapter 2

Emittance Growth in Staged Plasma Wakefield Accelerators

Accelerating particles to high energy is key to advancing elementary particle physics, and plasma wakefield acceleration is a promising technique to do so in a significantly more compact manner. The plasma wake, however, is in principle nothing exotic—it simply acts as an energy redistributor, transferring energy from the driver to the trailing bunch. Reaching TeV collisions therefore requires about 1 kJ of energy to be transfered to each colliding bunch in some way or another. This large amount of energy can either be transferred all in a single stage by one high energy driver (e.g., using high energy protons), or by using a number of lower energy drive bunches successively transferring their energy to the accelerating bunch, each in their own separate plasma accelerator: a process known as *staging*. This way, it is comparably easier to produce the drive bunches, especially for electrons, but it also adds the complexity of coupling driving and accelerating bunches in and out of successive stages—difficult to do without degrading the beam quality, i.e., increasing the emittance. Moreover, this is only one of a wealth of detrimental effects that can occur in a plasma accelerator, including problems like scattering, ion motion and various instabilities. In this chapter, we will discuss all these effects and how they can be mitigated, with some added emphasis on staging.

Before we dive into various mechanisms of emittance growth, however, it is necessary to review both classical transverse beam dynamics as well as some basic theory of plasma wakefield acceleration.

2.1 Review of transverse beam dynamics

At a fundamental level, a particle beam can be thought of as a large number of points in 6D phase space, i.e., 3D positions and momenta. However, while keeping track of millions or more particles is possible (and is routinely done) in a computer, it is often not very instructive for a human. Luckily, the motion of the beam particles is often highly coherent, and can therefore be described by their first and second order moments (mean and variance). The mean trajectory of the particles defines its *orbit*, which is followed by an imaginary *reference particle* with some nominal energy. The position of all other particles are defined relative to this reference particle in a comoving 3D coordinate system. We will refer to x and y as the horizontal and vertical transverse directions, respectively, and z as the longitudinal direction (see Fig. 2.1). The variable s denotes the distance traveled along the orbit.

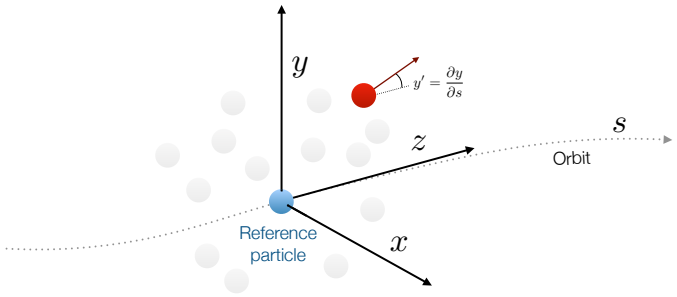

Figure 2.1: Schematic of the coordinate system used to refer to particles: x and y are the horizontal and vertical transverse coordinates, while z is the longitudinal coordinate relative to an imaginary reference particle (the bunch centroid) which follows the orbit. Also shown in the vertical plane is the angle y' of the particle to the forward axis (the corresponding angle x' is not indicated).

2.1.1 Single-particle dynamics

Instead of using the transverse momentum, it is useful to work with the particle's angle to the longitudinal axis, usually denoted with a prime:

$$x' = \frac{\partial x}{\partial s} = \frac{p_x}{p}, \tag{2.1}$$

where p_x and p denote the momentum in the x and forward directions. This angle evolves based on external electric and magnetic fields, which are independent of the presence of the particle bunch (*space charge* [160] is typically negligible for high energy electron beams). It is therefore possible to model the evolution of the entire

beam by considering it as an ensemble of non-interacting single particles.

To keep a beam focused, transversely offset particles must be brought towards the axis. This can be achieved with a field that provides a force linearly proportional to the offset. The conventional choice is a magnetic quadrupole, which provides exactly this kind of field: $\mathbf{B} = (gy, gx, 0)$, where $g = \frac{\partial B}{\partial r}$ is the radial magnetic field gradient—exerting a Lorentz force $\mathbf{F} = q\mathbf{v} \times \mathbf{B} = qvg(-x, y, 0)$. Applying Newton's second law in, say, the horizontal direction we get

$$F_x = \gamma m\ddot{x} = \gamma m v^2 x'' = -qgvx, \tag{2.2}$$

where γ is the relativistic Lorentz factor. This can be simplified to the so-called *Hill's equation*

$$x'' = -k(s)x, \tag{2.3}$$

where the focusing strength $k(s) = qg(s)/p$ can vary along the orbit and where we have used $p = \gamma mv$. Note that the corresponding equation in the vertical plane $y'' = k(s)y$ has the opposite sign, implying that a quadrupole focuses in one plane and defocuses in the other.

In a constant focusing field, a particle will undergo simple harmonic motion. However, in general $k(s)$ is not constant and therefore the amplitude of the particle motion also changes:

$$x(s) = \sqrt{\epsilon\beta(s)}\cos(\sqrt{k(s)}s + \phi_0), \tag{2.4}$$

where ϕ_0 is an initial phase, while ϵ and $\beta(s)$ are the constant and varying parts of the amplitude, respectively. Substituting this solution into Hill's equation, we obtain a differential equation for $\beta(s)$ given by

$$\frac{1}{2}\beta(s)\beta''(s) - \frac{1}{4}\beta'(s)^2 + k(s)\beta(s)^2 = 1. \tag{2.5}$$

Note that the constant ϵ can take any positive value, and it does not change during linear or no focusing—this quantity is known as the *single-particle emittance*, or the *Courant-Snyder invariant* after E. D. Courant and H. S. Snyder who first described it in 1957 [161]. It can be intuitively thought of as the degree to which the particle deviates from traveling parallel and on-axis, like the reference particle (which by definition has zero emittance).

2.1.2 Matrix formalism

Since focusing fields are linear, they can be described by linear operators—or in this case as matrices. The 4D transverse phase space vector of a particle is

$$\mathbf{x} = \begin{bmatrix} x \\ x' \\ y \\ y' \end{bmatrix}, \tag{2.6}$$

and the effect of a quadrupole can be encapsulated in a 4×4 *transfer matrix*

$$\mathbf{M_q} = \begin{bmatrix} \cos(\sqrt{k}l) & \frac{1}{\sqrt{k}}\sin(\sqrt{k}l) & 0 & 0 \\ -\sqrt{k}\sin(\sqrt{k}l) & \cos(\sqrt{k}l) & 0 & 0 \\ 0 & 0 & \cosh(\sqrt{k}l) & \frac{1}{\sqrt{k}}\sinh(\sqrt{k}l) \\ 0 & 0 & \sqrt{k}\sinh(\sqrt{k}l) & \cosh(\sqrt{k}l) \end{bmatrix}, \tag{2.7}$$

where l is the length of the quadrupole. The effect of a field-free vacuum, also called a *drift*, is the limit of $\mathbf{M_q}$ where $k \to 0$:

$$\mathbf{M_d} = \begin{bmatrix} 1 & l & 0 & 0 \\ 0 & 1 & 0 & 0 \\ 0 & 0 & 1 & l \\ 0 & 0 & 0 & 1 \end{bmatrix}. \tag{2.8}$$

Note that all transfer matrices have unitary determinants: $\det(\mathbf{M}) = 1$.

Propagating a particle through all the accelerator elements (e.g., quadrupoles and drifts)—collectively known as a *lattice*—is then simply a matter of premultiplying the particle vector successively by each matrix

$$\mathbf{x} = \mathbf{M_n}...\mathbf{M_2}\mathbf{M_1}\mathbf{x}_0. \tag{2.9}$$

This formalism readily extends from a single particle to an ensemble, simply by generalizing the single particle 4×1 vector to a multi-particle $4 \times N$ matrix that includes all N beam particles:

$$\mathbf{X} = \begin{bmatrix} \mathbf{x}_1 & \mathbf{x}_2 & ... & \mathbf{x}_N \end{bmatrix}. \tag{2.10}$$

2.1.3 Beams and Courant-Snyder parameters

A beam of many particles can be characterized by its mean and variance in transverse phase space—if the beam is Gaussian, this is in fact a complete description. The covariance matrix can be calculated from the multi-particle matrix using a normalized outer product

$$\mathbf{\Sigma} = \frac{\mathbf{X}\mathbf{X}^\intercal}{N}, \tag{2.11}$$

often termed the *sigma matrix* or *beam matrix*, which in a single plane takes the form

$$\mathbf{\Sigma} = \begin{bmatrix} \langle x^2 \rangle & \langle x x' \rangle \\ \langle x' x \rangle & \langle x'^2 \rangle \end{bmatrix}. \tag{2.12}$$

Transferring this beam matrix through an accelerator lattice follows from substituting $\mathbf{X} = \mathbf{M}\mathbf{X}_0$ into Eq. 2.11:

$$\mathbf{\Sigma} = \frac{\mathbf{M}\mathbf{X}_0 \left(\mathbf{M}\mathbf{X}_0\right)^\intercal}{N} = \mathbf{M}\frac{\mathbf{X}_0\mathbf{X}_0^\intercal}{N}\mathbf{M}^\intercal = \mathbf{M}\mathbf{\Sigma}_0\mathbf{M}^\intercal, \tag{2.13}$$

i.e., by pre- and postmultiplying the beam matrix by the transfer matrix. Importantly, the determinant of the beam matrix does not change during such a transfer

$$\det(\mathbf{\Sigma}) = \det(\mathbf{M}\mathbf{\Sigma}_0\mathbf{M}^\intercal) = \det(\mathbf{M})\det(\mathbf{\Sigma}_0)\det(\mathbf{M}^\intercal) = \det(\mathbf{\Sigma}_0), \tag{2.14}$$

because the determinant of a transfer matrix is always equal to 1. This determinant is in fact connected to the root mean square (rms) of all the single particle emittances

$$\epsilon_{\mathrm{rms}}^2 = \det(\mathbf{\Sigma}), \tag{2.15}$$

a quantity also known as the *geometric emittance* of the beam. Factoring this rms emittance out of the beam matrix leaves us with

$$\mathbf{\Sigma} = \epsilon_{\mathrm{rms}}\mathbf{B} = \epsilon_{\mathrm{rms}} \begin{bmatrix} \beta_x & -\alpha_x \\ -\alpha_x & \gamma_x \end{bmatrix}, \tag{2.16}$$

where β_x, α_x and γ_x are known as the Courant-Snyder or *Twiss* parameters. The *beta function* β_x, quantifying the beam size envelope, is connected via a derivative to the *alpha function* $\alpha_x = -\beta_x'/2$, which represents the x–x' correlation of the beam. The *gamma function* γ_x is completely determined by $\det(\mathbf{B}) = 1$ to be

$$\gamma_x = \frac{1 + \alpha_x^2}{\beta_x}, \tag{2.17}$$

implying that knowledge of the emittance, beta and alpha functions is sufficient to fully characterize a beam (ignoring third and higher order moments) at a given location s.

It is possible to express the single particle emittance that each particle in the distribution has in terms of the three Twiss parameters (see Fig. 2.2):

$$\epsilon(x, x') = \gamma_x x^2 + 2\alpha_x x x' + \beta_x x'^2. \tag{2.18}$$

While this single particle emittance is conserved throughout the accelerator, the particle will change its location in phase space by traversing an ellipse of constant emittance. The "angular location" on this ellipse, also known as the *phase*, changes according to

$$\phi_x(s) = \int_0^s \frac{1}{\beta_x(s')} ds', \tag{2.19}$$

i.e., it rotates quickly in phase space when the beta function is small and slowly when it is large.

Finally, the single particle emittance presents a simple way to define a continuous beam distribution in phase space. A bivariate Gaussian beam, as shown in Fig. 2.2, with a normalized charge density is given by

$$\psi(x, x') = \frac{1}{2\pi\epsilon_{\text{rms}}} e^{-\frac{1}{2}\frac{\epsilon(x,x')}{\epsilon_{\text{rms}}}}. \tag{2.20}$$

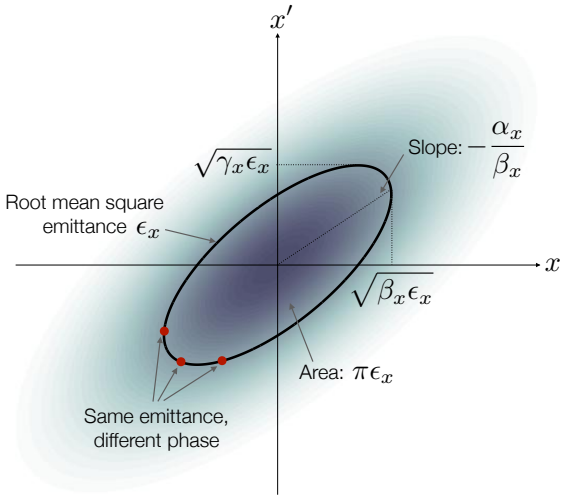

Figure 2.2: Phase space distribution of a bivariate Gaussian beam, where physical interpretations of the (geometric) emittance, phase and Courant-Snyder parameters are indicated.

2.1.4 Normalized emittance

While the geometric emittance is conserved in drifts or any linear focusing devices, it is not conserved during acceleration of the beam. This can be understood by considering the phase space it represents: positions and angles (sometimes also known as the *trace space*). When a particle experiences longitudinal acceleration, its forward momentum increases, but its transverse momentum does not. This therefore reduces the angle with respect to the axis ($x' = p_x/p$), which effectively compresses the x–x' phase space in the x' direction with a factor proportional to the forward momentum. It is thus necessary to normalize the geometric emittance by the forward momentum to get a quantity which is conserved also during acceleration. In practice, however, it is more useful to normalize not by the full forward momentum, but instead $p/mc = \beta\gamma$ as this allows better comparison between particles of different mass. The *normalized emittance* is therefore defined as

$$\epsilon_n = \beta\gamma\epsilon_{\mathrm{rms}}, \tag{2.21}$$

where $\beta = v/c$ and $\gamma = 1/\sqrt{1 - v^2/c^2}$ are relativistic factors (and not Courant-Snyder parameters). The β-factor is typically dropped when considering electron beams as it equals 1 for energies higher than a few MeV.

This normalized emittance, often known as the "beam quality", is a particularly important concept in transverse beam dynamics. Once a beam is produced, its normalized emittance can typically only increase—its beam quality can only degrade, bar a few clever exceptions. Normally, therefore, the emittance can at best be preserved at the initial value, with the use of aberration-free linear optics all the way from start to finish. If a high quality beam is required at the output, as in linear colliders or FELs, sources of emittance growth along the accelerator must be carefully accounted for in a sometimes-termed "emittance budget".

The reason why the emittance cannot decrease in an accelerator lattice can be traced to Liouville's theorem, which states that the density in phase space is conserved under linear transformations (e.g., linear optics). There are few ways to circumvent this limitation, however, one of which involves using synchrotron radiation (SR): particles are made to emit SR in, e.g., a ring (known as a damping ring), which causes them to lose momentum in all directions including the transverse, and are then re-accelerated in the longitudinal direction. Repeated enough times (typically over several ms), this process of damping is able to significantly reduce the beam emittance. However, this is not a viable option for reducing the emittance of a TeV-scale electron beam, as it would require an extremely large damping ring—which with a linear collider is what we wanted to avoid in the first place. Emittance

preservation at every step is therefore of prime importance in linear colliders.

2.2 Review of plasma wakefield theory

Although there has been much recent progress in the field of plasma wakefield acceleration, the basic mechanisms have long been understood. The theory of plasma wakefields separates into two main regimes: (1) *linear*, considering only small perturbations of the plasma density, and (2) *nonlinear*, where also large density perturbations are considered. The latter is considerably more complex than the former, often requiring computationally heavy simulations, but is also the focus of much attention due to its many attractive properties.

2.2.1 Linear perturbation theory

The original concept of plasma wakefield acceleration only considered small perturbations of the plasma density, as the density of laser and particle beams at the time was not high enough for further excitation. In this case, the perturbation of the plasma density from each infinitesimal particle can be added in a linear superposition to calculate the full perturbation, hence the term *linear regime*. In this section, we will follow a shortened description of the linear theory first laid out by Keinigs and Jones [162], and later pedagogically reproduced by Blumenfeld [127].

Density perturbations

We start by considering the plasma electron continuity equation

$$\frac{\partial n_e}{\partial t} + \nabla \cdot (n_e \mathbf{v}_e) = 0, \tag{2.22}$$

where n_e is the electron density, t is time and $\mathbf{v}_e$ is the fluid velocity—representing fluid-like electron movement in the absence of sources or sinks. The plasma electrons also obey the Lorentz force equation

$$\frac{\partial \mathbf{p}_e}{\partial t} = -e(\mathbf{E} + \mathbf{v}_e \mathbf{B}), \tag{2.23}$$

where $\mathbf{E}$ and $\mathbf{B}$ are the electric and magnetic fields, and $\mathbf{p}_e$ is the electron fluid momentum. Assuming that the fields are sufficiently weak to not cause relativistic motion ($\mathbf{p}_e = m_e \mathbf{v}_e$) the magnetic field term is negligible compared to that of the electric field. Using this and assuming only small density perturbations $n_e = n_0 + \delta n$,

we can linearize Eq. 2.22 to get

$$\frac{\partial \delta n}{\partial t} + \nabla \cdot (n_0 \mathbf{v}_e) = 0, \tag{2.24}$$

as well as a simplified force equation

$$\frac{\partial \mathbf{v}_e}{\partial t} = -\frac{e\mathbf{E}}{m_e}. \tag{2.25}$$

Differentiating Eq. 2.24 with respect to t and substituting in Eq. 2.25, we get a single equation

$$\frac{\partial^2 n_e}{\partial t^2} - \frac{n_0 e}{m_e} \nabla \cdot \mathbf{E} = 0. \tag{2.26}$$

Finally, we make use of Gauss' law to express the electric field divergence in terms of the net charge density

$$\nabla \cdot \mathbf{E} = -\frac{e}{\epsilon_0}(\delta n + n_b), \tag{2.27}$$

where n_b is the beam electron density and ϵ_0 is the vacuum permittivity. Substitution results in

$$\frac{\partial^2 \delta n}{\partial t^2} + \frac{n_0 e^2}{\epsilon_0 m_e} \delta n = -\frac{n_0 e^2}{\epsilon_0 m_e} n_b, \tag{2.28}$$

which can be further simplified to

$$\frac{\partial^2 \delta n}{\partial z^2} + k_p^2 \delta n = -k_p^2 n_b, \tag{2.29}$$

where $k_p = \sqrt{n_0 e^2/\epsilon_0 m_e c^2}$ is the plasma wavenumber introduced in Chapter 1.5.1, and a we have substituted time t for the co-moving coordinate $z = s - ct$. This equation indicates that the plasma behaves like a driven harmonic oscillator, where the beam charge drives density waves in the ambient plasma—also known as *wakes*. Equation 2.29 can be solved using Green's functions (in this case a simple sinusoid) to give us an analytic expression for the density perturbation

$$\delta n(z, \mathbf{r}) = -k_p \int_z^\infty n_b(z', \mathbf{r}) \sin k_p (z - z') dz', \tag{2.30}$$

where $\mathbf{r} = (x, y)$ is a transverse 2D vector. Each particular location in space is only affected by the beam charge directly in front, and can therefore be calculated independently at each transverse location $\mathbf{r}$.

Figure 2.3 shows examples of 1D density perturbations for two different bunches: a long bunch ($k_p \sigma_z > 1$) and a short bunch ($k_p \sigma_z < 1$), defining different regimes of plasma response based on their rms bunch length σ_z. For long beams, the plasma

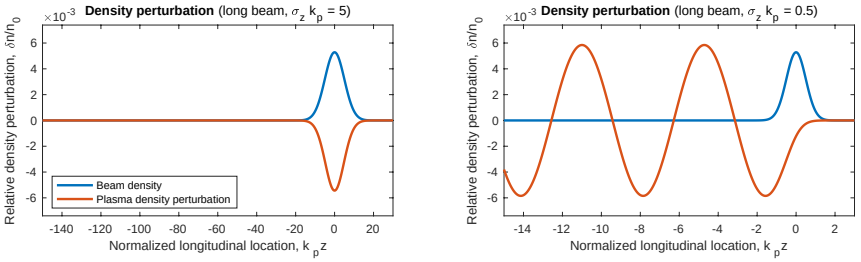

Figure 2.3: Plasma density perturbation in the linear regime from a long bunch (left) and a short bunch (right). The plasma has time to cancel out the beam charge imbalance for long beams, but does not for short beams, where the plasma keeps ringing at the plasma frequency.

has sufficient time to cancel out the charge imbalance set up by the beam ($\delta n \approx -n_b$), whereas for short beams the plasma starts ringing at the plasma frequency ($\delta n \sim \sin k_p z$ for $z < 0$). This response is similar to that of a tuning fork being slowly bent (long bunch) or experiencing a fast strike (short bunch).

Longitudinal and transverse electric fields

Armed with the ability to calculate plasma density perturbations, we are now able to find the resulting electric fields due to charge separation. To find the longitudinal field, it is sufficient to use a 1D approach—however, since we are also interested in knowing also the transverse fields, we will skip directly to the 2D treatment.

First, we consider the inhomogeneous wave equation for electric fields

$$\frac{1}{c^2}\frac{\partial^2 \mathbf{E}}{\partial t^2} - \nabla^2 \mathbf{E} = -\frac{1}{\epsilon_0}\nabla(\nabla \cdot \mathbf{E}) - \mu_0 \frac{\partial \mathbf{J}}{\partial t}, \tag{2.31}$$

where $\mathbf{J}$ is the current density and μ_0 is the permeability of the vacuum. The source terms on the right hand side corresponds to free charges (Eq. 2.27) and currents, respectively, the latter of which can be written as

$$\mathbf{J} = -en_b c\hat{\mathbf{z}} - en_0 \mathbf{v}_e, \tag{2.32}$$

where $\hat{\mathbf{z}}$ is the longitudinal unit vector—an expression representing both relativistic beam currents and sub-relativistic plasma currents. Substituting Eqs. 2.27 and 2.32 into the wave equation, we obtain

$$\frac{1}{c^2}\frac{\partial^2 \mathbf{E}}{\partial t^2} - \nabla^2 \mathbf{E} = \frac{e}{\epsilon_0}\nabla(\delta n + n_b) + \mu_0 e \frac{\partial}{\partial t}(n_b c\hat{\mathbf{z}} + n_0 \mathbf{v}_e). \tag{2.33}$$

Transforming to comoving coordinates, the left hand side simplifies, and using Eq. 2.25 we can substitute for $\partial \mathbf{v}_e/\partial t$ to get

$$-\nabla_\perp^2 \mathbf{E} = \frac{e}{\epsilon_0}\nabla\delta n + \frac{e}{\epsilon_0}\nabla n_b + \hat{\mathbf{z}}\frac{e}{\epsilon_0}\frac{\partial n_b}{\partial z} + \frac{n_0 e^2}{\epsilon_0 m_e c^2}\mathbf{E}, \tag{2.34}$$

where $\nabla_\perp$ is the transverse gradient operator. This can be further simplified to

$$(\nabla_\perp^2 - k_p^2)\mathbf{E} = -\frac{e}{\epsilon_0}\nabla\delta n - \frac{e}{\epsilon_0}\nabla_\perp n_b, \tag{2.35}$$

a second-order differential equation for $\mathbf{E}$ which can be solved independently in the longitudinal and transverse directions. The last term represents the electric "pancake field" from the beam, which can be ignored, as it is canceled (to order $1/\gamma^2$) by the beam's intrinsic magnetic field. Assuming cylindrical symmetry, we arrive at equations for the longitudinal electric field,

$$(\nabla_\perp^2 - k_p^2)E_z = -\frac{e}{\epsilon_0}\frac{\partial \delta n}{\partial z}, \tag{2.36}$$

and the radial electric field,

$$(\nabla_\perp^2 - k_p^2)E_r = -\frac{e}{\epsilon_0}\frac{\partial \delta n}{\partial r}. \tag{2.37}$$

Their solution can be derived using Green's functions, as shown by Keinigs and Jones, to be

$$E_z(r,z) = \frac{e}{\epsilon_0}\int_0^\infty \frac{\partial \delta n(r',z)}{\partial z} K_0(k_p r_>) I_0(k_p r_<) r' dr', \tag{2.38}$$

$$E_r(r,z) = -\frac{e}{\epsilon_0}\int_0^\infty \frac{\partial \delta n(r',z)}{\partial r'} K_1(k_p r_>) I_1(k_p r_<) r' dr', \tag{2.39}$$

where $r_<$ is the lesser of r and r' and $r_>$ is the greater. I_n and K_n are the nth order modified Bessel function of the first and second kind, respectively. The combination of Eqs. 2.30, 2.38 and 2.39 constitute linear plasma wakefield theory, allowing us to calculate the plasma density perturbation and resulting electric fields induced by a relativistic beam.

2.2.2 Nonlinear perturbations

Linear plasma wakefield theory applies well when its assumptions are satisfied: low beam density compared to the plasma density and non-relativistic motion of plasma electrons. If these assumptions are broken [163], however, the plasma response is

nonlinear—and in general very hard to model.

While the linear regime is charge symmetric—i.e., electrons and positrons have equal and opposite plasma responses—this is not the case for the nonlinear regime: for electron bunches, increasing the beam density beyond that of the plasma ($n_b > n_0$) results in a bubble-like cavity structure devoid of plasma electrons, as described in Chapter 1.5.2 and shown in Fig. 1.6. For positron bunches, the plasma interaction is more complex, gradually evolving to an non-Gaussian equilibrium bunch shape, sometimes in the form of an arrowhead (for radially asymmetric beams) [130].

Pioneering work on nonlinear plasma oscillations was done by Akhiezer and Polovin (1956) [164] and Dawson (1959) [165], even before plasma wakefields were conceptualized for acceleration. More recently, the nonlinear dynamics of the electron "blowout regime" was modeled by Lu (2006) [123, 124], allowing calculation of the exact shape of the bubble as well as the accelerating fields inside it. An alternative theoretical approach was later presented by Stupakov (2018) [166], where the beam is considered point-like and the trajectory of single plasma electrons trace out the blowout structure. However, these models go beyond what is necessary for understanding this thesis, and therefore only a few basic concepts from nonlinear theory will be considered in detail.

The wave breaking field

It is very useful to be able to estimate the characteristic accelerating field of a nonlinear plasma wave. We start by considering the electric field from complete charge separation over the length scale of a plasma wave in 1D. Mathematically, this is expressed using Gauss's law

$$\nabla \cdot \mathbf{E} = \frac{\rho}{\epsilon_0}, \tag{2.40}$$

which for a 1D plasma wave of characteristic wavenumber k_p reduces to

$$k_p E_z = \frac{e n_0}{\epsilon_0}. \tag{2.41}$$

Expanding k_p and rearranging, we find the so-called *wave breaking field* [167]

$$E_z = \sqrt{\frac{m_e c^2 n_0}{\epsilon_0}}, \tag{2.42}$$

or in engineering terms $E_z[\mathrm{V/m}] \approx 96\sqrt{n_0[\mathrm{cm}^{-3}]}$. For instance, for a plasma density of 10^{16} cm^{-3} the accelerating field can reach approximately 10 GV/m. Interestingly,

with some rearranging, Eq. 2.42 can be stated very simply in terms of the rate of change of the Lorentz factor

$$\frac{\partial \gamma}{\partial s} = k_p, \tag{2.43}$$

i.e., the Lorentz factor increases by 1 for every plasma skin depth. Therefore, the smaller the skin depth, the faster the acceleration.

The matched beta function

The accelerating beam experiences not only longitudinal fields, but also transverse fields. When the plasma electrons are completely "blown out", a bare ion column remains—exerting a focusing force for negatively charged beams (defocusing for positively charged beams).

To determine the transverse electric field inside the plasma blowout, we again start with Gauss's law for electric charges (Eq. 2.40). Applying the divergence theorem for a thin Gaussian pillbox volume with a radius r and width δ centered on the longitudinal axis, we obtain

$$\int \mathbf{E} \cdot \mathbf{dS} = \int \frac{\rho}{\epsilon_0} dV \tag{2.44}$$

$$2\pi r \delta E_r = \pi r^2 \delta \frac{e n_0}{\epsilon_0} \tag{2.45}$$

$$E_r = \frac{e n_0 r}{2\epsilon_0}. \tag{2.46}$$

Interpreting this electric field as an equivalent magnetic field, we can determine the focusing gradient to be

$$g_{\text{ion}} = \frac{\partial B_\phi}{\partial r} \equiv \frac{1}{c}\frac{\partial E_r}{\partial r} = \frac{e n_0}{2c\epsilon_0}. \tag{2.47}$$

The *matched* beta function β_m in such a focusing channel is defined to be that which does not change over time, i.e., $\alpha(s) = 0$. This can be found by solving Hill's equation for $\beta(s)$ (Eq. 2.5) setting all derivatives to zero, which gives

$$\beta_m = \frac{1}{\sqrt{k}} = \sqrt{\frac{p}{e g_{\text{ion}}}} = \sqrt{\frac{2c\epsilon_0 \gamma m_e c}{e^2 n_0}}, \tag{2.48}$$

where $k = e g_{\text{ion}}/p$ has been used and the Lorentz β is assumed to be 1 (ultra-relativistic beams). This can be simplified to the expression

$$\beta_m = \frac{\sqrt{2\gamma}}{k_p}, \tag{2.49}$$

indicating that the matched beta function increases with energy and decreases with higher plasma density. For instance, for a 1 GeV beam in a plasma of density 10^{16} cm^{-3}, the matched beta function is only 3.3 mm—which is very small.

If an electron bunch is injected into a blowout-based plasma accelerator with the wrong beta function, the beam size will rapidly oscillate—also known as *beta beating*. If the energy spread is nonzero, the emittance will increase due to different phase space rotation frequencies (smearing in phase space) [168]. Therefore, to avoid this beam degradation, it is important to match the beta function. This will be further discussed in Section 2.3.4.

Particle-in-cell simulations

While the above concepts make up zeroth order estimates of acceleration and focusing in the nonlinear regime, more detailed calculations are exceedingly more difficult. While some simple situations have analytical solutions, as outlined by Lu [123, 124] and Stupakov [166], the general approach is to instead use numerical simulations. These simulations are typically based on the particle-in-cell (PIC) method, where a large number of (macro-)particles are moved in a stepwise fashion through a 3D grid of cells with associated electric and magnetic fields. PIC simulations operate with a four-step cycle:

(1) Push the macro-particles using Newton-Lorentz equations of motion based on the forces present.

(2) Calculate charge and current density distributions by interpolation.

(3) Use Maxwell's equations to calculate the electric and magnetic fields in each cell.

(4) Determine the forces on particles based on their positions and velocities, adding any additional, external forces as required.

Typically, the grid used is in the mm^3 scale and using a μm resolution, implying around a 10^4–10^7 cells. Each cycle must be recalculated up to several times per plasma oscillation period $2\pi/\omega_p$, corresponding to approximately 1-100 μm of beam propagation. Simulating propagation on the mm-scale (laser plasma accelerators), or even the m-scale (beam-driven plasma accelerators) can therefore be extremely computationally intensive, requiring the use of supercomputing and massively parallel processing. Many different code implementations exist, of which OSIRIS [169] and VSIM [170] are examples of mature codes (benchmarked with experiment).

A multitude of codes attempt to significantly speed up the calculation time by applying various assumptions, appropriate in different situations. One such code is QuickPIC [171], using the so-called *quasistatic approximation*, where the timescale of the beam is assumed to be much slower than that of the plasma evolution—by a relativistic factor $\sqrt{2\gamma}$ (see Eq. 2.49)—particularly relevant for beam-driven PWFAs with ultra-relativistic beams. The plasma wakefields are therefore recalculated only once the relativistic beam has evolved, which allows a speed-up of several orders of magnitude. Given our focus on beam-driven PWFA, QuickPIC is the code of choice throughout this thesis. Figure 2.4 shows a QuickPIC simulation of an electron beam in the blowout regime, with the associated transverse and longitudinal forces.

For a more complete description of plasma accelerator simulations, a review is given by Vay and Lehe in Ref. [172].

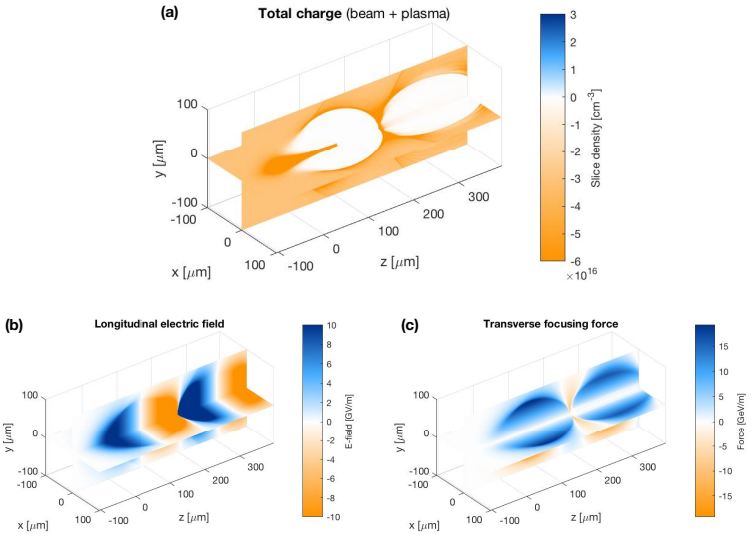

Figure 2.4: QuickPIC simulation of an electron bunch in the blowout regime, showing a clear bubble structure in the plasma electron density (a). Also shown are the corresponding longitudinal electric fields (b) and transverse focusing forces (c).

2.3 Sources of emittance growth in a plasma accelerator

Not exceeding the emittance budget is important in any high brightness accelerator, and especially so in a linear collider. Using a plasma wakefield accelerator introduces additional sources of emittance growth not present in conventional ac-

celerators. Here we cover the most important such sources, and discuss how they can be mitigated.

2.3.1 Multiple Coulomb scattering

One of the most obvious ways in which plasma accelerators differ from conventional accelerators is by the presence of a gas/plasma in the beam path, as opposed to a high vacuum. Most beam particles interact elastically with the particles of the gas (soft collisions)—i.e., with no energy loss and only a small angle change—and only a few particles will interact inelastically (hard collisions), leading to energy loss and large angle scattering. The latter particles form a non-Gaussian halo around the Gaussian core, and can typically be ignored for applications such as linear colliders.

Elastic scattering occurs when a particle passes within an unshielded region of the atomic nucleus. For a neutral gas, this is between the nuclear radius and the atomic radius, beyond which there is no scattering. In an ionized gas, ions can also scatter outside the atomic radius, based on the degree of ionization—i.e., singly ionized atoms will all behave like hydrogen etc. The largest impact parameter (scattering radius) depends on the type of plasma. For a quasineutral plasma—like that of linear PWFA or an active plasma lens—it will be the Debye length, outside of which the electric field is shielded, and for a non-neutral ion column—such as for blowout PWFA—it will be the full radius of the ion column. The total emittance growth is then simply the sum of the contributions from gas scattering and ion scattering.

Beam–gas scattering is a well-understood topic, starting with Blachman and Courant in 1948 [173] and Bethe in 1953 [174], then later in more detail by, e.g., Harita, Yokoya [175] and Raubenheimer [176]. Extensions for ion scattering was added by Montague [177] and later generalized by Kirby *et al.* [178]. The normalized emittance growth rate can be expressed as

$$\frac{d\epsilon_n}{ds} = \frac{4\pi r_e^2 n_0 \beta_x}{\gamma}\left(Z_i^2 \ln\left(\frac{\lambda}{R_a}\right) + 1.64Z(Z+1)\ln\left(\frac{287}{\sqrt{Z}}\right)\right), \tag{2.50}$$

where β_x is the beta function, n_0 is the neutral vapor density, r_e is the classical electron radius, Z is the atomic number, $Z_i e$ is the ion charge, $R_a \approx 10^{-10}$ m is the atomic radius and λ is either the Debye length λ_D (quasineutral plasma) or the plasma wavelength λ_p (blowout ion channel). The added effect of ionization (first term in Eq. 2.50) is only significant for hydrogen and helium, assuming a singly ionized plasma ($Z_i = 1$), and is generally negligible for higher-Z gases.

One interesting question is how the emittance growth in a plasma wakefield

accelerator scales with plasma density and final beam energy. Do we have to trade accelerating gradient for emittance? Using the matched beta function in a blowout (Eq. 2.49) and $k_p^2 = 4\pi r_e n_0$ we can integrate the instantaneous emittance growth to find the total added emittance along the full length L of the accelerator

$$\Delta\epsilon_n = \int_0^L \frac{d\epsilon_n}{ds} ds = \sqrt{2} r_e f(Z, Z_i, \lambda) \int_0^L \frac{k_p}{\sqrt{\gamma}} ds, \tag{2.51}$$

where $f(Z, Z_i, \lambda)$ corresponds to the outer parentheses in Eq. 2.50. Using $d\gamma = k_p ds$, this evaluates to

$$\Delta\epsilon_n = \sqrt{8} r_e (\sqrt{\gamma_f} - \sqrt{\gamma_0}) \left(Z_i^2 \ln\left(\frac{\lambda_p}{R_a}\right) + 1.64 Z(Z+1) \ln\left(\frac{287}{\sqrt{Z}}\right)\right), \tag{2.52}$$

where γ_0 and γ_f are the initial and final Lorentz factors, and we use $\lambda = \lambda_p$ assuming the blowout regime. We also assume that all particles are accelerated at the wave breaking field. Remarkably, this emittance does not depend on plasma density (only weakly through $\ln \lambda_p$), as increased scattering is compensated by decreased accelerator length and vice versa. Note, however that if instead the quasilinear PWFA regime is used, the matched beta function is larger and consequently the emittance growth increases, as was reported by Schroeder *et al.* in Ref. [155].

The only practical mitigation strategy against scattering is to use a low-Z gas species—ideally hydrogen. In this case, the emittance growth is very reasonable: around 1 nm rad for a 1 TeV beam. Use of heavier gas species will quickly lead to unacceptable emittance growth, due to the approximate Z^2 scaling.

An interesting point about gas/ion scattering studies is the lack of experimental verification of the theory. Although perhaps a somewhat dull topic of study, such an experiment would be of great value to the field.

2.3.2 Ion motion

Most plasma wakefield research assumes a stationary ion column with a perfectly linear focusing force. However, in the presence of sufficiently intense bunches, background ions will also undergo significant oscillation [179]. Contrary to the outward (blowout) motion of plasma electrons, ions are pulled closer to the axis by an electron beam, leading to nonlinear focusing forces and rapid emittance growth. Rosenzweig *et al.* [180] derived the phase advance of this ion motion to be

$$\Delta\phi_i \simeq \sqrt{\frac{2\pi r_p Z_i N \sigma_z}{A\epsilon_n}} (r_e n_0 \gamma)^{1/4} \tag{2.53}$$

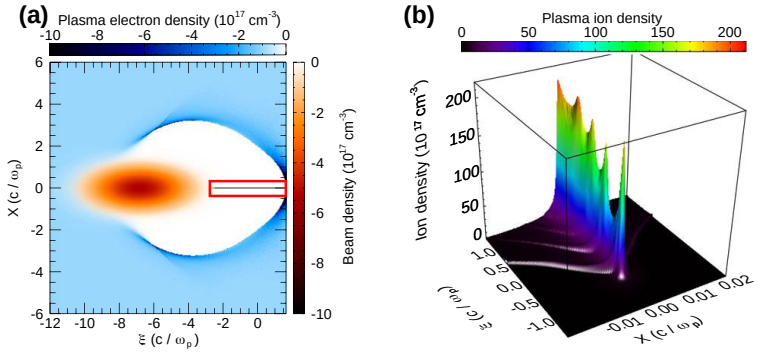

Figure 2.5: Simulation of ion motion by An *et al.* showing (a) the blowout structure and resulting ion motion (red square) and (b) a close-up of the significantly increased ion density on axis. Note the scale difference between the electron and ion wake structures. Source: An *et al.*, Phys. Rev. Lett **118**, 244801 (2017) [183].

where $r_p = 1.55 \times 10^{-18}$ m is the classical proton radius, A is the atomic mass number, and N is the number of beam particles. To avoid emittance growth, this phase advance must be limited to $\Delta\phi_i \ll \pi/2$—a significant limitation to the freedom of parameter choice for, e.g., a linear collider. Rosenzweig shows that the parameters used for proposed PWFA linear collider "afterburners" [181,182] (single-stage energy doublers) will lead to catastrophic emittance growth (100% in 1 mm). Figure 2.5 shows a simulation of ion motion.

Mitigating the effects of ion motion can be challenging. Since the bunch length typically scales with the plasma wavelength (constant $\sqrt{n_0}\sigma_z$), ion motion is approximately independent of plasma density. Using a heavier gas (large A) is possible, but will lead to more scattering and potentially multiple ionization where the bunch is most intense, both of which will increase emittance. This leaves only decreasing the bunch charge N or increasing the emittance ϵ_n, two options that will also reduce the collider luminosity.

If ion motion is left unmitigated, the accelerating beam will evolve to a transversely non-Gaussian equilibrium distribution. One promising approach is to match the beam directly to this distribution [183,184], in which case the emittance can be made reasonably small (sub-mm mrad) and does not increase during acceleration. Matching to this exact transverse distribution can be very difficult in practice, but may be possible using a plasma ramp of gradually decreasing ion masses (using different gases) to adiabatically shape the beam into the equilibrium distribution [185]. It is, however, unclear whether this non-Gaussian shape could be preserved between stages in a staged accelerator.

Finally, removing the ions altogether—a hollow channel accelerator—would solve all the above problems, including gas/ion scattering. Unfortunately, this comes at the cost of other problems; most notably a beam breakup instability, whereby the beam is deflected away from the channel axis (see Section 2.3.6 and Chapter 3).

2.3.3 Positron transverse beam loading

When an intense positron bunch propagates in a plasma, the plasma electrons are sucked towards the axis and create a region of higher electron density, which again provides focusing fields—sometimes called *transverse beam loading*. This is exactly analogous to ion motion, which is a form of transverse beam loading for electrons. While this so-called *self-loaded regime* has been shown by Corde [130] and Doche *et al.* [11, 145] to simultaneously focus and accelerate positrons, the emittance of the accelerated bunch increases dramatically (to 10^3 mm mrad or more) [186].

The positron beam gradually evolves to a non-Gaussian equilibrium state (see Fig. 1.6). Lotov [187] calculated this equilibrium state for a linear plasma wakefield, showing that the distribution has a strong peak on axis with long tails—a result which is expected to be similar also for a nonlinear plasma response. The final emittance is much larger than that for ion motion because plasma electrons produce a larger wake structure than that of plasma ions (see Fig. 2.5). Presently, it remains uncertain whether this mode of positron acceleration can be used for low emittance applications like a linear collider.

Another idea proposed to provide simultaneous focusing and acceleration for positrons is to use a donut-shaped drive beam [188, 189]—sometimes called *wake inversion*. This leaves a high density trail of plasma electrons on-axis and has been shown to provide linear focusing for positive test particles. However, using a high charge positron beam to efficiently load the accelerating field would result in a similar transverse beam loading and emittance growth as in the self-loaded regime.

As for mitigation, there are currently no good options for high gradient acceleration of low emittance positron beams. The four main options that exist all have their own problems: (1) the blowout regime defocuses positrons, (2) the self-loaded regime produces very high equilibrium emittances, (3) wake inversion does not allow high efficiency and (4) the hollow plasma channel accelerator, which in principle treats positrons and electrons identically, suffers from the beam breakup instability. This status quo is a big road block for the PWFA linear collider community, and must be solved either by identifying some agreeable parameter compromise in one of these regimes or by discovering some new regime.

2.3.4 Mismatching

In a plasma accelerator where the beam is injected from the plasma itself, the beam will intrinsically have a matched beta function β_m (Eq. 2.49). However, this is not necessarily the case for externally injected beams, e.g., in the case of a staged PWFA where the beam is coupled in and out of successive stages. If the beta function of the beam is *mismatched* [190], the beam size will oscillate at twice the betatron frequency $\omega_\beta = c/\beta_m$—also known as betatron beating.

Since the rate of this betatron beating is energy dependent, any energy spread in the beam will lead to *decoherence*, i.e., smearing of the beam envelope in phase space. Throughout this process, the emittance increases and the oscillating beta function gradually converges to the matched beta function, at which point the emittance saturates—known as complete decoherence. The relative emittance growth as stated by Mehrling *et al.* [168] is

$$\frac{\epsilon_{n,\mathrm{sat}}}{\epsilon_{n,0}} = \frac{1}{2}\left((1+\alpha_0^2)\frac{\beta_m}{\beta_0} + \frac{\beta_0}{\beta_m}\right), \tag{2.54}$$

where $\epsilon_{n,0}$ and $\epsilon_{n,\mathrm{sat}}$ are the initial and final normalized emittances, and β_0 and α_0 are the initial Courant-Snyder parameters. This ratio is also sometimes referred to as β_{mag} or colloquially "b-mag" [191]. Decoherence occurs faster for higher energy spreads, and complete decoherence occurs approximately after a distance $L_{dc} = \beta_m/\sigma_\delta$ [192], where σ_δ is the rms relative energy spread ($\delta = \Delta E/E$). Clear evidence for betatron beating was shown experimentally at FFTB and at FACET by Clayton *et al.* [193, 194].

Clearly, this emittance growth can be avoided by correctly matching the beta function of the incoming beam to the channel, $\beta_0 = \beta_m$ and $\alpha_0 = 0$—the only way to reduce Eq. 2.54 to unity. A subtle point is that for perfect matching, each energy slice needs to be matched slightly differently, as the matched beta function varies with energy ($\beta_m \sim \sqrt{\gamma}$).

For a typical high-gradient plasma accelerator, the matched beta function is very small. As an example, at density 10^{17} cm^{-3} (giving 30 GV/m accelerating fields) the matched beta function is only 3.3 mm for a 10 GeV beam. Such small beta functions are difficult to achieve with conventional focusing (quadrupoles) without inducing aberrations and emittance growth, which makes staging very difficult (see Section 2.4).

An immediate solution to this problem is to reduce the plasma density, increasing the matched beta function, but this also reduces the accelerating gradient. However, if the density is initially low and then gradually increased to the desired density—a

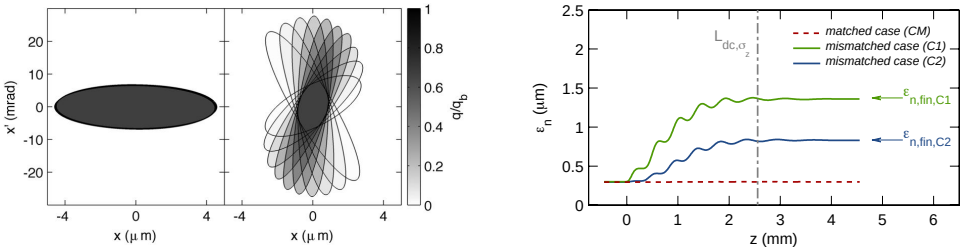

Figure 2.6: Mismatching of beams in a plasma wakefield accelerator. The phase space (left) of a mismatched beam before and after decoherence. The emittance (PIC-simulated) is seen to increase for mismatched beams, but not for matched beams. Source: Mehrling *et al.*, Phys. Rev. ST Accel. Beams **15**, 111303 (2012) [168].

so-called *plasma ramp* [195]—the beam is continually matched and the emittance preserved. If the ramp approximately sustains $\alpha = 0$ throughout, it is called an *adiabatic ramp* [196, 197], which is typically considered the safest option as it does not require very exact input matching and works for large energy spreads. However, if compactness is essential, it is possible to use more optimal ramps [198] at the cost of tighter tolerances. Note that in the ramp, the accelerating bunch is not in the correct phase of the longitudinal wakefield, and the incorrect beam loading will therefore typically induce an energy spread—this should be accounted for with an opposite beam loading in the flat-top accelerating region.

Typically, the matched beta function will still be small even after a ramp, in which case the remaining beam capture and refocusing must be done with external optical components between the stages (more details in Section 2.4).

2.3.5 Misalignments

A problem closely related to mismatching is that of misalignments between the incoming beam and the plasma accelerating structure. Misalignments cause emittance growth in two different ways: (1) through centroid decoherence and (2) through "hosing" and beam breakup. The former is just the first-order moment equivalent to mismatching (which is a second order moment phenomenon). The latter is caused by a feedback loop between the beam and the plasma cavity (coupled via transverse wakefields). Here we will only consider decoherence, as the beam breakup or hose instability deserves its own section—see Section 2.3.6.

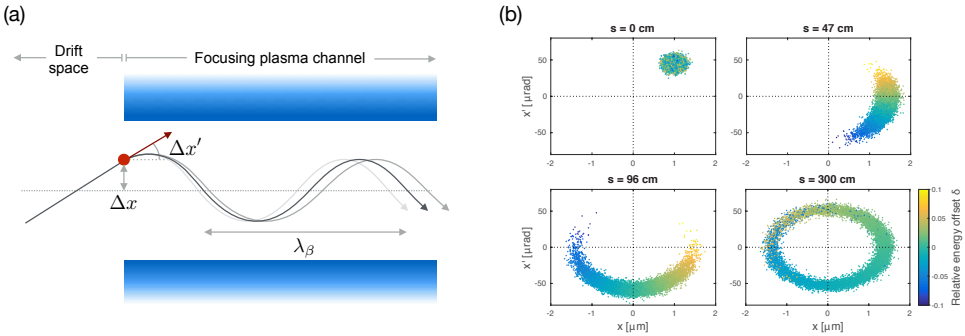

Figure 2.7: (a) Schematic view of a beam undergoing decoherence in a focusing plasma channel. (b) Decoherence as seen in trace space, gradually approaching full decoherence. Source: Lindstrøm *et al.*, Proceedings of IPAC2016 (2016), p. 2561 [1].

Decoherence

The process of centroid decoherence is illustrated in Fig. 2.7. When a bunch is injected off-axis, it starts to oscillate—each energy slice with a different frequency. This smears the bunch out in phase space until full decoherence is reached.

Generally, the smaller the accelerating structure, the tighter the tolerance. For CLIC, the alignment tolerance of elements is of the order 10 μm rms [49]. Plasma accelerators, however, with several orders of magnitude smaller accelerating structures, will have much tighter alignment tolerances. Another important difference between conventional accelerators and PWFAs is that the alignment of the plasma cell itself is irrelevant: the drive beam creates its own accelerating cavity in the uniform plasma and is therefore always on-axis. Instead, the drive-to-trailing beam offset is the important quantity, making the production of ultra-stable drive beams vital to high beam brightness. We should note that for inhomogeneous plasmas such as a hollow channel, both the plasma structure and the drive beam must be stabilized with respect to the accelerating beam.

Given that plasma accelerators are still being developed at a conceptual level, limited research effort has gone into the "higher order" problem of tolerances. Nevertheless, early studies by Assmann and Yokoya [199] showed that the tolerance of a conceptual PWFA-based TeV-scale collider would be very small, around 20 nm, simply based on the expected matched beam size. Further studies by Cheshkov *et al.* [200–203], using dynamical maps, concluded that the tolerance of a typical laser–plasma linear collider was indeed well below 100 nm and hence recommended the use of weaker focusing, e.g., by using hollow plasma channels.

Core Publication [1]

C. A. Lindstrøm, E. Adli, J. Pfingstner, E. Marin and D. Schulte,
Transverse tolerances of a multi-stage plasma wakefield accelerator,
Proceedings of IPAC2016, Busan, Korea (JACoW, Geneva, 2016), p. 2561.

A theoretical and simulation-based study performed as part of this thesis (Core Publication [1]) made a similar finding—approximately 40 nm rms and 1 μrad rms position and angular offsets, respectively, assuming a 1 TeV plasma wakefield accelerator linear collider (PWFA-LC) suggested in Ref. [152]. Further, for a beam-driven PWFA-LC it was found that the overall emittance growth is approximately given by

$$\Delta\epsilon_{n,LC} \approx \frac{l_s^2 k_p^2 N^{3/2} \sigma_\delta^2 \sigma_J}{16\sqrt{3}}, \tag{2.55}$$

where l_s is the length of each stage, N is the number of stages, σ_δ is the relative rms energy spread, and σ_J is the rms spread of the *error action* defined as

$$J = \frac{\Delta x^2}{2\beta_x} + \frac{\beta_x \Delta x'^2}{2}, \tag{2.56}$$

i.e., a combination of squared position (Δx) and angular ($\Delta x'$) offsets. Equation 2.55 is predicated on the assumption that beams will not reach full decoherence within each plasma cell—counter to what was assumed in Ref. [200], but typically the case for high-energy PWFA-LCs (backed up by simulation for the specific parameters). In Ref. [96], Schulte later noted that the alignment tolerance will likely be further reduced by considering the beam–beam overlap at the collision point.

Looking at Eq. 2.55 there appears to be a wealth of options for mitigating emittance growth from misalignments. However, adding the constraint of a constant final energy, most of these options fall away: $E_{\text{final}} \sim l_s N k_p$ and hence $\Delta\epsilon_{n,LC} \sim \sigma_J \sigma_\delta^2 E_{\text{final}}^2/\sqrt{N}$. From this we conclude that using more stages is beneficial, however, this ignores the added length and potential for emittance growth between stages. In fact, the only real options are to (1) reduce the energy spread, (2) break the correspondence between high gradient and strong focusing—e.g., by using a hollow channel—or (3) to actually produce ultra-stable drive beams on the scale of 40 nm/1 μrad rms or better. The energy spread in a PWFA will likely not be much below 1%; weak focusing introduces a host of new problems (see Section 2.3.6); and production of such ultra-stable beams is beyond the current state of the art—such as the 100–200 nm rms vibration level at LCLS [204]—and would therefore require significant R&D. A final note is that using plasma ramps does not

necessarily loosen tolerances, as it simply trades better position tolerance for worse angular tolerance (see Eq. 2.56).

In conclusion, misalignment tolerances currently represent a big hurdle to low emittance PWFAs and a potential linear collider application. A large research effort will likely be necessary to chart out how to deal with this challenge.

2.3.6 Beam breakup and the hose instability

The hose instability is an important challenge for plasma accelerators. However, before we discuss hosing, it is instructive to consider a very similar effect: the *beam breakup instability* [205].

The conventional beam breakup instability

Both longitudinal and transverse wakefields (i.e., force fields trailing a bunch) exist in a conventional accelerator due to the finite radius of metallic beam pipes—a phenomenon extensively studied by among others Chao [160] and Bane [206]. Transverse wakefields were quickly found to wreak havoc in high intensity linacs, first observed by Kelliher and Beadle in 1960 [207] and later in the SLAC linac by Panofsky and Bander in 1968, who subsequently presented their theory of beam breakup [208].

The beam breakup instability is best illustrated with a two-particle model. A single particle will set up a short-range transverse wakefield $W_\perp$ per charge per offset, with a corresponding force $F_\perp(z) = qx_1W_\perp(z)$. Typically this wakefield is sinusoidal in z with a slowly decaying amplitude. If this particle is in a focusing channel (e.g., made of quadrupoles) it will oscillate with a wavenumber k_β, i.e., $x_1(s) = x_0\cos(k_\beta s)$, where x_0 is the initial offset. A second particle is placed some distance Δz behind, observing both the transverse wakefield from the leading particle and the external focusing force:

$$\frac{\partial^2 x_2}{\partial s^2} + k_\beta^2 x_2 = \frac{qW_\perp(\Delta z)x_0}{E}\cos(k_\beta s). \tag{2.57}$$

This driven harmonic oscillator has a resonant behavior and an amplitude that grows without bound, as seen from the solution

$$x_2(s) = x_0\cos(k_\beta s) + \frac{qW_\perp(\Delta z)x_0}{2k_\beta E}s\sin(k_\beta s). \tag{2.58}$$

Although this model only considers two particles, its conclusions apply also to real beams: the head drives a resonant buildup of the tail amplitude, eventually leading

to beam breakup.

The standard mitigation technique for beam breakup is to introduce a head-to-tail energy chirp, also known as BNS damping after Balakin, Novokhatsky and Smirnov who first suggested it [209]. Simply put, this changes the oscillation frequencies of each longitudinal slice of the beam, which then decohere—inhibiting any resonant buildup. In the context of the two-particle model, we consider the second particle having a different focusing wavenumber $k_\beta + \Delta k_\beta$, giving instead

$$\frac{\partial^2 x_2}{\partial s^2} + (k_\beta + \Delta k_\beta)^2 x_2 = \frac{qW_\perp(\Delta z)x_0}{E}\cos(k_\beta s). \tag{2.59}$$

This equation has the solution

$$x_2(s) = x_0\cos(k_\beta + \Delta k_\beta)s + \frac{qW_\perp(\Delta z)x_0}{2k_\beta \Delta k_\beta E}\left(\cos(k_\beta + \Delta k_\beta)s - \cos k_\beta s\right), \tag{2.60}$$

which is not resonant, but oscillating. Ideally, the chirp is negative—i.e., lower energies further behind—as this enables cancellation of the transverse wakefield, which initially increases linearly from zero. This defines a criterion for the energy chirp required for BNS damping

$$\frac{\Delta k_\beta}{k_\beta} = \frac{qW_\perp(\Delta z)}{2k_\beta^2 E}, \tag{2.61}$$

where q represents the approximate charge of the bunch head.

In the case of beam breakup, the best options are therefore to (1) increase the energy spread, (2) reduce the transverse wakefield (e.g., by shortening the bunch or increasing the pipe radius), (3) reduce the bunch charge, or (4) increase the strength of the focusing. In principle, the difference in wavenumber Δk_β could also be generated with the rapidly changing fields of a high-frequency focusing device.

The hose instability

The hose instability—a variation of the beam breakup instability—was first described as a potential problem for plasma accelerators by Whittum *et al.* [116], who concluded that it would lead to very rapid beam breakup. Likening the hose instability to the *transverse two-stream instability*, he noted how it differs from the beam breakup instability by being independent of the beam charge (as higher charge beams create larger radius channels) and depending not on beam offset, but instead on beam tilts or kinks. However, challenging Whittum's assumption of long bunches and adiabatic channel formation, Huang *et al.* [125] showed that hosing does in fact

depend on beam parameters like charge, and that the effect is not as catastrophic as feared. This was backed up by experiments [210], none of which had managed to observe the hosing instability. Later, it was found by Mehrling *et al.* [131] that the intrinsic energy chirp induced by the strong deceleration effectively works to BNS-damp the hosing instability. In addition, Deng *et al.* [211] showed that for beams in a self-ionized plasma, a slightly different and less severe hosing occurs—and it is possible to find a working point where the gradual head-to-tail buildup of the ion column BNS-damps without the need for an energy chirp.

All the above research on the hose instability has, however, been focused on the drive bunch. While relevant to an afterburner [182], for an all-out PWFA linear collider we need to consider the trailing bunch. In the blowout regime, the trailing bunch will also be subject to a beam breakup instability [212]. This instability grows slowly (low exponential power), but appears to set a limit to the maximum achievable energy, beyond which the amplitude of the beam oscillation grows too large. Ref. [212] gives the example of a 10^{17} cm^{-3} plasma density, 6×10^{10} drive beam particles, 6×10^{9} trailing beam particles and tolerating an amplitude growth of a factor 10, in which case we can only accelerate up to about 500 GeV.

Interestingly, Lebedev *et al.* found that beams are subject to a fundamental *efficiency–instability relation* [213]: i.e., to avoid beam breakup, the power transfer efficiency from the driver to the trailing bunch must be limited. The ratio of the transverse wakefield to the focusing field is given by

$$\eta_t \approx \frac{\eta_P}{4(1-\eta_P)}, \tag{2.62}$$

where η_P is the ratio of power lost by the drive to that gained by the trailing bunch. This implies that it is not possible to be close to 100% efficient without beam loss, and instead the power efficiency must be kept sufficiently low to ensure $\eta_t \ll 1$. It is, however, unclear whether this relation also holds for trains of bunches, which may allow us to circumvent the criterion and increase efficiency by extracting energy over many accelerating buckets. A moderate amount of ion motion is also likely to mitigate beam breakup [214].

2.3.7 Radiative cooling

Before discussing out-of-plasma sources of emittance growth, it is useful to consider the exception to the rule that emittance can only increase: radiative cooling. In damping rings, the emittance cools on the time scale of milliseconds, and one would therefore not expect a single-pass linac to provide any significant emittance decrease.

However, in the presence of very strong focusing and very high energies, this damping can be non-negligible even in a linac [215]. It is worth noting that radiative damping does not in principle impose an upper limit to the achievable energy in a PWFA [216].

Studies by Michel *et al.* [192] confirms that the emittance can indeed be reduced this way, but also highlights the significant increase in energy spread as a result of this radiation. Reference [217] suggests that PeV-level beams with nm·rad emittance can be achieved by way of radiative damping in a plasma accelerator, although this study does not consider misalignments and may therefore be overly optimistic. Nevertheless, it will be important to include this effect in future studies—especially for TeV-scale energies—as it will affect the beam emittance.

2.4 Staging

Staging is the process of extracting the accelerating beam from one plasma accelerator stage and matching it into the next, simultaneously dumping the drive beam and replacing it with a fresh one. Historically, the staging problem has been considered mostly at the level of "insert quadrupoles here". More recently, however, it has been realized that staging is nontrivial and may lead to significant emittance growth and lengthening of the overall accelerator. A major difficulty is the combination of highly diverging beams and relatively large energy spreads, leading to large *chromaticity*.

Before discussing chromaticity in more detail, however, it should be noted that there *are* ways to avoid staging altogether. This includes using highly energetic drivers such that a single, long stage is sufficient—a strategy employed by for instance the AWAKE experiment [137], which uses a 400 GeV proton bunch that self-modulates [135] into hundreds of bunches and then accelerates a bunch of electrons [136]. Another way is to avoid strong focusing fields—e.g., by partially or completely removing the on-axis ions (hollow plasma channels: see Chapter 3). While in this section we will focus on staging, it is clear that alternative methods like these should be investigated in parallel.

2.4.1 Chromaticity

Chromaticity refers to the difference in focusing of different energy slices of a beam. Strictly speaking, chromaticity is often assumed to refer to *tune chromaticity* in rings, $\xi = (\partial\mu/\partial\delta)/2\pi$, which quantifies the chromatic error of single particles. Instead, we are referring to *focusing chromaticity* or *chromatic amplitude*, defined

by Montague [218] as

$$W_x = \sqrt{\left(\frac{\partial \alpha_x}{\partial \delta} - \frac{\alpha_x}{\beta_x}\frac{\partial \alpha_x}{\partial \delta}\right)^2 + \left(\frac{1}{\beta_x}\frac{\partial \beta_x}{\partial \delta}\right)^2}, \tag{2.63}$$

which quantifies the chromatic error of the beam distribution as a whole.

Unmitigated chromaticity can lead to severe relative emittance growth. Considering a hypothetical single lens that both captures and refocuses the beam, this will induce an approximate chromatic amplitude $W_{\text{staging}} \simeq L^*/\beta_m$ [219], where L^* is the distance from the lens center to the plasma entry/exit from which the beam diverges with a matched beta function β_m. Note that this "lens" can either be a collection of several quadrupoles or some form of plasma lens (discussed in Chapter 4). Assuming that the lens is made to focus beams that diverge from just upstream and refocuses to just downstream—i.e., that the focal length is about half the length of the lens, $f/2 \approx l_{\text{lens}} \approx L^*$—it will obey the relation $L^* = \sqrt{2E/(g_r ec)}$, where g_r is the radial magnetic field gradient (or equivalent for quadrupoles). Substituting for $\beta_m = \sqrt{2\gamma}/k_p$ and then simplifying, we find that

$$W_{\text{staging}} \approx \sqrt{\frac{n_0 e}{g_r \epsilon_0 c}}, \tag{2.64}$$

which interestingly is independent of the beam energy. Moreover, the emittance growth from this chromaticity can be expressed as [2]

$$\frac{\Delta\epsilon_n^2}{\epsilon_n^2} = W^2\sigma_\delta^2 + \mathcal{O}(\sigma_\delta^4). \tag{2.65}$$

This implies an approximate emittance growth for staging given by

$$\frac{\Delta\epsilon_n^2}{\epsilon_n^2} \approx \frac{n_0 e \sigma_\delta^2}{g_r \epsilon_0 c}. \tag{2.66}$$

As an example, using a 1% energy spread, a quadrupole channel with a g_r-equivalent of 60 T/m and a plasma density of 10^{17} cm^{-3}, we get more than 200% emittance growth at each stage. Using instead a strong active plasma lens with $g_r = 2$ kT/m at the same density, the growth can be reduced to about 14%—clearly a significant improvement. Nevertheless, it does not take many stages of even moderate relative growth before exponential compounding explodes the beam, especially if the plasma accelerator decoheres the phase space completely between each stage.

Mitigation of this emittance growth is therefore important. Use of stronger focusing elements such as active plasma lenses is one potential method, but may

not be a viable option as the accelerated beam can create its own plasma wakefield in the lens—a topic explored further in Chapter 4. Beyond reducing the energy spread, the simplest mitigation strategy, as discussed in Section 2.3.4, is to use a plasma ramp: i.e., decreasing the entry/exit plasma density. While it may be difficult to create a plasma ramp that fully resolves the staging problem, as that would require a very long ramp, it is likely to be an integral part of any staging system. To deal with the residual chromaticity, however, we will need some form of *achromatic* optics between the stages.

2.4.2 Sextupole correction

The conventional method to correct for chromaticity is to use *sextupoles* in regions of large dispersion [220]: these are magnets which provide a different focal length at each transverse offset. Combining this with dispersion therefore allows a sextupole to cancel the energy–focal length correlation inherent in quadrupoles. However, sextupoles also add a number of geometric aberrations to the beam which must be canceled with clever lattice design, often involving families of repeating sextupoles separated by a $-\mathbf{I}$ transfer matrix.

This method is used in final focusing systems, both new [219] and old [221], to cancel the detrimental effects on emittance caused by focusing beams with percent-level energy spreads down to very small (sub-mm) beta functions. These systems are very complex and typically hundreds of meters long. In many ways, one can think of PWFA staging as requiring two back-to-back final focusing systems: one to capture and the other to refocus the beam. This highlights the difficulty of using conventional magnetic optics for staging—if hundreds of meters of magnetic optics is required between stages, this would defeat the purpose of using a high-gradient acceleration scheme.

However, it is possible to make reasonable staging optics using this method, partly thanks to the symmetry of the problem. Figure 2.8 shows a non-optimized solution of this type—note the length, complexity and shear number of magnets required.

While use of sextupoles is certainly an option for chromaticity-corrected staging, it is not ideal. The main problem is that sextupoles require large dispersion to work properly, which in turn requires strong dipole bending, in particular if the system is to be compact. This will inevitably lead to strong synchrotron radiation and resulting energy spread, and therefore sextupole-based staging scales unfavorably with increasing energy. This could be avoided with a no-bend, no-sextupole based chromaticity correction method.

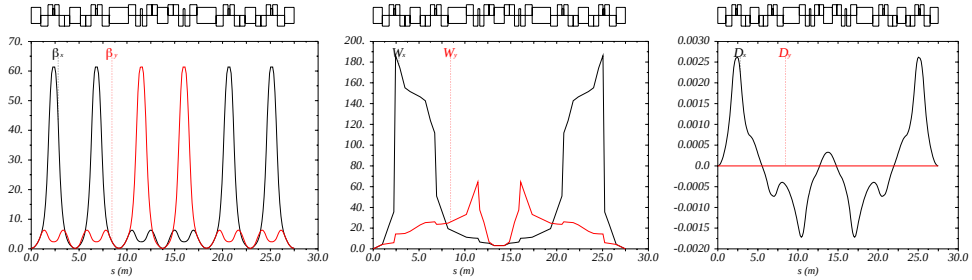

Figure 2.8: Example of staging optics using sextupoles, calculated using MADX [222]. The beta functions (left), chromatic amplitude (middle) and dispersions (right) are all simultaneously matched or canceled (to first order), but the system is long and complex—not ideal for compact staging.

2.4.3 Apochromatic correction

Fortunately, it is possible to cancel chromatic focusing errors using nothing but linear optics—no need for sextupoles and dipoles—using a method known as *apochromatic correction*. First proposed by Montague and Ruggiero [223], the energy dependence of the beam envelope is canceled for small variations in energy at a certain location along the orbit. This method is very similar to that used by camera lens makers to construct achromatic objectives out of glass lenses (where no sextupole-equivalent is available): see Fig. 2.9 for illustration.

As can be seen from Fig. 2.10, the mechanism behind apochromatic beam optics is that although single particles do indeed have chromatic errors, the overall beam distribution does not. It is in fact impossible to cancel the single-particle chromaticity using only linear optics—sextupoles are required [224]. Fortunately, as opposed to circular accelerators, in a single-pass linac the exact phase advance of particles is normally unimportant, and can therefore safely be ignored.

Typically it is sufficient to do apochromatic matching to first order in energy offset (δ) only, but in principle it can be done to arbitrary order. This serves to further flatten the chromatic dependence of the Courant-Snyder parameters around the nominal energy, as is illustrated up to second order in Fig. 2.11. A general method for designing apochromatic beam lines of any order was developed in Core Publication [2].

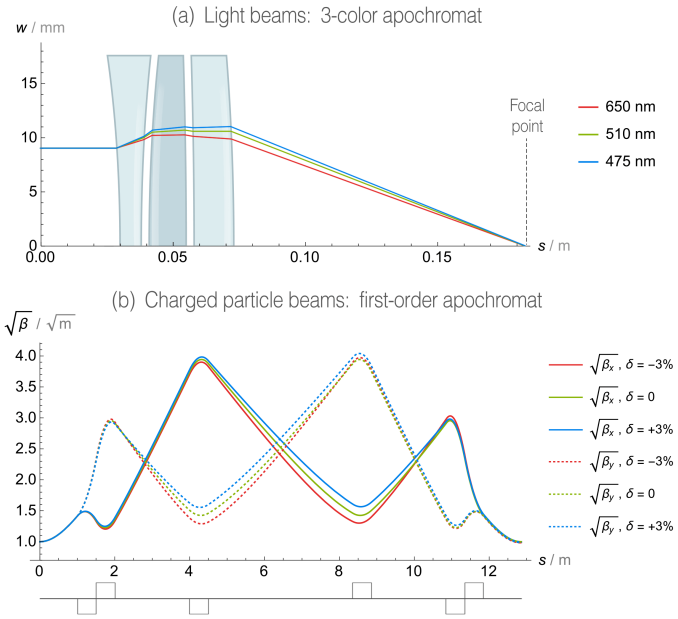

Figure 2.9: Apochromatic focusing, illustrated both by its use in (a) light-optics and (b) beam optics. Three colored lines (red, green, blue) demonstrate how the energy dependence of the focusing is canceled at the exit location (right hand side)—using (a) actual light rays (b) and the rms beam size envelope, respectively. Source: Lindstrøm and Adli, Phys. Rev. Accel. Beams **19**, 071002 (2016) [2].

Core Publication [2]

Carl A. Lindstrøm and Erik Adli
Design of general apochromatic drift-quadrupole beam lines,
Phys. Rev. Accel. Beams **19**, 071002 (2016).

So what are the limits of apochromatic correction? It is not possible to create a fully achromatic apochromat, regardless of how high the apochromatic correction order is. Instead, the current conjecture is that chromatic offsets that have less than about 100% emittance growth can be made arbitrarily achromatic, whereas energies outside this region can not be mitigated. The implication of this is that an apochromatic lattice can be successfully applied to the staging problem, but only if the beam exiting and re-entering the plasma starts at a sufficiently high beta function. This necessitates the use of plasma ramps, particularly if high plasma densities are used. The required plasma density at the end of these ramps can be

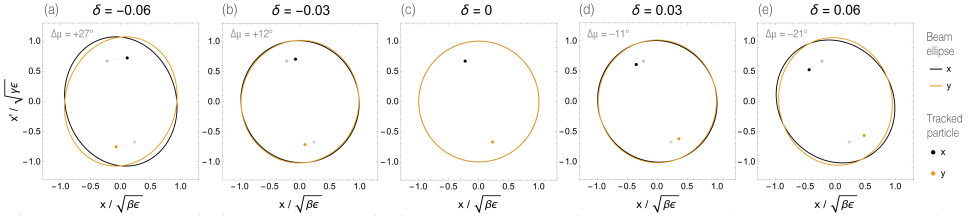

Figure 2.10: Trace space of different energy offsets (a–e), showing both the beam ellipse (solid lines) and a single tracked particle (points), for an apochromatic beamline. Although the single particle observes different phase advance at different energies (tune chromaticity), the beam ellipse is preserved to first order ($W = 0$). At higher energy offsets, the effect of higher order chromaticity is apparent. Source: Lindstrøm and Adli, Phys. Rev. Accel. Beams **19**, 071002 (2016) [2].

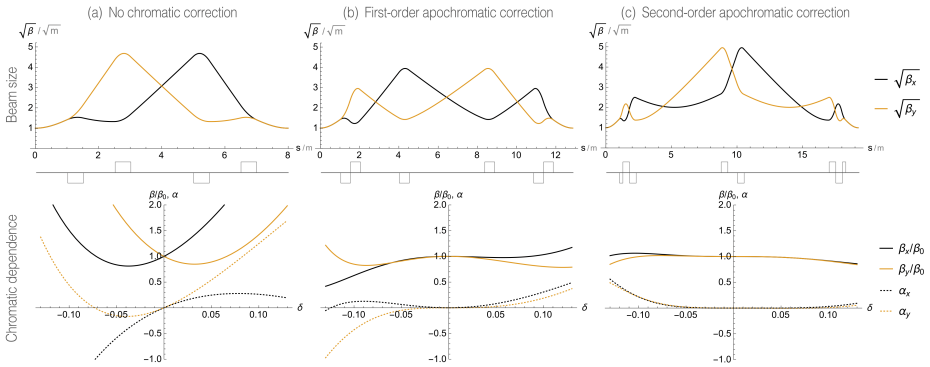

Figure 2.11: Comparison of quadrupole-based staging with no chromatic correction (a), first-order apochromatic correction (b) and second-order apochromatic correction (c). The chromatic error can be flattened more effectively for higher order apochromats, at the cost of a somewhat longer lattice. Source: Lindstrøm and Adli, Phys. Rev. Accel. Beams **19**, 071002 (2016) [2].

expressed (using Eq. 2.66) as

$$n_{\mathrm{ramp}} \ll \frac{g_r}{\sigma_\delta^2} \frac{\epsilon_0 c}{e}. \tag{2.67}$$

As an example, using a beam with 1% energy spread and a 60 T/m lens, the plasma density at the end of the ramp should be much less than 10^{16} cm^{-3}.

2.4.4 Proposed staging optics

Based on the idea of apochromatic correction, a schematic solution for staging optics was proposed in Core Publication [3], assuming parameters from the PWFA linear

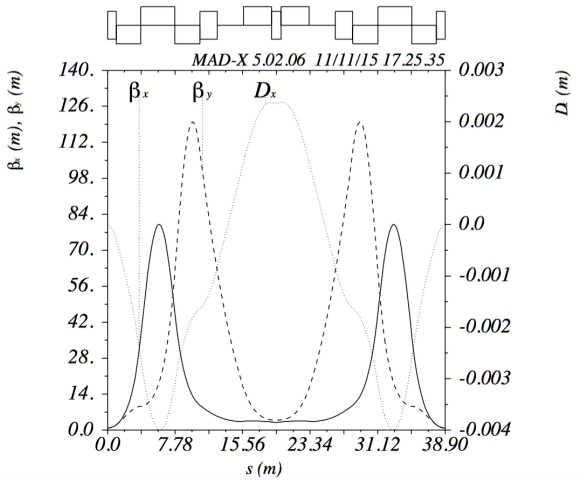

Figure 2.12: Proposed solution for staging optics of a 500 GeV beam with 0.5% energy spread. Chromaticity, dispersion and longitudinal chirp (R_{56}) are all canceled to the required level. However, for lower energies and higher energy spreads, second-order dispersion induces non-negligible emittance growth. Source: Lindstrøm *et al.*, Nucl. Instrum. Methods Phys. Res. A **829**, 224 (2016) [3].

collider study in by Adli *et al.* [152].

Core Publication [3]

C. A. Lindstrøm, E. Adli, J. M. Allen, J. P. Delahaye, M. J. Hogan, C. Joshi, P. Muggli, T. O. Raubenheimer and V. Yakimenko
Staging optics considerations for a plasma wakefield acceleration linear collider, Nucl. Instrum. Methods Phys. Res. A **829**, 224 (2016).

While the problem of capture and rematching is universal to both particle and laser drive beams, it will likely be harder to extract particle drive beams without affecting the accelerating beam. This imposes important constraints on the staging design. In particular, it will require meter-scale beam separation sections before and after each plasma stage, during which no focusing can occur as it would affect the drive and accelerating beam differently. The accelerating beam may therefore diverge significantly, inducing chromatic effects during capture. Additionally, these dipoles induce dispersion and longitudinal chirping (R_{56}) which must be canceled by the time of refocusing. All this was simultaneously accomplished for a 500 GeV beam of up to 0.5% energy spread in approximately 39 m, using 8 quadrupoles and 5 dipoles (see Fig. 2.12).

Although the chromaticity (mismatching) problem may be solved in this design, this solution is not final: by increasing the energy spread from 0.5% to 1%, an unmitigated second order dispersion blows up the emittance by 40%. Moreover, applying the same solution to lower energy stages only makes this problem worse. Further work is therefore required to either (1) mitigate also higher-order dispersion or (2) find a non-dipole-based method for separating the two beams. Note that the solution would work for a laser-driven wakefield accelerator, as extraction/injection of laser drivers do not require dipole separators.

In principle, assuming a workaround for second-order dispersion is found, a solution that works for one energy can be scaled to work for all energies. As the energy increases, the matched beta function scales as $\beta_m \sim \sqrt{\gamma}$. If also the length of focusing elements are scaled as $l \sim \sqrt{\gamma}$, keeping the magnetic field gradient constant, then a scaled version of the same optics applies: $\beta(s)\sqrt{\gamma/\gamma_0}$. While this is a relatively weak scaling (square root), it is important to note that the space between stages will increase, and therefore the total length of the accelerator scales as $\gamma^{3/2}$. Extrapolating, this means that at some energy a staged plasma accelerator will provide less effective acceleration gradient than a conventional, unstaged RF accelerator. We should, however, note that this may not be a problem since for sufficiently high energy the matched beta function will be large enough to not require any staging optics.

A final note is that the distribution of drive beams also represents a challenge, although strictly decoupled from the staging itself. Suggested schemes include a magnetic multi-chicane structure [152] (see Fig. 1.7) as well as an improved tree-like structure [16].

In summary, the combination of plasma ramps and apochromatic correction is able to solve the chromatic mismatching problem. Use of stronger focusing devices is highly beneficial, both in terms of chromaticity and compactness. The separation and re-merging of driving and accelerating beams presents a particularly difficult challenge for beam-driven PWFA, not present in LWFA, for which R&D is required.

2.5 Conclusions

It is apparent that plasma accelerators face many challenges in preserving low emittance beams. Some problems do seem surmountable: ion scattering can be mitigated by using low-Z gases; mismatching can be avoided by using longitudinally tailored plasma density ramps; and staging now seems feasible by the introduction of apochromatic corrective optics. Ion motion will likely set stringent limits on beam intensity, although it may be possible to mitigate by using transversely

Figure 2.13: Conceptual sketch of a qualitative cross-term "matrix" of interfering effects between different sources of emittance growth in a plasma accelerator, which may lead to more (red) or less (green) emittance degradation. Note that this is a first attempt, and should only serve as a template for further work.

shaped bunches.

Two aspects, however, remain particularly worrisome: (1) misalignments, as a source of instability and/or decoherence, and (2) transverse beam loading of positrons. For accelerating electrons, the beam breakup instability places extremely strict limits on misalignments—perhaps as low as the few nm-level to achieve reasonable luminosity. Moreover, the main method to suppress this instability—BNS-damping with an energy spread—works only to amplify the other problem of beam decoherence.

Even *if* a suitable parameter set can be found for electron acceleration, the positron problem is even more severe: there is currently no known way to efficiently accelerate low-emittance positron beams at high gradient. This is because we are forced to choose only two out of the three requirements: (1) no transverse beam loading, (2) efficiency via longitudinal beam loading and (3) strong focusing to avoid beam breakup.

It is in no way a given that plasma acceleration will eventually be compatible with a high luminosity linear collider: this is currently an open question. The only way to find out is by charting out the known parameter space and keep looking for new solutions.

One option for moving forward with theoretical studies of emittance preserving plasma accelerators is to start mapping out "cross term" effects. The above-mentioned sources of emittance growth have, with some exceptions, typically been studied in isolation. However, some sources of emittance growth—say, ion motion or radially nonuniform fields—will interfere with and possibly mitigate other effects—

such as the beam breakup instability [214, 225]. In this case, the emittance growth from one effect cannot simply be added to the emittance growth from another: there are cross terms. Charting out the full matrix of how these effects interfere with each other, both constructively and destructively, would be an interesting addition to the field: see Fig. 2.13 for a first qualitative-only attempt.

Another way forward is to make experimental progress toward a complete and emittance preserving single stage by using low plasma density (i.e., with sub-GV/m accelerating fields), where most problems are relaxed—especially misalignment and mismatching. When this prototype is proven to work optimally, consistent with linear collider requirements, we can incrementally improve the technology and move to higher densities. Current demonstrations of 10–100 GV/m fields are no doubt impressive, but also somewhat misleading to the linear collider effort, since such fields have not yet been used for efficient acceleration of low emittance beams. Just look to computer chip manufacturers: they did not start out making nm-scale transistors although this may have been understood to be theoretically possible!

Chapter 3

Hollow Plasma Channels

Positron acceleration is a major challenge for plasma wakefield accelerators. The combination of high gradient, high efficiency and low emittance all in one scheme is currently not available. That said, several methods *do* provide high positron acceleration gradient using plasmas—including the quasilinear regime [11], the self-loaded regime [130] and potentially wake inversion [188, 189]—but all suffer from the same problem of beam collapse into high-emittance, non-Gaussian equilibrium states [187]. This motivates instead changing the geometry of the plasma itself—the idea behind the *hollow plasma channel* [226–228]: a tubular plasma through which the beam is accelerated in the absence of focusing. At the face of it, hollow channel acceleration is the only method that encompasses all our three requirements: high gradient, high efficiency and emittance preservation [229]. Unfortunately, hollow channels are also highly unstable as accelerators due to the presence of very strong transverse wakefields [230]. This leads to a beam breakup instability which, combined with zero focusing, causes significant emittance growth or even beam loss.

Despite this gloomy outlook, it would be premature to conclude that plasmas are incompatible with high brightness positron acceleration—the parameter space is too rich and unexplored. Only by closely examining the advantages and drawbacks of each technique can we make progress. This chapter is therefore focused on the transverse wakefield problem in hollow plasma channels—in particular reporting on experimental work done at SLAC, where these transverse wakefields were measured for the first time.

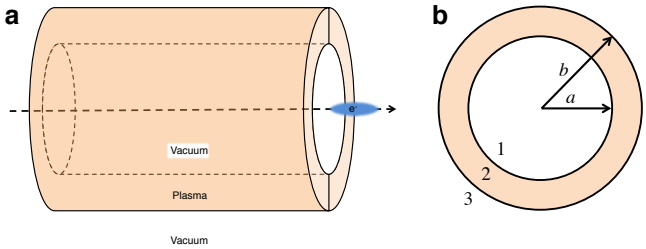

Figure 3.1: Schematic view of a hollow plasma channel, showing the (1) interior and (3) exterior vacuum regions separated by a (2) tubular plasma. Source: Gessner, Ph.D. thesis (Stanford University, 2016) [253].

3.1 Introduction

The hollow plasma channel did not originate as a solution to the positron problem: it was first proposed by Tajima [226] for laser guiding to overcome the diffraction and dephasing limit of laser wakefield accelerators. Only later was it envisioned as a positron accelerator [231]. Table 3.1 presents a detailed history of hollow plasma channel acceleration—from 1983 to the present.

3.1.1 Linear hollow plasma channel theory

One of the main appeals of the hollow plasma channel is its ability to respond symmetrically to positrons and electrons. This occurs only when the plasma behaves perturbatively, i.e., it is in the linear regime—which therefore constitutes the main theoretical framework used to study hollow plasma channels.

As opposed to uniform plasmas, hollow channels provide virtually infinite freedom in choice of radial density distributions. However, for this work we will assume a hard-walled flat-top channel with finite inner and outer radii a and b, respectively, as illustrated in Fig. 3.1. The next central assumption is that the plasma can be treated as a non-evolving dielectric channel [254] with a plasma dielectric constant

$$\epsilon(\omega) = 1 - \frac{\omega_p^2}{\omega^2}, \tag{3.1}$$

which varies with the frequency ω, and where ω_p is the plasma electron frequency given by Eq. 1.8. Using a similar approach to that used for dielectric channels [255], the longitudinal and transverse wakefields can be calculated. This was done for the hollow plasma channel by Schroeder *et al.* [230]—assuming an infinitely wide channel ($b \to \infty$)—and later generalized to finite channels by Gessner [253]. In the interest of brevity, we will simply reproduce the findings of Ref. [253].

Year	Milestone (hollow plasma channels)
1983	Tajima [226] proposes partially or completely hollow plasma channels for laser guiding to overcome the diffraction and dephasing limit in laser wakefield accelerators—dubbing it the *plasma fiber accelerator*.
1985	Further studies by Zaidman *et al.* [232], utilizing simple 2D simulations.
1987	Barnes *et al.* [233] show that lasers can be "self-trapped" in plasma fibers given sufficient laser power.
1992	First hollow channel PIC simulations by Katsouleas *et al.* [227].
1995	Hollow channel theory is consolidated by Chiou *et al.* [228, 234], who notes that the achievable accelerating field is approximately half that of a uniform plasma, including the existence of a wake-damping resonant wall layer where the plasma frequency matches the channel frequency.
1996	Arbitrary transverse density profiles are described by Shvets *et al.* [235, 236], also introducing an effective Q-factor for wake dissipation.
1999	Schroeder *et al.* [230] uses a multimode expansion to describe beam loading and beam breakup in hollow channels—the first mention of the transverse wakefield problem.
2000	A hollow channel is generated by Fan *et al.* [237], based on a kinoform (phase plate) design by Andreev *et al.* [238].
2001	Lee *et al.* [231] proposes hollow channels for positron acceleration.
2003	Marsh *et al.* [239] compares positron acceleration and guiding in uniform- and (nearly) hollow plasmas in an experiment at the FFTB facility at SLAC National Accelerator Lab—the first experimental demonstration of a hollow channel.
2009	Kirby *et al.* [240, 241] studies use of an obstructed gas jet for hollow channel generation.
2011	Kimura *et al.* [242] simulates positron acceleration in a realistic kinoform-based hollow channel—laying the groundwork for future experiments.
2013	Independent control of acceleration and focusing (for electrons) in *near-hollow* channels is studied by Schroeder *et al.* [243], who also find that ramped triangular beams provide optimal beam loading [244]).
2014	Yi *et al.* [245] proposes to accelerate positrons with a proton-driven hollow channel (later expanded on by Li *et al.* [246, 247]).
2016	Schroeder *et al.* [248] proposes a hollow channel-based linear collider concept (beam breakup is not addressed).
2016	*Nonlinear* hollow plasma channels are simulated by Amorim *et al.* [249].
2016	Gessner *et al.* [9, 10] demonstrates positron-driven plasma wakefields using a kinoform-produced hollow channel at the FACET facility at SLAC.
2017	Penn *et al.* [250] studies the hollow channel beam breakup instability.
2018	Wu *et al.* [251] proposes to use the hollow channel as a dechirper.
2018	First measurements of transverse wakefields in a hollow channel at FACET by Lindstrøm *et al.* [4] (part of this thesis)—consistent with theory—as well as the first observation of positron energy gain in a hollow channel plasma [252].

Table 3.1: Selected milestones in hollow channel plasma acceleration, listed by year of publication, including the work performed as part of this thesis.

Longitudinal wakefields

The hollow channel supports mainly two dominant wakefield modes: an $m = 0$ longitudinal (TM) mode and an $m = 1$ transverse (HEM) mode, where m denotes the azimuthal index. The longitudinal mode provides a uniform accelerating field across the width of the channel (assuming a high energy driver), varying sinusoidally in the comoving z-direction:

$$W_{z0}(z) = -\frac{ek_p\chi_\parallel^2}{2\pi\epsilon_0 a}\frac{B_{00}(a,b)}{B_{10}(a,b)}\cos(\chi_\parallel k_p z)\Theta(z) \tag{3.2}$$

per particle. Here, k_p is the plasma wavenumber, e and ϵ_0 are the positron charge and vacuum permittivity, $\Theta(z)$ is the Heaviside step function and

$$\chi_\parallel = \sqrt{\frac{2B_{10}(a,b)}{2B_{10}(a,b) - k_p a B_{00}(a,b)}} \tag{3.3}$$

is a longitudinal wavelength modification factor. The "Bessel-boundary function" is defined as

$$B_{ij}(a,b) = I_i(k_p a)K_j(k_p b) + (-1)^{i-j+1}I_j(k_p b)K_i(k_p a), \tag{3.4}$$

where I_n and K_n are the nth order modified Bessel functions of the first and second kind, respectively. This accelerating mode is independent of the transverse offset of the driver ($m = 0$).

Transverse wakefields

Similarly, the transverse wakefield is uniform across the channel width (dipole-like), but with an amplitude that varies linearly with the driver offset ($m = 1$). For a drive beam horizontally offset by Δx, the horizontal transverse wakefield per particle is

$$W_{x1}(z) = -\frac{e\Delta x\chi_\perp}{\pi\epsilon_0 a^3}\frac{B_{11}(a,b)}{B_{21}(a,b)}\sin(\chi_\perp k_p z)\Theta(z), \tag{3.5}$$

where the transverse wavelength modification factor is given by

$$\chi_\perp = \sqrt{\frac{4B_{21}(a,b)}{4B_{21}(a,b) - k_p a B_{11}(a,b)}}. \tag{3.6}$$

Given that the plasma response is linear, the total wakefield from a beam can be found by convolving the wakefields (Eqs. 3.2 and 3.5) with the longitudinal charge

distribution of the beam. Figure 3.2 shows the wakefields of a simulated hollow channel [4], where in particular the longitudinal field agrees very well with linear theory (Eq. 3.2). The transverse field also initially agrees well with theory (Eq. 3.5), but gradually diverges: this is an effect of plasma electrons being sucked into the channel—i.e., the assumption of a *non-evolving* plasma is broken. To understand the limits of when linear theory can be applied, it is therefore instructive to consider such nonlinear phenomena.

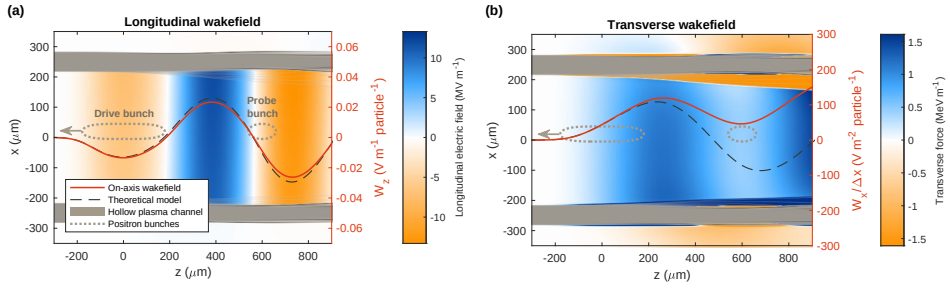

Figure 3.2: QuickPIC [171] simulation of a hollow channel with 215 μm and 280 μm inner and outer radius, respectively, and a plasma density of 3×10^{15} cm^{-3}. A 410 pC drive bunch transversely offset by 20 μm drives both a longitudinal wakefield (a) and a transverse wakefield (b), observed by a trailing 100 pC probe bunch. Source: Lindstrøm *et al.*, Phys. Rev. Lett. **120**, 124802 (2018) [4].

3.1.2 Nonlinear phenomena and PIC simulations

In the literature, there is some confusion about the exact condition for linearity. Reference [243] points out that the channel field can not exceed the wavebreaking field in the plasma wall: $E_z < E_{\mathrm{WB}}$, where E_{WB} is defined by Eq. 2.42. This limits the bunch charge (for a short bunch) to about $N < E_{\mathrm{WB}}/W_z$, where the longitudinal wakefield per particle W_z is given by Eq. 3.2. Further, Ref. [230] claims that the drive bunch can not exceed $N \ll k_p a^2/r_e$ particles in order to avoid excessive wall surface charge density, where r_e is the classical electron radius. Reference [253] instead quantifies this same constraint by limiting the drive bunch current to $N/\sigma_z \ll k_p a/2r_e$, where σ_z is the rms bunch length. In any case, it is clear that for high charge/current beams the wall is perturbed, and nonlinear phenomena akin to the blowout may occur. A useful tool in this regard is use of PIC simulations—as described in Chapter 2.2.2 and shown in Fig. 3.2.

Another effect that occurs in a hollow plasma channel is a resonance in the channel wall, first noted by Chiou [228] and Shvets *et al.* [235,236]. If the inner wall is "soft" (i.e., has a finite-width density ramp), there will be a thin layer wherein the

plasma frequency matches the frequency of the wakefield—leading to a resonance, and hence damping of the wakefield. Reference [235] introduces a corresponding Q-factor for the dissipation of the wake, which can be quite low unless the plasma boundary is very sharp—in some cases dissipating up to 70% of the wake energy in a single oscillation. This wake dissipation mechanism will be present in an otherwise linear plasma response, which has implications for the efficiency of, e.g., hollow channel acceleration of trains of multiple bunches.

3.1.3 The Panofsky-Wenzel theorem and short-range wakes

In light of the above discussion, there may appear to be many opportunities for tweaking the hollow channel in such a way as to suppress unwanted transverse wakefields. However, there are clear limits to this game set by the so-called *Panofsky-Wenzel theorem* [256]. This fundamental theorem ties together the longitudinal and transverse wakefields by their derivatives:

$$\nabla_\perp W_z = \frac{\partial}{\partial z}\mathbf{W}_\perp, \tag{3.7}$$

where $\mathbf{W}_\perp = (W_x, W_y)$ is a transverse wakefield vector.

For a hollow channel, using Eqs. 3.2 and 3.5 from linear theory, the Panofsky-Wenzel theorem can for short distances behind the driver be reduced to

$$\frac{W_x(z)}{\Delta x} = -\frac{\kappa(a,b)}{a^2}\int_0^z W_z(z')dz', \tag{3.8}$$

i.e., a direct connection between the short-range longitudinal and transverse wakefields induced by a drive bunch offset by Δx—a result derived in Core Publication [4]. Here $\kappa(a,b) = (4\chi_\parallel^2 - 2)/(\chi_\perp^2 - 1)$ is a numerical coefficient with a value close to 2. Interestingly, Eq. 3.8 is an instance of what Lebedev *et al.* [213] calls the *short-range wake theorem*.

We will eventually use this connection as a method for independently estimating the transverse wakefield from experimental measurements of the longitudinal wakefield (see Section 3.2.2).

3.1.4 Transverse wakefields and beam breakup

Clearly, short-range transverse wakefields are unavoidable in a hollow channel—or any accelerating structure for that matter. What makes the problem particularly bad in this case is the combination of small apertures (a) needed for strong accelerating fields (Eq. 3.2), and the lack of focusing fields—one of the main attractions for

positrons and easy staging (see Chapter 2.4). Equation 3.8 shows that the transverse wakefield increases significantly faster with decreasing channel radius a than the longitudinal wakefield does (by $1/a^2$), which leads to more rapid beam breakup—an instability discussed in Chapter 2.3.6. These transverse wakefields are likely similar to those present in a PWFA blowout structure with the same radius, but the lack of focusing fields means that any deflection will eventually lead to beam loss.

Reference [253] shows that for a single bunch the growth length of this instability—defined as the distance to double the transverse offset of the tail—in the case of no focusing is given by

$$L_g = \frac{1}{4}\sqrt{\frac{E}{eNw_x\Sigma_z}}, \tag{3.9}$$

where $w_x = \frac{\partial}{\partial z}\frac{W_x}{\Delta x}|_{z=0}$ is the initial slope of the transverse wakefield per offset per particle, and Σ_z is the full length of an assumed flat-top bunch with energy E. As an example, using FACET-like drive bunch parameters from Fig. 3.2 gives a growth length of about 4 cm—shorter than the length required for any significant acceleration, while clearly short enough for experimental detection in the 25 cm long channel at FACET.

3.2 The FACET E225 hollow channel experiment at SLAC

The SLAC linac has for many years produced high energy electron and positron bunches—initially for particle physics, and later for plasma accelerator research (among other uses). Plasma wakefield experiments at the Final Focus Test Beam (FFTB) facility at SLAC National Accelerator Laboratory were operated over many years (1998–2006), providing intense single bunches of energy up to 42 GeV by using the entire 3 km SLAC linac (up to 28.5 GeV for positrons). The follow-up Facility for Advanced aCcelerator Experimental Tests (FACET) [257] (2010–2016) was developed to improve on the experiments done at the FFTB, while also sharing 1 km of the linac with the new Linac Coherent Light Source (LCLS) [258]. Crucially, the FACET facility had the same high charge (3 nC) bunches as FFTB, but with the added ability to split these bunches into a two-bunch structure, allowing clean drive–trailing bunch acceleration of both electrons [129,144] and positrons [11,130], as well as the ability to also compress positron bunches. See Fig. 3.3 for a schematic of the FACET facility and the SLAC linac.

Following some early positron hollow channel experiments at the FFTB by Marsh *et al.* [239], a new hollow channel experiment was proposed for FACET: the E225

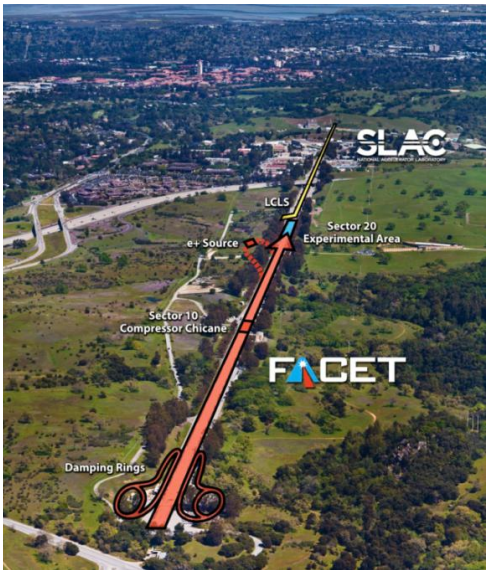

Figure 3.3: Bird's eye view and schematic layout of the FACET facility, using the first 2 km of the SLAC linac. Source: Mark Hogan, © SLAC.

hollow channel experiment. This experiment was led by S. Gessner and was extensively reported on in Ref. [253]. In this Section, a short overview of the FACET facility and the experimental setup is presented, as well as two major results obtained in the E225 experiment reported in Ref. [10] and Core Publication [4].

Core Publication [4]

C. A. Lindstrøm, E. Adli, J. M. Allen, W. An, C. Beekman, C. I. Clarke, C. E. Clayton, S. Corde, A. Doche, J. Frederico, S. J. Gessner, S. Z. Green, M. J. Hogan, C. Joshi, M. Litos, W. Lu, K. A. Marsh, W. B. Mori, B. D. O'Shea, N. Vafaei-Najafabadi and V. Yakimenko,
Measurement of transverse wakefields induced by a misaligned positron bunch in a hollow channel plasma accelerator,
Phys. Rev. Lett. **120**, 124802 (2018).

3.2.1 Experimental setup

The FACET facility comprised a highly complex setup, serving a large number of different accelerator research experiments. We will cover only those aspects relevant to the hollow channel experiment—more details beyond this can be found in

Refs. [129, 130, 253, 257].

Positron production and acceleration in the SLAC linac

Positron production at FACET utilized a technique developed for the SLAC Linear Collider (SLC) [259, 260]. First, an electron gun produced and accelerated high-charge, high-emittance electron bunches to about 1 GeV, which then entered an electron damping ring (see Fig. 3.3). After damping the horizontal and vertical normalized emittances down to 50 and 5 mm mrad, respectively, the electron bunches were re-entered into the linac, where they were accelerated to about 20 GeV. While these bunches could be used for electron experiments in the FACET experimental area, instead they were diverted to a positron source [261, 262] just upstream—consisting of a target made from W–26Re (a tungsten–rhenium alloy with 26% rhenium), followed by a solenoid and a *flux concentrator* (a pulsed eddy current transformer magnet). High energy electrons are required for a positron-per-electron yield higher than 1 in the resulting electromagnetic showers. The resulting low-energy positrons were then accelerated in a short linac to 200 MeV, transported back 2 km along the main linac, accelerated to about 1.2 GeV, then transferred to a positron damping ring, after which it was accelerated to 20 GeV in the main linac—just like the electrons, but surfing the radio frequency (RF) wave half a period out.

Note that a similar system is proposed also for FACET-II [138], where the electron source and damping ring will be exchanged for a photocathode, and a new ultra-compact positron damping ring [263] will be installed.

Longitudinal and transverse beam shaping

An important aspect of plasma wakefield acceleration is the need for very short bunches. FACET therefore employed a three-stage bunch compression technique using large chicanes in (1) the damping ring-to-linac transfer line, (2) half-way along the linac (Sector 10) and (3) just before the experimental area (Sector 20). A correlated energy spread (about 1%) was introduced along the bunch by accelerating it off crest or at the zero-crossing of the RF wave, and in this way the longitudinal phase space could be compressed to a minimum bunch length of approximately 20 μm rms.

However, the real innovation at FACET was the use of a beam notching device [129] that allowed splitting the bunches longitudinally into a two-bunch structure (see Fig. 3.4). Using a specifically designed multi-dipole *W-chicane* directly upstream of the experiment, the beam was energetically dispersed in the horizontal

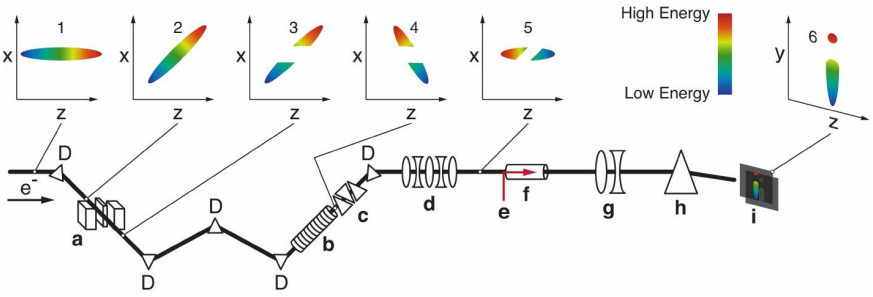

Figure 3.4: Schematic overview of the FACET experimental area: (a) beam notching device, (b) transverse deflecting cavity, (c) upstream energy spectrometer, (d) final focusing magnets, (e) ionizing laser, (f) heat-pipe oven, (g, h) imaging spectrometer with (i) LANEX and Cherenkov screens. Plots 1–5 show the process of generating the two-bunch structure (notching). Source: Litos *et al.*, Nature **515**, 92 (2014) [129].

plane and then cut into two parts using an adjustable mask, before finally canceling the induced dispersion prior to entering the plasma.

In order to achieve sufficiently high beam density for plasma wakefield excitation, FACET also featured a quadrupole-based final focusing system able to focus the beam down to about 20×20 μm rms in the transverse plane—with beta functions of approximately $\beta_x = 0.5$ and $\beta_y = 5$ m.

Plasma channel production

Two techniques were used at FACET for making a plasma: (1) *field ionization* [264, 265], where the electric field of the intense particle bunch itself ionizes the gas/vapor, and (2) high-power laser ionization, which allowed also more complex plasma channels to be formed—such as a hollow channel. The plasma was created by ionizing lithium vapor contained in a heat-pipe oven [266, 267], with a helium buffer gas on the upstream and downstream ends. While the use of lithium vapor was the standard solution at FACET—including for the E225 experiment—a long chamber filled with (harder-to-ionize) hydrogen was also used: enabling experiments that needed access to the plasma from the transverse direction, such as the E210 plasma photocathode injection experiment [18].

The FACET laser [268] was a 10 TW Ti:sapphire (chirped pulse amplified [74]) laser system providing short pulses—as low as 50 fs FWHM (full width at half maximum)—with an energy up to 500 mJ at a central wavelength of 800 nm (infrared). While the laser itself was at ground level, the beam was transported down into the experimental area (15 m below the surface), where it entered an in-vacuum

compressor before being focused and coupled into the plasma source via a holed mirror. To avoid excessive heating of the lithium vapor (from the energy loss of the beam) and burning of the mirrors, the repetition rate was limited to 10 Hz—and typically run at 1 Hz.

Uniform plasma operation required use of an *axicon* [269]—a shallow cone-shaped transmissive optic—to focus the laser into a long uniform column: a zeroth-order Bessel intensity profile (J_0^2). However, to make a hollow channel, a spiral phase plate (kinoform) was used. This method—first introduced by Andreev *et al.* [238]—creates instead a *higher-order* Bessel intensity profile. The specific kinoform used in the E225 experiment was an $m = 7$ phase plate (giving a J_7^2 radial intensity profile) with a first maximum at 250 μm: see Fig. 3.5.

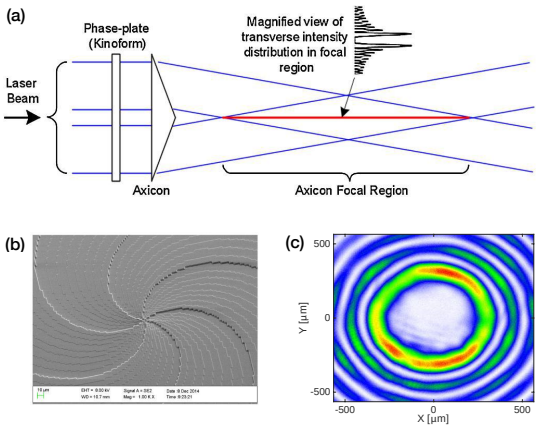

Figure 3.5: (a) Operation of a kinoform in combination with an axicon. (b) Scanning electron microscope image of an $m = 6$ kinoform. (c) The resulting laser image in the focal region—a hollow channel. Sources: (a) Kimura *et al.*, Phys. Rev. ST Accel. Beams **14**, 041301 (2011) [242], (b) © NIL Technology ApS [270] and (c) Gessner, Ph.D. thesis (Stanford University, 2016) [253].

Diagnostics

Given the multitude of experiments performed at FACET, a large number of diagnostics were available—only some of which were used in the hollow channel experiment. One central diagnostic consisted of a dispersive dipole with two quadrupoles—an *imaging spectrometer*—enabling energy measurements where angular kicks from the plasma could be canceled out using point-to-point imaging between the plasma exit and the LANEX or Cherenkov [271] detector screens. The transverse beam profile could be directly observed on a thin yttrium aluminum garnet (YAG) screen just

downstream of the plasma source. Moreover, the beam centroid was measured using two beam position monitors (BPMs)—one upstream and one downstream—such that the beam trajectory through the hollow channel could be found.

Measurements of the longitudinal bunch profile was normally accomplished with the use of a transverse deflecting cavity [272]. However, another option was to use an electro-optical sampler (EOS) [273–275], a technique whereby a beam-synchronous laser pulse is sent through a pair of crossed polarizers with a birefringent crystal in between. The electric pancake field of the beam induces a polarization change in the crystal, such that the transmitted laser power is proportional to the beam current profile. This allowed *non-destructive* shot-by-shot characterization of the longitudinal separation between the driver and the trailing bunch.

Laser cameras downstream of the plasma were also installed to monitor the transverse profile of the hollow channel—such as its roundness, intensity and transverse offset. After out-coupling via a holed mirror, the laser beam passed through a lens that allowed several cameras placed at different distances to simultaneously image several object planes inside the channel [see Fig. 3.5(c)]. Figure 3.7 shows the overall experimental setup.

3.2.2 Experimental results

Two main results were produced in the E225 hollow channel experiment: (1) the successful demonstration of a positron-driven hollow channel accelerator, and (2) the precise verification of the wakefields in such a channel. The data for these results were obtained using a fast-iteration data acquisition and analysis technique that was developed at FACET—see Appendix B for more details.

Demonstration of a positron-driven hollow channel plasma accelerator

In work by Gessner, reported in Ref. [10], a positron-driven hollow channel plasma accelerator was generated and characterized. While positron acceleration was not explicitly demonstrated until later [252], the measured deceleration of the drive bunch was in excellent agreement with linear theory (Eq. 3.2)—a bunch tail energy loss of 19 MeV in an 8 cm long channel, consistent with the predicted 220 MV/m decelerating field (see Fig. 3.6). Furthermore, the channel was confirmed to be hollow (i.e., zero on-axis plasma density) as the transverse beam size measured on the downstream YAG screen was unchanged when the positron beam propagated on-axis—not the case if propagated through the channel wall.

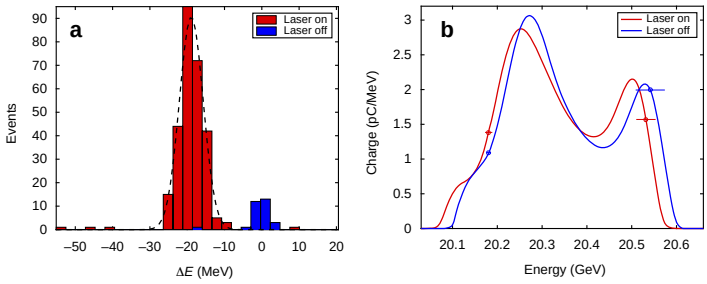

Figure 3.6: (a) Histogram of energy loss for a positron bunch in a hollow plasma channel (315 shots) for both laser off (blue) and laser on (red). (b) The energy distribution of a typical shot, indicating that the energy drops in the presence of a channel. Source: Gessner *et al.*, Nat. Commun. **7**, 11785 (2016) [10].

Measurements of the transverse wakefield

In many ways the natural continuation of Ref. [10] and a counterpart to the successful demonstration of the scheme, was the precise measurement of perhaps its main Achilles' heel—the transverse wakefield. This was the topic of a large fraction of the work done for this thesis, and was reported on in Core Publication [4].

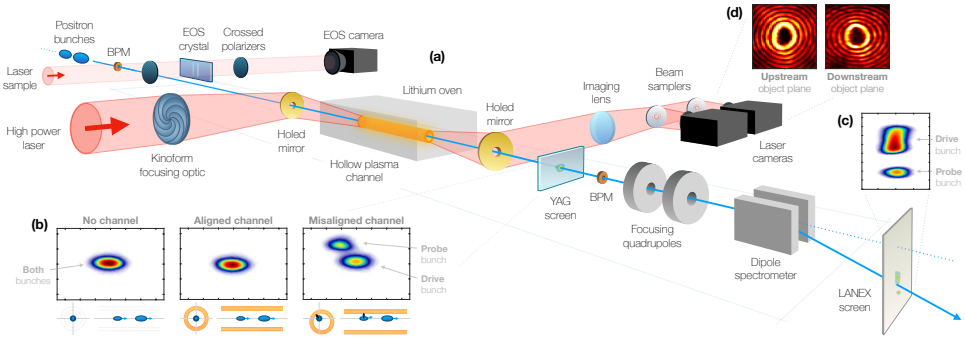

Figure 3.7: FACET E225 experimental setup (a) showing the incoming positron bunches entering a hollow plasma channel, before being diagnosed with a downstream YAG screen (b) and imaging spectrometer (c). The kinoform-focused high power laser beam is coupled in and out via holed mirrors, then imaged onto downstream laser cameras (d). Source: Lindstrøm *et al.*, Phys. Rev. Lett. **120**, 124802 (2018) [4].

The goal of this experiment was to measure the longitudinal variation of the transverse wakefield in a hollow plasma channel. This was accomplished by way of a bunch separation scan, observing the angular deflection of a trailing positron probe bunch by the offset of the leading drive bunch. Figure 3.7 illustrates the overall setup of this particular experiment, as well as how it was measured.

Instead of offsetting the drive bunch itself, the laser-generated channel was randomly offset by a significant transverse pointing jitter (30–40 μm rms)—with a negligible angular alignment error as the source was far upstream. At each bunch separation, the angular deflection of the probe bunch was measured on the imaging spectrometer (in the undispersed plane) as well as the offset of the channel (using laser cameras). Since the transverse wakefield (Eq. 3.5)—and hence the probe bunch deflection—scales with the channel offset, the deflection–offset correlation could be used as a direct measure of the transverse wakefield. Figure 3.8 shows such a correlation over several hundred shots at a particular bunch separation.

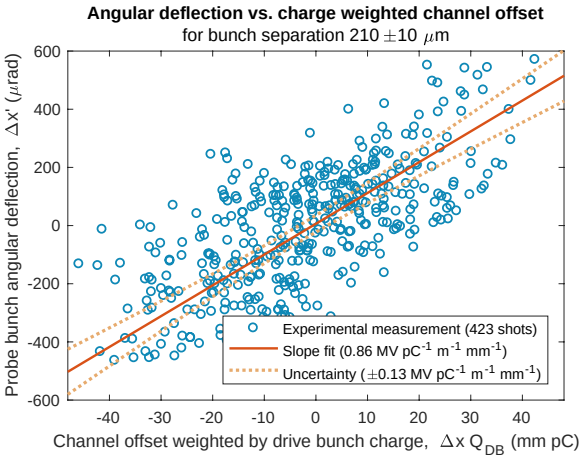

Figure 3.8: Correlation between the channel offset (weighted by the charge of the drive bunch) and the resulting angular deflection of the probe bunch, measured for a specific drive–probe bunch separation. Note that this plot represents the third data point in Fig. 3.9. Source: Lindstrøm *et al.*, Phys. Rev. Lett. **120**, 124802 (2018) [4].

A nine-step bunch separation scan was performed by tweaking the bunch compressor phase while simultaneously adjusting the beam notching device, producing bunch separations up to a maximum of 600 μm—enough for a half period of the wakefield. Figure 3.9(a) shows the result of this scan.

As an additional, independent measurement of the transverse wakefield, the short-range wakefield theorem (Eq. 3.8) was utilized. This way, a measurement of the longitudinal variation of the *longitudinal* wakefield could be used to estimate the transverse wakefield, given knowledge of the channel radius. Figure 3.9(b) shows a measurement of the longitudinal wakefield—i.e., probe bunch energy loss per drive bunch charge as measured on the spectrometer—which was used for the transverse wakefield estimate in Fig. 3.9(a).

The overall agreement between these transverse wakefield measurements is very

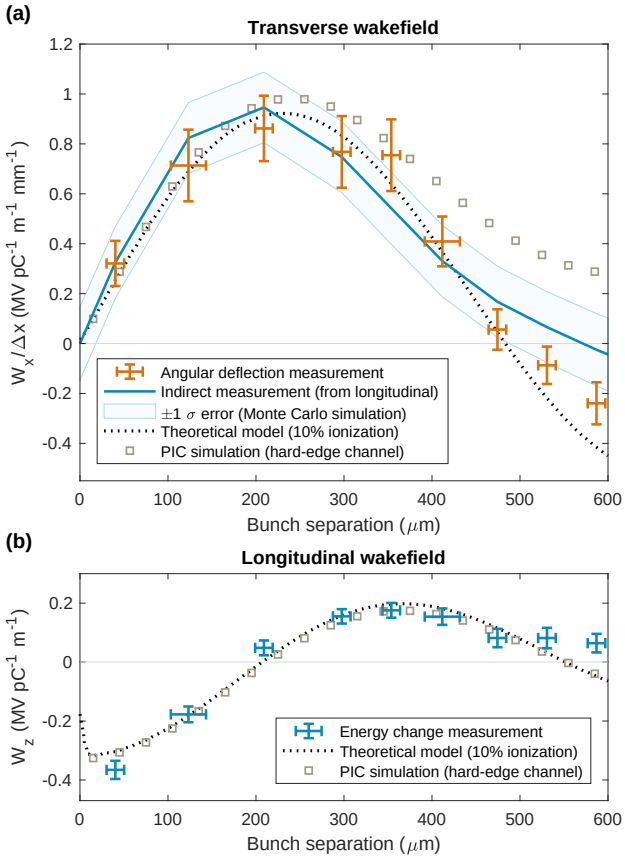

Figure 3.9: (a) Transverse wakefield in a hollow plasma channel from a direct angular deflection measurement (red crosses) and indirectly estimated via the Panofsky-Wenzel theorem (blue line). There is overall good agreement with linear theory (dotted black line), diverging only somewhat at larger bunch separations—although not exactly matching PIC simulations (gray squares). (b) The longitudinal wakefield (blue crosses), as measured on the spectrometer, used for estimating the transverse wakefield—in excellent agreement with theory. Incidentally, this measurement represents the first observation of positron acceleration in a hollow plasma channel. Source: Lindstrøm *et al.*, Phys. Rev. Lett. **120**, 124802 (2018) [4].

good: both the direct angular deflection measurement and the estimate based on the longitudinal field overlap to within the error of the measurement. Both also agree well with linear theory, with the exception of bunch separations larger than 500 μm. Here, the measurement diverges somewhat—an expected effect when plasma electrons are pulled into the channel (see Fig. 3.2). However, PIC simulations appear to overestimate this divergence—a problem which was not resolved, despite a large QuickPIC [171] simulation campaign searching for suitable beam and channel profiles (including soft walls).

The implication of this measurement is that the presence of a strong transverse wakefield has been confirmed. This result is not particularly surprising, given the robustness of the theory, but it is nonetheless an important incremental step towards an understanding of which plasma acceleration techniques can and can not be used for a linear collider.

The next step is to devise a strategy for mitigating the beam breakup instability.

3.3 Mitigation of the beam breakup instability

When considering whether the hollow plasma channel can be used for a linear collider, it is natural to first compare it to existing accelerator technologies used in current, mature linear collider designs. The beam breakup instability is not a novel problem in this regard—it was already a problem in the SLAC linac [208] and it is one of the main design constraints for CLIC [49]. The typical scale of short-range transverse wakefields in a CLIC cavity is about 100 V/pC/m/mm [276], while in a E225-like hollow plasma channel it was measured to be close to 1 MV/pC/m/mm (Fig. 3.9)—10,000 times larger! This is not related to the plasma, but rather due to the characteristic scale of the structure (i.e., the aperture). In fact, since the transverse wakefield scales as

$$\frac{W_x}{\Delta x} \sim \frac{1}{a^{3.5}}, \tag{3.10}$$

assuming $k_p a > 1$ (see Eq. 3.5), we would get CLIC-scale transverse wakefields also in a hollow plasma channel if it had the same aperture as a CLIC cavity (3 mm [277] instead of 215 μm). Moreover, the transverse wakefield will always increase faster relative to the longitudinal wakefield when the structure gets smaller, as evident from the short-range wake theorem (Eq. 3.8): $W_x/W_z \sim a^{-2}$.

In light of this, it is clear that the transverse wakefield must somehow be reduced—a challenging task given the fundamental nature of the above scalings. Several methods for mitigating the beam breakup instability have been proposed, the most promising of which will be discussed below.

3.3.1 External focusing

The conventional method for mitigating detrimental effects of transverse wakefields in any accelerator is to use strong external focusing, and has consequently been suggested for hollow channels by, e.g., Schroeder *et al.* [230, 243, 244, 248]. The focusing strength must be at least as strong as the transverse wakefield per offset, i.e., $F_{\text{wake}} < F_{\text{focus}}$ or equivalently

$$g_r > \frac{Q}{c}\frac{W_x}{\Delta x}\bigg|_{\text{tail}}, \tag{3.11}$$

where the transverse wakefield is evaluated at the bunch tail. Another way to view this is as an upper limit to the amount of charge, based on the strength of the focusing and the wakefields in the channel. The question, then, is how strong the external focusing can be.

Ideally, we would like to have radially symmetric focusing. However, this is not possible if the channel is to be truly hollow (i.e., a vacuum), as will be discussed in Chapter 4.1.1. The main option is therefore to go for quadrupole focusing—typically in the form of a FODO lattice (focus–drift–defocus–drift). For maximum focusing power, let us assume zero gap between the alternating-polarity quadrupoles. Exactly this kind of focusing has not been studied in detail for hollow plasma channels, but it *was* for the closely related dielectric channel already in 1997 by Gai *et al.* [278] at Argonne National Lab. They concluded that a single 150 MeV bunch could successfully be transported over several meters if external focusing and BNS damping (Chapter 2.3.6) was used. A later study by Li *et al.* [279] (same group) expanded on this by setting limits on the achievable acceleration gradient given efficient energy extraction—found to be of the order a few hundred MeV/m, depending on the channel radius and bunch charge. While plasmas differ somewhat from purely dielectric materials, it is reasonable to believe that this limit also applies to hollow plasma channels—at least as a first approximation.

While this gradient limit is already problematically low, another problem is even more worrisome. Net quadrupole focusing is a second-order effect, and requires the beam to be carefully matched. Figure 3.10 shows the general condition for optimum focusing in a quadrupole channel: the minimum average beta function in a (no-gap) quadrupole channel is $\bar{\beta} \approx \sqrt{10/k}$, where k is the quadrupole strength—which occurs only when the FODO period length is $L \approx \bar{\beta} \approx \sqrt{10/k}$. However, if the focusing is too strong in relation to the period length, i.e., $k \gtrsim 14/L^2$, the channel is *defocusing*. If the channel is too weak, on the other hand, the focusing ability of the channel is very marginal. The significance of these details is that it is not

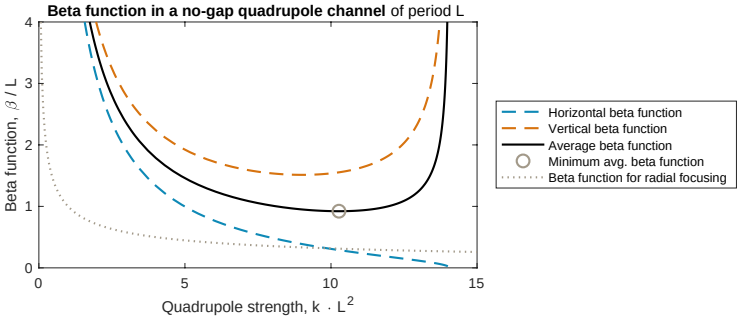

Figure 3.10: Beta functions in a FODO channel with no gaps between alternating quadrupoles, and a period length of L. The periodic input beta function in the horizontal (dashed blue) and vertical planes (dashed red) planes vary greatly with the quadrupole strength k. The minimum (x–y) averaged beta function occurs when $k \approx 10/L^2$—giving $\bar{\beta} \approx \sqrt{10/k}$. This implies that the quadrupole channel requires approximately 10 times higher magnetic field gradients (T/m) than an equivalent radial focusing channel (e.g., active or passive plasma lens: see Chapter 4).

possible to use external focusing to focus both a driver and an accelerating bunch, since these will in general have different energies (unless time-dependent focusing can be made). Focus the drive beam, and you will lose your accelerating beam from beam breakup—focus the accelerating beam and the drive beam will eventually be strongly defocused. Note that this problem does not apply to *laser-driven* hollow channels, as the laser is unaffected by magnetic fields.

3.3.2 Bunch trains

One way to circumvent the transverse wakefield problem is to split the bunch into a train of many small bunches with lower charge [230, 280]. This includes building up the wakefield with a train of drive bunches, as well as extracting the energy using a train of accelerating bunches. While the single bunch beam breakup (SBBU) is clearly mitigated this way, the new problem of resonant buildup of transverse wakefields arises. This can, however, potentially be hindered by the use of *stagger tuning* [281]—changing the frequency of the transverse wakefield while keeping that of the longitudinal wakefield constant—such that the transverse wakefield is not allowed to grow, but the accelerating field is. This is possible because different combinations of plasma density, channel radius and thickness can be made to have the same longitudinal frequency, but not transverse (see the wavelength modification factors Eqs. 3.3 and 3.6). Overall, this reduces the need for external focusing and therefore (partially) mitigates any problems discussed in Section 3.3.1.

There is, however, one problem with this approach: the thin resonant layer in the channel wall, and in general the potentially low Q-factor—as argued by Shvets *et al.* [235] (see Section 3.1.2). By spreading the buildup of the wake over many oscillations, the wall resonance is given time to grow. This and other nonlinear plasma behaviors are therefore likely to damp or otherwise perturb the wake—detrimental to both the efficiency and emittance preservation. Properly mapping out this problem will likely require some amount of simulation-based R&D as well as experimental verification.

Lastly, splitting the bunch into many smaller bunches also directly impacts the luminosity (Eq. 1.10). This is because the luminosity scales as the square of the number of particles per bunch N^2—each individual particle has less particles to hit in the colliding bunch. While this scaling does not hold for large bunch charges due to beamstrahlung constraints—in which case the luminosity instead scales linearly with N [49]—there is a limit to how much a bunch can be split up without impacting luminosity.

3.3.3 Near-hollow channels and electron lensing

Given the seemingly limited ability of external focusing and bunch trains to mitigate the transverse wakefield problem, it seems like the only viable option for the hollow channel is to somehow introduce strong focusing. This can be done by adding a low-density plasma inside the hollow channel—yet another proposal by Schroeder *et al.* [243], who dubbed it the *near-hollow plasma channel*. Working effectively as a hybrid blowout–hollow channel regime, this allows independent control of the accelerating fields, provided by the high density channel, and the focusing fields, provided by the on-axis ion column. The only drawback, of course, is that it does not work for positrons, which is why we went to the hollow channel in the first place.

Inspired by the near-hollow channel, we may propose a new scheme that might work for positrons. Clearly, for strong focusing of both drive and accelerating beams, the ideal situation would be to have a column of negative charges—an inverse ion column. Short of an anti-plasma, we must therefore introduce an excess of electrons on-axis. While this is the principle behind the self-loaded positron acceleration regime [130], transverse beam loading leads to significant emittance growth (see Chapter 2.3.3). The same thing would happen if we used a *Gabor lens* [282]—i.e., an electron cloud (see Table 4.1)—the problem is simply that electrons are too light. The solution is therefore to increase the mass of the electrons—relativistically! Using a long, ultrarelativistic, *counter-propagating* bunch of electrons in the hollow plasma channel would provide strong focusing of positron beams—the same effect

that provides e^+e^- pinching at the interaction point of a linear collider. This is a variation of the concept known as *electron lensing* [283, 284]—a low energy counter-propagating electron beam—which was both proposed [285] and demonstrated [286] for conventional accelerators by Shiltsev *et al.* at Fermilab (see Fig. 3.11).

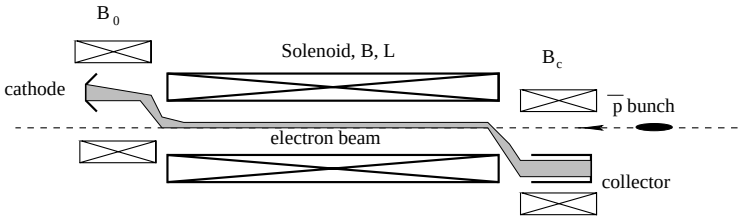

Figure 3.11: Electron lensing, as used to improve the lifetime of the 980 GeV proton bunches in the Tevatron at Fermilab. By increasing the energy of the counter-propagating electron beam, this could allow positron focusing for hollow plasma channels. Source: Shiltsev *et al.*, Phys. Rev. ST Accel. Beams **2**, 071001 (1999) [285].

The strength of this electron lens would depend mainly on the average beam density of the counter-propagating beam. If the transverse charge distribution of the electrons is uniform, and the energy sufficiently high to not be perturbed during the passage of the positrons, the emittance of the positron beam should be preserved—just like in an equivalent near-hollow channel. Increasing the energy of the electron beam from MeV to GeV, we would see a gradual shift from transverse beam loading effects to the equivalent of (negligible) ion motion: a 1 GeV-scale counter-propagating electron beam should provide similar properties to that of an ion column. Although the beam energy in the Fermilab electron lens [286, 287] was merely 10 keV, one could imagine increasing the energy of the electrons to be ultrarelativistic by use of a small electron ring or recirculating linac.

While clearly the high-energy electron lensing scheme is speculative at present, if it could help move high-gradient, high-efficiency, low-emittance positron acceleration out of the impossible and into the impractical, *that* would constitute progress.

3.4 Conclusions

Hollow channel plasma wakefield acceleration is to date the only positron acceleration scheme that may simultaneously provide high gradient, high efficiency and emittance preservation. It does not yet, however, constitute the solution to compact plasma-based linear colliders—strong transverse wakefields caused by even slight misalignments lead to a severe beam breakup instability.

In this chapter, the cause and possible mitigations of this instability was ex-

amined. Although hollow channels were originally proposed for laser guiding, they were later realized to be ideal positron accelerators due to their charge symmetry—evident from the linear theory that describes them (Eqs. 3.2 and 3.5). The E225 hollow channel experiment at SLAC's FACET facility, which constituted a major part of the work for this thesis, was able to show not only acceleration of positrons in a hollow plasma channel, but also to do precision measurements of the transverse and longitudinal fields in it. While the experiment and analysis was technically very challenging, the results are clear and consistent with theory. Transverse wakefields will indeed be the major challenge ahead for hollow channels.

Many ideas for how to mitigate the beam breakup instability have been proposed, many of which seem promising at first glance, but less so with the second. External focusing—the typical go-to solution—appears especially challenging in light of the difficulties associated with quadrupole FODO channels. However, a novel solution based on high-energy counter-propagating electron lensing may (or may not) prove to be the necessary solution. Only with continued research and innovation can this significant road block to a plasma-based linear collider be moved aside.

Chapter 4

Active Plasma Lenses

Active plasma lensing is a promising method for strong focusing of particle beams, as it provides radially symmetric kT/m focusing fields [94], with possible applications to staging, final focusing or even positron sources. Although not as strong as the closely related passive plasma lens [95], active plasma lenses have many advantages, including being independent of the exact beam distribution as well as being charge symmetric—important for positron focusing.

However, the active plasma lens concept suffers from several types of aberrations—especially plasma wakefields and nonuniform plasma temperatures—both of which must be tackled if the technology is to be viable for use with high brightness beams. This is therefore the topic of the following Chapter, which reports on both theoretical investigations of the limits set by plasma wakefields, as well as experimental studies of nonuniform plasma temperatures (and how to mitigate it) performed at the CLEAR User Facility at CERN.

4.1 Introduction

The idea of making a plasma lens stems from considering the ideal form of beam optics. Just as in light optics, we would prefer focusing in both the horizontal and vertical plane simultaneously. This would make net 2D focusing a first-order effect, and not a second-order effect like in quadrupoles and solenoids. There are only two ways to accomplish this: (1) using radial electrostatic fields or (2) using azimuthal (circular) magnetic fields. The former (1) is the basis of the *passive plasma lens*, where the ion column of a plasma blowout is used for focusing the beam—"passively" as the beam provides its own blowout. The latter (2), on the other hand, is the principle behind the *active plasma lens* and requires a radially uniform longitudinal

current—"active" because it needs to be externally driven. See Tables 4.1 and 4.2 for historical reviews of passive and active plasma lenses, respectively. The focus of this Chapter, however, will mainly be on active plasma lenses.

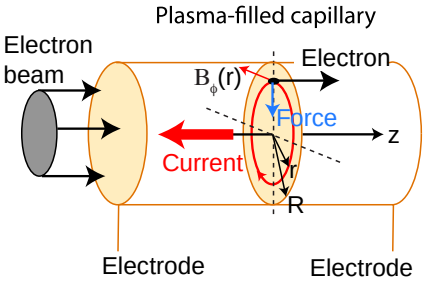

Figure 4.1: Illustration of the basic function of an active plasma lens. A longitudinal current is passed between two electrodes: the current density forms an azimuthal magnetic field, linearly increasing with distance from the axis. An electron beam propagating through the plasma will then observe a radial focusing force. Source: van Tilborg *et al.*, Phys. Rev. Lett. **115**, 184802 (2015) [94].

4.1.1 Basic theory

An active plasma lens consists of a thin gas-filled tube—a *capillary*—with high-voltage electrodes on either end for supplying the discharge current (see Fig. 4.1). Most often, this capillary has internal gas inlets and holed ends where the gas escapes into a vacuum. When the gas is discharged, a longitudinal current flows through the capillary. Ampere's law states that

$$\nabla \times \mathbf{B} = \mu_0 \mathbf{J} + \frac{1}{c^2}\frac{\partial \mathbf{E}}{\partial t}, \tag{4.1}$$

where $\mathbf{B}$ and $\mathbf{E}$ are the magnetic and electric (vector) fields, $\mathbf{J}$ is the current density and μ_0 is the permeability of free space. Based on the last term in this equation, one might suspect that it is possible to use a strong, high frequency electric field to generate a focusing B-field via *displacement currents*, however this turns out to be fundamentally impossible as the effect is canceled by radial E-fields (by Gauss' law) [324]. Assuming cylindrical symmetry and only a longitudinal current, Ampere's law can therefore be simplified to

$$\frac{1}{r}\frac{\partial}{\partial r}(rB_\phi) = \mu_0 J_z(r), \tag{4.2}$$

where r, ϕ and z are the radial, azimuthal and longitudinal coordinates. In principle, the current density can vary with radius—a source of aberration discussed in

Year	Milestone (passive plasma lenses)
1922	First electrostatic focusing of a continuous low-energy (300 eV) electron beam in a cathode ray tube by Johnson [288] from an excess of on-axis positive ions—an early precursor to the passive plasma lens.
1932	Von Borries and Ruska [289, 290] consider cathode ray focusing by space charge in a gas discharge—calling it a *space charge lens*.
1934	Bennett [291] introduces the idea of magnetically self-focused electron streams, where the electric space-charge field of the stream is neutralized by a plasma, leaving only magnetic focusing fields.
1947	Gabor [282] proposes to use an electron cloud for focusing low energy ion beams—now known as a *Gabor lens*.
1955	Bennett [292] generalizes his theory of self-focused streams.
1966	Magnetically self-focused electron streams are observed by Graybill and Nablo [293] in an experiment at the Ion Physics Corp.
1969	Gabor lensing is experimentally demonstrated for the first time by Zhukov *et al.* [294], who also coins the term "plasma lens".
1978	More Gabor lenses are demonstrated by Booth and Lefevre at Lawrence Livermore [295], and by Mobley *et al.* at Brookhaven [296].
1982	*Foil focusing* is proposed and demonstrated by Adler and Miller [297, 298], where radial currents in a thin metallic foil leads to electrostatic ion focusing—conceptually similar to passive plasma lensing.
1987	Chen [95] proposes to use the strong transverse electrostatic fields of beam-driven PWFAs for the final focus of a linear collider—the inception of the modern passive plasma lens.
1990	Aberrations of passive plasma lenses are studied by Su *et al.* [299].
1990	Self-pinching of a 21 MeV electron beam by (overdense) plasma wakefields is observed at Argonne National Lab by Rosenzweig *et al.* [300], in a first demonstration of the passive plasma lens.
1991	Similar experiments are performed at Tokyo University by Nakanishi *et al.* [301], also demonstrating electron focusing by plasma wakefields.
1994	A time-resolved passive plasma lens experiment is performed at UCLA by Hairapetian *et al.* [302] using 25 ps long electron bunches, demonstrating that focusing occurs mainly in the denser beam core.
1999	The plasma return current effect, whereby the focusing of a passive plasma lens is reduced by electrons flowing back through the beam (effectively active plasma lensing), is observed at LBNL by Govil *et al.* [303].
2001	A 28.5 GeV positron beam is focused by a 3 mm long passive plasma lens in the FFTB facility at SLAC by Ng *et al.* [304].
2010	Thompson *et al.* [305] demonstrates a low-aberration plasma lens at the underdense threshold in an experiment at Fermilab.
2015	Laser-driven passive plasma lensing is demonstrated by Thaury *et al.* [306] at the Laboratoire d'Optique Appliquée.
2017	Marocchino *et al.* [307] perform a 6D beam phase space characterization at INFN Frascati of passive plasma lensing effects in a discharge capillary.

Table 4.1: Selected milestones from the nearly one-century long history of *passive* plasma lenses, listed by year of publication.

Year	Milestone (active plasma lenses)
1950	Panofsky and Baker [308] construct an "arc lens" with an externally driven current to focus their 350 MeV ion beam in the 184-inch cyclotron at the Berkeley Radiation Laboratory—the first active plasma lens.
1965	A similar lens is operated in the AGS at Brookhaven National Lab by Forsyth *et al.* [309] for the purpose of increasing the neutrino yield in a spark chamber experiment—the first z-pinch plasma lens, where the current is large enough to magnetically pinch the plasma.
1990	A z-pinch plasma lens proposed [310, 311] for the CERN antiproton source is demonstrated by Dallic [312] and Kowalewicz *et al.* [313].
1991	z-pinch plasma lensing is used for focusing heavy-ion beams in the SIS accelerator at GSI-Darmstadt by Boggasch *et al.* [314].
1992	Braun [89] proposes to use active plasma lenses for more efficient positron capture.
1992	A wall-stabilized, unpinched active plasma lens is operated in the UNILAC accelerator at GSI-Darmstadt by Boggasch and Stetter *et al.* [315, 316], demonstrating fine-focusing of heavy-ion beams.
2001	Bobrova *et al.* [317] shows that a nonuniform discharge current forms in a discharge capillary due to radial temperature gradients, using a magnetohydrodynamical approach.
2005	Broks *et al.* [318] presents an alternative non-LTE model for the formation of nonuniform discharge currents, claiming negligible electron-to-wall heat flow due to an electron-free sheath, which produces similar radial current density profiles, but different plasma density profiles.
2007	Transverse interferometry measurements of the plasma density in a discharge capillary at Oxford University by Gonsalves *et al.* [319] agrees with the Broks model, but not with the Bobrova model.
2015	Discharge capillary-based (unpinched) active plasma lenses are used for strong (3000 T/m) focusing of laser-wakefield accelerated beams in BELLA at Lawrence Berkeley National Lab by van Tilborg *et al.* [94].
2016	The BELLA plasma lens is used by Steinke *et al.* [320] to demonstrate staging of two laser plasma accelerators.
2017	Van Tilborg *et al.* [321] presents indirect evidence of the nonuniform current density in helium, by observation of ring-shaped beams and an enhanced focusing gradient.
2017	Experimental characterization of a hydrogen-based active plasma lens at INFN Frascati by Pompili *et al.* [322], displaying some emittance growth.
2018	A DESY experiment performed by Röckemann *et al.* [323] at the Mainz Microtron measures directly the expected gradient enhancement and emittance growth in a hydrogen-filled capillary lens.
2018	Demonstration of emittance preservation in an active plasma lens by Lindstrøm *et al.* [7] (part of this thesis), based on the discovery that use of a heavy gas species (argon) suppresses the aberration from radial temperature gradients.

Table 4.2: Selected milestones in *active* plasma lensing, listed by year of publication, including the work performed as part of this thesis.

Section 4.2.2. However, an ideal lens has a uniform current density, in which case Eq. 4.2 can be multiplied by r and integrated to give

$$B_\phi(r) = \frac{\mu_0 J_z r}{2}, \tag{4.3}$$

i.e., an azimuthal magnetic field proportional to the distance from the axis—exactly what is needed for linear focusing in both planes. This is often stated in terms of the magnetic field gradient

$$g_r = \frac{\partial B_\phi}{\partial r} = \frac{\mu_0 I_0}{2\pi R^2}, \tag{4.4}$$

where the current density $J_z = I_0/\pi R^2$ is expanded in terms of the total current I_0 going through a capillary of radius R.

One might argue that there is nothing special about the plasma in this case—any conductor would behave the same. This is correct, and there is indeed a metallic conductor counterpart to the active plasma lens, often called the *lithium lens* [325]. Why lithium? Because it is the metal that minimizes beam scattering, although it still scatters significantly more than a plasma. Lithium lenses are therefore not typically considered for use in high brightness beam focusing, but have instead mainly been used for capture of (highly diverging) antiproton beams [326, 327]. Additionally, lithium lenses have been considered for positron capture [328,329] and for use in muon colliders [330, 331].

4.1.2 Pinch limit of uniform focusing

For a passive plasma lens, the ultimate limit of the focusing field is set by the ion density (Eq. 2.47). For an active plasma lens, however, the achievable focusing field is limited by the z-pinch effect. The plasma current will start to self-pinch—i.e., concentrate towards the axis—when the magnetic pressure surpasses the regular pressure of the plasma, in which case the focusing becomes nonuniform, leading to emittance growth. To avoid this pinching, the pressure at the outermost radius ($r = R$) must satisfy

$$\frac{B_\phi^2}{2\mu_0} < n_0 k_B T, \tag{4.5}$$

where k_B is the Boltzmann constant, n_0 is the plasma electron density and T is the plasma temperature: representing the magnetic pressure (left hand side) versus the ideal gas pressure (right hand side). Using Eq. 4.4 and $B_\phi(R) = g_r R$ we arrive at the (inverse) *Bennett relation* [291, 310]

$$\frac{\mu_0 I_0^2}{8\pi} < \pi R^2 n_0 k_B T, \tag{4.6}$$

which describes the condition for no pinching. Recasting this in terms of maximum magnetic field gradient, we find

$$g_r < \frac{\sqrt{2\mu_0 n_0 k_B T}}{R}. \tag{4.7}$$

Evaluated for a typical active plasma lens with density 10^{17} cm^{-3} (4 mbar), temperature 3 eV and capillary radius 500 μm, the gradient is limited to about 700 T/m for the plasma to not undergo pinching.

While early active plasma lens prototypes [309, 312, 314] were mostly operated in the z-pinched regime, recent mm-scale wall-stabilized active plasma lenses [6, 94, 322, 323] have not yet experimentally probed the limits set by the Bennett relation.

It should be noted that the Bennett relation is only the steady-state limit of z-pinch dynamics. The characteristic time scale of pinching was first calculated by Rosenbluth [332] (later recounted by Christiansen [310]) to be approximately given by

$$\tau_{\text{pinch}} \approx 1.5R \left(\frac{2\pi^2 n_0 A m_u}{\mu_0}\right)^{\frac{1}{4}} \left(\frac{dI}{dt}\right)^{-\frac{1}{2}}, \tag{4.8}$$

where A is the atomic mass number, m_u is the atomic mass unit, and dI/dt is the current rise rate (assuming a linearly increasing current). As an example, for a 500 μm radius lens filled with 4 mbar argon and with a 5 A/ns current rise rate, approximately 200 ns passes before pinching starts. It may therefore be possible to push the Bennett limit by using very short current pulses, such that the plasma does not have time to z-pinch before the magnetic field is sampled by the beam.

4.2 Aberrations

Assuming an active plasma lens is operated in the unpinched regime, there are still two sources of aberration which can cause significant emittance growth: plasma wakefields in the case of intense bunches, and radial temperature gradients—a plasma-dynamical problem intrinsic to the lens itself. Additionally, there will be some emittance growth from ion scattering—a topic discussed in Chapter 2.3.1.

4.2.1 Plasma wakefield distortion

In principle, if we ignore the longitudinal current, an active plasma lens is just another plasma source: for many plasma accelerator labs in fact their primary source of plasma. It is therefore no wonder that when an intense particle bunch enters the plasma lens that strong plasma wakefields will arise, resulting in nonuniform passive

plasma lensing. For this reason, it is currently unclear whether active plasma lenses can be used for staging—one of its main applications as envisioned by the advanced accelerator community.

Core Publication [5]

Carl A. Lindstrøm and Erik Adli,
Analytic plasma wakefield limits for active plasma lenses,
submitted to Phys. Rev. Accel. Beams, arXiv:1802.02750 (2018).

A theoretical and simulation-based investigation of the limits set by plasma wakefields was performed as part of this thesis, and was reported in Core Publication [5]. The main finding of this work was a closed-form expression for the maximum focusing gradient experienced by a bunch in an active plasma lens as caused by passive plasma lensing, as well as an expression for the corresponding rate of emittance growth. This allows fast exploration of the full 4-dimensional parameter space of plasma and beam variables (i.e., plasma density, bunch charge, bunch length and transverse beam size).

Using a combination of linear and nonlinear plasma wakefield theory, the maximum focusing gradient inside the bunch was found to be

$$g_{\max} \approx -\frac{\mu_0 c}{2} \min\left(en_0, \frac{Qk_p^2\sigma_z}{\pi\sigma_x\sigma_y\left(1+\frac{k_p^2\sigma_x\sigma_y}{2}\right)\left(1+\sqrt{8\pi}k_p^2\sigma_z^2\right)} \right), \tag{4.9}$$

where k_p is the plasma wavenumber, Q is the bunch charge, σ_z is the rms bunch length, and $\sigma_{x/y}$ is the rms transverse beam size in the lens. This gradient occurs on-axis and longitudinally centered for long bunches, and in the bunch tail for short bunches (defined arbitrarily at $z = -2\sigma_z$, as the field increases linearly with z). The corresponding emittance growth can, surprisingly, be found without any knowledge of the incoming beam optics except the beam size, given that we use the *thin lens approximation* (the beam size does not change inside the lens). This results in an approximate expression for a rate of absolute emittance growth

$$\frac{d\epsilon_{Nx}}{ds} \approx \frac{\sqrt{7}\mu_0 eQk_p^2\sigma_z\sigma_x}{12\sqrt{2\pi}^3 m\sigma_y\left(1+\frac{k_p^2\sigma_x\sigma_y}{2}\right)\left(1+2\sqrt[4]{3}k_p^2\sigma_z^2\right)}, \tag{4.10}$$

which should then be added in quadrature with the initial emittance. Note that this represents the rms emittance growth, whereas in reality the phase space is distorted in a non-Gaussian fashion. These expressions work well also for x–y asymmetric

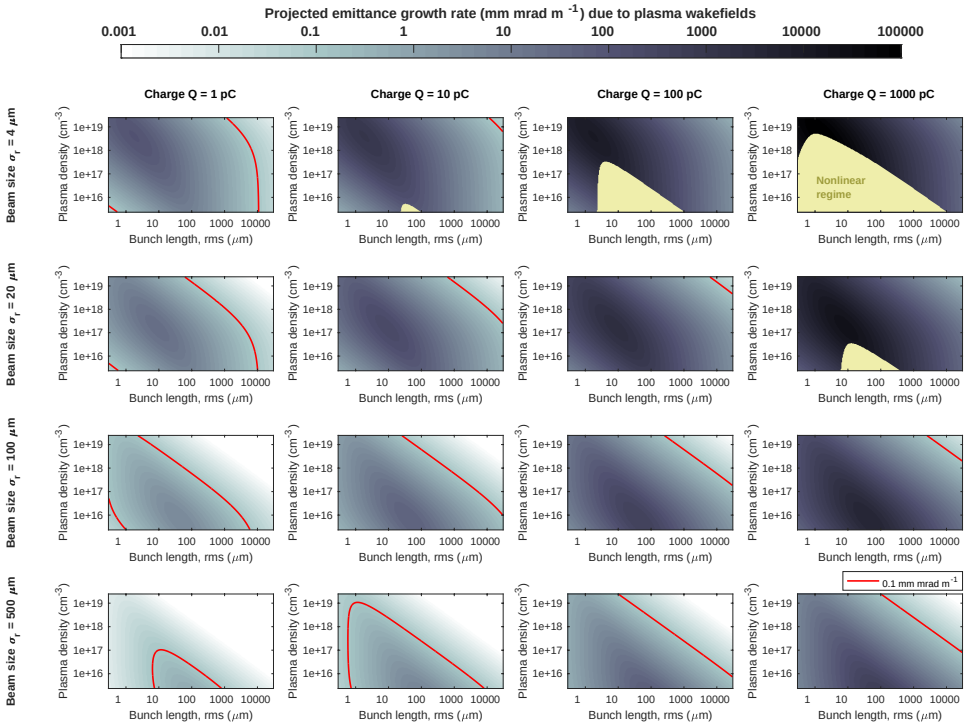

Figure 4.2: Visualization of the 4D parameter space for round e^-/e^+ beams. The 2D grid of density plots shows different beam size (outer vertical) and charge (outer horizontal), and within each plot the maximum focusing gradient from plasma wakefields is plotted against the plasma density (inner vertical) and the bunch length (inner horizontal). Red lines indicate contours for 0.1 mm mrad of emittance growth per meter—an approximate upper bound for acceptable growth in high energy, low emittance machines. Clearly high intensity (upper left) is not easily compatible with emittance preservation. Source: Lindstrøm and Adli, arXiv:1802.02750 (2018) [5].

bunches, at least up to a reasonable aspect ratio (about 10 or more).

Although Eqs. 4.9 and 4.10 might appear lengthy, they are many orders of magnitude faster to compute than a PIC simulation. This allows estimation of emittance growth rate across the entire relevant 4D parameter space, as shown in Fig. 4.2. Combined with the Bennett limit (Section 4.1.2), we can probe whether there is any part of this parameter space which allows active plasma lenses to be used in the context of high brightness beams—see Fig. 4.3.

In conclusion, by inspecting Fig. 4.3, the only way to avoid significant emittance growth for linear collider or FEL-type beams is to increase the beam size to the 100–1000 μm level. This is far too large for low emittance bunches (sub-mm·mrad), as extremely large beta functions (10^3–10^7 m) would be required. This is a problem

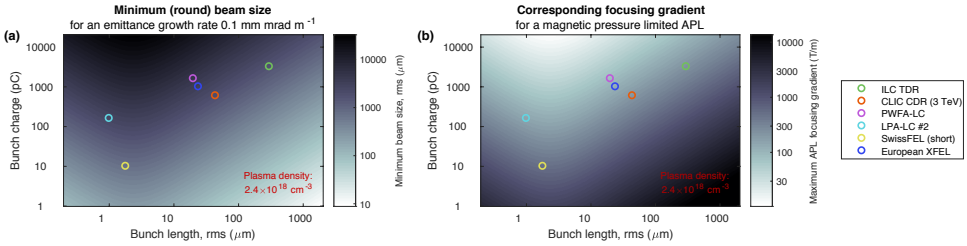

Figure 4.3: (a) Minimum beam size required in an active plasma lens for emittance growth rate 0.1 mm mrad m^{-1} assuming round electron/positron beams, and (b) the corresponding active plasma lens gradient in a 10-beam-sigma radius capillary (minimum 250 μm). A high plasma density (100 mbar) is chosen to increase the Bennett limit. Beam parameters for FELs and colliders are indicated (circles). Source: Lindstrøm and Adli, arXiv:1802.02750 (2018) [5].

especially in staging, as it would induce large chromaticity and large emittance growth from scattering (which scales with β). However, there is a hypothetical chance that an active plasma lens can be used for final focusing—a single lens at the end of the linac—as it will improve on the already large chromaticity of a final quadrupole doublet, assuming that the emittance growth and detector background from ion scattering can be controlled. This option is explored briefly in Section 4.4.1.

4.2.2 Radial temperature gradients

Ideally, an active plasma lens consists of a plasma with uniform density and temperature, resulting in a uniform current density. However, this is not necessarily the case. The current density is given by Ohm's law

$$J_z(r) = \sigma(r) E_z, \tag{4.11}$$

where E_z is a uniform high-voltage electric field and $\sigma(r)$ is the plasma conductivity [333], given by

$$\sigma(r) = \frac{32\epsilon_0^2 (k_B T_e)^{3/2}}{e^2 \sqrt{m_e} \ln \Lambda}. \tag{4.12}$$

Here T_e is the electron temperature, $\ln \Lambda$ is the Coulomb logarithm, while m_e and ϵ_0 are the electron mass and vacuum permittivity, respectively. Note that the conductivity does not depend on the electron density n_e, except weakly via the Coulomb logarithm as $\Lambda = n_e \lambda_D^3 = n_e (\epsilon_0 k_B T_e / n_e e^2)^{3/2}$. Instead, the conductivity scales with the electron temperature, such that

$$J_z(r) \sim T_e^{3/2}(r). \tag{4.13}$$

Any temperature gradient in the plasma will therefore cause a nonuniform current density and consequently a nonuniform focusing gradient—a source of emittance growth.

During a discharge, exactly such a temperature gradient does form, as first shown by Bobrova *et al.* in 2001 [317]. The formation can be broken into a four-step process, as claimed by Broks *et al.* [318,319]:

1. The plasma is ionized.
2. Electrons are Joule-heated by the current.
3. The hot electrons transfer their heat to the ions, as a virtually electron-free sheath near the wall stops them from heating the wall directly.
4. Ions subsequently transfer heat to the wall, preferentially cooling the plasma closer to it—forming a temperature gradient.

Using a simplified magnetohydrodynamics (MHD) approach, Bobrova *et al.* calculated the steady-state solution of this electron temperature distribution, which follows the differential equation (as expressed by van Tilborg *et al.* [321])

$$\frac{1}{x}\frac{\partial}{\partial x}\left(x\frac{\partial u}{\partial x}\right)+u^{3/7}=0, \tag{4.14}$$

where $x = r/R$ is a scaled radius and $u = (T_e/A)^{7/2}$ is a scaled temperature for which $A = \sqrt{7R^2E_z^2\sigma_0/2\kappa_0}$. In this case, the thermal and electrical conductivities scale according to $\kappa = \kappa_0 T_e^{5/2}$ and $\sigma = \sigma_0 T_e^{3/2}$, respectively. Equation 4.14 can be solved numerically to give the scaled temperature distribution $u(r)$, which then via Eq. 4.13 can be substituted to find the current density profile

$$J_z(r) = \frac{I_0}{\pi R^2}\frac{u(r)^{3/7}}{2m_I}. \tag{4.15}$$

Here the scaled temperature is normalized by the numerical factor

$$m_I = \int_0^1 u(x)^{3/7}xdx \tag{4.16}$$

in order to obtain the correct total current $2\pi\int_0^R J_z(r)rdr = I_0$. This model is often referred to as the *JT model*, based on the variables in Eq. 4.13.

A good overview of the JT model was given by van Tilborg *et al.* in Ref. [321], who confirmed that it agrees well with MHD simulations, as shown in Fig. 4.4.

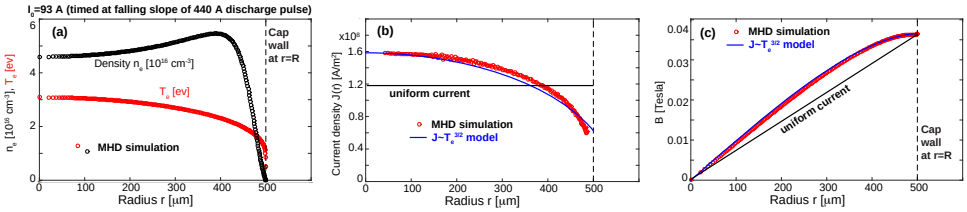

Figure 4.4: Comparison of the JT model and MHD simulations, showing (a) the plasma density and temperature profile, (b) the current density and (c) the resulting nonlinear magnetic field distribution—overall in good agreement. Source: adapted from van Tilborg *et al.*, Phys. Rev. Accel. Beams **20**, 032803 (2017) [321].

4.3 The CLEAR plasma lens experiment at CERN

The CLEAR plasma lens experiment is an ongoing experiment at the CLEAR User Facility [12] at CERN, spearheaded by the University of Oslo and backed by collaborators at DESY, CERN and the University of Oxford. A large part of the work for this thesis consisted of planning, designing, installing and testing the setup for this experiment, followed by several runs of beamtime. This resulted in two separate Core Publications: one about the experimental setup and aims [6] and one reporting on the discovery of how to suppress the temperature gradient aberration [7], both of which will be briefly summarized in this section.

Core Publication [6]

C. A. Lindstrøm, K. N. Sjobak, E. Adli, J. H. Röckemann, L. Schaper, J. Osterhoff, A. E. Dyson, S. M. Hooker, W. Farabolini, D. Gamba and R. Corsini,
Overview of the CLEAR plasma lens experiment,
Nucl. Instrum. Methods Phys. Res. A **909**, 379 (2018).

The overall goal of the CLEAR plasma lens experiment was to perform investigations complementary to those conducted using similar setups in BELLA at LBNL [94, 321], SPARC LAB at INFN [307, 322] and the Mainz Microtron by DESY [323]. In particular, three overall goals were envisioned:

- Testing a novel low-cost design.
- Characterizing the nonuniformity of the radial magnetic field distribution using a direct beam-based measurement.
- Probing the limits imposed by plasma wakefields.

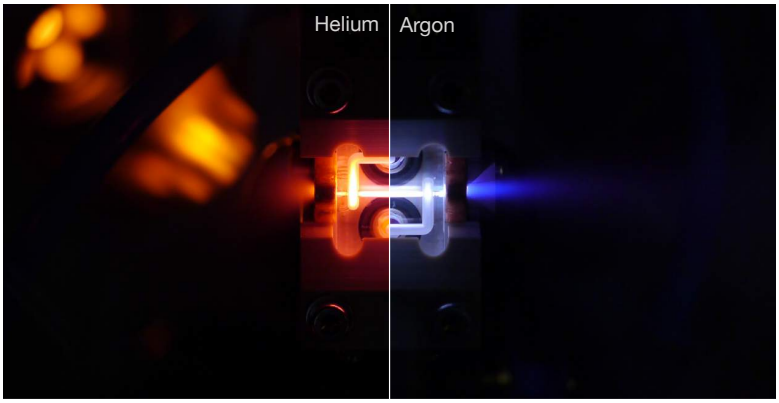

Figure 4.5: Split image showing the CLEAR plasma lens during discharge, both in helium (left) and in argon (right)—the two gases used in the experiment. The background light in helium (left) is produced by a cold cathode pressure gauge.

Additionally, with a working and well-characterized single lens, a longer term move towards demonstrating apochromatically corrected staging (see Chapter 2.4.3) using multiple lenses was proposed as an option.

4.3.1 Experimental setup

Although an active plasma lens is very compact, this comes at the cost of some complexity. A number of subsystems need to work together for seamless operation. This includes a capillary; a gas flow system; a vacuum chamber with pumps; a high voltage pulsed current source; a timing system; and a method to stop gas flowing into the upstream accelerator. Additionally, to perform beam-based tests, a suitable beam must be produced and aptly diagnosed.

Beam production in the CALIFES beam line

The CLEAR User Facility consists of the upstream CALIFES accelerator [334]—formerly used as a witness beam injector at the CLIC Test Facility (CTF3) [335]—and a downstream experimental area. This 25 m long linac uses a Cs_2Te photocathode and three S-band structures to accelerate 1–200 pC bunches up to approximately 220 MeV. For low charge, these bunches can be produced with emittances as low as 1–3 mm mrad. A dipole energy spectrometer, toroids for charge measurement and an RF deflecting cavity for characterizing the longitudinal profile is also available. Lastly, a quadrupole triplet just upstream of the plasma lens enabled tight focusing of the electron bunches, down to approximately 50×50 μm rms.

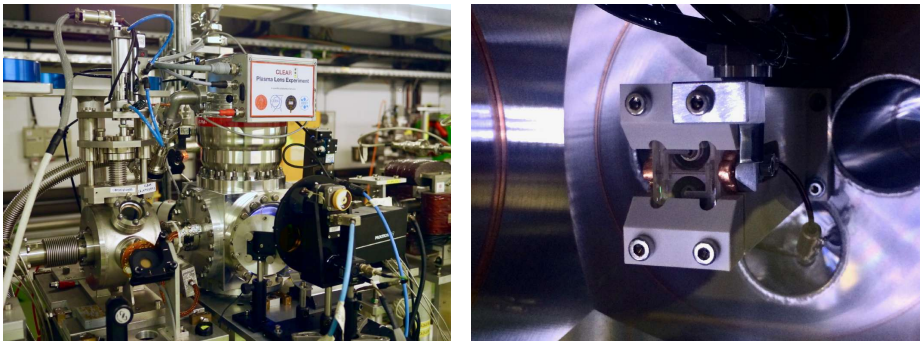

Figure 4.6: Images of the experimental setup, showing the vacuum chamber installed in the CLEAR beam line (left) and a close-up of the plasma lens itself (right). Source: Lindstrøm *et al.*, Nucl. Instrum. Methods Phys. Res. A **909**, 379 (2018) [6].

Capillary and holder

Perhaps the most central piece of equipment—the capillary—consists of two sandwiched blocks of sapphire (Al_2O_3) with a milled 1 mm diameter, 15 mm long tube—produced by collaborators at DESY. Internal gas inlet pipes in the sapphire (see Fig. 4.5) are connected to the capillary holder, which is made of an ultrahigh vacuum (UHV)-compatible plastic called polyether ether ketone (PEEK) and mounted horizontally on the back wall of a 20×20×20 cm cubic vacuum chamber, which then is mounted on a two-axis mover [336]. On the upstream and downstream sides of the capillary, two holed copper electrodes are attached and connected to the outside high voltage source.

Gas injection and vacuum

The capillary gas inlets are connected to an external gas flow regulator with a buffer volume for a smooth and controllable flow rate, allowing capillary pressures of approximately 1–100 mbar. This regulator is connected to long gas lines feeding gas (helium, nitrogen, neon or argon) from outside the accelerator hall.

Inside the chamber, it was found that a 2 m long, electrically non-conductive polyurethane pipe was required to avoid discharging to ground via the gas in the pipe (particularly for helium and neon). This roughly aligned with expectations from Paschen's law [337], which quantifies the breakdown voltage threshold for a given pressure and distance (but for parallel metal plates).

The steady flow of gas into the capillary naturally escapes through the holed electrodes and contaminates the beam line—a significant problem for the accelerating structures. Therefore a very large turbo pump is mounted on the chamber (see

Fig. 4.6), capable of reducing the pressure surrounding the lens to 10^{-4}–10^{-2} mbar during steady gas flow, depending on the gas species and capillary pressure. Additionally, to ensure UHV conditions upstream, a very thin 3 μm polymer (Mylar) window is mounted in a retractable gate valve just upstream of the lens (also visible in Fig. 4.6)—an idea inspired by a similar setup at PITZ [338]. Scattering in this window *does* increase the emittance by a small amount, but was found to not be a significant limitation.

The pressure in the buffer volume and vacuum chamber was measured using a capacitance gauge and a combined Pirani/cold cathode gauge, respectively. To determine the actual pressure in the capillary, one end was connected to a capacitance gauge while the closest inlet was sealed—a method also used in Ref. [339]. It was found that the pressure drop from the buffer to the capillary was approximately 70%.

High voltage discharge using a Compact Marx Bank

A Compact Marx Bank [340] with a fast rise time, produced by collaborators at Oxford University, is used for supplying short (200 ns), high voltage (25 kV), current pulses with a peak current of 400–500 A, as shown in Fig. 4.7(d), at a repetition rate of about 1 Hz. This device is significantly cheaper to produce than a thyratron—the conventional choice for discharge capillaries—and hence represents a novel, lower-cost and perhaps more scalable solution for active plasma lensing.

Beam diagnostics

To diagnose the beam and measure the effect of plasma lensing, a number of diagnostics is available. This includes an optical transition radiation (OTR) foil just downstream for measuring beam focusing and centroid deflections, a dipole spectrometer for accurate energy measurements, and a quadrupole doublet for measuring the emittance in both planes. Additionally, a camera is used for observing both discharge and scintillation light from the beam passing through the sapphire, a diode for time-resolving the plasma recombination light, and a photomultiplier tube (PMT) for detecting beam loss.

Figure 4.7 shows an overview of the full experimental setup.

4.3.2 Experimental results

The first experimental result was the successful commissioning of the novel plasma lens design and setup—one of the three main goals. Despite some initial reliability problems, eventually the plasma lens could operate stably over tens of thousands

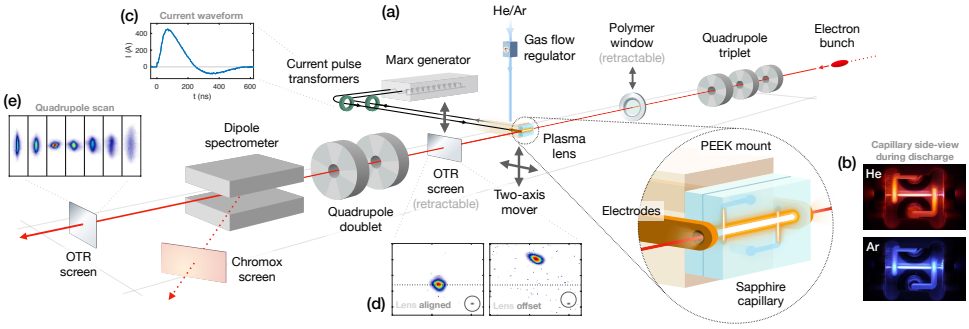

Figure 4.7: Schematic of the CLEAR plasma lens experiment—showing (a) the overall experimental setup, (b) helium and argon discharges, (c) the Marx generator current waveform, (d) beam deflections on the downstream OTR screen, and (e) raw images from a quadrupole scan emittance measurement. Source: Lindstrøm *et al.*, Phys. Rev. Lett. **121**, 194801 (2018) [7].

of shots without problem. This served as a valuable baseline for conducting real experiments. Based on experience from FACET (Chapter 3.2), a refined version of the fast-iteration data acquisition and analysis technique (see Appendix B) was employed—with great efficiency and success.

Radial uniformity and emittance preservation

Using a pencil beam of 50×50 μm rms, a transverse scan across the full 1 mm aperture of the capillary was performed, measuring the angular centroid deflection to the downstream OTR screen. This allowed an accurate characterization of the magnetic field distribution in the lens. The result of this scan, performed both in 23 mbar helium and in 6 mbar argon is shown in Fig. 4.8—both taken at peak current (about 80 ns after the initial discharge).

Two important conclusions can be drawn from this measurement. Firstly, in helium, there is a clear nonlinearity, in excellent agreement with the JT model and overall consistent with Ref. [321]. This is the first complete direct measurement of this focusing nonuniformity, leaving no doubt as to whether it exists. However, secondly—and rather surprisingly—the same measurement in argon shows no evidence of any nonlinearity: the field is linear to within the (small) error of the measurement. This was an unexpected finding that was stumbled upon when helium initially proved too hard to ionize (argon has a lower ionization potential). The implication of this discovery is that the temperature gradient aberration can be fully suppressed by changing from a light gas species to a heavy gas species, as reported in Core Publication [7].

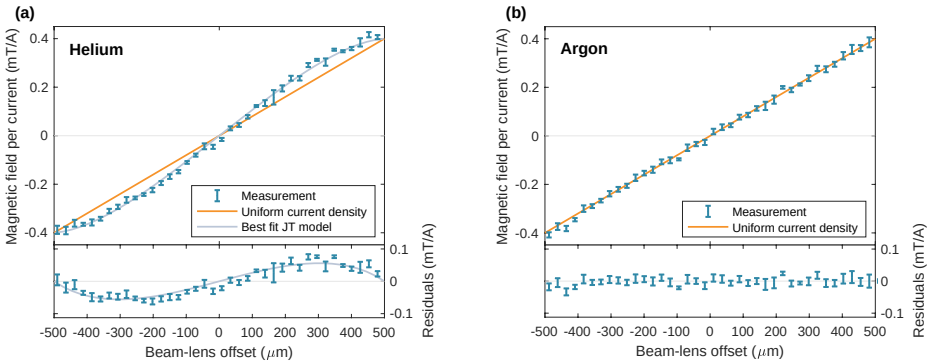

Figure 4.8: Transverse offset scan of the magnetic field distribution in an active plasma lens filled with (a) helium and (b) argon. The field is observed to be nonlinear in helium—evidence for radial temperature gradients. In argon, however, the field is linear to within the measurement error—allowing emittance preservation. Source: Lindstrøm *et al.*, Phys. Rev. Lett. **121**, 194801 (2018) [7].

Core Publication [7]

C. A. Lindstrøm, E. Adli, G. Boyle, R. Corsini, A. E. Dyson, W. Farabolini, S. M. Hooker, M. Meisel, J. Osterhoff, J. H. Röckemann, L. Schaper and K. N. Sjobak,
Emittance preservation in an aberration-free active plasma lens,
Phys. Rev. Lett. **121**, 194801 (2018).

The lack of aberrations further implies that the beam emittance should be preserved during lensing, assuming that plasma wakefields are controlled for. A number of quadrupole scan multi-shot emittance measurements were therefore performed in both helium and argon (see Fig. 4.9), however this time using a large beam size in order to sample as much nonlinearity as possible—and only 2 pC of charge per bunch. As expected, emittance growth was observed in helium—consistent with tracking simulations using the measured nonlinear field—and emittance preservation was observed in argon. Error analysis excludes any emittance growth above 0.25 mm mrad at a 90% confidence level.

The physical mechanism that prevents an aberration forming in argon is hypothesized to be the decreased thermal conductivity of heavier ions. As mentioned in Section 4.2.2, the existence of a virtually electron-free sheath close to the sapphire wall forces the electrons to only conduct heat to the plasma ions, which subsequently transfers it to the wall. Since both the electron–ion thermal transfer rate and the ion lattice thermal conductivity decreases with ion mass ($\sim 1/m_i$) [317],

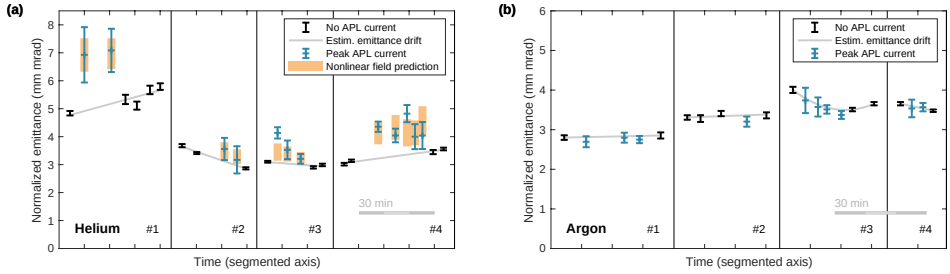

Figure 4.9: Emittance measurements from quadrupole scans (a) in helium and (b) in argon. Helium shows clear evidence of emittance growth during lensing—consistent with the expected nonlinear fields. The argon-based lens, on the other hand, is consistent with emittance preservation. Source: Lindstrøm *et al.*, Phys. Rev. Lett. **121**, 194801 (2018) [7].

it takes significantly longer to build up the nonuniformity. Therefore, sampling the field very early in this process is possible in argon with a fast-pulse current source, but not in helium, as the nonlinearity develops effectively instantaneously. A two-temperature MHD simulation study will be conducted to verify whether this is the correct explanation.

Regardless of the mechanism, this work shows that the aberration can be suppressed—a fact that was utilized to demonstrate emittance preservation in an active plasma lens for the first time. It should, however, be noted that a similar unpinched, argon-filled plasma lens was used already in 1991 by Boggasch *et al.* [315] for "fine focusing" of heavy ion beams, but the emittance was not quantified and anyway the aberration was not known at the time.

Lastly, this aberration suppression will inevitably lead to increased emittance growth from scattering, as argon scatters significantly more than hydrogen or helium. In our experiment, operating at 6 mbar argon, the emittance was found to not measurably increase, as verified by quadrupole scans with and without gas. However, in general, scattering *will* be a problem—placing restrictions on the gas pressure, and hence on the maximum focusing gradient (via the Bennett relation). A possible mitigation strategy here is to use a lighter gas species, like nitrogen or neon, assuming that these gases are also able to suppress the aberration for a sufficiently long time.

Effect of plasma wakefields

The other, somewhat less encouraging line of investigation involved measuring distortions of the beam caused by plasma wakefields. While fairly successful, this

turned out to be much more challenging than anticipated, as the achievable bunch charge density from the CALIFES accelerator was only barely sufficient to observe the passive plasma lensing effect—mainly due to low photocathode quantum efficiency. Nevertheless, some interesting scans were performed, with results in general agreement with the proposed theory (see Section 4.2.1).

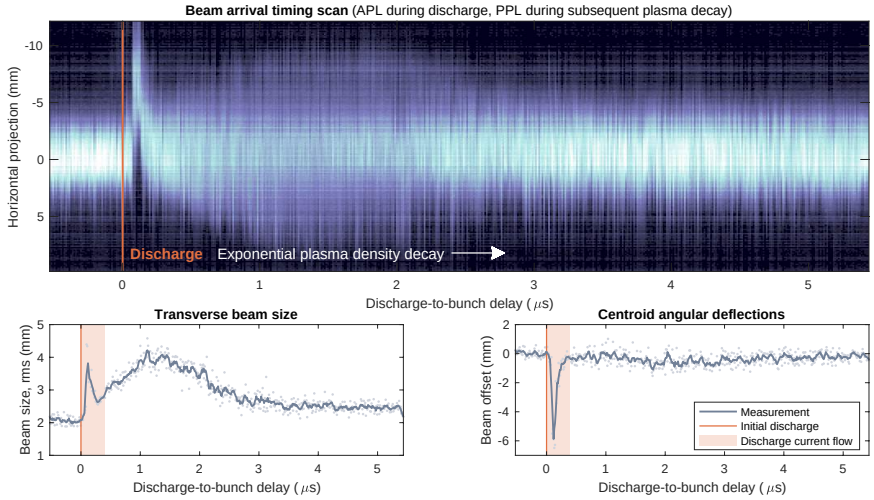

Figure 4.10: A scan of beam arrival time relative to the discharge demonstrates the passive plasma lensing effect, particularly during the subsequent (exponential) plasma density decay—the beam couples most strongly to the wakefield when the plasma wavelength matches the bunch length. Use of an offset capillary also allows decoupling of the active and passive plasma lens effects, as only the former provides a centroid deflection (red area).

In particular, a μs-scale scan of the relative discharge–beam delay functioned as a logarithmic plasma density scan, since the plasma density decays exponentially after the discharge current is gone. A similar experiment was independently performed at INFN by Marocchino *et al.* [307]. However, by using a transversely offset lens our experiment was able to decouple the active and passive plasma lensing effects, as the former provides a centroid deflection and the latter does not. Figure 4.10 shows the result of this measurement, which qualitatively agrees with the expected effect—initial defocusing and centroid deflection by the current, then a gradual increase in defocusing as the plasma wavelength approaches the bunch length (strongest coupling), and finally a gradual decrease in defocusing as the plasma wavelength grows too long (see Fig. 4.2). Only defocusing could be observed as the observation screen was further away than the beta function in the lens, such that any beam waist would occur prior to reaching the screen.

A scan of transverse beam sizes in the lens was also performed (60–130–200 μm), where the passive plasma lensing effect diminished with each beam size increase, as expected.

Although not quantitatively very precise, the overall trend of these measurements suggests that plasma wakefields will likely prove to be a significant limitation for active plasma lenses—especially in the context of low-emittance, high-charge beams for high energy physics.

4.4 Potential applications

Use of active plasma lenses for staging will clearly be challenging due to plasma wakefields, but there are several other interesting applications of this technology that may be relevant to linear colliders. Two examples include (1) replacing the final doublet of the final focusing system, and (2) high-yield positron beam capture.

4.4.1 Final focusing

The passive plasma lens has long been envisioned as a final focusing device for linear colliders [95, 341], with its MT/m radial focusing fields. However, there are a number of fundamental challenges with this concept, including difficulty focusing positrons and large detector backgrounds [342]. In addition, the practical problem of alignment stability is significantly increased for self-focused beams, due to the nm-scale tolerances at the interaction point (IP). In a quadrupole-based final focusing system, however, this is less of a concern as the alignment of the IP beam waist is tied directly to the sub-nm alignment stability of the quadrupoles [343] and not primarily the beam.

Several of these problems fall away by switching to an active plasma lens: positrons are as easily focused as electrons, and IP waist alignment is tied to the alignment of the capillary. The remaining problem is then to ensure negligible plasma wakefield distortion and scattering, the latter of which leads to both detector backgrounds and emittance growth. In addition, the use of heavy gases may be required [7] in order to avoid nonuniform plasma temperature gradients, although this increases scattering.

Using expressions for emittance growth rates from scattering and wakefields (Eqs. 2.50 and 4.10), while assuming a typical lens–IP distance and beam parameters for a collider, it is straightforward to calculate the maximum capillary length to have acceptable emittance growth (defined here as 100%). To achieve the required focal length, we must satisfy a minimum current requirement—see Fig. 4.11 for a

parameter scan of varying plasma density, bunch length and charge. Importantly, the required current can then be compared to the maximum current allowed by the Bennett relation (Eq. 4.1.2). Clearly, operation of an active plasma lens final focusing device will require significantly higher currents than that required for producing a z-pinch, which if unmitigated will lead to strong aberrations. The only exception to this is to use very short bunch lengths (1 μm or less) in combination with low plasma densities (less than 10^{15} cm^{-3}). As discussed in Section 4.1.2, however, the Bennett limit can potentially be circumvented with the use of very fast current pulses—an interesting future research direction.

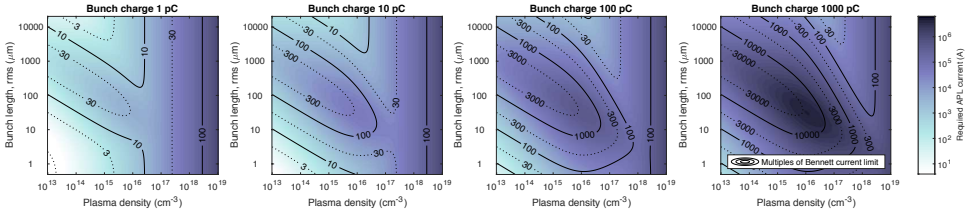

Figure 4.11: Parameter scan of the required active plasma lens current for distortion-limited (100% emittance growth) final focus operation for varying plasma density (inner horizontal), bunch length (inner vertical), and bunch charge (outer horizontal). We assume a round 1 TeV beam with 1 mm mrad initial emittance focused to 1 mm beta function at the IP—producing a 30×30 nm rms IP beam size. The plasma lens is assumed to be nitrogen-filled (triply ionized), with a plasma temperature 3 eV, have a capillary diameter 550 μm (8 beam sigmas), and be placed 3 m from the IP. Most of the parameter space requires large currents—many times larger than the z-pinch current limit (ratio to the Bennett limit given by black contours).

While the use of active plasma lenses for final focusing will be challenging, it is interesting to consider its potential advantages over conventional designs. First of all, an active plasma lens could be significantly more compact than a quadrupole final doublet—especially interesting if it could fit inside the detector (shorter lens–IP distance). Focusing in both directions also imply that the beta function can on average be smaller in the lens compared to a focusing–defocusing quadrupole doublet—this reduces the chromaticity. Moreover, an active plasma lens can focus a round beam to be very small in *both* planes, not only in *one* plane as in normal final focus systems [219]—perhaps not useful for an e^+e^- collider, which uses flat beams to suppress beamstrahlung, but may be attractive to other concepts [344] such as a $\gamma\gamma$ collider [345] (see Chapter 5.2).

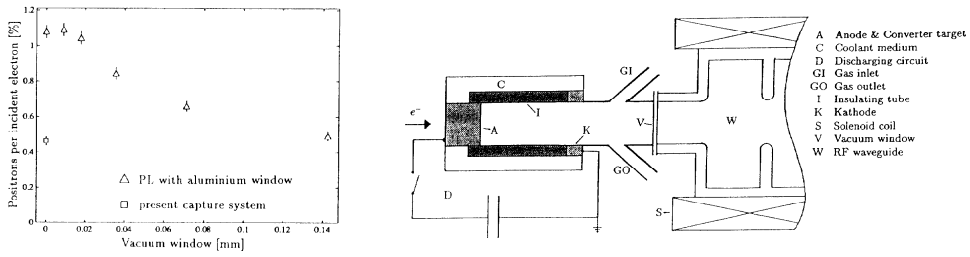

Figure 4.12: Schematic design by Braun *et al.* of a positron source based on active plasma lensing (right), providing higher energy acceptance and electron filtering. This produces approximately doubled positron-per-incident electron yield compared to solenoid-based positron sources (left). Source: Braun *et al.*, Proceedings of EPAC1992 (1992), p. 1650 [89].

4.4.2 High-yield positron sources

Compact positron acceleration is clearly a major challenge in advanced accelerator research—one that requires both theoretical and experimental work. One road block for experiments is that positron bunches are prohibitively expensive to make: typically it requires an intense, high-energy electron beam focused onto a high-Z metallic target, producing showers of electrons and positrons [261,346]—often with a low positron-per-electron yield. Improvements to the cost and yield of positron production would therefore benefit the field greatly.

Active plasma lenses may be useful in this regard. Already in 1992 Braun *et al.* proposed to use an unpinched active plasma lens as an integral part of a positron source [89]. This idea had already been used for anti-proton capture at CERN [311–313]. The idea is to simply swap out the conventional solenoid with an active plasma lens directly after the positron target. This has three main advantages beyond its compactness:

- Electrons are immediately defocused in the plasma lens, whereas in a solenoidal field both electrons and positrons are focused. This removes the problem of electron beam loading in subsequent structures, and any need for electron/positron filtering.

- The energy acceptance is approximately doubled because the focusing field in a plasma lens scales as $1/\gamma$, whereas in a solenoid it scales as $1/\gamma^2$—doubly sensitive to energy offsets.

- Lastly, the longitudinal distortion (phase slippage) is decreased as the path difference for different initial angles is smaller in a plasma lens (sinusoidal arcs)

compared to in a solenoid, where particles move in spirals along the magnetic field lines.

This concept does of course rely on uniform focusing fields for emittance preservation. As shown in Section 4.3.2, this is possible in high-Z gases like argon. Scattering is not likely to be a significant problem—despite the low positron energy (1–25 MeV)—because the initial divergence is large enough that any additional divergence (at the few mrad-level) will be negligible.

While the proposed positron source was never tested experimentally, in principle the concept can be easily tested at CLEAR or any of the other current plasma lens experiments with the addition of for instance a tungsten target in front of the upstream end of the capillary.

4.5 Conclusions

Active plasma lensing, with its rich and interesting history (Table 4.2), is undoubtedly an important concept with clear applications to future, compact accelerators. Its use for high-intensity, low-emittance beams is, however, not so straightforward—as discussed in this chapter. Two main causes of aberration, plasma wakefields and plasma temperature gradients, can both lead to significant emittance growth in the beams being focused. Additionally, the current in the lens is limited by the so-called Bennett relation, indicating when self-pinching of the plasma will occur—something to be avoided if uniform focusing is desired.

The findings of this work has been two-fold: (1) it is possible to suppress the plasma temperature gradient aberration by using a high-Z gas species like argon—discovered in an experiment at the CLEAR User Facility at CERN—enabling the first demonstration of emittance preservation in an active plasma lens. The conventional JT model for nonuniform focusing was also experimentally verified for low-Z helium. However, importantly, the increased ion mass will also dramatically increase emittance growth from scattering—careful trade-offs will be required. Unfortunately, (2) another finding is that emittance preservation appears to be severely limited by plasma wakefields. This is especially true for intense bunches, and linear collider staging with active plasma lenses is effectively ruled out.

Overall, while unsuccessful at making linear colliders more compact, these findings nevertheless represent a small step forward in terms of understanding the true potential of active plasma lenses.

Chapter 5

Conclusion

The big, underlying question inspiring this work has been: "*is it possible to make a compact, high-energy, high-luminosity electron–positron collider with the use of plasmas?*" The scope of this thesis, however, has been focused on one important aspect in this regard: whether emittance growth in a plasma-based accelerator can be mitigated to the required level. Specifically, this was studied in three main lines of investigation relating to emittance preservation: in chromaticity-dominated staging (Chapter 2), for positrons in hollow plasma channels (Chapter 3), and in active plasma lenses (Chapter 4). Below is a brief summary of the findings from this work (Core Publications [1–7]), as well as some final thoughts about the future directions of the field.

5.1 Executive summary

Going from a conventional RF accelerator to a plasma wakefield accelerator, we introduce a number of new sources of emittance growth—with potentially dire consequences for the luminosity of a collider. The most important of these—as covered in Chapter 2.3—are multiple Coulomb scattering from the background ions; ion motion for dense electron beams; transverse beam loading for positrons; mismatching of the transverse beam size; drive–trailing bunch misalignments through energy-based decoherence; and beam breakup or hosing due to strong transverse wakefields. Many of these problems have straightforward mitigation strategies, whereas others do not. Beam breakup and decoherence appear particularly challenging in this regard—imposing stringent limits on beam current and very tight (10–100 nm-scale) misalignment tolerances [1].

Staging adds another layer of complexity to this already difficult task—as beams

exiting a plasma stage diverge rapidly, leading to emittance growth due to chromaticity during refocusing. A partial solution to this problem was presented—apochromatic corrective optics [2]—whereby a combination of linear-only optical components can be made to cancel chromaticity locally (at the entry to the next stage): a concept inspired by camera-lens optics. This, in combination with plasma density ramps, was the basis of a proposed rudimentary staging optics design for a high energy linear collider [3]. Some extra work will be required, however, relating to the in- and out-coupling of drive beams—a particularly challenging aspect specific to *beam-driven* plasma wakefield acceleration.

Bypassing staging in its entirety, and attempting to solve the daunting positron acceleration problem, is hollow channel plasma acceleration—one of the few concepts to simultaneously allow high-gradient, high-efficiency and emittance preserving acceleration of positron bunches. However, the transverse wakefields induced in these channels may lead to catastrophic beam breakup. The E225 hollow channel experiment at FACET, SLAC was able to not only demonstrate first acceleration of positrons in a hollow plasma channel, but also to perform precision measurements of its transverse wakefield [4]. Consistent with theory, these measurements provide a firm stepping stone for future research into mitigation of this problem. While many of the currently proposed strategies (like external focusing) appear unsuited, some novel ideas inspire hope—such as a combination of near-hollow channels (for e^-) and high energy counter-propagating electron lensing (for e^+). A significant effort will likely be required to find a suitable scheme.

Lastly, active plasma lensing is a promising scheme for compact focusing in any novel accelerator. Using a large longitudinal plasma current, it provides strong and radially symmetric focusing—for electrons *and* for positrons. However, application to a linear collider are hindered by the existence of aberrations, leading to unacceptable emittance growth. This includes, in particular, nonuniform passive plasma lensing effects and intrinsic plasma temperature gradients. The distortion from plasma wakefields was quantified analytically [5] and used to search the parameter space for feasible active plasma lens staging optics—unfortunately showing little promise for high-charge, low-emittance beams. On the other hand, a plasma lens experiment designed and conducted at the CLEAR User Facility at CERN—successfully demonstrating lensing with a novel, scalable setup [6]—found that the seemingly intrinsic plasma temperature-based aberration could be fully suppressed by switching from a light gas species (helium) to a heavy gas species (argon) [7]. This lead to the first demonstration of emittance preservation in an active plasma lens. Despite this success, however, it seems active plasma lensing is unsuited for linear collider staging due to the plasma wakefields—but will likely be useful for

lower intensity machines or specific applications like high-yield positron capture.

5.2 Future directions

Short term, the field will be occupied with small- and large-scale experiments investigating various aspects of plasma wakefield acceleration. Two experiments stand out in this respect, with their ability to address arguably the most important question relating to a linear collider: emittance preservation—for both electron and positron acceleration schemes. FACET-II [138] at SLAC, with its extremely high-brightness beam, is aiming to demonstrate a high-gradient, high-efficiency, emittance preserving plasma stage—an extremely challenging task, if we are to believe Chapter 2.3. FLASHForward [132] at DESY, with its similar capabilities, aims to do the same—among other goals. Clearly, these highly capable facilities will make big strides toward demonstrating the ultimate plasma wakefield electron accelerator.

However, true progress toward a linear collider can only be made by addressing positron acceleration—the biggest unsolved problem. Importantly, FACET-II will likely have the ability to continue the positron legacy started by FFTB and continued at FACET. Even if the challenge is currently conceptual—and not experimental—it is often that theoretical advances are made in the vicinity of pioneering experimental work. It remains to be seen, however, whether these advances can keep up with the ambitious schedules of proposed road maps [147, 148].

Long term, the direction of the field will depend on the progress in coming years. In the best case scenario, we follow the course charted by the road maps and do higher-than-ever-energy-physics with our new plasma-based linear collider. But, there is a real chance that this may never happen—we can perhaps already see the contours of a fundamental inverse relationship between acceleration gradient and luminosity. In this case, we must turn the original question on its head: "*what interesting physics can we do with this powerful new acceleration technique?*" While the answer to this question might not involve high-energy e^+e^- collisions, there are some exciting other options to consider.

One possible alternative to an electron–positron collider is a photon- or *gamma–gamma* ($\gamma\gamma$) collider [345, 347, 348]—colliding two intense beams of gamma rays produced by Compton scattering of laser beams off high energy electrons. The particle beam requirements of a $\gamma\gamma$ collider are similar to those of a linear collider, but—crucially—without the need for positrons. Proposed designs include high-quality 250 GeV electron beams and intense 1 J laser beam at a wavelength 1 μm [349]—which seems achievable using a compact plasma wakefield accelerator.

Another alternative is to probe non-perturbative quantum electrodynamics (QED)

with the intense electromagnetic fields created by colliding 100 GeV-class, very short and tightly focused electron beams [344]—again, no positrons required. While some experiments [350, 351] have probed the weakly non-perturbative QED regime, including the SLAC E144 experiment [352, 353], a e^-e^- collider of this type could explore the *strongly* non-perturbative regime for the first time.

Finally, a related and exotic option is to use the ultrahigh fields in a high density plasma *directly* [354,355]—with the goal of observing the *Unruh effect* [356]. Unruh radiation is thought to be observed by strongly accelerating observers—seemingly coming from a "hot" surrounding horizon—and is equivalent to the Hawking radiation [357] emitted at the event horizon of a black hole (via the equivalence principle [358]). If viable, this could allow effective probing of quantum gravity in relatively small-scale experiments—a much-needed step forward in a field currently starved of experimental progress.

In conclusion, while the work presented in this thesis is only an incremental step in relation to the gargantuan leap required to build a plasma-based linear collider—or any of its alternatives—it is with pebbles like this that we pave the road to success!

Appendix A

Core Publications

This appendix contains the seven first-authored core publications around which this thesis is structured.

A.1 Transverse tolerances of a multi-stage plasma wakefield accelerator

Authors

C. A. Lindstrøm, E. Adli, J. Pfingstner, E. Marín and D. Schulte

Conference proceedings

Proceedings of IPAC2016, Busan, Korea (JACoW, Geneva, 2016), p. 2561

Abstract

Plasma wakefield acceleration (PWFA) provides GeV/m-scale accelerating fields, ideal for applications such as a future linear collider. However, strong focusing fields imply that a transversely offset beam with an energy spread will experience emittance growth from the energy dependent betatron oscillation. We develop an analytic model for estimating tolerances from this effect, as well as an effective simplified simulation tool in Elegant. Estimations for a proposed 1 TeV PWFA linear collider scheme indicate tight tolerances of order 40 nm and 1 μrad in position and angle respectively.

(4 pages)

TRANSVERSE TOLERANCES OF A MULTI-STAGE PLASMA WAKEFIELD ACCELERATOR

C.A. Lindstrøm*, E. Adli, J. Pfingstner
Department of Physics, University of Oslo, 0371 Oslo, Norway
E. Marin, D. Schulte, CERN, Geneva, Switzerland

Abstract

Plasma wakefield acceleration (PWFA) provides GeV/m-scale accelerating fields, ideal for applications such as a future linear collider. However, strong focusing fields imply that a transversely offset beam with an energy spread will experience emittance growth from the energy dependent betatron oscillation. We develop an analytic model for estimating tolerances from this effect, as well as an effective simplified simulation tool in Elegant. Estimations for a proposed 1 TeV PWFA linear collider scheme indicate tight tolerances of order 40 nm and 1 μrad in position and angle respectively.

INTRODUCTION

Plasma wakefield acceleration (PWFA) is an emerging technology promising GeV/m acceleration gradients [1], orders of magnitude higher than conventional technologies. A potential application is a future linear collider of significantly shorter lengths than current designs like ILC [2] and CLIC [3]. Schemes have been proposed where multiple consecutive PWFA cells are staged such that the energy-depleted drive bunch is swapped for a fresh one at regular intervals, accelerating the witness bunch to TeV-scale.

The drive bunch creates a 100 μm-scale wake in the plasma, in which strong electric fields accelerate the witness bunch longitudinally, but also focus the witness bunch transversely. In the non-linear "blowout" regime, these focusing fields are mostly linear in radius r, and hence the transverse emittance is conserved. However, much like in a quadrupolar FODO-lattice, a transverse offset will disperse a beam with an energy spread and increase its projected emittance. In this paper, we study transverse tolerances due to this effect. Plasma-beam interaction may also lead to emittance growth through the hosing instability [4] or the beam break-up instability [5], but this is not considered here.

Note that since the drive beam defines the channel, stage-to-stage alignment of plasma cells is irrelevant, and only relative drive-to-witness alignment matters. Also, static offsets are assumed to be tunable, leaving dynamic offsets (shot-to-shot jitter) as the main source of emittance growth.

MODEL

We adopt a simple analytic model: the witness bunch enters the plasma channel, defined by the drive bunch, with a relative offset position Δx and angle $\Delta x'$ (see Figure 1), and matched to the channel with a Twiss beta-function

$$\beta_m = \frac{\sqrt{2\gamma}}{k_p}, \tag{1}$$

where γ is the Lorentz factor of the witness beam and the k_p is the wavenumber of the plasma. Since inside the channel, the beam x and x' centroids will oscillate, but we don't care about the phase, it is useful to instead work with an *action*

$$J = \frac{\Delta x^2}{2\beta} + \frac{\beta}{2}\Delta x'^2, \tag{2}$$

where β is the beta-function of the incoming beam and we assume $\alpha = 0$. The model neglects the effect of acceleration, synchrotron radiation, beam loading and other collective effects.

For verification, analytic results are compared to a simplified simulation setup. Since we are working in the blowout regime, where fields are mostly linear, conventional particle tracking in Elegant [6] can be used to emulate the effect of the plasma channel. A long radially symmetric "quadrupole" is used for focusing, and thin accelerating cavities are distributed along the channel to include also the effect of acceleration.

EMITTANCE GROWTH

When the witness bunch enters the channel, its centroid starts oscillating in phase space with a conserved action J, with a wavelength $\lambda_\beta = 2\pi\beta_m$ along s. Since λ_β is energy dependent, higher energy particles oscillate more slowly, and

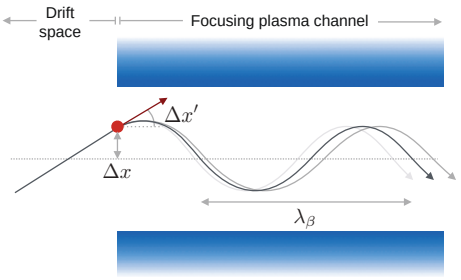

Figure 1: The witness beam enters the plasma channel with a positional offset Δx and angular offset $\Delta x'$ relative to the drive beam (which defines the channel). Each energy slice then oscillates with wavelength $\lambda_\beta(\gamma) = 2\pi\beta_m(\gamma)$, resulting in increased projected emittance.

* c.a.lindstrom@fys.uio.no

ISBN 978-3-95450-147-2

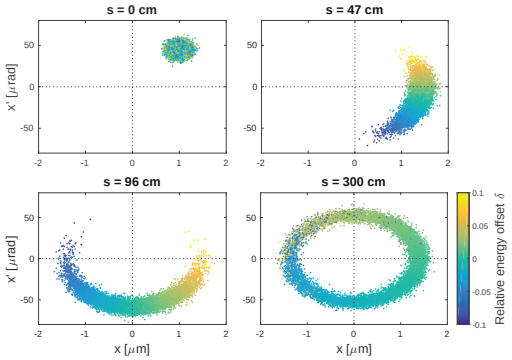

Figure 2: Evolution of the witness bunch in phase space, where colors indicate the relative energy offset. The initial beam, offset by 1 μm and 40 μrad in x and x' respectively, gets progressively stretched while it traverses the circumference of the offset ellipse (unsaturated regime) until ending up as a steady-state ring (saturated regime).

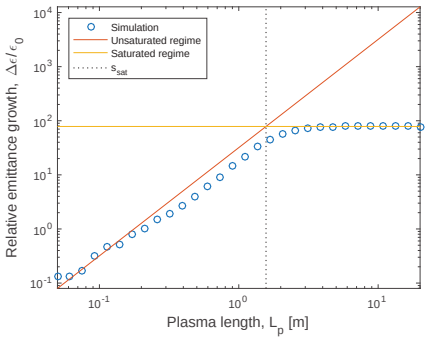

Figure 3: Emittance growth vs. plasma length for a 100 GeV beam with 3 % rms energy spread, normalized emittance 100 nm and an initial offsets of 1 μm and 40 μrad. Emittance growth is seen to transition from the unsaturated regime (red line) to the saturated regime (yellow line) at the predicted saturation length (dotted line).

hence the bunch smears out in phase space until it finally forms a ring (see Figure 2). To describe this behavior, we differentiate between the *unsaturated regime* of continuous smearing and the steady-state *saturated regime* where bunch is fully smeared.

Unsaturated Emittance Growth

Consider a beam of transverse rms size σ_x and geometric emittance ϵ. Without loss of generality, we assume the offset is purely positional, $\Delta x = \sqrt{2\beta J}$, giving an rms phase spread

$$\sigma_{\mu 0} = 2\pi \frac{\sigma_x}{2\pi \Delta x} = \frac{\sqrt{\beta\epsilon}}{\sqrt{2\beta J}} = \sqrt{\frac{\epsilon}{2J}}. \quad (3)$$

Different energies advance their phase by $\mu(s) = 2\pi s/\lambda_\beta = s/\beta_m$, giving an energy dependence (chromaticity) of

$$\xi = \left.\frac{\partial \mu}{\partial \delta}\right|_{\delta=0} = \left.\frac{\partial}{\partial \delta}\left(\frac{s}{\sqrt{1+\delta}\beta_m}\right)\right|_{\delta=0} = -\frac{s}{2\beta_m}. \quad (4)$$

Their new phase spread, assuming Gaussian distributions, can be found by adding sigmas in quadrature

$$\sigma_\mu{}^2 = \sigma_{\mu 0}{}^2 + (\sigma_E \xi)^2. \quad (5)$$

Since all smearing occurs along the circumference of the offset ellipse, the relative increase in phase spread equals the relative increase in emittance

$$\frac{\epsilon}{\epsilon_0} = \frac{\sigma_\mu}{\sigma_{\mu 0}} = \sqrt{1 + \frac{\sigma_E{}^2}{\sigma_{\mu 0}{}^2}\xi^2} = \sqrt{1 + \frac{\sigma_E{}^2 s^2 J}{2\epsilon_0 \beta_m{}^2}}. \quad (6)$$

Expanding the square root by assuming the emittance growth is small, we obtain the unsaturated emittance growth

$$\left.\frac{\Delta\epsilon}{\epsilon_0}\right|_{\text{unsat}} = \frac{\sigma_E^2 s^2 J}{4\epsilon_0 \beta_m{}^2} = \frac{\sigma_E^2 s^2 k_p^2 J}{8\epsilon_{N0}}. \quad (7)$$

Saturated Emittance Growth

To find the saturated emittance growth of a plasma channel given an action J, we must find the emittance of the offset ellipse. A ring of radius $j = \sqrt{2J}$ has a 2D rms radius of $j_{rms} = j/\sqrt{2}$, and since the geometric emittance is $\epsilon = {j_{rms}}^2$ we get the saturated emittance growth

$$\left.\frac{\Delta\epsilon}{\epsilon_0}\right|_{\text{sat}} = \frac{J}{\epsilon_0} = \frac{\gamma J}{\epsilon_{N0}}, \quad (8)$$

where we assume the final emittance is much greater than the initial emittance.

Saturation Length

To determine the length required for saturation, we solve for when the unsaturated emittance growth, Eq. (7), equals the saturated emittance growth, Eq. (8), and find

$$s_{\text{sat}} = \frac{2\beta_m}{\sigma_E}. \quad (9)$$

This saturation length is energy dependent, growing with higher energy. Using plasma cells of the same length L_p, emittance growth will transit from the saturated to the unsaturated regime when $s_{\text{sat}} = L_p$, at energy

$$\gamma_{\text{swap}} = \frac{(\sigma_E k_p L_p)^2}{8}. \quad (10)$$

PLASMA DENSITY RAMPS

The effective matched β as seen from outside can be significantly increased while preserving the emittance, as well as the action, by using plasma density ramps [7]. This can be used to trade between angular and positional offset tolerances.

ISBN 978-3-95450-147-2

Consider a ramp of demagnification $\beta_0/\beta_m > 1$, where β_0 is the initial beta-function. To minimize emittance growth from offsets, in either regime, we must minimize J with respect to β_0, and since the offsets Δx and $\Delta x'$ are stochastic, we use their rms values $\sigma_{\Delta x}$ and $\sigma_{\Delta x'}$:

$$\frac{\partial \sigma_J}{\partial \beta_0} = \frac{\partial}{\partial \beta_0}\left(\frac{\sigma_{\Delta x}^2}{\beta_0} + \beta_0 \sigma_{\Delta x'}^2\right) = 0 \tag{11}$$

$$\beta_{0,\min} = \frac{\sigma_{\Delta x}}{\sigma_{\Delta x'}} \tag{12}$$

The above result indicates that if the plasma ramp demagnification is determined by other considerations (e.g. chromatic effects in staging optics [8]), the drive beam injector should be constructed such as to match the ratio of positional and angular jitter to β_0.

MULTIPLE STAGES

Generalizing to multiple stages necessarily introduces randomness to the system, with an offset jitter in each stage. Since the number of stages N will likely be small (a few to a few dozen), the total emittance growth is subject to significant relative jitter $\sim 1/\sqrt{N}$. Nevertheless, we make an estimate of the tolerances.

The emittance growth starts in the saturated regime, where after every cell the action has been canceled by smearing, and hence the normalized emittances add in quadrature. After this, and more importantly as γ_{swap} is often small, in the unsaturated regime, the beam is not fully smeared and the action is largely preserved. Action jitters σ_J therefore add (i.e. offsets add in quadrature) over n stages to give

$$\sigma_{J,n} = \sum_{i=1}^{n} \frac{i}{n}\sigma_J \approx \frac{n}{2}\sigma_J, \tag{13}$$

where acceleration damping of the action ($J \sim 1/\gamma$) is accounted for. The normalized emittance added at stage n and in total after N stages are thus given by

$$(\Delta\epsilon_N)_n = \frac{\sigma_E^2 L_p^2 k_p^2 n \sigma_J}{16} \tag{14}$$

$$(\Delta\epsilon_N)_{\text{tot}} = \sqrt{\sum_{n=1}^{N} (\Delta\epsilon_N)_n^2} = (\Delta\epsilon_N)_1 \sqrt{\sum_{n=1}^{N} n^2} \tag{15}$$

$$\approx N^{\frac{3}{2}} \frac{\sigma_E^2 L_p^2 k_p^2 \sigma_J}{16\sqrt{3}}. \tag{16}$$

Equivalently, we can express this as a tolerance for the square root of the action jitter (proportional to the offset jitters)

$$\sqrt{\sigma_{J,\max}} = \frac{\sqrt{16\sqrt{3}\,(\Delta\epsilon_N)_{\text{tot}}}}{\sigma_E L_p k_p N^{\frac{3}{4}}}, \tag{17}$$

where dependence on plasma density n_p is found by $k_p^2 = n_p e^2/m_e \epsilon_0 c^2$. This can be converted to positional and angular offset tolerances via $\sigma_{\Delta x} = \sqrt{2\beta_1 \sigma_J}$ and $\sigma_{\Delta x'} = \sqrt{2\sigma_J/\beta_N}$ where β_1 and β_N are evaluated at the first and last cell, respectively, as they require the tightest tolerances.

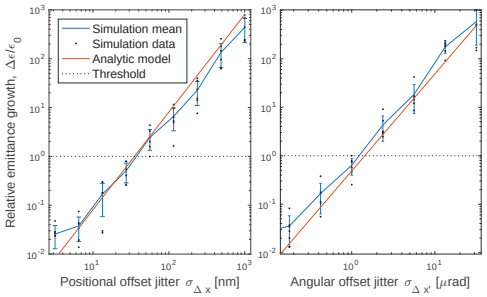

Figure 4: Emittance growth vs. positional and angular offset jitter for the worked example. Tolerances are individually approximately 40 nm and 1 μrad. As predicted by the model, emittance growth scales with the square of the rms offset, and is numerically consistent (35 nm and 1.5 μrad).

WORKED EXAMPLE

The 1 TeV PWFA linear collider scheme in Ref. [9] uses the following parameter set: 20 stages of 25 GeV energy gain, 3 m long, density 2×10^{16} cm^{-3}, and a beam of 1% energy spread and initial normalized emittance of 100 nm. The regime-swap occurs at 40 GeV, which means the unsaturated regime is dominant throughout the accelerator. Assuming a maximum of 100 % emittance growth, Eq. (17) estimates approximately a tolerance in position and angle of 35 nm and 1.5 μrad respectively, in good agreement with simulation (40 nm and 1 μrad) in Figure 4.

CONCLUSIONS

Plasma wakefield accelerators, while providing very large acceleration gradients, will require very tight alignment jitter tolerances. An analytic model was developed to estimate the emittance growth from position and angle offsets in the plasma channel, backed by a simplified simulation setup using conventional particle tracking. Tolerances were estimated for the 1 TeV PWFA linear collider scheme in Ref. [9] to approximately 40 nm and 1 μrad in position and angle rms jitter, respectively.

ACKNOWLEDGEMENTS

Work supported by the Research Council of Norway.

REFERENCES

[1] R. Ruth, A. W. Chao, P. L. Morton and P. B. Wilson, SLAC-PUB-3374, 1985.

[2] ILC Technical Design Report, `www.linearcollider.org/ILC/TDR`, 2007.

[3] CLIC Conceptual Design Report, `http://project-clic-cdr.web.cern.ch/project-clic-cdr/CDR_Volume1.pdf`, 2012.

[4] C. Huang *et al.*, Phys. Rev. Lett. **99**, 255001 (2007).

[5] A. Burov, V. Lebedev, and S. Nagaitsev, FERMILAB-FN-1008-AD, 2016.

ISBN 978-3-95450-147-2

[6] M. Borland, User's Manual for Elegant, 2012.

[7] X. L. Xu *et al.*, arXiv:1411.4386, 2014.

[8] C. A. Lindstrøm *et al.*, Nucl. Instrum. Methods Phys. Res. A (2016), http://dx.doi.org/10.1016/j.nima.2015.12.065.

[9] E. Adli *et al.*, CSS2013 and arXiv:1308.1145 (2013).

ISBN 978-3-95450-147-2

A.2 Design of general apochromatic drift-quadrupole beam lines

Authors

Carl A. Lindstrøm and Erik Adli

Journal

Phys. Rev. Accel. Beams **19**, 072001 (2016)

Abstract

Chromatic errors are normally corrected using sextupoles in regions of large dispersion. In low emittance linear accelerators, use of sextupoles can be challenging. Apochromatic focusing is a lesser-known alternative approach, whereby chromatic errors of Twiss parameters are corrected without the use of sextupoles, and has consequently been subject to renewed interest in advanced linear accelerator research. Proof of principle designs were first established by Montague and Ruggiero and developed more recently by Balandin *et al.* We describe a general method for designing drift-quadrupole beam lines of arbitrary order in apochromatic correction, including analytic expressions for emittance growth and other merit functions. Worked examples are shown for plasma wakefield accelerator staging optics and for a simple final focus system.

(9 pages)

Design of general apochromatic drift-quadrupole beam lines

C. A. Lindstrøm* and E. Adli

Department of Physics, University of Oslo, 0316 Oslo, Norway

(Received 24 March 2016; published 15 July 2016)

Chromatic errors are normally corrected using sextupoles in regions of large dispersion. In low emittance linear accelerators, use of sextupoles can be challenging. Apochromatic focusing is a lesser-known alternative approach, whereby chromatic errors of Twiss parameters are corrected without the use of sextupoles, and has consequently been subject to renewed interest in advanced linear accelerator research. Proof of principle designs were first established by Montague and Ruggiero and developed more recently by Balandin *et al.* We describe a general method for designing drift-quadrupole beam lines of arbitrary order in apochromatic correction, including analytic expressions for emittance growth and other merit functions. Worked examples are shown for plasma wakefield accelerator staging optics and for a simple final focus system.

DOI: 10.1103/PhysRevAccelBeams.19.071002

I. INTRODUCTION

Chromatic errors are inherent to charged particle beam optics, due to the energy dependent kick exerted by a magnetic quadrupole, as seen explicitly in the normalized quadrupole strength

$$k = \frac{eg}{p_0(1+\delta)}, \tag{1}$$

where g is the quadrupole field gradient, e is the particle charge, p_0 is the nominal particle momentum, and δ is the relative momentum offset. Coupled with an energy spread, this results in mostly unwanted nonlinear distortions of the beam.

Correcting chromatic errors is conventionally done using sextupoles in regions of large dispersion [1]. This method introduces nonlinear force terms, of which some may be canceled by careful lattice design, and adds additional dispersion and synchrotron radiation in the case of linear accelerators. In particular, this results in unfavorable energy vs length scaling laws for future high-energy, low emittance advanced accelerator concepts [2].

Fortunately, another method known as apochromatic focusing can be used to correct chromatic effects in linear accelerators without sextupoles or dipoles. Inspired by light ray optics, the aim is to simultaneously focus a range of colors (energies) to the same focal point using lenses (quadrupoles) only. Figure 1 illustrates this mechanism for both light beams and charged particle beams. In (a) three distinct colors are focused, while in (b) the energy dependence of the focusing is canceled to first order.

This method was introduced in 1987 by Montague and Ruggiero [3] in an attempt to meet the requirements of the Compact Linear Collider (CLIC) [4] final focus system. Presenting an analytical solution for a thin-lens first-order

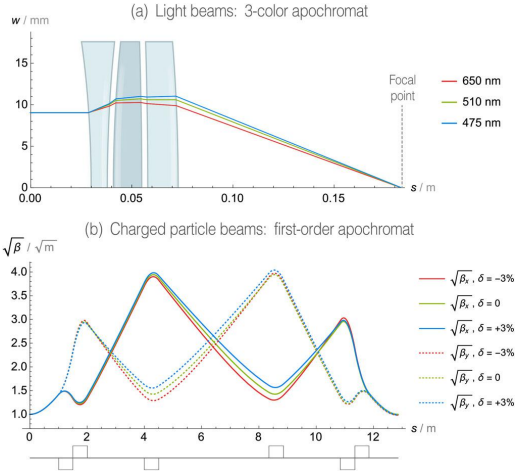

FIG. 1. Plot (a) shows width w of three light beams vs the optical axis s for a 3-color apochromat. Plot (b) shows transverse beam size $\sqrt{\beta}$ in x and y vs s for a first-order apochromat. Both apochromats use the same principle: beams of different color/energy are focused differently through the system, but end up focused to the same point. However, the two examples are different in a subtle way: In plot (a) three distinct colors are focused to the same point, leaving intermediate colors slightly unfocused. This is how achromatic lenses for light optics are often designed. In contrast, in plot (b) the nominal energy is perfectly focused, and the focusing error is canceled to first order in δ, leaving small-offset energies well focused. In this paper, we study arbitrary order apochromats for charged particle beams.

*c.a.lindstrom@fys.uio.no

apochromatic telescope of arbitrary magnification, they concluded that while not providing sufficient energy acceptance for CLIC, the method was of considerable interest in less extreme cases. However, their contribution has until recently remained largely ignored.

Now, a surge in advanced accelerator research has lead to a renaissance of interest in apochromatic focusing. Advances on the topic were made by Balandin *et al.* in work motivated by requirements at the European XFEL [5], showing e.g. that any drift-quadrupole beam line has a set of unique first-order apochromatic Twiss parameters [6], as well as finding a proof-of-principle 20-quad first-order apochromatic FODO-lattice [7]. Looking ahead, challenging demands for tightly focused beams, high emittance preservation and short beam lines in emerging accelerator technologies such as laser- and plasma wakefield accelerators highlight the need for apochromatic beam line design.

Although earlier work has successfully demonstrated the plausibility of apochromatic focusing, mostly by analytical means and by employing various symmetries, it has not been sufficiently illustrated how to systematically construct such lattices in general. In this paper, we take a more general approach and present a methodical framework for computing apochromatic beam lines corrected to arbitrary order, both with and without the use of symmetric lattices.

II. CHROMATICITY DEFINITIONS

Before delving into how chromatic errors are canceled, it is necessary to distinguish between two closely related, but different quantities. The *chromaticity*

$$\xi = \frac{1}{2\pi}\frac{\partial \mu}{\partial \delta}, \tag{2}$$

where μ is the betatron phase advance [8], quantifies the chromatic error of a single particle, whereas the *chromatic amplitude* [9] or *W-function*

$$W = \sqrt{\left(\frac{\partial \alpha}{\partial \delta} - \frac{\alpha}{\beta}\frac{\partial \beta}{\partial \delta}\right)^2 + \left(\frac{1}{\beta}\frac{\partial \beta}{\partial \delta}\right)^2} \tag{3}$$

quantifies the chromatic error of the beam as a distribution. In Eq. (3) we have used the definitions

$$\beta = \frac{\langle x^2 \rangle}{\epsilon} \tag{4}$$

$$\alpha = -\frac{\langle x x' \rangle}{\epsilon} = -\frac{1}{2}\frac{\partial \beta}{\partial s}, \tag{5}$$

where x, x', ϵ and s are transverse position, angle, geometric emittance and longitudinal position. β and α are better known as the Courant-Snyder or Twiss parameters [8] used to describe beam focusing in an accelerator lattice, and all conclusions in this paper are subject to the approximations of this framework. Note that throughout this paper, we will use $\frac{\partial}{\partial \delta}$ as shorthand for $\frac{\partial}{\partial \delta}|_{\delta=0}$, i.e. the chromatic derivative evaluated at $\delta = 0$.

Circular accelerators demand strict control of tune to avoid resonances, hence the chromaticity ξ must be

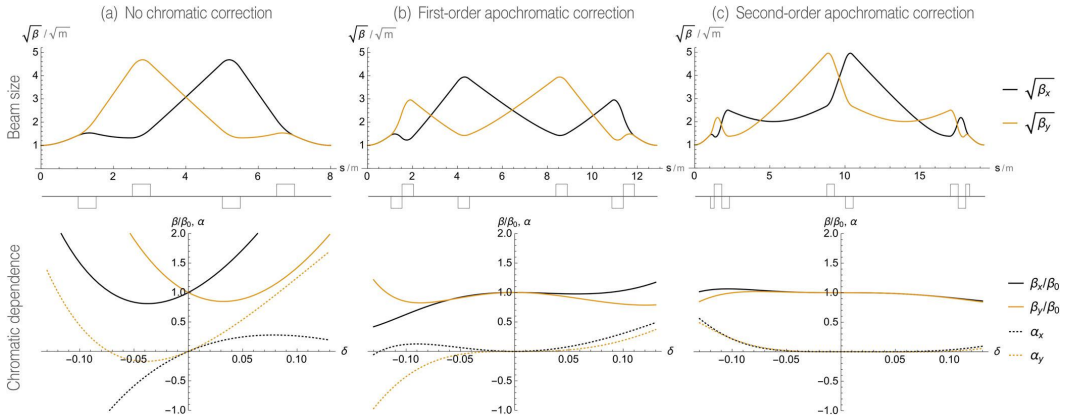

FIG. 2. Plots of $\sqrt{\beta}$ (proportional to rms beam size) vs beam line axis s, and chromatic dependence of $\beta(\delta)$ and $\alpha(\delta)$ vs δ, shown for different orders of apochromatic focusing. All solutions satisfy initial and final Twiss parameters $\beta = 1$ m and $\alpha = 0$ in both planes, with a 1 m drift before and after the first and last quadrupoles respectively. The chromatic dependence of the lattice flattens progressively with higher orders of apochromatic focusing; No chromatic correction (a) results in chromatic amplitude $W \neq 0$ (a slope) at nominal energy $\delta = 0$, whereas first order correction (b) removes this chromatic amplitude $W = 0$ (no slope), and second order correction (c) flattens it further by removing second order chromatic errors (curvature) around $\delta = 0$. Overall, the chromatic dependence can be decreased at the cost of longer lattices with more quadrupoles, where the appropriate order of the correction is determined by the energy spread of the beam.

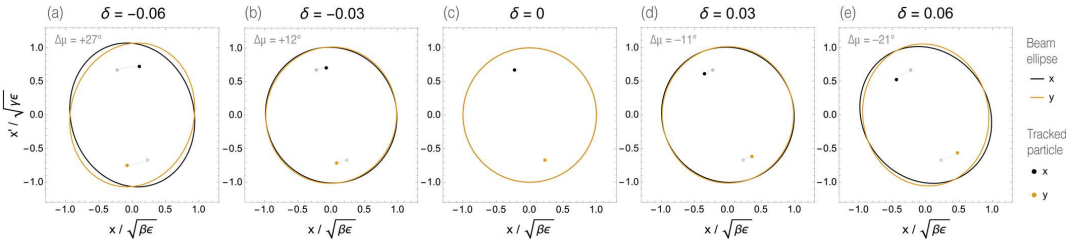

FIG. 3. Phase space plots with beam ellipses and a single tracked particle for several energy offsets δ, after transport through the first order apochromatic lattice shown in Fig. 2(b). As the energy increases [(a) → (e)], the particle experiences less phase advance ($\Delta\mu$), indicating a nonzero chromaticity $\xi < 0$ as defined by Eq. (2). However, since the distribution of particles retains the same shape around nominal energy [(b) and (d)], β and α are unchanged to first order and therefore chromatic amplitude $W = 0$. At larger energy offsets [(a) and (e)], the ellipse is distorted due to higher order errors.

canceled. This can only be done using nonlinear optics such as sextupoles [10]. However in single-pass linear accelerators, with no concept of tune and resonance, the chromaticity ξ usually does not need to be canceled. On the other hand, to ensure the correct focusing, it is important to cancel the W-function, which indeed can be corrected using sextupole-free apochromatic focusing. In colliding-beam storage rings, a combination of both methods can be used, where the chromaticity is canceled using sextupoles in the arcs and the W-function is canceled using apochromatic focusing in the intersection regions.

Figure 2 illustrates in more detail how apochromatic lattices are used to reduce the chromatic dependence of beam focusing, while Fig. 3 elaborates on how the W-function (focusing energy dependence) can be canceled when chromaticity ξ (phase advance energy dependence) is not.

III. CHROMATIC EXPANSIONS

In light ray optics, the standard approach to minimizing chromatic aberration for a given spectrum is to simultaneously focus a number of different colors [11]. This can also be done in beam optics. The underlying assumption is that by matching two narrowly offset energies, the energies between them are also approximately matched. To decrease the degree of mismatch in this region, more matched energies are added, requiring additional d.o.f.

In this paper, we employ a more systematic approach, namely to explicitly cancel terms in the chromatic expansion, defined as the Taylor series of a quantity with respect to relative energy offset δ, e.g.,

$$\beta(\delta) = \sum_{n=0}^{\infty} \frac{\delta^n}{n!} \frac{\partial^n \beta}{\partial \delta^n} \tag{6}$$

$$= \beta_0 + \frac{\partial \beta}{\partial \delta}\delta + \frac{1}{2}\frac{\partial^2 \beta}{\partial \delta^2}\delta^2 + \mathcal{O}(\delta^3). \tag{7}$$

A beam typically has a Gaussian or similarly distributed energy spread, where energies further from the nominal are progressively less populated. Minimizing the weighted average mismatch is accomplished most effectively by first canceling first order chromatic terms, then second order terms etc., adding only a constant number of additional d.o.f. per order. By directly taking control over the expansion Eq. (6), the lattice designer has more precise control of the chromatic performance of the beam line, as exemplified in the next section.

IV. EMITTANCE GROWTH IN DRIFT-QUADRUPOLE BEAM LINES

Using drift-quadrupole beam lines allows us to make relatively simple, yet exact expressions for measuring performance; orders of magnitude faster to compute compared to particle tracking. This is because focusing fields are linear, which ensures that every energy slice of the beam preserves its rms emittance, or equivalently [8]

$$\beta(\delta)\gamma(\delta) - \alpha(\delta)^2 = 1, \tag{8}$$

where the Twiss parameter $\gamma = \langle x'^2 \rangle / \epsilon$ represents the divergence of the beam. As we are interested only in effects due to focusing and not dispersion (which a drift-quadrupole beam line does not introduce), we can ignore correlations between energy and phase space ($\langle x\delta \rangle = \langle x'\delta \rangle = 0$), giving a squared projected emittance

$$\bar{\epsilon}^2 = \langle x^2 \rangle \langle x'^2 \rangle - \langle xx' \rangle^2 \tag{9}$$

$$= (\epsilon_0 \bar{\beta})(\epsilon_0 \bar{\gamma}) - (\epsilon_0 \bar{\alpha})^2 \tag{10}$$

$$= {\epsilon_0}^2 (\bar{\beta}\bar{\gamma} - \bar{\alpha}^2), \tag{11}$$

where ϵ_0 is the geometric emittance of each energy slice, and a bar denotes energy average (projection). In a transport beam line, a natural merit function is the relative projected squared emittance growth

$$\frac{\Delta\epsilon^2}{{\epsilon_0}^2} \equiv \frac{\bar{\epsilon}^2 - {\epsilon_0}^2}{{\epsilon_0}^2} = \bar{\beta}\,\bar{\gamma} - \bar{\alpha}^2 - 1. \tag{12}$$

Other applications, such as final focus systems or spectrometers, might use rms spot sizes ($\sim\sqrt{\bar{\beta}}$) as their merit function. We observe that in any drift-quadrupole lattice, chromatic correction of $\beta(\delta)$ and $\alpha(\delta)$ is sufficient, since $\gamma(\delta)$ is determined completely by Eq. (8).

Assuming a Gaussian energy distribution of rms energy spread σ_E and substituting for chromatic expansions, we find

$$\bar{\beta} = \int_{-\infty}^{\infty} \beta(\delta) \frac{e^{-\frac{\delta^2}{2{\sigma_E}^2}}}{\sqrt{2\pi}\sigma_E} d\delta \tag{13}$$

$$= \int_{-\infty}^{\infty} \sum_{n=0}^{\infty} \frac{\delta^n}{n!} \frac{\partial^n \beta}{\partial \delta^n} \frac{e^{-\frac{\delta^2}{2{\sigma_E}^2}}}{\sqrt{2\pi}\sigma_E} d\delta \tag{14}$$

$$= \sum_{n=0}^{\infty} \frac{1}{n!} \frac{\partial^n \beta}{\partial \delta^n} \frac{{\sigma_E}^n}{\sqrt{2\pi}} \int_{-\infty}^{\infty} \lambda^n e^{-\frac{1}{2}\lambda^2} d\lambda, \tag{15}$$

where the substitution $\lambda = \delta/\sigma_E$ is used. For odd offset orders the emittance growth at $+\delta$ and $-\delta$ are equal and opposite, canceling each other, such that only even orders ($n = 2m$) contribute a nontrivial Gaussian integral

$$\int_{-\infty}^{\infty} \lambda^{2m} e^{-\frac{1}{2}\lambda^2} d\lambda = \sqrt{2\pi}(2m-1)!!, \tag{16}$$

where !! is the double factorial: $n!! = n(n-2)(n-4)\ldots$. Substituting Eq. (16) into (14) and simplifying factorials using $(2m)!!(2m-1)!! = (2m)!$ and $(2m)!! = 2^m m!$, we are left with

$$\bar{\beta} = \sum_{m=0}^{\infty} \frac{{\sigma_E}^{2m}}{2^m m!} \frac{\partial^{2m}\beta}{\partial\delta^{2m}} \tag{17}$$

and similar expressions for $\bar{\alpha}$ and $\bar{\gamma}$ by simply substituting α or γ in place of β. Expanding Eq. (12) in terms of energy spread σ_E gives

$$\frac{\Delta\epsilon^2}{{\epsilon_0}^2} = \sum_{m=1}^{\infty} \chi_m {\sigma_E}^{2m} \tag{18}$$

with coefficients

$$\chi_m = \sum_{k=0}^{m} \frac{\left(\frac{\partial^{2l}\beta}{\partial\delta^{2l}}\frac{\partial^{2k}\gamma}{\partial\delta^{2k}} - \frac{\partial^{2l}\alpha}{\partial\delta^{2l}}\frac{\partial^{2k}\alpha}{\partial\delta^{2k}}\right)}{2^m l!k!}, \tag{19}$$

where $l = (m-k)$. The expansion in Eq. (18) starts at $m = 1$ because by Eq. (8) there is no constant term.

Somewhat misleadingly, Eq. (19) gives the impression that only even order chromatic derivatives contribute to emittance growth. However, different order chromatic derivatives of β, α, and γ are related by Eq. (8) and its derivatives

$$\frac{\partial^n}{\partial\delta^n}(\beta\gamma - \alpha^2) = 0, \tag{20}$$

where $n > 0$. To illustrate, we expand Eq. (20) for $n = 1$ and $n = 2$, giving

$$\beta\frac{\partial\gamma}{\partial\delta} = 2\alpha\frac{\partial\alpha}{\partial\delta} - \frac{\partial\beta}{\partial\delta}\gamma \tag{21}$$

$$\frac{\partial^2\beta}{\partial\delta^2}\gamma + \beta\frac{\partial^2\gamma}{\partial\delta^2} - 2\alpha\frac{\partial^2\alpha}{\partial\delta^2} = 2\left(\frac{\partial\alpha}{\partial\delta}\right)^2 - 2\frac{\partial\beta}{\partial\delta}\frac{\partial\gamma}{\partial\delta} \tag{22}$$

and simplify the lowest order emittance growth coefficient χ_1 by first using Eq. (21), then Eq. (22), rearranging and finally using Eq. (3):

$$\chi_1 = \frac{1}{2}\left(\frac{\partial^2\beta}{\partial\delta^2}\gamma + \beta\frac{\partial^2\gamma}{\partial\delta^2} - 2\alpha\frac{\partial^2\alpha}{\partial\delta^2}\right) \tag{23}$$

$$= \left(\frac{\partial\alpha}{\partial\delta}\right)^2 - \frac{\partial\beta}{\partial\delta}\frac{\partial\gamma}{\partial\delta} \tag{24}$$

$$= \left(\frac{\partial\alpha}{\partial\delta}\right)^2 + \frac{\partial\beta}{\partial\delta}\frac{1}{\beta}\left(\frac{\partial\beta}{\partial\delta}\frac{1+\alpha^2}{\beta} - 2\alpha\frac{\partial\alpha}{\partial\delta}\right) \tag{25}$$

$$= \left(\frac{\partial\alpha}{\partial\delta} - \frac{\alpha}{\beta}\frac{\partial\beta}{\partial\delta}\right)^2 + \left(\frac{1}{\beta}\frac{\partial\beta}{\partial\delta}\right)^2 \tag{26}$$

$$= W^2. \tag{27}$$

Substituting this into Eq. (18) gives an expression for the lowest order relative squared projected emittance growth

$$\frac{\Delta\epsilon^2}{{\epsilon_0}^2} = W^2{\sigma_E}^2 + \mathcal{O}({\sigma_E}^4) \tag{28}$$

or equivalently [using Eq. (12)] the relative rms projected emittance growth

$$\frac{\Delta\epsilon}{\epsilon_0} = \frac{\bar{\epsilon} - \epsilon_0}{\epsilon_0} = \sqrt{1 + \frac{\Delta\epsilon^2}{{\epsilon_0}^2}} - 1 \tag{29}$$

$$= \frac{1}{2}W^2{\sigma_E}^2 + \mathcal{O}({\sigma_E}^4). \tag{30}$$

This result shows that, to lowest order, relative projected emittance growth can be written simply in terms of energy spread and the W-function, implying that in order to cancel emittance growth to third order in energy spread, it is

sufficient to cancel first order chromatic derivatives. Balandin *et al.* defines such a lattice as a *third-order apochromat* [7], referring to emittance growth, whereas we will consistently call it a *first-order apochromat*, referring to the canceled chromatic derivatives.

For first-order correction, two d.o.f. are required per plane, one for each of the first order chromatic Twiss (α and β) derivatives, in addition to those needed for standard zeroth order matching. More generally, at order $2n$ in emittance growth, Eq. (20) can substituted into Eq. (19) to eliminate γ and all $2n$th chromatic Twiss derivatives, leaving derivatives of order $(2n-1)$ or lower. However, if also the lowest $(n-1)$ chromatic Twiss derivatives are canceled, only terms with zeroth and nth derivatives remain. We conclude that to cancel emittance growth to order $\mathcal{O}({\sigma_E}^{2n+1})$ in energy spread, we must cancel the first n chromatic Twiss derivatives in both planes; in total $4n$ d.o.f. Note the linear complexity $\mathcal{O}(n)$ of d.o.f. for apochromatic correction of order n.

V. METHOD

Our goal is to find an apochromatic beam line which satisfies appropriately chosen constraints. Previous work has found such solutions analytically in simple cases [3] or using symmetry [7,12]. To find solutions to a general nonsymmetric set of constraints, it is useful to take a computational approach. In particular, this requires calculation of chromatic derivatives, which can be accomplished in a number of ways. Given the simplistic equations describing apochromatic focusing, we have developed an analytic-numerical algorithm to find such beam lines: (1) Consider a beam line defined by a set of alternating drift spaces of lengths $\{d\} \in \mathbb{R}^+$, and quadrupoles of strengths $\{k\} \in \mathbb{R}$ and lengths $\{l\} \in \mathbb{R}^+$, of which some are left as variables $\{q\}$. (2) Insert a relative energy offset δ in the quadrupole strengths [see Eq. (1)]: $\{k\} \to \{k/(1+\delta)\}$. (3) Compute analytically the transfer matrix $\boldsymbol{R}(\{q\},\delta)$ of the overall beam line. This will be a complicated nonlinear function of δ. (4) Expand $\boldsymbol{R}$ as a series to the required order in δ about the nominal energy, $\delta = 0$. (5) Express the output Twiss parameters α and β in terms of $\boldsymbol{R}$ and input Twiss parameters α_0, β_0, γ_0 using

$$\begin{bmatrix} \beta \\ \alpha \\ \gamma \end{bmatrix} = \begin{bmatrix} C^2 & -2CS & S^2 \\ -CC' & CS'+SC' & -SS' \\ C'^2 & -2C'S' & S'^2 \end{bmatrix} \begin{bmatrix} \beta_0 \\ \alpha_0 \\ \gamma_0 \end{bmatrix} \tag{31}$$

where $(C,S,C',S') = (R_{11},R_{12},R_{21},R_{22})$ in x and $(C,S,C',S') = (R_{33},R_{34},R_{43},R_{44})$ in y [8]. (6) Truncate the $\alpha(\delta)$ and $\beta(\delta)$-series at the required order in δ. (7) Extract expressions for chromatic derivatives of α and β as given by Eq. (6) to form a set of constraints and/or a merit function. (8) Solve the constraints and/or minimize the merit function using the d.o.f. $\{q\}$ available. Apart from particularly simple cases, this must be solved numerically. (9) (Optional) Simplify the numerical solving by employing symmetries to reduce the number of constraints and d.o.f., including periodicity, mirror symmetry, and mirror antisymmetry (i.e., quadrupole polarities are switched).

This method can be applied both to thick and thin quadrupoles, although thin quadrupoles result in a great reduction in calculation time.

A simple, yet powerful code was developed based on this method, using a computer algebra package (*Mathematica*) for expressing constraints analytically and a numerical analysis package (MATLAB) for solving or minimizing them. This code was used to compute all solutions in Sec. VI, as well as Figs. 1(b), 2, and 3. Execution times using a standard laptop computer typically ranged from seconds to minutes.

It should be noted that first order apochromatic matching following this method can be achieved in existing accelerator design codes, including MAD [13], by matching chromatic amplitude W and phase Φ.

VI. APPLICATIONS

In order to demonstrate this method, two practical applications of apochromatic beam lines are considered: (i) Staging optics for a plasma wakefield accelerator and (ii) a simple final focus system. Together, these examples show varying degrees of symmetry (high and low, respectively), demagnifications (none and large, respectively), and different merit functions (emittance growth and spot size, respectively). However they both share requirements for localized small beam sizes with comparatively long adjacent drift spaces (L^*), hence large chromatic errors, and a strong incentive to minimize the overall beam line length. To illustrate higher order apochromats, two solutions are presented for the plasma wakefield accelerator: one first-order apochromat using conventional quadrupoles, and a third-order apochromat using axially symmetric plasma lenses.

A. PWFA staging optics

Plasma wakefield acceleration [14,15] is one of several emerging advanced accelerator concepts, in which energy is transferred from a laser (LWFA) or particle (PWFA) *drive* beam to a trailing *witness* beam via a wakefield in the plasma. To achieve much higher energies than that of the drive beam, this process must be repeated in multiple stages; the two beams must be separated and the witness beam reinjected behind a fresh drive beam into the next plasma cell.

To avoid significant emittance growth in the plasma channel, the staging optics between cells must match the witness beam to a specific Twiss β. Assuming parameters used in a recent beam-driven PWFA linear collider study

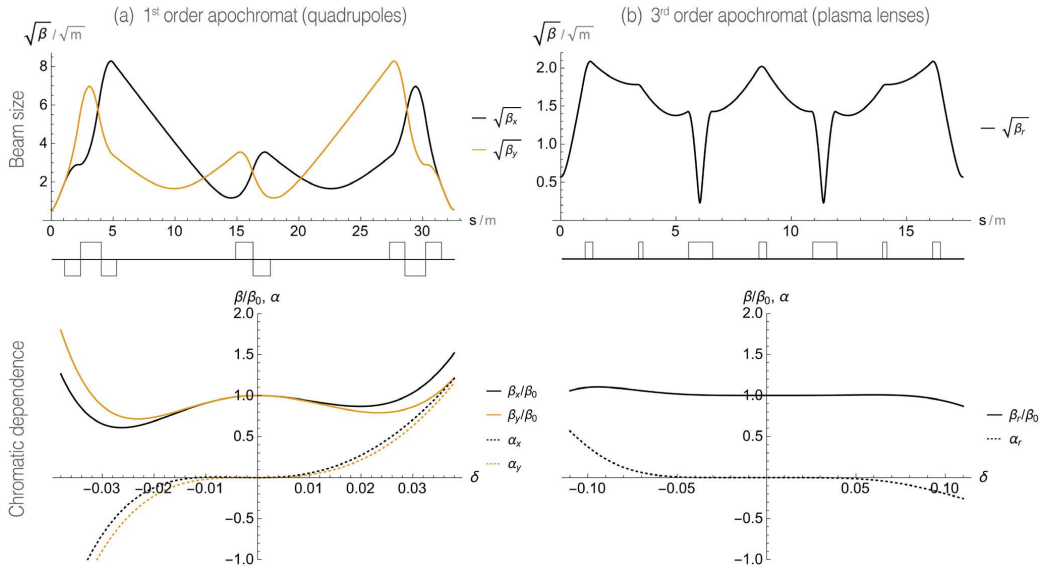

FIG. 4. Example A: PWFA staging optics, both using quadrupoles (a) and plasma lenses (b). Plots show $\sqrt{\beta}$ (proportional to rms beam size) vs beam line axis s, and chromatic dependence of $\alpha(\delta)$ and $\beta(\delta)$ vs offset δ. Both solutions capture a 100 GeV beam exiting a plasma (with density ramps) matched to $\beta_0 = 32.5$ cm and refocuses it back to 32.5 cm, with a 1 m drift space at the start and end for injection and extraction of drive beams. Solution (a) is a first-order apochromatic lattice using 8 quadrupoles with field gradient 160 T/m are placed antisymmetrically (mirrored with polarity switched), whereas solution (b) is a third-order apochromatic lattice using 7 discharge capillary plasma lenses [18] with field gradient 3000 T/m placed symmetrically. Transporting a beam with 1% rms energy spread leads to a projected emittance growth of 0.96% in lattice (a), and 0.000004% in lattice (b). Note the different δ-scales in the two chromatic dependence plots.

[16], we use $\beta_{\mathrm{mat}} = 2.5$ cm for a 100 GeV witness beam, which has an energy spread of approximately 1%. Using a plasma density ramp [17] of β-magnification 13, the staging optics must match to and from $\beta_0 = 32.5$ cm. Injection and extraction of drive beams introduce further considerations, discussed in Ref. [2]. Here we simply reserve 1 m of drift space at the beginning and end of the lattice for eventual injection and extraction sections.

The combination of large energy spread and tightly focused β-functions with long adjacent drift spaces results in significant chromatic errors that require cancellation. A naive beam line with no chromatic correction produces a projected emittance growth of around 10%.

1. First order quadrupole solution

We start by solving the problem with lowest (first) order apochromatic correction using conventional magnetic quadrupoles. Since the problem is mirror symmetric, we can work with the first half of the lattice only, reducing the original 4 constraints ($\beta_x = \beta_y = \beta_0$ and $\alpha_x = \alpha_y = 0$ at the end) to only 2 constraints. Two solutions exist: mirror symmetry ($\alpha_x = \alpha_y = 0$ halfway) and mirror antisymmetry ($\beta_x = \beta_y$ and $\alpha_x = -\alpha_y$ halfway), where quadrupole polarity is switched. We choose the latter for its similar emittance growth in both planes.

A first-order apochromat must satisfy both the zeroth order matching constraints and cancellation of their first-order chromatic derivatives, resulting in a total of 4 constraints at the halfway point:

$$\beta_x - \beta_y = 0 \tag{32}$$

$$\alpha_x + \alpha_y = 0 \tag{33}$$

$$\frac{\partial \beta_x}{\partial \delta} - \frac{\partial \beta_y}{\partial \delta} = 0 \tag{34}$$

$$\frac{\partial \alpha_x}{\partial \delta} + \frac{\partial \alpha_y}{\partial \delta} = 0. \tag{35}$$

Since this requires 4 d.o.f., we define a half-lattice of 4 quadrupoles. To minimize the total length, we use quadrupoles of alternating maximum field strength, assumed to be ± 160 T/m, and vary their lengths. Solving Eqs. (32)–(35)) using the method outlined in Sec. V produces the solution presented in Fig. 4(a): a 32.5 m long lattice of 8 quadrupoles transporting a 100 GeV beam of 1% energy spread

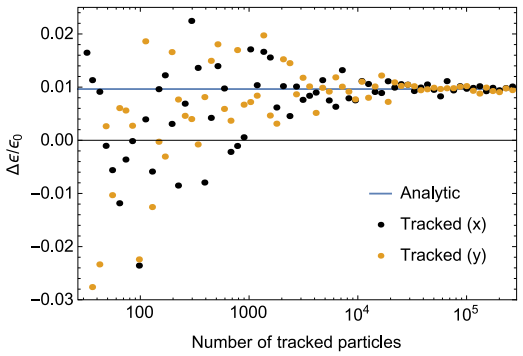

FIG. 5. Plot of relative projected emittance growth vs number of tracked particles, after Elegant-tracking [19] a beam with 1% rms energy spread through the apochromatic lattice shown in Fig. 4(a). Approaching large particle numbers, the tracked emittance growth converges to the analytic estimate given by Eq. (18), with an expected statistical error ($\sim 1/\sqrt{N}$). Since the lattice is antisymmetric, the emittance growth is (very nearly) identical in both planes.

with a projected emittance growth of 0.96%, which is around the limit for a linear collider application.

To illustrate the accuracy of the analytic expression for emittance growth Eq. (18), it is compared to the emittance growth of particles tracked through this example using Elegant [19], shown in Fig. 5. It verifies that as the number of tracked particles increase, the tracked emittance growth indeed converges to the analytically calculated value, which is many orders of magnitude faster to compute.

2. Third-order plasma lens solution

Emittance preservation can be dramatically improved with the use of axially symmetric lenses since the number of constraints is halved, which allows correction to higher order at low computational cost. An implementation of axially symmetric plasma lenses, based on strong discharge capillaries, has recently been presented by BELLA [18]. Constructing a third-order apochromat, using mirror symmetry, requires 4 constraints at the halfway point:

$$\alpha_r = \frac{\partial \alpha_r}{\partial \delta} = \frac{\partial^2 \alpha_r}{\partial \delta^2} = \frac{\partial^3 \alpha_r}{\partial \delta^3} = 0. \tag{36}$$

We define a half-lattice of 4 focusing-only plasma lenses of variable lengths, operating at 3000 T/m [18]. Solving Eqs. (36) using the method in Sec. V, we obtain the solution shown in Fig. 4(b): a 17.4 m long lattice of 7 plasma lenses transporting a 100 GeV beam of 1% energy spread with a projected emittance growth of only 0.000004%, which is far below the requirements for a linear collider. In fact, the solution is almost completely achromatic up to an energy offset of ±5%.

A similarly performing solution of approximately half the length (8.9 m) can be found by using both focusing and defocusing lenses, as is possible in discharge capillary plasma lenses. However, the above example is used to show that apochromatic focusing can be used also in solenoids and plasma lenses where only focusing fields are available.

B. Final focus system

Apochromatic beam lines can also be used to magnify or demagnify charged particle beams, as shown analytically in Ref. [3], in which case the beam line will be asymmetric unlike in the previous example. A first-order apochromatic telescope can be constructed by matching $R_{12} = R_{21} = R_{34} = R_{43} = 0$ and canceling their chromatic derivatives $T_{126} = T_{216} = T_{346} = T_{436} = 0$, using the method in Sec. V. However, for this example, we will consider a simple final focus system, using a similar, but not identical, criterion of a locally minimized average spot size for a given energy spread. This is useful in applications like colliders and fixed target experiments.

With no symmetry to reduce the number of constraints, we must simultaneously match to

$$\beta_x = \beta_x^* \tag{37}$$

$$\beta_y = \beta_y^* \tag{38}$$

$$\alpha_x = \alpha_y = 0 \tag{39}$$

at the interaction point (IP). This requires 4 d.o.f., and any additional d.o.f. will be used to maximize the appropriate merit function: relative luminosity,

$$\frac{\mathcal{L}}{\mathcal{L}_0} = \sqrt{\frac{\beta_x^* \beta_y^*}{\bar{\beta}_x \bar{\beta}_y}}, \tag{40}$$

or equivalently minimizing $\bar{\beta}_x \bar{\beta}_y$, where a bar denotes momentum averaging. According to Eq. (17), this is to lowest order the same as minimizing

$$\frac{\partial^2 \beta_x}{\partial \delta^2} + \frac{\partial^2 \beta_y}{\partial \delta^2}. \tag{41}$$

In practice, however, the numerical search is helped by also adding first order apochromatic correction:

$$\frac{\partial \beta_x}{\partial \delta} = \frac{\partial \beta_y}{\partial \delta} = \frac{\partial \alpha_x}{\partial \delta} = \frac{\partial \alpha_x}{\partial \delta} = 0. \tag{42}$$

In total this amounts to 8 constraints requiring 8 d.o.f., and a merit function to be minimized by any additional variables.

Since our goal is to greatly demagnify the beam, our system has a large inherent scale difference: $\beta^* \ll \beta_0$. This complicates the numerical search, as parameters are

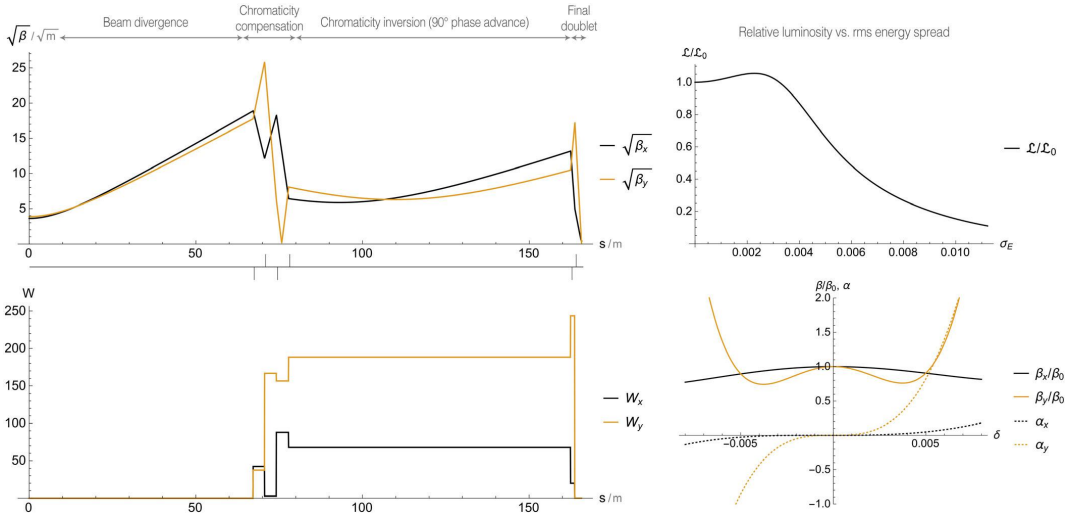

FIG. 6. Example B: Final focus. A 166 m long first-order apochromatic lattice using 6 (thin) quadrupoles, focuses a beam of 0.5% rms energy spread with about 30% luminosity loss. The beam is focused from $\beta_{x0} = 13.1$ m, $\beta_{y0} = 15$ m down to $\beta_y^* = 16.3$ cm, $\beta_y^* = 1.33$ cm, in total a β-demagnification of 80 in x and 1125 in y. The W-function is intentionally increased, then transported and inverted, until it is finally canceled in the final doublet, which focuses the beam to the interaction point.

simultaneously on large and small scales, resulting in a large fine-grained parameter space to be searched. Two methods are useful in mitigating this problem: (i) Back-propagate Twiss parameters for matching, starting with β_x^*, β_y^* and matching to β_{x0}, β_{y0}. This greatly loosens matching tolerances. (ii) Find a solution for small demagnification (larger β_x^*, β_y^*), then use this solution as an initial guess for a slightly larger demagnification. Repeat this process until the desired demagnification is reached.

We start with Twiss parameters $\beta_{x0} = 13.1$ m, $\beta_{y0} = 15$ m, and $\alpha_{x0} = \alpha_{y0} = 0$, focusing to $\beta_x^* = 16.3$ cm, $\beta_y^* = 1.33$ cm, using a lattice of 6 quadrupoles where the last drift space is $L^* = 2$ m, we have 12 available d.o.f. (6 quadrupole strengths, 6 drift space lengths). Thin quadrupoles are used to speed up the numerical search. Applying the method in Sec. V, we obtain the solution shown in Fig. 6: a 166 m long lattice, focusing a beam of energy spread 0.5% by β-demagnifications 80 in x and 1125 in y, with a luminosity loss of about 30% according to Eq. (40). Conceptually, this solution consists of four separate modules (see Fig. 6): the beam diverges to large β's; large chromatic amplitude W is introduced; the chromatic amplitude is inverted by a 90° phase advance; the beam is strongly focused and the first-order chromatic amplitude is canceled. Note, however, that this structure was never imposed, but is simply a solution that results from applying the algorithm.

Ultimately, the performance of the presented solution compares unfavorably to state-of-the-art linear collider final focus systems, consistent with the conclusion in Ref. [3]. For instance, the design proposed by Seryi and Raimondi [20] offers orders of magnitude larger demagnification at the same energy acceptance by employing *local chromaticity correction*, whereby sextupoles compensate chromatic errors as close to the source as possible, unlike our example which uses *global chromaticity correction*, by transporting artificially induced chromatic errors for some distance until it is finally canceled. Nevertheless, many applications require more moderate demagnification, in which case there can be significant benefits to using linear quadrupole optics, which does not distort the phase space as much as nonlinear sextupole optics.

An apochromatic final focus may, however, prove beneficial in future high energy circular electron-positron colliders, such as CEPC [21] or FCC-ee [22]. A major problem for these machines is hard X-rays hitting the particle collision detectors, produced in dipoles close to the IP as a nonzero dispersion is required for local chromaticity correction. By removing dipoles entirely from the IP area, an apochromat constitutes an interesting alternative approach to this problem, although only a careful study of all constraints can determine whether it provides a net improvement.

VII. CONCLUSION

Apochromatic correction of chromatic focusing errors, which makes use of linear optics (quadrupoles) only, can be applied to preserve projected emittance of charged particle beams of significant energy spreads, in cases where tune

resonances do not occur. This is especially relevant in emerging accelerator technologies like plasma wakefield acceleration. The method presented has been shown through examples to produce drift-quadrupole beam lines of any order in apochromatic correction, using both thick and thin quadrupoles, as well as varying degrees of symmetry. In addition, simple analytic expressions for emittance growth reduce the need for particle tracking to measure performance. We believe that apochromatic correction could be part of any advanced accelerator lattice designer's toolbox in the future.

ACKNOWLEDGMENTS

We thank A. Chao, Y. Nosochkov, R. Tomas, D. Schulte and J. Pfingstner for useful discussions. This work is supported by the Research Council of Norway.

[1] H. Zyngier, LAL Report No. 77/35, 1977.
[2] C. A. Lindstrøm, E. Adli, J. M. Allen, J. P. Delahaye, M. J. Hogan, C. Joshi, P. Muggli, T. O. Raubenheimer, and V. Yakimenko, Staging optics considerations for a plasma wakefield acceleration linear collider, Nucl. Instrum. Methods Phys. Res., Sect. A **829**, 224 (2016).
[3] B. W. Montague and F. Ruggiero, CLIC Report No. Note 37, 1987.
[4] CLIC Conceptual Design Report, http://project-clic-cdr.web.cern.ch/project-clic-cdr/CDR_Volume1.pdf, 2012.
[5] V. Balandin, R. Brinkmann, W. Decking, and N. Golubeva, TESLA-FEL Report No. 2007-05, 2007.
[6] V. Balandin, R. Brinkmann, W. Decking, and N. Golubeva, Apochromatic beam transport in drift-quadrupole systems, arXiv:1305.1549.
[7] V. Balandin, R. Brinkmann, W. Decking, and N. Golubeva, Third-order apochromatic drift-quadrupole beamline, in *Proceedings of the 3rd International Particle Accelerator Conference, New Orleans, LA, 2012* (IEEE, Piscataway, NJ, 2012), p. 1329.
[8] E. D. Courant and H. S. Snyder, Theory of the alternating-gradient synchrotron, Ann. Phys. (N.Y.) **3**, 1 (1958).
[9] B. W. Montague, CERN LEP Report No. Note 165, 1979.
[10] A. Wolski, *Beam Dynamics in High Energy Particle Accelerators*, (Imperial College Press, London, 2014), p. 277.
[11] M. J. Herzberger and N. R. McClure, The design of superachromatic lenses, Appl. Opt. **2**, 553 (1963).
[12] V. Balandin, R. Brinkmann, W. Decking, and N. Golubeva, Apochromatic Twiss parameters of drift-quadrupole systems with symmetries, in *Proceedings of the 2nd International Particle Accelerator Conference, San Sebastián, Spain, 2011* (EPS-AG, Spain, 2011), p. 2163.
[13] F. C. Iselin, The MAD Program: Physical Methods Manual, 1994.
[14] R. Ruth, A. W. Chao, P. L. Morton, and P. B. Wilson, Report No. SLAC-PUB-3374, 1985.
[15] T. Tajima and J. M. Dawson, Laser Electron Accelerator, Phys. Rev. Lett. **43**, 267 (1979).
[16] E. Adli, J. P. Delahaye, S. J. Gessner, M. J. Hogan, T. O. Raubenheimer, W. An, C. Joshi, and W. Mori, A beam driven plasma-wakefield linear collider: From Higgs factory to multi-TeV, arXiv:1308.1145.
[17] X. L. Xu *et al.*, Exact phase space matching for staging plasma and traditional accelerator components using longitudinally tailored plasma profiles, arXiv:1411.4386.
[18] J. van Tilborg *et al.*, Active Plasma Lensing for Relativistic Laser-Plasma-Accelerated Electron Beams, Phys. Rev. Lett. **115**, 184802 (2015).
[19] M. Borland, User's Manual for Elegant, 2012.
[20] P. Raimondi and A. Seryi, Novel Final Focus Design for Future Linear Colliders, Phys. Rev. Lett. **86**, 3779 (2001).
[21] F. Su *et al.*, CEPC partial double ring lattice design, in *Proceedings of the 7th International Particle Accelerator Conference, Busan, Korea, 2016* (JACoW, Geneva, 2016), p. 3785.
[22] K. Oide *et al.*, Design of beam optics for the FCC-ee collider ring, in *Proceedings of the 7th International Particle Accelerator Conference, Busan, Korea, 2016* (JACoW, Geneva, 2016), p. 3821.

A.3 Staging optics considerations for a plasma wakefield acceleration linear collider

Authors

C. A. Lindstrøm, E. Adli, J. M. Allen, J. P. Delahaye, M. J. Hogan, C. Joshi, P. Muggli, T. O. Raubenheimer and V. Yakimenko

Journal

Nucl. Instrum. Methods Phys. Res. A **829**, 224 (2016)

Abstract

Plasma wakefield acceleration offers acceleration gradients of several GeV/m, ideal for a next-generation linear collider. The beam optics requirements between plasma cells include injection and extraction of drive beams, matching the main beam beta functions into the next cell, canceling dispersion as well as constraining bunch lengthening and chromaticity. To maintain a high effective acceleration gradient, this must be accomplished in the shortest distance possible. A working example is presented, using novel methods to correct chromaticity, as well as scaling laws for a high energy regime.

(5 pages)

Nuclear Instruments and Methods in Physics Research A 829 (2016) 224–228

Contents lists available at ScienceDirect

Nuclear Instruments and Methods in Physics Research A

journal homepage: www.elsevier.com/locate/nima

Staging optics considerations for a plasma wakefield acceleration linear collider

C.A. Lindstrøm [a,b,*], E. Adli [a,b], J.M. Allen [b], J.P. Delahaye [b], M.J. Hogan [b], C. Joshi [d], P. Muggli [c], T.O. Raubenheimer [b], V. Yakimenko [b]

[a] Department of Physics, University of Oslo, Oslo 0316, Norway
[b] SLAC National Accelerator Laboratory, Menlo Park, CA 94025, USA
[c] Max Planck Institute for Physics, 80805 Munich, Germany
[d] Department of Electrical Engineering, UCLA, Los Angeles, CA 90095, USA

ARTICLE INFO

Available online 13 January 2016

Keywords:
PWFA
Staging
Emittance preservation
Beam optics
Linear collider

ABSTRACT

Plasma wakefield acceleration offers acceleration gradients of several GeV/m, ideal for a next-generation linear collider. The beam optics requirements between plasma cells include injection and extraction of drive beams, matching the main beam beta functions into the next cell, canceling dispersion as well as constraining bunch lengthening and chromaticity. To maintain a high effective acceleration gradient, this must be accomplished in the shortest distance possible. A working example is presented, using novel methods to correct chromaticity, as well as scaling laws for a high energy regime.

1. Introduction

A demand for TeV-scale electron–positron colliders has resulted in linear collider design studies which, if built, will be tens of kilometers long and cost billions of dollars. This has motivated an interest in cheaper and more compact accelerator technologies seeking to provide higher acceleration gradients.

Plasma wakefield acceleration (PWFA) is one of several new concepts, in which two consecutive charged particle beams are sent through a plasma, quickly and efficiently transferring energy from one beam (the drive beam) to the other (the main beam). These beams need to be very small, both transversely and longitudinally, in order to excite a sufficiently large electric field (the wakefield) to form an accelerating cavity in the plasma.

In order for the main beam to reach energies significantly higher than that of the drive beam, this process must be repeated in multiple stages. The plasma cells must be separated by beam optics which swaps out the depleted drive beam and focuses the diverging main beam back into the next cell. Since a shorter optics section gives a higher effective acceleration gradient, it is important to minimize its length.

2. Requirements

A linear collider requires very low emittance beams to reach the luminosity target. In order to preserve these emittances, all the way to the interaction point, a number of requirements must be met by the optics section between plasma cells. The goal is to find the shortest lattice which satisfy all these requirements.

We will assume beam and plasma parameters as defined in the PWFA linear collider study [1], where plasma cells operate in the non-linear blowout regime [2]. The main beam has an rms energy spread σ_E around 1%, a bunch length of $\sigma_z = 20$ μm, and normalized emittances of $\epsilon_{N,x} = 10$ μm and $\epsilon_{N,y} = 35$ nm. The drive beam has energy $E_d = 25$ GeV, and the plasma has an electron density of $n_p = 2 \times 10^{16}$ cm^{-3}, providing a gain of $\Delta E = 25$ GeV per cell. The emittance budget requires each stage to preserve emittance to the 1%-level.

2.1. Drive beam injection and extraction

Injecting the drive beam only a few 100 μm in front of the main beam is too short for any kicker. However, dipoles can be used to combine and separate the two beams by utilizing their difference in energy.

2.2. Beta matching

The plasma cavity formed by the drive beam has strong linear focusing forces. If the β-function of the main beam is not properly

* Corresponding author.
E-mail address: c.a.lindstrom@fys.uio.no (C.A. Lindstrøm).

http://dx.doi.org/10.1016/j.nima.2015.12.065
0168-9002/

matched [2], the beam envelope will oscillate and the projected emittance increases. The Twiss [3] matching condition at the plasma cell is

$$\beta_x = \beta_y = \beta_{mat} = \frac{\sqrt{2\gamma}}{k_p}, \tag{1}$$

$$\alpha_x = \alpha_y = 0, \tag{2}$$

where k_p is the plasma wavenumber and γ is the Lorentz factor. For our parameters, $\beta_{mat} = 2.3$ cm at 100 GeV.

2.3. Dispersion cancellation

The drive beam injection/extraction dipoles also disperse the main beam, due to its energy spread. Very small emittances require cancellation of dispersion:

$$D_x = D_x' = 0, \tag{3}$$

where D_x is the first-order dispersion. Higher order dispersions may also require cancellation to avoid emittance growth.

2.4. Isochronicity

The dipoles form a chicane with a non-zero longitudinal dispersion R_{56}. This leads to bunch lengthening or compression, which alters beam loading and the energy spread might increase. To avoid this we require

$$R_{56} \ll \frac{\sigma_z}{\sigma_E}, \tag{4}$$

which is $O(1\text{ mm})$ for our parameters.

2.5. Chromaticity cancellation

Placing quadrupoles immediately before and after the plasma will focus the drive and main beams differently due to their energy difference, hence injection/extraction dipoles should be placed between the plasma and quadrupoles. However, this allows tightly focused main beams to diverge significantly after exiting the plasma, resulting in a large chromatic amplitude W. Since emittance growth from chromaticity is given by $\Delta\epsilon/\epsilon_0 = 1/2W^2\sigma_E^2 + O(\sigma_E^4)$, we require

$$W_x = W_y = 0, \tag{5}$$

in which case the σ_E^4-term will dominate chromatic emittance growth.

3. Drive beam injection and extraction

3.1. Symmetry between injection and extraction

After plasma interaction, particles in the rear of the drive beam will have lost a significant fraction of their energy, but those in the front will remain at the injected energy. We assume that injection and extraction may be treated as inverse processes using the same optics, but in reverse order. This enforces either a mirror symmetric (C) or rotationally (S) symmetric chicane (Fig. 1). The C-chicane has less total bending, producing less synchrotron radiation, whereas the S-chicane places injection and extraction on opposite sides, freeing up space for beam dumps and diverting radiation away from drive beam distribution and injection systems.

3.2. Injection/extraction dipole length

In order to reduce chromaticity, the distance to the first quadrupole should be minimized. The two beams will separate in the dipole by a distance

$$\Delta x = \frac{1}{2} l_d^2 Bce\left(\frac{1}{E_d} - \frac{1}{E_m}\right), \tag{6}$$

where l_d is the dipole length, B is the dipole magnetic field strength, and E_m is the main beam energy.

A defocusing quadrupole placed next to the dipole can be used to further separate the beams, hence shortening the necessary dipole length. However, it also focuses the drive beam and leads to larger dispersion. Injector/extractor design has not been studied in detail in this work.

3.3. Dispersion cancellation

Although C and S-chicanes intrinsically cancel dispersion, they do not in the presence of quadrupoles. This can be corrected by either appropriately matching quadrupoles or by introducing extra dipoles. However, quadrupole dispersion matching is not independent of beta and chromaticity matching, further complicating their simultaneous matching. Adding extra dipoles allows dispersion cancellation independently of quadrupole matching.

Using a mirror symmetric quadrupole lattice, a single extra dipole per side is necessary, satisfying $D_x' = 0$ for C-chicanes or $D_x = 0$ for S-chicanes at the point of symmetry.

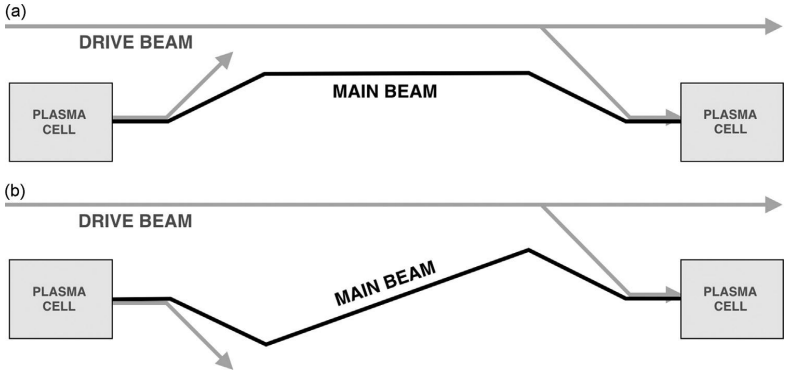

Fig. 1. Symmetric layouts for injection/extraction dipoles. A mirror symmetric C-chicane is shown in (a), and a rotationally symmetric S-chicane is shown in (b).

3.4. R_{56} correction

The longitudinal dispersion R_{56} is given by [4]

$$R_{56} = \int \frac{D_x(s)}{\rho(s)}\, ds, \tag{7}$$

where ρ is the bending radius, indicating that the longitudinal dispersion can be decreased by placing dipoles in regions of low D_x, and canceled by introducing new dipoles with opposing R_{56}.

4. Main beam focusing and emittance preservation

4.1. Beta matching

Symmetry dictates that quadrupoles must form either a longitudinally mirror symmetric (same polarity) or anti-symmetric (opposite polarity) lattice. If both injection and extraction require assistive defocusing quadrupoles, the lattice cannot be anti-symmetric.

Matching α and β-functions in both planes requires in general four degrees of freedom; e.g. four quadrupoles. Only two degrees of freedom are required for symmetric lattices ($\alpha_x = \alpha_y = 0$ or $\beta_x = \beta_y$, $\alpha_x = -\alpha_y$ at the symmetry point), which greatly simplifies matching.

Using plasma density ramps [5], which adiabatically relaxes the β-function, it may be possible to match to an order of magnitude larger β. This dramatically improves chromaticity (as $W \sim \beta_{quads} \sim 1/\beta_{mat}$) as well as dispersion tolerances.

4.2. Chromaticity correction

Chromaticity is conventionally corrected using sextupoles. Although very effective, sextupoles require large dispersion and introduce non-linear terms whose cancellation result in more complex lattices. Since dispersion needs to stay constant with energy, dipoles must get longer or stronger, resulting in a poor synchrotron radiation scaling with main beam energy. Motivated by this, a novel method was developed to correct chromaticity using linear lattices only [6], giving both shorter lattices and a better energy scaling.

5. Working example

A working example for a high main beam energy of 500 GeV is shown in Fig. 2; a 39 m long C-chicane with 8 quadrupoles and 5 dipoles. This example assumes an energy spread of 0.5%, a 1 m injection/extraction dipole with field strength 1 T, quadrupole field gradients 95 T/m, and a plasma density ramp β-magnification of 15, giving an effective $\beta_{mat} = 79$ cm. Note that this is neither a general nor an optimized solution.

Particle tracking in Elegant [7] (Fig. 3), shows that emittance growth due to chromaticity is just 0.03% and 0.04% in x and y respectively, and the bunch length is preserved with $R_{56} = 1.2$ μm. Emittance growth in x from second-order dispersion is 2%. However, at 1% energy spread, this emittance growth is 40%. In addition, this problem gets worse at lower energies as dispersion increases, indicating that second-order dispersion needs to be actively canceled to achieve a higher energy acceptance. This will be addressed in further work.

6. Scaling laws

Since the drive beam energy stays constant, dipoles will bend the main beam less at higher energies. In addition, quadrupoles must increase in length to still focus the main beam. We can identify two regimes, where E_d and E_m are the drive and main beam energies respectively:

1. Low energy ($O(E_m) = O(E_d)$): dominated by relatively strong dipoles.
2. High energy ($E_m \gg E_d$): dipoles are weak and quadrupoles dominate the lattice.

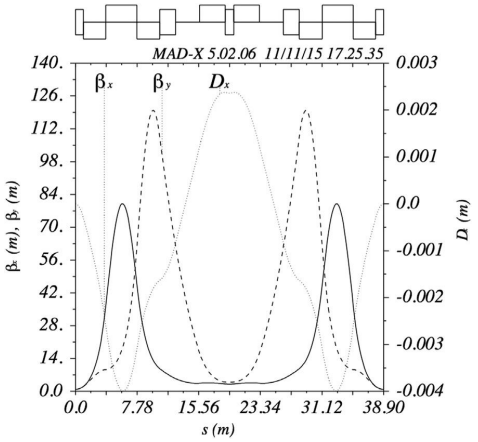

Fig. 2. Working example for 500 GeV, where 5 dipoles and 8 quadrupoles form a 39 m long C-chicane. Chromaticity is canceled by a linear lattice without sextupoles, however an uncorrected second-order dispersion leads to a 2% emittance growth.

6.1. Low energy regime

Dipoles produce large dispersion, demanding higher order cancellation. In addition, the length of injection/extraction dipoles is larger relative to β_{mat}, which requires chromaticity to also be canceled to higher order. This results in complex lattices custom made for each energy, with no clear scaling. In this case, with large dispersions and low energies, a solution using sextupoles may be favorable.

6.2. High energy regime

Assuming a constant quadrupole filling factor, where all quadrupoles operate at maximum field gradient, the lattice length scales as $\sqrt{\gamma}$, where γ is the main beam Lorentz factor. Since also β_{mat} scales as $\sqrt{\gamma}$, the β-profile scales with energy without changing shape. Hence the same scaled lattice can be used for all (high) energies. Scaling laws are listed in Table 1.

Two options exist for scaling dipole lengths: constant length ($l_d = \text{const}$, $B = \text{const}$), or constant filling factor ($l_d \sim \sqrt{\gamma}$, $B \sim 1/\sqrt{\gamma}$). Based on energy loss from synchrotron radiation $W_{SR} \sim P_{SR} l_d \sim \gamma^2 B^2 l_d$, the latter is preferable ($W_{SR} \sim \gamma^{1.5}$ compared to $W_{SR} \sim \gamma^2$).

Emittance growth scales as σ_E^4 (if $W=0$), strongly encouraging lower energy spreads. Moreover, increasing the plasma density ramp magnification M_{pdr} or the quadrupole field gradient g_{max} suppresses emittance growth roughly as $1/M_{pdr}^3$ and $1/g_{max}^{1.5}$ and shortens the total lattice length by $1/\sqrt{g_{max}}$.

It is worth noting that laser wakefield acceleration (LWFA) operates in the "high energy regime" at any energy, as laser injection/extraction does not require dipoles.

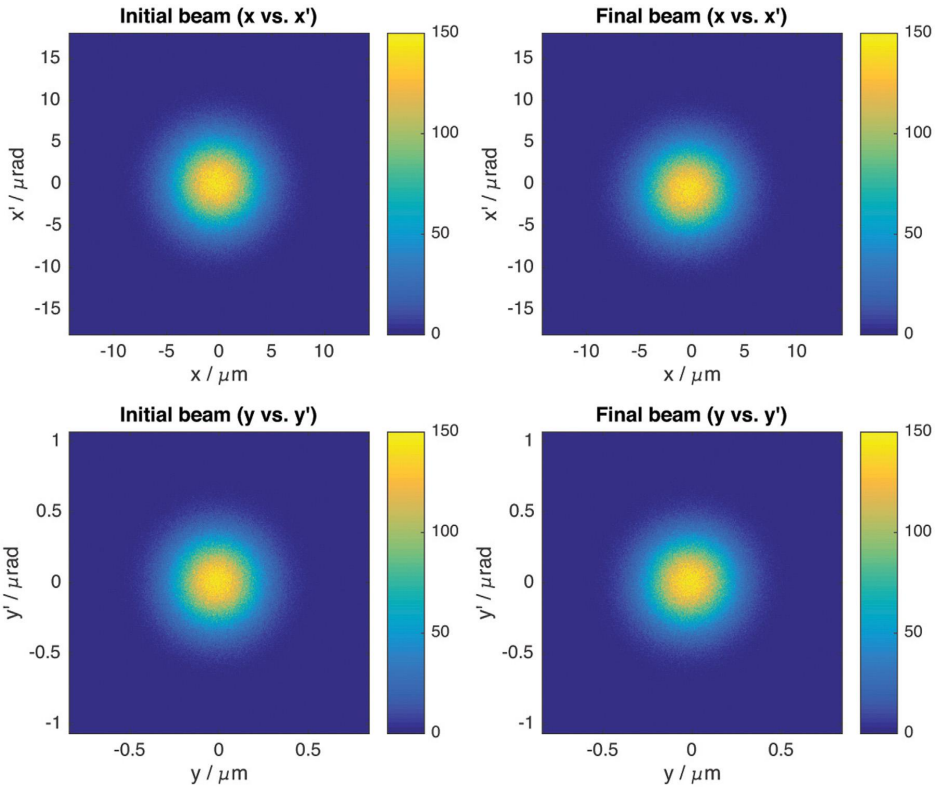

Fig. 3. Phase space in x (upper) and y (lower) for initial (left) and final beam (right) of the 0.5% rms energy spread example in Section 5, tracked in Elegant [7] using 1.5×10^6 particles. Emittance is well-preserved, however the final x-phase space (upper right) shows a small 2% emittance growth due to uncorrected second-order dispersion.

Table 1
Energy scaling laws for the high energy regime ($E_m \gg E_d$). The same lattice is used for all energies, by scaling lengths as $\sqrt{\gamma}$, where γ is the main beam Lorentz factor.

Variable	Symbol	Energy scaling
Lattice length	L	$\sqrt{\gamma}$
Dipole, quad. length	l_d, l_q	$\sqrt{\gamma}$, $\sqrt{\gamma}$
β-functions	β	$\sqrt{\gamma}$
Spot size	σ_x	$1/\sqrt[4]{\gamma}$
Dispersion	D_x	$1/\sqrt{\gamma}$
Isochronicity	R_{56}	$1/\sqrt{\gamma}$
Chromatic amplitude	W	Const.
Emittance growth	$\frac{\Delta\epsilon}{\epsilon_0}$	Const.
Quad. field gradient	g_{max}	Const.
SR power, energy loss	P_{SR}, W_{SR}	γ, $\gamma^{1.5}$

7. Further work

Further work includes finding emittance preserving lattices at lower energies by considering second-order dispersion and chromaticity cancellation, incorporating the inherent chromaticity of plasma channels ($W = \partial\beta/\partial\delta/\beta = 1/2$) into the linear lattice chromaticity correction, and studying the use of a positive R_{56} combined with the energy chirp in the plasma cavity in order to reduce the energy spread of the main beam.

8. Conclusions

The optics section between plasma cells in a staged PWFA linear accelerator needs to extract and inject drive beams using bending magnets, which sets stringent requirements on dispersion and R_{56} cancellation. Focusing of the highly diverging main beam leads to large chromaticity, which must be canceled to avoid emittance growth. Based on these constraints, using the symmetry of the system and a linear lattice without sextupoles for chromaticity correction, a high energy solution was found that meets these requirements. Scaling laws were found, which allow solutions to be scaled to very high main beam energies, however low energies will require higher order cancellation of dispersion and chromaticity for sufficient energy acceptance.

Acknowledgements

This work is supported by the Research Council of Norway.

References

[1] E. Adli, et al., A Beam Driven Plasma-Wakefield Linear Collider: From Higgs Factory to Multi-TeV, *Electronic Proceedings of the Snowmass 2013*, arXiv:1308.1145v2, 2013.

[2] J.B. Rosenzweig, et al., Physical Review A44 R6189(R), 1991.
[3] E.D. Courant and H.S. Snyder, Annals of Physics 1958.
[4] K. Wille, The Physics of Particle Accelerators (pp. 76-77), Oxford, UK: Oxford University Press, 2000.
[5] X. Xu, et al., arXiv:1411.4386v2, 2015.
[6] C.A. Lindstrøm, E. Adli, to be submitted.
[7] M. Borland, ANL Advanced Photon Source Report No. LS-287, 2000.

A.4 Measurement of transverse wakefields induced by a misaligned positron bunch in a hollow channel plasma accelerator

Authors

C. A. Lindstrøm, E. Adli, J. M. Allen, W. An, C. Beekman, C. I. Clarke, C. E. Clayton, S. Corde, A. Doche, J. Frederico, S. J. Gessner, S. Z. Green, M. J. Hogan, C. Joshi, M. Litos, W. Lu, K. A. Marsh, W. B. Mori, B. D. O'Shea, N. Vafaei-Najafabadi and V. Yakimenko

Journal

Phys. Rev. Lett. **120**, 124802 (2018)

Abstract

Hollow channel plasma wakefield acceleration is a proposed method to provide high acceleration gradients for electrons and positrons alike: a key to future lepton colliders. However, beams which are misaligned from the channel axis induce strong transverse wakefields, deflecting beams and reducing the collider luminosity. This undesirable consequence sets a tight constraint on the alignment accuracy of the beam propagating through the channel. Direct measurements of beam misalignment-induced transverse wakefields are therefore essential for designing mitigation strategies. We present the first quantitative measurements of transverse wakefields in a hollow plasma channel, induced by an off-axis 20 GeV positron bunch, and measured with another 20 GeV lower charge trailing positron probe bunch. The measurements are largely consistent with theory.

(5 pages)

Measurement of Transverse Wakefields Induced by a Misaligned Positron Bunch in a Hollow Channel Plasma Accelerator

C. A. Lindstrøm,[1,*] E. Adli,[1] J. M. Allen,[2] W. An,[3] C. Beekman,[4] C. I. Clarke,[2] C. E. Clayton,[3] S. Corde,[4] A. Doche,[4] J. Frederico,[2] S. J. Gessner,[2,†] S. Z. Green,[2] M. J. Hogan,[2] C. Joshi,[3] M. Litos,[5] W. Lu,[6] K. A. Marsh,[3] W. B. Mori,[7] B. D. O'Shea,[2] N. Vafaei-Najafabadi,[3,‡] and V. Yakimenko[2]

[1]*Department of Physics, University of Oslo, 0316 Oslo, Norway*
[2]*SLAC National Accelerator Laboratory, Menlo Park, California 94025, USA*
[3]*Department of Electrical Engineering, University of California-Los Angeles, Los Angeles, California 90095, USA*
[4]*LOA, ENSTA ParisTech, CNRS, Ecole Polytechnique, Université Paris-Saclay, 91762 Palaiseau, France*
[5]*Department of Physics, University of Colorado Boulder, Boulder, Colorado 80309, USA*
[6]*IFSA Collaborative Innovation Center, Department of Engineering Physics, Tsinghua University, Beijing 100084, China*
[7]*Department of Physics and Astronomy, University of California-Los Angeles, Los Angeles, California 90095, USA*

(Received 7 November 2017; published 23 March 2018)

Hollow channel plasma wakefield acceleration is a proposed method to provide high acceleration gradients for electrons and positrons alike: a key to future lepton colliders. However, beams which are misaligned from the channel axis induce strong transverse wakefields, deflecting beams and reducing the collider luminosity. This undesirable consequence sets a tight constraint on the alignment accuracy of the beam propagating through the channel. Direct measurements of beam misalignment-induced transverse wakefields are therefore essential for designing mitigation strategies. We present the first quantitative measurements of transverse wakefields in a hollow plasma channel, induced by an off-axis 20 GeV positron bunch, and measured with another 20 GeV lower charge trailing positron probe bunch. The measurements are largely consistent with theory.

DOI: 10.1103/PhysRevLett.120.124802

Precision tests of the standard model of particle physics can be performed with a linear electron-positron collider. However, these machines will be very large and expensive to build. Plasma wakefield acceleration (PWFA) [1–3] is a promising new technique for building a more compact, more cost-effective accelerator: an intense charged particle bunch is propagated through a uniform plasma, where it induces a highly nonlinear wake structure with strong accelerating and focusing fields. While this mechanism has been shown to sustain large acceleration gradients [4] and high energy transfer efficiency [5] for a second trailing electron bunch, the success does not immediately extend to positrons due to the inherently charge-asymmetric response of nonlinear plasmas. Positron bunches have been transported through and accelerated by meter long plasma wakes [6–9]. However, the extremely nonlinear focusing fields of such wakes make it very difficult to preserve the emittance of the accelerating beam [10].

A possible solution for symmetrizing the acceleration of electrons and positrons while preserving the emittance is to use a hollow channel surrounded by an annular plasma [11–13]. This is so because a drive bunch propagating exactly on the channel axis drives an oscillating longitudinal wakefield that moves synchronously with the beam and is transversely uniform, while the transverse (deflecting) wakefield is zero everywhere in the channel. This method [14] has been experimentally demonstrated to accelerate positrons [15]. However, if the bunch propagates off-axis, it is expected to induce a strong dipolelike transverse wakefield that deflects both the drive beam and the accelerating trailing beam away from the axis. This leads to significantly reduced collider luminosity or even beam loss.

In this Letter, we present the first experimental measurements of transverse wakefields in a hollow channel plasma accelerator, performed at the Facility for Advanced aCcelerator Experimental Tests (FACET) [16] at SLAC National Accelerator Laboratory. The plasma channel was formed by ionizing lithium vapor with the high power FACET laser [17], which delivered a maximum of 10 mJ on target in as little as 50 fs (full width at half maximum). A high-order Bessel intensity profile (J_7^2) with the first maximum at 250 μm was obtained using a kinoform optic that focused the laser close to the center of a 46 cm heat-pipe oven [18], giving a 25 ± 1 cm long hollow channel.

The vapor pressure was set to 3.4 Torr at temperature 1095 K, giving a neutral vapor density of 3×10^{16} cm^{-3}. The laser pulse energy was attenuated to ionize only the channel wall, ensuring a truly zero plasma density on axis. A 20.35 GeV two-bunch positron beam was synchronized to arrive a few picoseconds after the laser pulse. The two bunches were obtained from a single bunch by giving it a head-to-tail energy chirp and energetically dispersing it onto a beam notching device, allowing a tunable bunch separation up to 600 μm. The positron beam was focused at the channel center with rms beam sizes $\sigma_x = 35$ and $\sigma_y = 25$ μm and beta functions $\beta_x = 0.5$ and $\beta_y = 5$ m, which ensured that the beam size was approximately constant throughout the channel. A total charge of 0.51 ± 0.04 nC, sufficiently low to not ionize the on-axis lithium vapor, was distributed between the leading drive bunch and the trailing probe bunch with a ratio $(4.1 \pm 1.1):1$.

The experiment consisted of measuring the transverse wakefield in a hollow plasma channel by observing the angular deflection of the probe bunch caused by an offset channel. In particular, the longitudinal variation of the transverse wakefield was measured by means of a bunch separation scan. Figure 1 shows the experimental setup. Although the two bunches originated from one bunch, scanning the bunch separation was possible by stretching the bunch and adjusting the beam notching device [5]. An electro-optical sampler (EOS) was used to measure the longitudinal bunch profile of the incoming beam, and an yttrium aluminum garnet (YAG) crystal in a horizontally dispersive region functioned as an upstream energy spectrometer for the positron beam. Two beam position monitors (BPMs) were used to measure the beam trajectory. Downstream of the channel, a nondestructive YAG screen was used to measure the transverse profile of the outgoing beam. A spectrometer with a vertically dispersive dipole magnet and a phosphorescent LANEX screen was used to measure energy changes of the probe bunch. Two quadrupole magnets were adjusted such that deflections by transverse fields induced in the channel were canceled in the vertical plane for increased energy resolution, but not completely in the horizontal plane to allow angular deflection measurements of the probe bunch. The offset of the channel, which was varied by a random laser pointing jitter, was measured downstream by imaging the laser profile at multiple object planes using cameras at different distances from the same lens.

The expected wakefields can be modeled by assuming the plasma behaves like a nonevolving dielectric medium [12] and that the timescale of the evolution of the beam is long compared to that of the wakefields (quasistatic approximation). Reference [15] shows that this results in a single-particle longitudinal wakefield dominated by the fundamental $m = 0$ mode, where m denotes the azimuthal index, which is cosinelike in the comoving longitudinal coordinate z,

$$W_{z0}(z) = -\frac{ek_p\chi_\parallel^2}{2\pi\epsilon_0 a}\frac{B_{00}(a,b)}{B_{10}(a,b)}\cos(\chi_\parallel k_p z)\Theta(z). \quad (1)$$

Here e is the positron charge, ϵ_0 is the vacuum permittivity, k_p is the plasma wave number, a and b are the channel inner and outer radii, $\Theta(z)$ is the Heaviside step function, and

$$\chi_\parallel = \sqrt{\frac{2B_{10}(a,b)}{2B_{10}(a,b) - k_p a B_{00}(a,b)}} \quad (2)$$

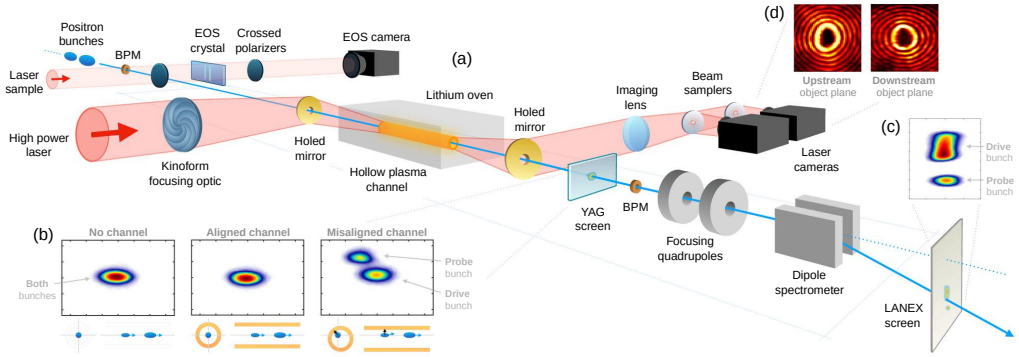

FIG. 1. (a) Experimental setup: Two positron bunches first pass an electro-optical sampler. A Ti:sapphire laser focused with a kinoform into a lithium vapor oven produces the hollow plasma channel. Two beam position monitors measure the trajectory of the beam and an yttrium aluminum garnet screen is used to measure the transverse profile (b). A dipole spectrometer with two quadrupoles focuses the beam onto a LANEX screen for energy and angular deflection measurements (c) before it is dumped. Meanwhile, the outgoing laser pulse is focused onto cameras imaging the kinoform profile (d) at different object planes inside the channel, which appears asymmetric due to aberrations induced by the transmissive optics. The upstream spectrometer does not appear in this figure.

is a longitudinal wavelength modification factor using the "Bessel-boundary function,"

$$B_{ij}(a,b) = I_i(k_p a)K_j(k_p b) + (-1)^{i-j+1} I_j(k_p b)K_i(k_p a).$$

The most significant mode of the single-particle transverse wakefield is the sinelike $m = 1$ dipole mode

$$W_{x1}(z) = -\frac{e\Delta x \chi_\perp}{\pi\epsilon_0 a^3}\frac{B_{11}(a,b)}{B_{21}(a,b)}\sin(\chi_\perp k_p z)\Theta(z), \quad (3)$$

whose amplitude is in the direction of the transverse offset Δx of the driving particle and where

$$\chi_\perp = \sqrt{\frac{2B_{21}(a,b)}{4B_{21}(a,b) - k_p a B_{11}(a,b)}} \quad (4)$$

is a transverse wavelength modification factor. Wakefields from arbitrary longitudinal bunch profiles can be obtained by convolving the single-particle wakefield with the particle distribution.

More detailed estimates of the expected wakefields can be obtained from particle-in-cell (PIC) simulations. Figure 2 shows a QuickPIC [19] simulation of a transversely offset beam in a hollow plasma channel using parameters from the experiment. Note the discrepancy between theory and simulation in the transverse wakefield. This is caused by electrons in the wall being pulled into the channel (numerically validated with OSIRIS [20]), which breaks the assumption of a nonevolving medium.

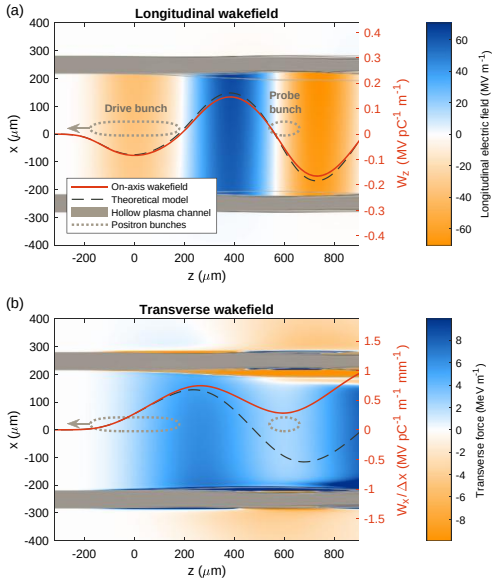

FIG. 2. PIC simulation using experimental parameters: a hollow channel with 215 μm inner and 280 μm outer radius at density 3×10^{15} cm^{-3}, driven by a 0.41 nC drive bunch transversely offset by 20 μm and probed by a 0.1 nC probe bunch at a bunch separation of 600 μm. The high beam energy ensures that both the beam and the longitudinal (a) and transverse wakefields (b) stay approximately constant throughout the channel. The on-axis wakefields (red lines) are consistent with the model (black dashed lines) in the longitudinal, but diverges from the modeled transverse wakefield when electrons are pulled into the channel.

In addition to a direct measurement, a second independent measurement of the transverse wakefield can be made using the longitudinal wakefield via the Panofsky-Wenzel theorem [21], which states that

$$\frac{\partial W_x}{\partial z} = \frac{\partial W_z}{\partial x}. \quad (5)$$

Since the $m = 0$ mode of the longitudinal wakefield [Eq. (1)] cancels due to no x dependence, we must include the much smaller amplitude $m = 1$ mode [15]

$$W_{z1}(z,x) = -\frac{xe\Delta x \chi_\perp^2 k_p}{\pi\epsilon_0 a^3}\frac{B_{11}(a,b)}{B_{21}(a,b)}\cos(\chi_\perp k_p z)\Theta(z). \quad (6)$$

Integrating Eq. (5) with respect to z gives to lowest order

$$W_x(z) = \int_0^z \frac{\partial W_{z1}(z',x)}{\partial x} dz'. \quad (7)$$

Since for our parameters $\chi_\perp \approx \chi_\parallel$, we can relate the x derivative of W_{z1} to the measured $W_z \approx W_{z0}$ by comparing only their amplitudes. This gives the approximate relation

$$\frac{\partial W_{z1}}{\partial x} \approx -\frac{\Delta x}{a^2}\kappa(a,b)W_z, \quad (8)$$

where we have simplified the numerical coefficients to

$$\kappa(a,b) = \frac{4\chi_\perp^2 - 2}{\chi_\parallel^2 - 1}. \quad (9)$$

Finally, we arrive at an equation which allows us to use the longitudinal wakefield to estimate the transverse wakefield per offset,

$$\frac{W_x(z)}{\Delta x} \approx -\frac{\kappa(a,b)}{a^2}\int_0^z W_z(z')dz'. \quad (10)$$

Experimentally, the longitudinal wakefield per particle at the location of the probe bunch z_{PB} can be determined by the probe bunch energy change δE_{PB}, normalized by the charge of the drive bunch Q_{DB},

$$W_z(z_{\mathrm{PB}}) = \frac{\delta E_{\mathrm{PB}}}{L_c Q_{\mathrm{DB}}}, \quad (11)$$

where we have assumed that the channel is uniform along its length L_c and beam loading [22] is ignored.

Transverse wakefields depend on the transverse offset of the drive bunch. An offset from the channel axis by distance Δx drives a transverse wakefield $W_x \propto \Delta x$ [see Eq. (3)], giving the probe bunch an angular deflection $\Delta x'$. Applying

Newton's second law to particles of energy E_{PB} (large compared to their energy change), we can express the transverse wakefield per particle per offset as

$$\frac{W_x(z_{\mathrm{PB}})}{\Delta x} = \frac{\Delta x'}{\Delta x Q_{\mathrm{DB}}} \frac{E_{\mathrm{PB}}}{L_c}. \tag{12}$$

The slope of the correlation $\Delta x'$ vs $\Delta x Q_{\mathrm{DB}}$ for a large number of shots was measured (see Fig. 3). Note that the offset Δx is weighted by the drive bunch charge Q_{DB} as it varied noticeably across the thousands of shots collected.

The relative beam-channel offset was mainly caused by a random transverse laser jitter of 30–40 μm rms, measured by laser cameras downstream, whereas the beam orbit in the channel was stable to 5 μm rms or less. The charge of the drive bunch was determined using the spectrometer upstream of the channel, and the angular deflection of the probe bunch in the horizontal plane as well as its energy change was measured on the spectrometer downstream. For large deflections where the offset was larger than the size of the drive bunch, the probe bunch was also visible on the YAG screen, as seen in Fig. 1(b). This was used to verify the calibration of the spectrometer angular deflection measurement.

Figure 4(a) shows the measured transverse wakefield per particle per offset for a scan of drive-to-probe bunch separations. The transverse wakefield estimated from the longitudinal wakefield [Fig. 4(b)] using the Panofsky-Wenzel theorem is also shown in Fig. 4(a) and found to be in good agreement with the measured values. Note that to minimize beam loading effects, only shots with less than 20% probe-to-drive charge ratio were used to calculate the longitudinal wakefield. The expectation from the theoretical model is found by convolving the single-particle wakefields [Eqs. (1) and (3)] with the longitudinal charge distribution measured using EOS. The plasma was found to not be fully ionized, and the plasma density was derived from the wavelength of the measured wakefields, which only depends on the plasma density and the well-known radius of the channel. This measurement implies 10% ionization (3×10^{15} cm^{-3}), which is also consistent with known laser parameters.

Both measurements are largely in agreement with the theoretical model, but diverge somewhat at larger bunch

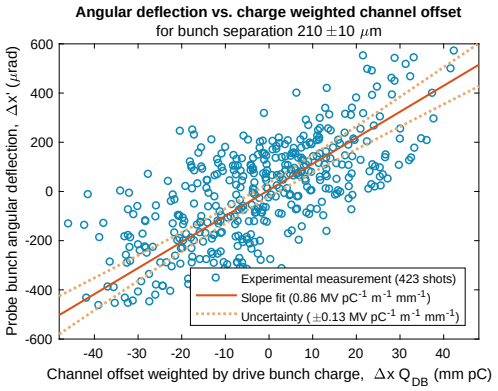

FIG. 3. Correlation between probe bunch angular deflection and channel offset weighted by drive bunch charge from a random laser pointing and charge jitter, for the third step (210 ± 10 μm) of the bunch separation scan. The linear trend line corresponds to a transverse wakefield $W_x/\Delta x = 0.86 \pm 0.13$ MV pC^{-1} m^{-1} mm^{-1}, where the uncertainty is defined by the rms from the trend line increasing by 3%. The error of each shot is negligible compared to the spread of the data points, caused by a combination of jitters in beam orbit, beam energy, bunch separation, plasma density, and channel length.

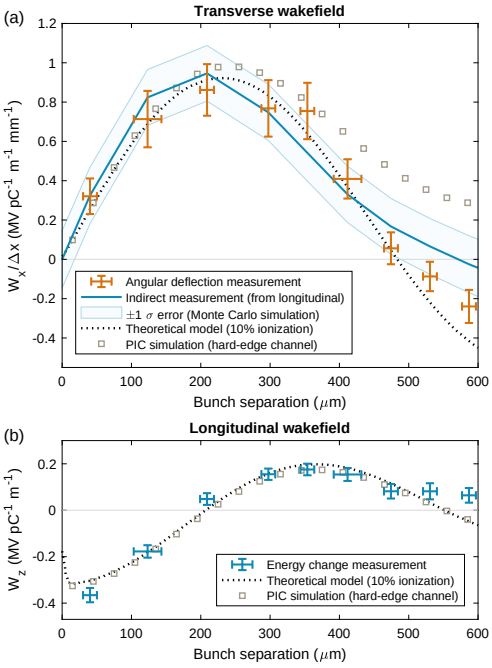

FIG. 4. (a) Transverse wakefield from direct measurements (red crosses) and indirectly estimated via the Panofsky-Wenzel theorem (blue line) against bunch separation measured using EOS. Both measurements are initially consistent with theory (dotted black line), but diverge somewhat for larger separations, although not quite matching QuickPIC simulations (gray squares). Notice that the slope in Fig. 3 is represented by the third data point. (b) The longitudinal wakefield (blue crosses), largely consistent with theory, is the basis of the indirect transverse wakefield estimate using Eq. (10). The longitudinal wakefield error, dominated by spectrometer resolution (±1 pixel), is Monte Carlo simulated to find the indirect measurement error [blue area in (a)].

separations. This behavior is expected from the nonlinear response of a plasma [see Fig. 2(b)]; however, the measured transverse wakefield does not quite match PIC simulations. We have investigated the effect of more complex radial plasma density profiles, including softer channel walls, but no simulation was found to fully account for the observed discrepancy.

This measurement shows that a hollow plasma channel generally has the expected transverse wakefield when beams are misaligned with respect to the channel axis. Note, however, that this is mainly an intrabunch problem, as the deflection of the accelerated bunch can potentially be canceled by placing it at the zero crossing of the transverse wakefield (i.e., close to 500 μm bunch separation in this measurement). Nevertheless, the issue of transverse deflection of off-axis beams remains, which sets stringent limits on misalignment if used for TeV-scale energy gain. To alleviate this problem, suppression mechanisms must be applied. Suggestions include external focusing or using trains of multiple drive bunches [12], where the longitudinal wakefield is resonantly driven, but the transverse wakefield is not. These and other mechanisms should be further explored to determine whether hollow plasma channels are suitable for high gradient acceleration of positrons.

In summary, the transverse wakefield induced by a misaligned positron bunch in a hollow plasma channel has been measured for the first time. These measurements are critical for devising mitigation strategies and alignment tolerances when using hollow plasma channels as accelerating structures.

The FACET E200 plasma wakefield acceleration experiment was built and has been operated with funding from the United States Department of Energy. Work at SLAC was supported by DOE Contract No. DE-AC02-76SF00515 and also through the Research Council of Norway (Grant No. 230450). Work at UCLA was supported by DOE Contract No. DE-SC0010064 and NSF Contract No. PHY-1415386. Simulations were performed on the UCLA Hoffman2 cluster through NSF OCI-1036224. Simulation work at UCLA was supported by DOE Contracts No. DE-SC0008491 and No. DE-SC0008316, and NSF Contracts No. ACI-1339893 and No. PHY-0960344. The work of C. B., S. C., and A. D. was supported by the European Research Council (M-PAC project, Contract No. 715807) and by the France-Stanford Center for Interdisciplinary Studies. The work of W. L. was partially supported by NSFC 11425521, 11535006, 11175102, and the National Basic Research Program of China Grant No. 2013CBA01501.

*c.a.lindstrom@fys.uio.no
†Present address: CERN, Geneva, Switzerland.
‡Present address: Department of Physics and Astronomy, Stony Brook University, Stony Brook, New York 11794, USA.

[1] P. Chen, J. M. Dawson, R. W. Huff, and T. Katsouleas, Phys. Rev. Lett. **54**, 693 (1985).
[2] R. D. Ruth, A. W. Chao, P. L. Morton, and P. W. Wilson, Part. Accel. **17**, 171 (1985).
[3] C. Joshi and T. Katsouleas, Phys. Today **56**, No. 6, 47 (2003).
[4] I. Blumenfeld *et al.*, Nature (London) **445**, 741 (2007).
[5] M. Litos *et al.*, Nature (London) **515**, 92 (2014).
[6] M. J. Hogan *et al.*, Phys. Rev. Lett. **90**, 205002 (2003).
[7] B. Blue *et al.*, Phys. Rev. Lett. **90**, 214801 (2003).
[8] S. Corde *et al.*, Nature (London) **524**, 442 (2015).
[9] A. Doche *et al.*, Sci. Rep. **7**, 14180 (2017).
[10] P. Muggli *et al.*, Phys. Rev. Lett. **101**, 055001 (2008).
[11] T. C. Chiou, T. Katsouleas, C. Decker, W. B. Mori, J. S. Wurtele, G. Shvets, and J. J. Su, Phys. Plasmas **2**, 310 (1995).
[12] C. B. Schroeder, D. H. Whittum, and J. S. Wurtele, Phys. Rev. Lett. **82**, 1177 (1999).
[13] W. D. Kimura, H. M. Milchberg, P. Muggli, X. Li, and W. B. Mori, Phys. Rev. ST Accel. Beams **14**, 041301 (2011).
[14] S. J. Gessner *et al.*, Nat. Commun. **7**, 11785 (2016).
[15] S. J. Gessner, Ph.D. thesis, Stanford University, Palo Alto, California, 2016.
[16] M. J. Hogan *et al.*, New J. Phys. **12**, 055030 (2010).
[17] S. Z. Green *et al.*, Plasma Phys. Controlled Fusion **56**, 084011 (2014).
[18] P. Muggli, K. A. Marsh, S. Wang, C. E. Clayton, S. Lee, T. C. Katsouleas, and C. Joshi, IEEE Trans. Plasma Sci. **27**, 791 (1999).
[19] W. An, V. K. Decyk, W. B. Mori, and T. M. Antonsen, Jr., J. Comput. Phys. **250**, 165 (2013), https://github.com/UCLA-Plasma-Simulation-Group/QuickPIC-OpenSource.
[20] R. A. Fonseca *et al.*, Lect. Notes Comput. Sci. 2329 (Springer-Verlag, Heidelberg, 2002), p. III-342.
[21] W. K. H. Panofsky and W. A. Wenzel, Rev. Sci. Instrum. **27**, 967 (1956).
[22] T. Katsouleas, Phys. Rev. A **33**, 2056 (1986).

A.5 Analytic plasma wakefield limits for active plasma lenses

Authors

Carl A. Lindstrøm and Erik Adli

Journal

Submitted to Phys. Rev. Accel. Beams, arXiv:1802.02750 (2018)

Abstract

Active plasma lensing is a promising technology for compact focusing of particle beams that has seen a recent surge of interest. While these lenses can provide strong focusing gradients of order kT/m and focusing in both transverse planes, there are limitations from nonlinear aberrations, causing emittance growth in the beams being focused. One cause of such aberrations is beam- driven plasma wakefields, present if the beam density is sufficiently high. We develop simple, but powerful analytic formulas for the effective focusing gradient from these wakefields, and use this to set limits on which parts of the beam and plasma parameter space permits distortion-free use of active plasma lenses. It is concluded that the application of active plasma lenses to conventional and plasma-based linear colliders may prove very challenging, except perhaps in the final focus system, unless the typical discharge currents used are dramatically increased, and that in general these lenses are better suited for accelerator applications with lower beam intensities.

(10 pages)

A.6 Overview of the CLEAR plasma lens experiment

Authors

C. A. Lindstrøm, K. N. Sjobak, E. Adli, J.-H. Röckemann, L. Schaper, M. Meisel, G. Boyle, J. Osterhoff, A. E. Dyson, S. M. Hooker, W. Farabolini, D. Gamba and R. Corsini

Journal

Nucl. Instrum. Methods Phys. Res. A **909**, 379 (2018)

Abstract

Discharge capillary-based active plasma lenses are a promising new technology for strongly focusing charged particle beams, especially when combined with novel high gradient acceleration methods. Still, many questions remain concerning such lenses, including their transverse field uniformity, limitations due to plasma wakefields and whether they can be combined in multi-lens lattices in a way to cancel chromaticity. These questions will be addressed in a new plasma lens experiment at the CLEAR User Facility at CERN. All the subsystems have been constructed, tested and integrated into the CLEAR beam line, and are ready for experiments starting late 2017.

(4 pages)

Nuclear Inst. and Methods in Physics Research, A 909 (2018) 379–382

Contents lists available at ScienceDirect

Nuclear Inst. and Methods in Physics Research, A

journal homepage: www.elsevier.com/locate/nima

Overview of the CLEAR plasma lens experiment

C.A. Lindstrøm [a,*], K.N. Sjobak [a], E. Adli [a], J.-H. Röckemann [b], L. Schaper [b], J. Osterhoff [b], A.E. Dyson [c], S.M. Hooker [c], W. Farabolini [d], D. Gamba [d], R. Corsini [d]

[a] Department of Physics, University of Oslo, 0316 Oslo, Norway
[b] DESY, Notkestraße 85, 22607 Hamburg, Germany
[c] University of Oxford, Clarendon Laboratory, Parks Road, Oxford OX1 3PU, United Kingdom
[d] CERN, Geneva, Switzerland

ARTICLE INFO

Keywords:
Active plasma lens
Discharge capillary
Compact Marx Bank
CLEAR user facility

ABSTRACT

Discharge capillary-based active plasma lenses are a promising new technology for strongly focusing charged particle beams, especially when combined with novel high gradient acceleration methods. Still, many questions remain concerning such lenses, including their transverse field uniformity, limitations due to plasma wakefields and whether they can be combined in multi-lens lattices in a way to cancel chromaticity. These questions will be addressed in a new plasma lens experiment at the CLEAR User Facility at CERN. All the subsystems have been constructed, tested and integrated into the CLEAR beam line, and are ready for experiments starting late 2017.

1. Introduction

Recent novel accelerator research has delivered several intriguing technologies, some of which can provide accelerating fields of several GV/m, paving the way to building significantly more compact particle accelerators. Many of these emerging concepts, e.g. plasma wakefield accelerators [1,2] or direct laser accelerators [3], require tightly focused input beams. Unless the components used to focus particle beams are also made more compact, not much will be gained from these advances.

Active plasma lensing is a promising technique providing strong and compact focusing, and has already been used in high gradient accelerator staging [4]. After breaking down a diffuse gas to a plasma, a large on-axis current density is used to form a radially increasing azimuthal magnetic field which, unlike a quadrupole, provides focusing in both planes simultaneously. Such a device, typically a thin gas filled capillary with high voltage electrodes on either side, can readily create magnetic field gradients upwards of kT/m [5].

Although finding stronger focusing elements is necessary, it is not sufficient for compact staging of advanced accelerator structures. Highly divergent beams and %-level energy spreads imply that the chromaticity of the staging optics needs to be controlled [6]. Typically this requires sextupoles, however these magnets have other adverse effects on the beam. The newly developed concept of apochromatic focusing [7] is therefore of interest, where only a lattice of linear optics lenses (like quadrupoles or active plasma lenses) are used to cancel chromaticity at specific locations in the beam line. In this paper, we outline an ongoing experiment aimed at eventually demonstrating such an apochromatic lattice of active plasma lenses, as a path towards compact and chromatically controlled staging of high gradient accelerators.

2. Experimental goals

The ultimate goal of demonstrating an apochromatic plasma lens lattice will be approached in two phases: (1) by commissioning and characterizing a single plasma lens and (2) by using three such lenses and measuring their chromaticity as well as alignment and synchronization tolerances. The first of these two phases is underway at the CLEAR User Facility at CERN, and will investigate two important limitations of active plasma lenses: radially nonuniform focusing fields and interference from plasma wakefields.

2.1. Successful operation of a novel, low-cost setup

Several implementations of active plasma lenses have already been successfully demonstrated by LBNL [5], INFN [8] and DESY [9]. Emphasis is therefore placed on developing a novel low-cost, scalable setup. This is attempted in two ways: using a Marx bank instead of the bulkier and more expensive thyratron, and using a thin polymer foil beam window instead of differential pumping to ensure sufficient vacuum in

* Corresponding author.
E-mail address: c.a.lindstrom@fys.uio.no (C.A. Lindstrøm).

https://doi.org/10.1016/j.nima.2018.01.063
Received 22 November 2017; Received in revised form 16 January 2018; Accepted 17 January 2018
Available online 31 January 2018
0168-9002/

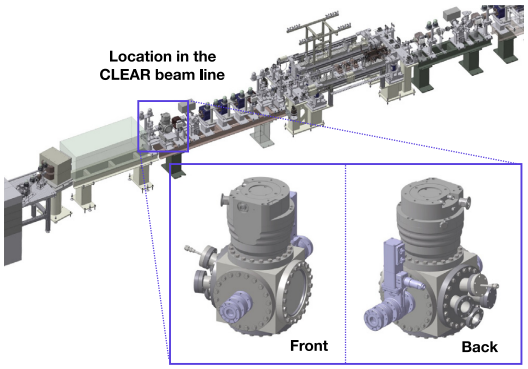

Fig. 1. Location of the plasma lens experimental setup as installed in the CLEAR beam line. The inset shows a 3D sketch of the experimental chamber setup.

the rest of the accelerator. Our goal is to demonstrate stable operation over tens of thousands of shots.

2.2. Field gradient uniformity measurements

Transporting charged particle beams with a well defined energy without emittance growth requires linear beam optics. Any nonlinearities will, without compensation, lead to emittance growth. Active plasma lenses are ideally linear, but in practice they may have nonlinearities due to e.g. low partial ionization [8] or radial temperature gradients. For the latter case, reference [10] develops a theoretical model for such temperature gradient-based nonlinearities, found consistent with their indirect experimental measurements (halo formation). It is, however, important to verify the model further by measuring the nonlinearity directly (magnetic field vs. radius) before attempting to reduce or compensate for it.

In order to directly measure the uniformity of the focusing field, we will observe the centroid angular deflection of a transversely offset beam. This requires a tightly focused beam (compared to the plasma lens aperture) in order to not sample a large range of radii. A short lens should also be used to avoid transverse displacement of the beam inside the lens.

2.3. Limits set by plasma wakefield focusing

Plasma wakefields are intrinsically much stronger (MT/m) than those reachable in an active plasma lens (kT/m), but are generally both longitudinally and transversely nonuniform. Recent active plasma lens experiments have largely avoided interference from plasma wakefield focusing (often called passive plasma lensing) by using low charge, large beam sizes or long bunches. However, these low density beams are not representative of the beams planned for high intensity machines like a linear collider, and it is important to understand whether active plasma lenses can be used for such applications. Passive plasma lensing has already been demonstrated experimentally in an active plasma lens [11], but this should be further probed to determine what parts of the parameter space allows distortion free active plasma lensing.

We will perform this measurement over a wide range of charge, beam size, bunch length and plasma density, by looking for distortion of the beam in the presence of a plasma, but with no active plasma lens current. This is verified by transversely offsetting the beam in the plasma lens, and looking for focusing without a centroid angular deflection.

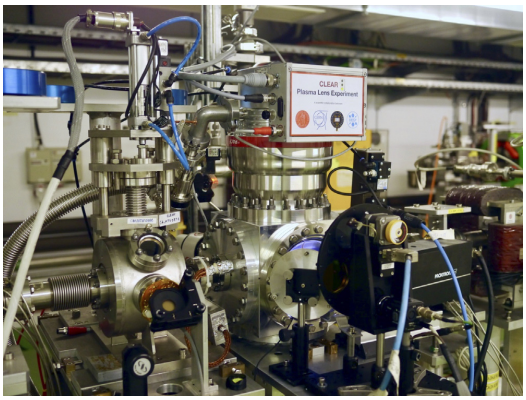

Fig. 2. Overview of the installed setup (beam direction: right to left). A cubic vacuum chamber is mounted on a precision mover, and is connected to the beam line via flexible bellows. A large turbo pump is mounted above. A viewport is used to view the capillary mounted inside, captured on both a regular and a 5 ns gated camera. An OTR screen is insertable in a smaller chamber just downstream. A low pressure gas injection system is mounted behind the chamber, as well as a Compact Marx Bank providing high voltage, high current pulses for discharging. A gate valve with a thin polymer foil is used to avoid gas leaking upstream.

3. The CLEAR User Facility

The CERN Linear Electron Accelerator for Research (CLEAR) [12] is a user facility well suited for an active plasma lens experiment, due to its versatility and rapid turnaround. Previously used as the probe beam injector for the CLIC Test Facility (CTF3), it uses a photocathode RF gun and three S-band accelerating structures to provide 50–220 MeV electron bunches to a dedicated experimental area. It can produce trains of up to a few hundred bunches with 1 pC to 1.5 nC of charge per bunch, at a repetition rate of maximum 5 Hz. The emittance of these bunches ranges from 3 mm mrad at 50 pC to 20 mm mrad at 1 nC. The bunch length can be varied between 300 μm and 1200 μm (1–4 ps).

Just upstream of the plasma lens experiment (see Fig. 1) there is a quadrupole triplet to provide tightly focused beams in the capillary. Calculations indicate beta functions of less than 10 cm such that a minimum rms beam size of 50 μm should be achievable.

4. Experimental setup

Although small in size, the experimental setup (Fig. 2) consists of several subsystems, all of which must work in unison to focus an electron beam.

4.1. Capillary and holder

The capillary itself is a 1 mm diameter, 15 mm long sapphire tube. A half tube is milled from each of two sapphire blocks using a drill bit (and not using laser ablation), as well as two separate gas inlet lines extending to the edges of the capillary. These gas lines continue into a capillary holder made from polyether ether ketone (PEEK): an ultra-high vacuum compatible, electrically insulating plastic. The internal gas lines in the holder exit via a non-conducting polyurethane gas pipe to a gas feedthrough out of the vacuum chamber inside which the capillary and holder is mounted (see Fig. 3). Two electrodes with a hole slightly larger than the capillary diameter are mounted on the upstream and downstream sides of the capillary, and connected to the outside via an electrical feedthrough.

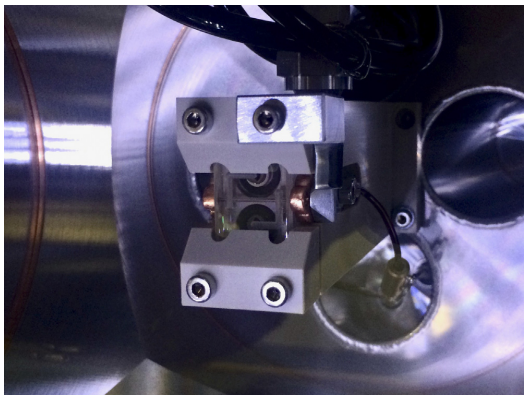

Fig. 3. Plasma lens sapphire capillary (1 mm diameter, 15 mm long) mounted in a PEEK holder, with connected copper electrodes. Gas inlet pipes internally in the holder and in the sapphire allow gas to flow from the external low pressure gas injection system into the capillary. Small surfaces angled at 45° on the upstream side produces OTR light for measuring of the beam size locally.

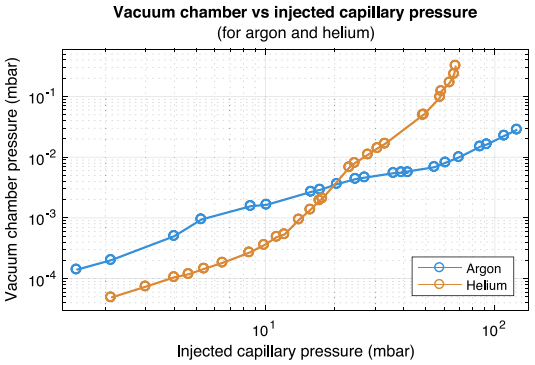

Fig. 4. Measurement of vacuum chamber pressure vs injected capillary pressure, for both helium and argon. Avoiding sparks to the chamber wall requires chamber pressures below 0.01 mbar, indicating safe operation up to about 30 mbar in the capillary for helium, and 70 mbar for argon.

4.2. Chamber and alignment

A $20 \times 20 \times 20$ cm^3 cubic aluminum vacuum chamber is used to electrically insulate the plasma lens from ground with approximately 8 cm of vacuum. The six DN160 CF flanges are used for connecting to the beam line (upstream and downstream), to a turbo pump (above), a borosilicate glass viewport (front), a supporting precision mover (below) and to a multi-port cluster flange (back). The PEEK holder is mounted on the cluster flange, which has four feedthroughs used for two high voltage electric leads rated for 25 kV DC, for gas, and for a pressure gauge measuring the chamber vacuum level.

Alignment and transverse movement is accomplished with a precision two-axis mover with μm resolution and range 13 mm horizontally and 8 mm vertically. The mover is external to increase movement range, avoid controls interference from the electric discharges and to save on cost. Angular pitch and yaw is manually aligned using adjustment screws on the mover and on the rotating mover-to-chamber connection plate. Longitudinal translation and angular roll adjustment is not necessary. The chamber is connected to the beam pipe with two flexible edge-welded bellows on each side, and the 13 mm horizontal range of the mover is sufficient to move the sapphire capillary completely out of the beam orbit.

4.3. Vacuum and gas flow

In this experiment we use both helium and argon, piped via gas lines from 200 bar, 50 l gas bottles outside the accelerator hall. These lines connect to a low-pressure precision gas injection system, consisting of a remotely controlled gas flow regulator (Pfeiffer EVR 116) and a buffer volume with a pressure gauge (Pfeiffer CMR 361). This capacitance-based gauge operates in a feedback loop with the gas flow regulator controller (Pfeiffer RVC 300). Gas pressures from 1 mbar up to 1 bar can be kept in this buffer volume, which is connected to the vacuum chamber gas feedthrough via a remotely controllable pneumatic shutter valve. A short gas line ensures that the pressure inside the capillary stays close to the measured pressure in the buffer. The gas is injected continuously to a operate at a stable, known pressure.

Inside the chamber, the gas which escapes the small aperture of the capillary must be rapidly pumped out. It is important to keep the chamber pressure below approximately 0.01 mbar to avoid discharging to ground rather than between the electrodes. A large turbo pump with magnetic bearings (Pfeiffer HiPace 700M) and a pumping speed of 700 l/s ensures a sufficient vacuum for capillary pressures up to 30 mbar of helium or up to 70 mbar of argon (see Fig. 4). The turbo pump is then connected in series with a 15 m^3/h scroll pump (Edwards nXDS15i) to ensure a fore vacuum of less than 0.1 mbar.

The chamber pressure is measured using a full range Pirani/cold cathode gauge (Pfeiffer PKR 361), which allows measurement down to 10^{-9} mbar. Typically the turbo pump reaches 10^{-8} mbar with no gas flow.

4.4. Polymer foil beam window

During operation of the CLEAR accelerator, the photocathode requires a very good vacuum and any gas flow upstream is unacceptable. Typically this is solved by differential pumping, which is expensive (many pumps) and requires much space. Instead, based on experience at the PITZ experiment at DESY Zeuthen [13], we have installed a thin polymer beam window just upstream (20 cm) of the plasma lens. Made from an 8 μm thick Kapton foil mounted in a small retractable gate valve, it can withstand pressure differentials of up to 1 bar. Early tests shows negligible gas permeation, but that the beam experiences a slight increase in beam emittance when passing through the window. Unless the chamber is erroneously filled with 1 bar of gas, the window never experiences large forces. The plan is therefore to change to a thinner 3 μm Kapton or Mylar foil, which reduces the scattering of the beam.

4.5. Compact Marx Bank high voltage discharge source

To break down the gas to a plasma and to supply the large current required for beam focusing, a 10-stage spark-gap based Compact Marx Bank [14] is used. When triggered, it releases a 20 kV sub-μs duration pulse of peak current up to 500 A. Two wide-band current transformers (Pearson 410) are used to measure both the incoming and outgoing current pulses (see Fig. 5 for a representable current trace). It is important to note that such a high current, high voltage source poses a significant safety risk, and must be handled accordingly.

4.6. Timing and synchronization

The discharge from the Compact Marx Bank must be synchronized with the passing of the beam to within a few ns. In addition, the relative timing of these two events should cover a range of μs in order to scan the beam through the full current pulse profile. This is accomplished by connecting the discharge first to a coarse trigger with 52 ns step resolution and a large range, and then through a smaller range fine delay trigger with 4 ps step resolution.

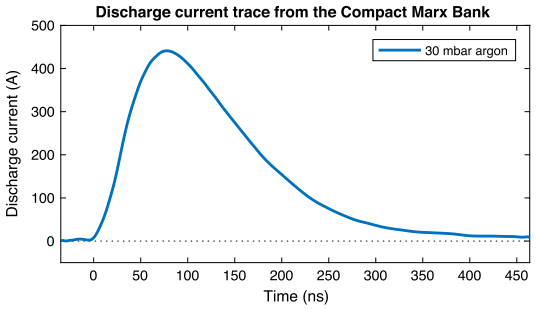

Fig. 5. Current trace (300 shot average) from the Compact Marx Bank during a discharge in the capillary, measured using a wide-band current pulse transformer, showing a peak current of 450 A. The gas pressure in the capillary was 30 mbar of argon.

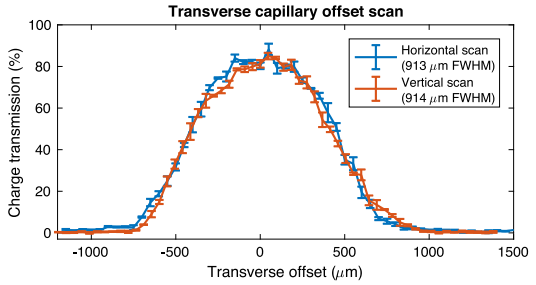

Fig. 6. Transmission scan of the beam through the 1 mm diameter capillary, both in the horizontal (blue) and the vertical direction (red), where the charge transmission is calculated as the ratio to the charge measured with the plasma lens completely out. The full width at half maximum (FWHM) corresponds to the capillary radius, but is slightly less due to small angular misalignment. Simulations indicate a beam size of 170 ± 10 μm rms in both planes, which can be decreased to less than 50 μm with further optimization. (For interpretation of the references to color in this figure legend, the reader is referred to the web version of this article.)

4.7. Diagnostics

Several diagnostics are used to measure the output of the experiment. To detect changes in beam size and any dipole kicks in the plasma lens is an insertable optical transition radiation (OTR) screen 30 cm downstream, with an image resolution of approximately 20 μm/pixel, and a thin aluminum blinder foil just upstream to stop any plasma light. Another camera looks directly at the sapphire capillary through the viewport, showing the transverse and longitudinal profile of the discharge in the capillary as well as any scintillation light from the beam passing through sapphire. A gated camera with a minimum gate duration of 5 ns is used to observe the temporal variation of the discharge, needed to understand the evolution of the plasma. Immediately downstream of the experimental chamber a photomultiplier tube (PMT) is installed to observe particle losses in the capillary. Further downstream is a charged particle beam dipole spectrometer to measure any energy changes caused by plasma wakefields, although this is expected to be a negligible effect. An in-air yttrium aluminum garnet (YAG) screen is used for measuring the transverse profile several meters downstream, before the beam is dumped. Lastly, two small OTR-producing surfaces are mounted on the upstream electrode to provide a beam size measurement as close to the capillary as possible, important for minimizing the beam size.

5. Status and future plans

The CLEAR plasma lens experiment started its design phase in early 2017 and is planned to last until at least late 2018.

Bench tests of the vacuum levels, the polymer beam window, gas injection, and high voltage discharges were all successfully performed during mid 2017. The setup was subsequently installed in the CLEAR beam line and integrated into the control system. Some distortion of the beam due to the plasma-current was observed during a preliminary beam time in late 2017, before further upgrades were initiated. The best charge transmission of the beam through the capillary is currently $87 \pm 5\%$ (see Fig. 6), but this number is expected to reach close to 100% as the beam size approaches the stipulated 50 μm rms. Experiments will be performed starting at the end of 2017 and is planned to last until mid 2018.

6. Conclusion

The CLEAR plasma lens experiment is a new experiment aimed at demonstrating successful operation of a novel low-cost setup, and at characterizing two important aspects of active plasma lenses: the non-uniformity of the focusing field, and limits due to plasma wakefields. After successful bench tests of all the subsystems, the setup is now installed and starting to produce scientific data. Experiments will continue until late 2018.

Acknowledgments

The authors wish to thank Reidar Lunde Lillestøl, Gianfranco Ravida, Gerard McMonogle, Franck Perret, Stephane Curt, Thibaut Lefevre, Bruno Cassany, Serge Lebet, Jose Antonio Ferreira Somoza, Alice Ingrid Michet, Herve Rambeau, Stefano Mazzoni, Michael John Barnes, Aimee Ross and Candy Capelli. We thank CERN for providing beam time at the CLEAR User Facility. This work was supported by the Research Council of Norway (NFR Grant No. 230450) and by the Helmholtz Association of German Research centers (Grant No. VH-VI-503).

References

[1] P. Chen, J.M. Dawson, R.W. Huff, T. Katsouleas, Phys. Rev. Lett. 54 (1985) 693–696.
[2] R.D. Ruth, A.W. Chao, P.L. Morton, P.W. Wilson, Part. Accel. 17 (1985) 171.
[3] E.A. Peralta, et al., Nature 503 (2013) 91–94.
[4] S. Steinke, et al., Nature 530 (2016) 190–193.
[5] J. van Tilborg, et al., Phys. Rev. Lett. 115 (2015) 184802.
[6] C.A. Lindstrøm, et al., Nucl. Instrum. Methods Phys. Res. A 829 (2016) 224–228.
[7] C.A. Lindstrøm, E. Adli, Phys. Rev. Accel. Beams 19 (2016) 071002.
[8] R. Pompili, et al., Appl. Phys. Lett. 110 (2017) 104101.
[9] Private communication with J.-H. Röckemann, DESY.
[10] J. van Tilborg, et al., Phys. Rev. Accel. Beams 20 (2017) 032803.
[11] A. Marocchino, et al., Appl. Phys. Lett. 111 (2017) 184101.
[12] D. Gamba, et al., Nucl. Instrum. Methods Phys. Res. A (2017). https://dx.doi.org/10.1016/j.nima.2017.11.080.
[13] O. Lishilin, et al., Nucl. Instrum. Methods Phys. Res. A 829 (2016) 37–42.
[14] A.E. Dyson, C. Thornton, S.M. Hooker, Rev. Sci. Instrum. 87 (2016) 093302.

A.7 Emittance preservation in an aberration-free active plasma lens

Authors

C. A. Lindstrøm, E. Adli, G. Boyle, R. Corsini, A. E. Dyson, W. Farabolini, S. M. Hooker, M. Meisel, J. Osterhoff, J.-H. Röckemann, L. Schaper and K. N. Sjobak

Journal

Phys. Rev. Lett. **121**, 194801 (2018)

Abstract

Active plasma lensing is a compact technology for strong focusing of charged particle beams, which has gained considerable interest for use in novel accelerator schemes. While providing kT/m focusing gradients, active plasma lenses can have aberrations caused by a radially nonuniform plasma temperature profile, leading to degradation of the beam quality. We present the first direct measurement of this aberration, consistent with theory, and show that it can be fully suppressed by changing from a light gas species (helium) to a heavier gas species (argon). Based on this result, we demonstrate emittance preservation for an electron beam focused by an argon-filled active plasma lens.

(6 pages)

Emittance Preservation in an Aberration-Free Active Plasma Lens

C. A. Lindstrøm,[1,*] E. Adli,[1] G. Boyle,[2] R. Corsini,[3] A. E. Dyson,[4] W. Farabolini,[3] S. M. Hooker,[4,5] M. Meisel,[2] J. Osterhoff,[2] J.-H. Röckemann,[2] L. Schaper,[2] and K. N. Sjobak[1]

[1]*Department of Physics, University of Oslo, 0316 Oslo, Norway*
[2]*DESY, Notkestraße 85, 22607 Hamburg, Germany*
[3]*CERN, CH-1211 Geneva 23, Switzerland*
[4]*Department of Physics, Clarendon Laboratory, University of Oxford, Parks Road, Oxford OX1 3PU, United Kingdom*
[5]*John Adams Institute for Accelerator Science, Denys Wilkinson Building, Keble Road, Oxford OX1 3RH, United Kingdom*

(Received 10 August 2018; published 7 November 2018)

Active plasma lensing is a compact technology for strong focusing of charged particle beams, which has gained considerable interest for use in novel accelerator schemes. While providing kT/m focusing gradients, active plasma lenses can have aberrations caused by a radially nonuniform plasma temperature profile, leading to degradation of the beam quality. We present the first direct measurement of this aberration, consistent with theory, and show that it can be fully suppressed by changing from a light gas species (helium) to a heavier gas species (argon). Based on this result, we demonstrate emittance preservation for an electron beam focused by an argon-filled active plasma lens.

DOI: 10.1103/PhysRevLett.121.194801

Advances in high gradient acceleration research [1–4] promise significantly more compact particle accelerators, key to next-generation free-electron lasers (FELs) [5] and linear colliders [6]. However, advances in high gradient acceleration must be matched by a similar miniaturization of beam focusing devices. Active plasma lensing [7] is one promising technique that provides compact, strong focusing in both planes simultaneously, by passing a large longitudinal current through a thin plasma-filled capillary [8,9], ideally creating an azimuthal magnetic field proportional to the distance from the axis. While the concept dates back to the 1950s [10] and was used for fine focusing of heavy ion beams [11], active plasma lenses (APLs) have recently gained attention based on their application to advanced accelerator research, such as beam capture and staging of laser plasma accelerators [12].

Although APLs provide kT/m focusing fields, orders of magnitude stronger focusing compared to conventional quadrupole magnets, they can suffer from aberrations that increase the emittance of the beam being focused [13,14]. One such aberration is caused by plasma temperature gradients in the capillary (colder plasma closer to the wall), which leads to a radially nonlinear magnetic field distribution [15,16] with enhanced focusing closer to the axis. This spherical aberration has been indirectly demonstrated in both helium [17] and hydrogen [18], by measurements of on axis field gradient enhancement and the formation of ring-shaped beams.

In this Letter, we show that this aberration can be fully suppressed by changing from a light gas species (helium) to a heavier gas species (argon). This discovery was made possible by the first complete characterization of the radial magnetic field distribution in an APL, in an experiment performed at the CERN Linear Electron Accelerator for Research (CLEAR) User Facility [19,20]. The beam emittance was subsequently measured using quadrupole scans, resulting in the first demonstration of emittance preservation in an APL.

The experimental setup [21], shown in Fig. 1, consisted of a 1 mm diameter and 15 mm long capillary milled from two sapphire blocks, mounted in the CLEAR beam line to allow passage of an electron beam. The capillary was filled with 1–100 mbar of gas through internal gas inlets, connected to an external flow regulator and a buffer volume. The gas escaping into the surrounding chamber was pumped out by a large turbo pump, which together with a 3 μm polymer (Mylar) window [22] preserved the ultrahigh vacuum in the upstream accelerator line. Holed copper electrodes on the up- and downstream side of the capillary were connected to a compact Marx bank [23], providing short 20 kV discharge pulses with a tunable 410–450 A peak current after 80 ns and a duration of 145 ns full width at half maximum (FWHM) [see Fig. 1(c)], as measured by in- and outgoing wideband current pulse transformers. A two-axis mover [24] was used to displace the capillary horizontally and vertically relative to the beam, with a 1 μm step resolution and an approximate range of 10 mm.

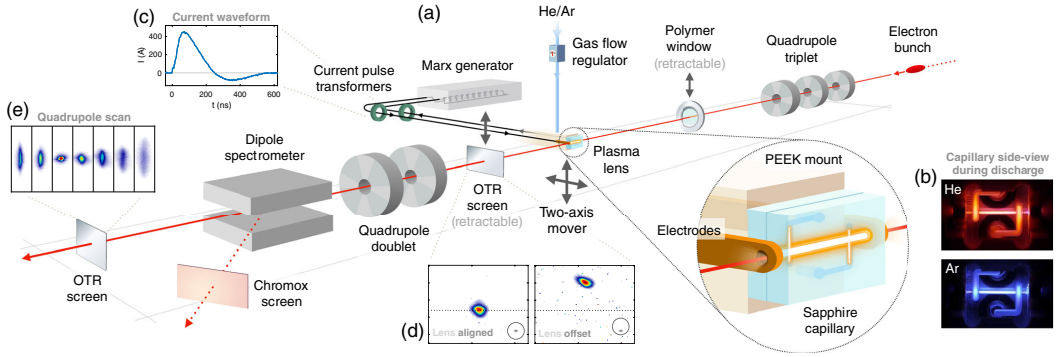

FIG. 1. (a) Experimental setup: an electron bunch was tightly focused by a quadrupole triplet into an APL after passing a thin polymer window. The lens consisted of a gas-filled sapphire capillary with internal gas inlets (b) connected to an external gas flow regulator, and was discharged using two copper electrodes connected to a Marx generator producing high-voltage pulses with 410–450 A peak current (c). A two-axis mover scanned the beam transversely across the capillary aperture, deflecting the beam onto an OTR screen immediately downstream (d). With this screen retracted, the beam was instead focused by a quadrupole doublet onto another OTR screen, allowing measurement of emittance using a quadrupole scan (e). Additionally, a dipole spectrometer with a Chromox screen was used to measure the beam energy and energy spread.

To ensure a high-resolution magnetic field measurement, a quadrupole triplet 1 m upstream of the lens was used to focus the beam to a spot size of about 50×50 μm root mean square (rms). This was measured and optimized at the plasma lens using optical transition radiation (OTR) from a stainless steel wedge mounted on the upstream electrode. Directly downstream of the lens (30 cm) was a retractable OTR screen to observe beam focusing and centroid angular deflections from the APL, mounted with a thin aluminum foil to block stray plasma light. Further downstream, a quadrupole doublet allowed multishot emittance measurements using quadrupole scans on another OTR screen, also with a noninvasive light-blocking foil. A dipole magnet was used as a spectrometer to measure the mean energy (200–220 MeV) and energy spread ($< 0.2\%$ rms) of the beam on a chromium-doped ceramic (Chromox) screen. Upstream of the experimental setup was a radio frequency (rf) transverse deflecting cavity used to measure the bunch length to be approximately 400 μm rms, as well as toroids used to measure the beam charge.

The measurement of the radial magnetic field distribution in the APL was performed by displacing the lens vertically across the full 1 mm aperture of the capillary with respect to a tightly focused fixed-orbit beam, while centered in the horizontal plane. Angular deflections of the beam centroid, as observed on the closest OTR screen, scale linearly with the local magnetic field averaged over the length of the capillary. A short capillary was therefore used to avoid any transverse displacement (betatron motion) inside the APL, as this would lead to unwanted radial averaging. Each offset was recorded over 5–10 shots to average any angular jitter, which was approximately 0.5 and 0.1 mrad rms in the horizontal and vertical plane, respectively. The scans were performed around the peak current timing (after approximately 80 ns), as this is the most stable and potent operating point and because later timings with lower discharge current tended to suffer from poor signal-to-noise ratio. One or two bunches (at a 667 ps interval) with 5–7 pC of charge per bunch were used to simultaneously ensure negligible distortion from plasma wakefields [25] and to get a sufficient signal on the OTR screen.

The expected magnetic field in an APL can be found using Ampère's law for a longitudinal current density,

$$\frac{1}{r}\frac{\partial}{\partial r}(rB_\phi) = \mu_0 J_z(r), \tag{1}$$

where B is the magnetic field, J is the current density, the permeability of the plasma is assumed to be that of the vacuum μ_0, and r, ϕ, and z are the radial, azimuthal, and longitudinal coordinates, respectively. If the current density is uniform, Eq. (1) integrates to give a linear magnetic field with a constant magnetic field gradient

$$g_r = \frac{\partial B_\phi}{\partial r} = \frac{\mu_0 I_0}{2\pi R^2}, \tag{2}$$

where I_0 is the total current and R is the capillary radius. This represents the ideal operation of an APL, providing emittance preservation and focusing in both planes.

However, this picture is complicated by the buildup of a radial temperature gradient inside the capillary, which leads to a nonuniform current density and a nonlinear magnetic field—detrimental to the beam quality. As described in Ref. [16] and supported by Ref. [26], this occurs

in a four-step process, starting with (1) the formation of a cold plasma. Then (2) the electron temperature increases sharply from Joule heating, but (3) due to a thin, virtually electron-free sheath near the capillary wall, the hot electrons only transfer their heat to the plasma ions, which (4) subsequently lose heat to the wall. This process preferentially cools the plasma closer to the capillary wall, leading to the formation of a nonuniform temperature profile with hotter plasma closer to the axis. Since the plasma conductivity σ increases with the plasma electron temperature T_e, the current concentrates closer to the axis, as given by [17]

$$J_z(r) = \sigma(r)E_z \propto T_e^{3/2}(r), \tag{3}$$

where E_z is a uniform longitudinal electric field.

A steady-state solution to this process was found by Ref. [15] through a simplified magnetohydrodynamics (MHD) approach, satisfying the radial heat flow equation

$$\frac{1}{x}\frac{\partial}{\partial x}\left(x\frac{\partial u}{\partial x}\right) + u^{3/7} = 0, \tag{4}$$

where $x = r/R$ is a scaled radius and $u = (T_e/A)^{7/2}$ is a scaled temperature for which $A = \sqrt{7R^2E_z^2\sigma_0/2\kappa_0}$. Here we assume a Maxwellian velocity distribution, such that the thermal and electrical conductivities scale according to $\kappa = \kappa_0 T_e^{5/2}$ and $\sigma = \sigma_0 T_e^{3/2}$, respectively [27]. Substituted into Eq. (3), we find the current density profile

$$J_z(r) = \frac{I_0}{\pi R^2}\frac{u(r)^{3/7}}{2m_I}, \tag{5}$$

where the scaled temperature is normalized by

$$m_I = \int_0^1 u(x)^{3/7} x dx, \tag{6}$$

to ensure the correct total current $2\pi\int_0^R J_z(r)rdr = I_0$. With this current density, Ampère's law (1) can be numerically integrated to find the steady-state radial magnetic field distribution—sometimes termed the "JT model." A nonuniformity will lead to an enhancement of the on axis focusing gradient 1–1.48 times larger than Eq. (2), depending on the wall temperature.

In order to avoid the nonuniformity, we must break the assumption of steady state. In a light gas, this is not trivial, as the timescale of electron–ion heat transfer, and hence the buildup of the nonuniformity, is shorter than the typical rise time of the current pulse. However, crucially, this timescale can be slowed down by changing to a heavier gas, where the rate of thermal transfer between electrons and ions as well as the ion thermal conductivity (both inversely proportional to the ion mass [15]) are significantly reduced. The discharge current can then rise to its peak before the current becomes nonuniform, ensuring a linear magnetic field when the beam passes. Two-temperature MHD simulations using FLASH [28] are currently under study to verify this explanation and will be the subject of a future publication.

Experimentally, this magnetic field distribution was found by measuring the angular deflection of the beam as an offset Δy_{OTR} on the downstream OTR screen for every offset y_0 of the lens. Since the current in the APL was fluctuating by a few percent, the measurement can be improved by considering the ratio of the magnetic field and the instantaneous discharge current observed by the beam

$$\frac{B_\phi(y_0)}{I_0} = \frac{E\Delta y_{\mathrm{OTR}}}{ecL\Delta s I_0}, \tag{7}$$

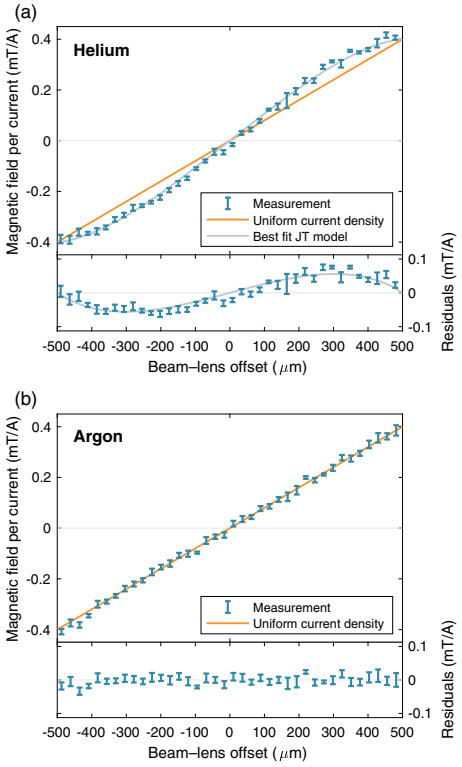

FIG. 2. Measurement of the magnetic field per discharge current for a scan of beam-to-lens offsets in (a) helium and (b) argon, where the uncertainty (blue error bars) represents the standard deviation of the mean. A strong nonlinearity is observed in helium, consistent with the JT model (gray line), whereas in argon the measurement is consistent with the expectation from a uniform current density (orange lines).

where L is the length of the capillary, Δs is the distance from the center of the capillary to the screen, E is the beam energy, and e and c are the electron charge and the speed of light in vacuum, respectively.

Figure 2 shows the measured magnetic field per current for both (a) helium and (b) argon, using a transverse step size of 26 μm. In helium, there is clear evidence of a nonlinearity, consistent with the JT model and indicating a best fit gradient enhancement factor of 1.34 and a scaled wall temperature $u(R) = 0.0114$. These results are in excellent agreement with Ref. [17]. In argon, there is no evidence of any nonlinearity—the magnetic field distribution is linear to within the error of the measurement. The flow of each gas was minimized while ensuring stable discharges at the few nanosecond level. The resulting neutral gas density in the capillary was 6 mbar in argon and 23 mbar in helium, both a 70% pressure drop from the buffer volume, measured by sealing one gas inlet and connecting the closest end of the capillary to a capacitance gauge—a method used also in Ref. [29].

To verify the expected emittance growth in helium and emittance preservation in argon, a number of quadrupole scans were performed in each gas. Instead of using a tightly focused beam, a larger beam (100–150 μm rms) covering a significant portion of the aperture was used—this way, the nonlinearity was sampled more extensively and the potential emittance growth increased. Simultaneously, to avoid any emittance growth from plasma wakefields, the beam charge was lowered to approximately 2 pC for the single bunch used in the measurement. Due to non-negligible horizontal dispersion, emittance measurements were only performed in the vertical plane. Additionally, for each measurement, at least two different current settings were used in the second (nonscanned) quadrupole, allowing an overall verification of length and current calibrations.

Figure 3 shows emittance measurements from multiple quadrupole scans in both (a) helium and (b) argon, repeated four times for each gas. Each segment consists of one or more control measurements before and after the shots with discharge to estimate any emittance drift over a 15–30 min interval, as well as several emittance measurements where the beam is focused by the APL at peak current (410 A). We clearly observe emittance growth in helium compared to the background emittance, in good agreement with predictions from particle tracking through the measured nonlinear field [see Fig. 2(a)]. This tracking simulation uses the measured spot size in the lens as well as a random centroid offset jitter (estimated to 1σ beam size), leading to a spread of predicted emittances as more offset beams sample the nonlinearity more strongly. The emittance error in each quadrupole scan is obtained from the covariance matrix produced when performing parabolic fits to the measured spot sizes. This error is observed to increase during discharges, both due to the centroid offset jitter as well as current fluctuations caused by a discharge timing jitter.

In argon, the measured emittance during peak discharge current is fully consistent with the background emittance to within the estimated error. This is clear evidence of emittance preservation, simultaneously confirming that there are no other sources of emittance growth. Assuming that additional emittance is added in quadrature and that errors are Gaussian, the argon measurement excludes emittance growth larger than 0.25 mm mrad at 90% confidence level. Moreover, the change in beam optics was measured across consecutive on-off quadrupole scans to be consistent with the expected focusing from a 326 T/m uniform magnetic field gradient [Eq. (2)] to within the error of the measurement, verifying that there is no gradient enhancement in argon.

We have shown that APLs can be made aberration-free by changing to a heavier gas species, but this comes at the

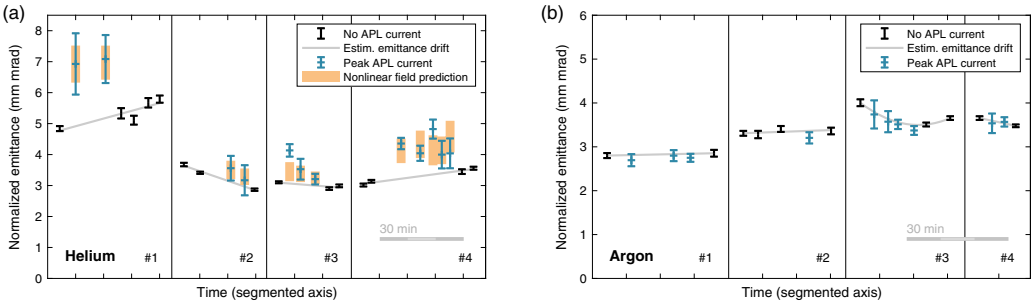

FIG. 3. Quadrupole scan emittance measurements for both (a) a helium and (b) an argon APL, performed multiple times at peak current timing (blue error bars). Additionally, the background emittance was measured in the absence of current (black error bars) before and after discharges to estimate any emittance drift (gray lines). The predicted emittance growth in helium (orange rectangles) based on the measured nonlinear field [see Fig. 2(a)] is in good agreement with the measured values. In argon, all measurements are consistent with emittance preservation. Emittance drift is modeled with a linear fit in all measurements except one (argon #3), where a quadratic fit produces a tighter bound.

cost of more scattering. Emittance growth from multiple Coulomb scattering [30,31] increases almost quadratically with atomic number, such that argon scatters 54 times more than helium and 280 times more than hydrogen. This effect can, however, be minimized by increasing the discharge current or decreasing the capillary radius, thereby requiring a shorter lens for the same focusing or by lowering the pressure. For this experiment, the pressure was sufficiently low to not increase the emittance, as verified by quadrupole scans with and without gas, but calculations indicate that higher pressures could result in non-negligible emittance growth. Moreover, scattering can potentially be reduced by using an intermediate gas species, like nitrogen or neon, if the aberration can still be suppressed. Use of nitrogen, which scatters 5.6 times less than argon, is currently a topic of active investigation.

One immediate application of the argon lens is as an emittance preserving beam capture device for laser plasma accelerators (LPAs). A challenge for LPAs is the highly diverging beams produced, typically 1 mrad rms, which combined with percent-level energy spreads lead to significant emittance growth due to large chromaticity during beam capture. This problem can be solved by using an aberration-free active plasma lens (e.g., 600 A peak current, 10 mm long, 400 μm capillary radius, 1 mbar argon) placed sufficiently close to a LPA source (10 cm downstream) to capture high-quality beams without degradation (1 mm mrad, 200 MeV, 1% rms energy spread, 1–2 μm rms bunch length, up to 200 pC)—potentially useful for an ultra-compact FEL.

Other applications may include radially symmetric final focusing for linear colliders or possibly staging of plasma accelerators [32], assuming plasma wakefield distortion is avoided by reducing the beam intensity. While in this measurement plasma wakefields were successfully controlled for, in general, they will impose limits to the application of APLs to low-emittance, high-intensity beams [25], such as those needed for linear colliders, unless compensation methods can be found. The nonlinearity suppression reported in this Letter contributes in this regard by increasing the effective aperture of the lens, allowing significant reduction of wakefields with the use of larger, lower density beams.

In conclusion, emittance preservation in an active plasma lens has been demonstrated for the first time with the use of an argon-based discharge capillary. Direct measurements of magnetic fields across the full aperture show linearity in argon and nonlinearity in helium. Quadrupole scans demonstrate the expected emittance preservation and growth, respectively, consistent with the measured field profiles. This development of a compact linear beam optics device is a critical step towards truly compact low-emittance accelerators.

The authors wish to thank Davide Gamba, Alessandro Curcio, Reidar Lunde Lillestøl, Gianfranco Ravida, Gerard McMonagle, Franck Perret, Stephane Curt, Thibaut Lefevre, Bruno Cassany, Serge Lebet, Jose Antonio Ferreira Somoza, Alice Ingrid Michet, Hervé Rambeau, Stefano Mazzoni, Michael John Barnes, Aimee Ross, and Candy Capelli. We thank CERN for providing beam time at the CLEAR User Facility. This work was supported by the Research Council of Norway (NFR Grant No. 230450) and by the Helmholtz Association of German Research Centers (Grants No. VH-VI-503 and No. ZT-0009).

*c.a.lindstrom@fys.uio.no

[1] T. Tajima and J. M. Dawson, Laser Electron Accelerator, Phys. Rev. Lett. **43**, 267 (1979).
[2] P. Chen, J. M. Dawson, R. W. Huff, and T. Katsouleas, Acceleration of Electrons by the Interaction of a Bunched Electron Beam with a Plasma, Phys. Rev. Lett. **54**, 693 (1985).
[3] R. D. Ruth, A. W. Chao, P. L. Morton, and P. W. Wilson, A plasma wake field accelerator, Part. Accel. **17**, 171 (1985).
[4] C. Joshi and T. Katsouleas, Plasma accelerators at the energy frontier and on tabletops, Phys. Today **56**, No. 6, 47 (2003).
[5] M. E. Couprie, A. Loulergue, M. Labat, R. Lehe, and V. Malka, Towards a free electron laser based on laser plasma accelerators, J. Phys. B **47**, 234001 (2014).
[6] W. P. Leemans and E. Esarey, Laser-driven plasma-wave electron accelerators, Phys. Today **62**, No. 3 44 (2009).
[7] J. van Tilborg *et al.*, Active Plasma Lensing for Relativistic Laser-Plasma-Accelerated Electron Beams, Phys. Rev. Lett. **115**, 184802 (2015).
[8] D. J. Spence and S. M. Hooker, Investigation of a hydrogen plasma waveguide, Phys. Rev. E **63**, 015401 (2000).
[9] A. Butler, D. J. Spence, and S. M. Hooker, Guiding of High-Intensity Laser Pulses with a Hydrogen-Filled Capillary Discharge Waveguide, Phys. Rev. Lett. **89**, 185003 (2002).
[10] W. K. H. Panofsky and W. R. Baker, A focusing device for the external 350-MeV proton beam of the 184-inch cyclotron at Berkeley, Rev. Sci. Instrum. **21**, 445 (1950).
[11] E. Boggasch, A. Tauschwitz, H. Wahl, K.-G. Dietrich, D. H. H. Hoffmann, W. Laux, M. Stetter, and R. Tkotz, Plasma lens fine focusing of heavy-ion beams, Appl. Phys. Lett. **60**, 2475 (1992).
[12] S. Steinke *et al.*, Multistage coupling of independent laser-plasma accelerators, Nature (London) **530**, 190 (2016).
[13] J. van Tilborg, S. K. Barber, C. Benedetti, C. B. Schroeder, F. Isono, H.-E. Tsai, C. G. R. Geddes, and W. P. Leemans, Comparative study of active plasma lenses in high-quality electron accelerator transport lines, Phys. Plasmas **25**, 056702 (2018).
[14] R. Pompili *et al.*, Experimental characterization of active plasma lensing for electron beams, Appl. Phys. Lett. **110**, 104101 (2017).
[15] N. A. Bobrova, A. A. Esaulov, J.-I. Sakai, P. V. Sasorov, D. J. Spence, A. Butler, S. M. Hooker, and S. V. Bulanov, Simulations of a hydrogen-filled capillary discharge waveguide, Phys. Rev. E **65**, 016407 (2001).

[16] B. H. P. Broks, K. Garloff, and J. J. A. M. van der Mullen, Nonlocal-thermal-equilibrium model of a pulsed capillary discharge waveguide, Phys. Rev. E **71**, 016401 (2005).
[17] J. van Tilborg *et al.*, Nonuniform discharge currents in active plasma lenses, Phys. Rev. Accel. Beams **20**, 032803 (2017).
[18] J.-H. Röckemann *et al.*, Direct measurement of focusing fields in active plasma lenses, arXiv:1803.06663.
[19] D. Gamba *et al.*, The CLEAR user facility at CERN, Nucl. Instrum. Methods Phys. Res., Sect. A, doi: 10.1016/j.nima.2017.11.080 (2017).
[20] R. Corsini *et al.*, First experiments at the CLEAR User Facility, *Proceedings of IPAC2018, Vancouver, BC, Canada* (JACoW, Geneva, 2018), p. 4066.
[21] C. A. Lindstrøm *et al.*, Overview of the CLEAR plasma lens experiment, Nucl. Instrum. Methods Phys. Res., Sect. A, doi: 10.1016/j.nima.2018.01.063 (2018).
[22] O. Lishilin *et al.*, First results of the plasma wakefield acceleration experiment at PITZ, Nucl. Instrum. Methods Phys. Res., Sect. A **829**, 37 (2016).
[23] A. E. Dyson, C. Thornton, and S. M. Hooker, A compact, low cost Marx bank for generating capillary discharge plasmas, Rev. Sci. Instrum. **87**, 093302 (2016).
[24] F. Toral *et al.*, Design, manufacturing and tests of a micrometer precision mover for CTF3 quadrupoles, *Proceedings of EPAC'08, Genoa, Italy* (JACoW, Geneva, 2008), p. 1517.
[25] C. A. Lindstrøm and E. Adli, Analytic plasma wakefield limits for active plasma lenses, arXiv:1802.02750.
[26] A. J. Gonsalves, T. P. Rowlands-Rees, B. H. P. Broks, J. J. A. M. van der Mullen, and S. M. Hooker, Transverse Interferometry of a Hydrogen-Filled Capillary Discharge Waveguide, Phys. Rev. Lett. **98**, 025002 (2007).
[27] L. Spitzer and R. Härm, Transport phenomena in a completely ionized gas, Phys. Rev. **89**, 977 (1953).
[28] B. Fryxell, K. Olson, P. Ricker, F. X. Timmes, M. Zingale, D. Q. Lamb, P. MacNeice, R. Rosner, J. W. Truran, and H. Tufo, FLASH: An adaptive mesh hydrodynamics code for modeling astrophysical thermonuclear flashes, Astrophys. J. Suppl. Ser. **131**, 273 (2000).
[29] J. van Tilborg, A. J. Gonsalves, E. H. Esarey, C. B. Schroeder, and W. P. Leemans, Density characterization of discharged gas-filled capillaries through common-path two-color spectral-domain interferometry, Opt. Lett. **43**, 2776 (2018).
[30] F. Zimmermann, Possible limits of plasma linear colliders, J. Phys. Conf. Ser. **874**, 012030 (2017).
[31] N. Kirby, M. Berry, I. Blumenfeld, M. J. Hogan, R. Ischebeck, and R. Siemann, Emittance growth from multiple Coulomb scattering in a plasma wakefield accelerator, *Proceedings of PAC2007, Albuquerque, NM, USA* (IEEE, Piscataway, NJ, 2007), p. 3097.
[32] C. A. Lindstrøm, E. Adli, J. M. Allen, J. P. Delahaye, M. J. Hogan, C. Joshi, P. Muggli, T. O. Raubenheimer, and V. Yakimenko, Staging optics considerations for a plasma wakefield acceleration linear collider, Nucl. Instrum. Methods Phys. Res., Sect. A **829**, 224 (2016).

Appendix B

Rapid Iteration Experimental Data Acquisition and Analysis

Accelerators are expensive machines to run: the electricity bill for SLAC's 3 km linac is of the order $30,000 or more *per day*. That means, time is precious when you're doing experiments—every second counts. It is therefore of vital importance that the method for taking data and deciding what to do next is efficient.

There is of course no right or wrong method for doing advanced accelerator experiments, as every lab and every user develops their own way. However, one very efficient method was developed at the FACET facility at SLAC, and later fine-tuned in the CLEAR facility at CERN. This is worth documenting in case it might boost the research output per hour of beam time also elsewhere. Many facilities will already be using some version of the same method, in which case there is little to be gained beyond a conceptual clarification!

B.1 Speeding up the acquisition–analysis cycle

Ideally, an experiment is conducted straightforwardly via the following steps:

1. Adjust the experimental setup to the desired setting
2. Record the data
3. Analyze and interpret the data (then publish)

However, a real world experiment is never this simple—especially because the measurement devices and the physical system you are measuring rarely behave exactly as expected. This can be due to noise, unknown calibration factors, misalignments and offsets, or just a plain misunderstanding. In reality, therefore, an experiment is always conducted many times over—gradually converging on the measurement initially planned. This feedback loop of attempting to take data, analyzing it, learning from the results and then repeating with an improved setup is something we will call the *acquisition–analysis cycle*.

Having to go through this iteration cycle is sometimes viewed as a failure of the original experiment—you failed to get the result, and now you have to try again. Quite the contrary: this cycle is inherent to experimental work. Consequently, the experimental methodology should reflect this fact and be built around it. In particular, it is very fruitful to shorten the time taken between data collection and data analysis. This gives the experimenters a clearer view of the true state of the machine and the measurement, and hence a better picture of what is best to do next.

We should note that this concept is widely applied in software engineering. Early software companies had a tendency to follow the so-called *waterfall model*, where one would first fully design the software on paper, then write the code, followed by testing and subsequent release—step by step flowing down the waterfall. Often, especially for large projects, this was not very successful—leading to large time and cost overruns, and a product that was nothing like what the customer had envisioned. An alternative approach was developed: RAD, or *rapid application development* (sometimes *rapid prototyping*), whereby a rudimentary and minimalistic prototype is quickly designed, built and tested—then iterated with another round of design, building and testing etc. This is now a widely adopted strategy in the software industry.

B.2 A two-part software concept

So how do we convert this somewhat vague concept to something tangible and useful in an accelerator environment? One answer to this question is a specific two-part software solution, and the way it is used: (1) a GUI-based data acquisition application and (2) a flexible, "quick and dirty" online analysis tool based on functional programming—to be used iteratively in quick succession.

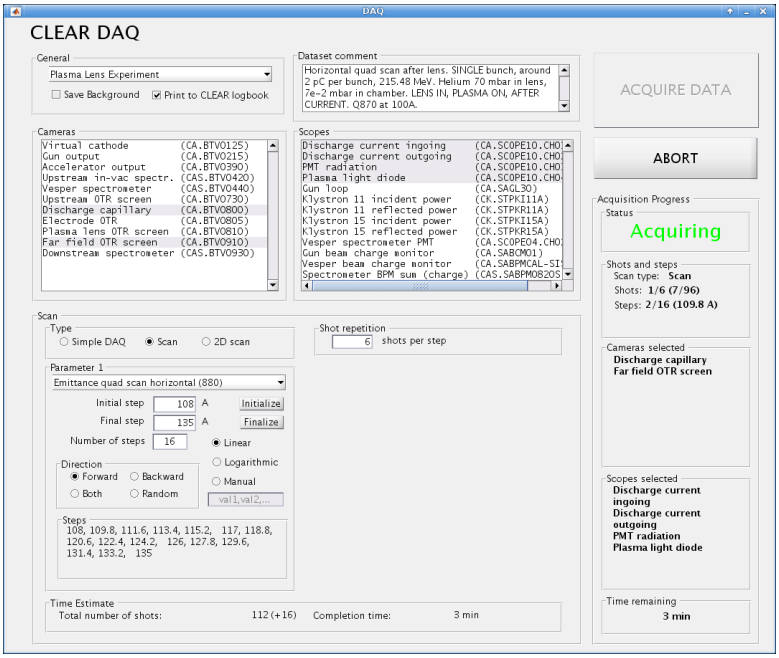

Figure B.1: Example of a GUI-based data acquisition (DAQ) application, as developed for the CLEAR User Facility [12] at CERN.

B.2.1 Part 1: GUI-based Data Acquisition (DAQ)

Almost every accelerator facility has some kind of data acquisition software—or *DAQ*—as it forms the backbone of the experimental data collection. The DAQ is typically built as a graphical user interface (GUI), as it gives the best overview of the many simultaneous pieces of information needed to define how and what data to collect. This data is then often placed in neatly packaged collections called *datasets*, which include images, scope traces and scalar values both beam-synchronously (every shot) and of the machine state (before the dataset).

A dataset is typically taken in one of three forms: a multi-shot recording of the state of the machine (sometimes called a "simple DAQ"); a single parameter scan, where the machine is progressively altered while taking several shots at each step; and a two-parameter (2D) scan, where a single parameter is scanned and rescanned while a second parameter is changed in between—often a very slow process.

Figure B.1 shows an example of such a GUI-based DAQ (from the CLEAR User Facility), developed as part of this thesis.

B.2.2 Part 2: One-liner command line Data Analysis (DAN)

While a good DAQ can certainly speed up the data taking process, making sure the *quality* of that data is high requires some form of fast feedback. The immediate reaction to this observation is that we should develop some highly mature GUI-based online data analysis tool. While this may be appropriate in certain situations, it is often not the best solution for a fast-paced advanced accelerator experiment—because it takes too much time to develop and is not very versatile once it has been written. On the other hand, writing an analysis script from scratch for every dataset is not practical either—infinite flexibility, but also very slow.

Another important consideration is the abstraction level at which the experimenter can work: ideally one would "ask" the software about the physical quantity in question and get an answer, and not have to resort to 50 lines of code (with all the associated bugs and other distractions).

Based on experience from FACET and CLEAR, it was found that a one-liner-based command line tool for data analysis—or *DAN*—is the best compromise. This system is left *intentionally* rough and rudimentary, as customizing the output too much toward a specific type of dataset goes against the more important point of being flexible. Combining high flexibility and short input syntax is therefore challenging, but is solved by employing so-called *anonymous functions*—a concept that stems from functional programming.

Anonymous functions

Functional programming is a way to program based solely on functions, i.e., completely without internal, hidden state variables—all data is passed as input and output function arguments. This paradigm is based on *lambda calculus*, a formal system to investigate computability developed back in the 1930's. A staple of this system is the anonymous function (or *lambda function*): a notation that allows writing functions without giving it a name such as "f" or "`foobar`". Mathematically, this is often written as (using the example $f(x, y) = x^2 y$):

$$(x, y) \mapsto x^2 y, \tag{B.1}$$

with a similar syntax in programming languages (like MATLAB): `@(x,y) x^2*y`.

The main advantage of this functional notation is that we can very compactly define the desired action on the data (say a background subtraction, a projection or a sum) and pass this directly to the function as an argument, and it all fits within a single line of code.

Three levels of abstraction

Especially when analyzing images, there is an overwhelming amount of information, and it is useful to approach the data in three levels of abstraction:

1. *Image-by-image*; where images from a dataset can be stepped through (or animated). This way, the full complexity of the data can be appreciated—very useful for understanding how to simplify it, e.g., by applying cuts ("region of interest": ROI) and background subtractions etc. It is, however, difficult to see trends and get a statistical overview of the dataset this way.

2. *Waterfall plotting*; where images are projected or otherwise transformed from a 2D matrix to a 1D vector (using an anonymous function as an argument)—such that the entire dataset can be put in a single figure. This also works well for 1D data such as a scope trace (where the full data is shown). Waterfall plots make it easy to see trends and correlations when sorted by the scan variable or other measurable quantities. However, sometimes waterfall plots can be difficult to read, as they pack a lot of information.

3. *Correlation* or *scan plots*; where images or vector data are distilled into a single scalar value for each shot (again using an anonymous function as an argument). This is very useful for a simplified, physically meaningful representation of the dataset, but should always be checked against a more complete waterfall plot. This is because sometimes in the process of information distillation, the single scalar value extracted does not accurately represent the intended physical quantity.

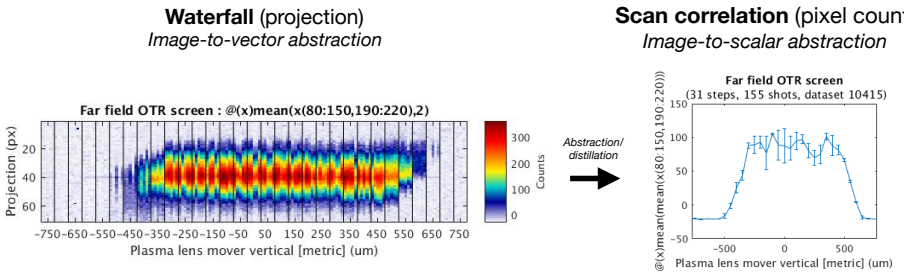

Figure B.2: Waterfall plot versus a scan-correlation plot: two different levels of abstraction of the same dataset. The waterfall contains more (sometimes useful) information, but the more distilled correlation plot is easier to interpret. The corresponding code is shown in Fig. B.3.

The process of analyzing a dataset typically follows these three steps: (1) first look at the raw data, (2) abstract it to look for trends, then (3) distill it down to the

desired quantity. Once this process has been completed and fine-tuned for a single dataset of a certain type, it is typically very fast to repeat it—just reuse (copy and paste) the same single-line functional calls, changing only the dataset ID. Over time, a "library" of one-liners are built up for use in different types of analyses. The use of a command line also conveniently saves the history of which analyses have been run and how they were gradually fine-tuned. See Fig. B.2 for an example output of abstraction levels (2) and (3).

Once an analysis one-liner script has been successfully written (typically takes only a few minutes), the data is interpreted and the quality is evaluated. If the quality is not sufficient—maybe finer scan steps or a different scan range is needed, or a camera/scope was not working—the dataset is simply retaken and the analysis quickly recalculated. This process is iterated until the desired measurement is reached.

A final note is that while these three functions should always be available (see the below code example), it may eventually be beneficial to write separate scripts for routine analyses that are repeated a large number of times. In this case, the sometimes considerable amount of time spent on polishing a script may be worthwhile.

Code example

Figure B.3 shows an example of such a one-liner code system. The goal in this specific example is to find the aperture of an active plasma lens capillary: if the beam passes through the capillary cleanly, it will appear on an OTR screen (far) downstream—if it hits the capillary wall, it will not. A scan was made where the capillary was vertically offset with a precision mover.

First the images are viewed individually to determine the appropriate ROI: x-pixels 190–220 and y-pixels 80–150. A waterfall plot with the vertical projection is then plotted—see Fig. B.2 (left). Having confirmed that this is a good scan, we plot the scan-correlation plot—see Fig. B.2 (right)—which shows clearly the relative transmission percentage as a function of the vertical offset of the capillary. From this final plot we can easily determine that the FWHM is approximately 900 μm. Since this is less than the desired full 1 mm aperture, we are likely dealing with an angular misalignment, such that the capillary must somehow be realigned before continuing. After realigning, we simply redo the scan and reuse the same one-liner script to quickly determine the new status of the alignment.

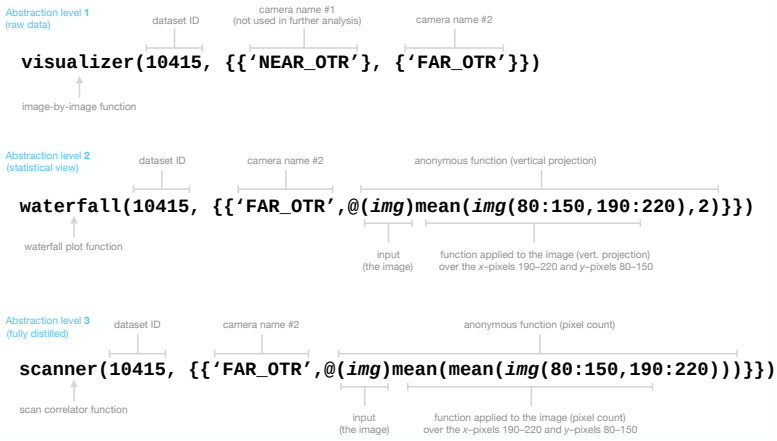

Figure B.3: Three-step code example based on the rapid-iteration data analysis tool. See Fig. B.2 for the corresponding output plots to lines 2 and 3. Note in particular the syntax similarity between the three functions—this helps to speed up the process of distilling the data, by allowing fine tuned inputs to be quickly moved to the next level of abstraction.

Code repositories

An example of such a two-part software structure can be found in the DAQ and DAN code repositories for the CLEAR User Facility, on the CERN GitLab (open). The software is written in MATLAB.

- DAQ: https://gitlab.cern.ch/CLEAR/CLEAR_DAQ
- DAN: https://gitlab.cern.ch/CLEAR/CLEAR_DAN

B.3 Conclusions

The method outlined in this appendix was used successfully in both the FACET and CLEAR facilities, with a typical turn-around time of 5–10 minutes per dataset (data collection and analysis). If the datasets were inconclusive or showing a bad state, the machine would be tweaked and then the dataset retaken. As soon as the desired machine state was achieved, having used this method to characterize the machine, real physics measurements were taken. Only after the "golden" datasets were gathered was the careful post-processing performed in preparation for a manuscript.

Clearly, this method is not suitable in all situations, e.g., if the rate of data taking is very slow such that each shot must be carefully planned out. Nevertheless, it may be useful to some—in which case more scientific output can hopefully be produced with less wasted beam time.

Bibliography

[1] C. A. Lindstrøm, E. Adli, J. Pfingstner, E. Marín and D. Schulte, "Transverse tolerances of a multi-stage plasma wakefield accelerator," *Proceedings of IPAC2016, Busan, Korea* (JACoW, Geneva, 2016), p. 2561.

[2] Carl A. Lindstrøm and Erik Adli, "Design of general apochromatic drift-quadrupole beam lines," Phys. Rev. Accel. Beams **19**, 071002 (2016).

[3] C. A. Lindstrøm, E. Adli, J. M. Allen, J. P. Delahaye, M. J. Hogan, C. Joshi, P. Muggli, T. O. Raubenheimer and V. Yakimenko, "Staging optics considerations for a plasma wakefield acceleration linear collider," Nucl. Instrum. Methods Phys. Res. A **829**, 224 (2016).

[4] C. A. Lindstrøm, E. Adli, J. M. Allen, W. An, C. Beekman, C. I. Clarke, C. E. Clayton, S. Corde, A. Doche, J. Frederico, S. J. Gessner, S. Z. Green, M. J. Hogan, C. Joshi, M. Litos, W. Lu, K. A. Marsh, W. B. Mori, B. D. O'Shea, N. Vafaei-Najafabadi and V. Yakimenko, "Measurement of transverse wakefields induced by a misaligned positron bunch in a hollow channel plasma accelerator," Phys. Rev. Lett. **120**, 124802 (2018).

[5] Carl A. Lindstrøm and Erik Adli, "Analytic plasma wakefield limits for active plasma lenses," arXiv:1802.02750 (2018).

[6] C. A. Lindstrøm, K. N. Sjobak, E. Adli, J.-H. Röckemann, L. Schaper, J. Osterhoff, A. E. Dyson, S. M. Hooker, W. Farabolini, D. Gamba and R. Corsini, "Overview of the CLEAR plasma lens experiment," Nucl. Instrum. Methods Phys. Res. A **909**, 379 (2018).

[7] C. A. Lindstrøm, E. Adli, G. Boyle, R. Corsini, A. E. Dyson, W. Farabolini, S. M. Hooker, M. Meisel, J. Osterhoff, J.-H. Röckemann, L. Schaper and K. N. Sjobak, "Emittance preservation in an aberration-free active plasma lens," Phys. Rev. Lett. **121**, 194801 (2018).

[8] E. Adli, C. A. Lindstrøm, J. Allen, C. I. Clarke, J. Frederico, S. J. Gessner, S. Z. Green, M. J. Hogan, M. D. Litos, G. R. White, V. Yakimenko, W. An, C. E. Clayton, K. A. Marsh, W. B. Mori, C. Joshi, N. Vafaei-Najafabadi, S. Corde and W. Lu, "Transverse oscillations in plasma wakefield experiments at FACET," Nucl. Instrum. Methods Phys. Res. A **829**, 94 (2016).

[9] S. J. Gessner, J. M. Allen, C. I. Clarke, J.-P. Delahaye, J. T. Frederico, S. Z. Green, C. Hast, M. J. Hogan, N. Lipkowitz, M. D. Litos, B. D. O'Shea, D. R. Walz, V. Yakimenko, G. Yocky, E. Adli, C. A. Lindstrøm, W. An, C. E. Clayton, C. Joshi, K. A. Marsh, W. B. Mori, N. Vafaei-Najafabadi, S. Corde, A. Doche, W. Lu, "Demonstration of the hollow channel plasma wakefield accelerator," *Proceedings of IPAC2016, Busan, Korea* (JACoW, Geneva, 2016), p. 3202.

[10] S. Gessner, E. Adli, J. M. Allen, W. An, C. I. Clarke, C. E. Clayton, S. Corde, J.-P. Delahaye, J. Frederico, S. Z. Green, C. Hast, M. J. Hogan, C. Joshi, C. A. Lindstrøm, N. Lipkowitz, M. Litos, W. Lu, K. A. Marsh, W. B. Mori, B. O'Shea, N. Vafaei-Najafabadi, D. Walz, , V. Yakimenko and G. Yocky, "Demonstration of a positron beam-driven hollow channel plasma wakefield accelerator," Nat. Commun. **7**, 11785 (2016).

[11] A. Doche, C. Beekman, S. Corde, J. M. Allen, C. I. Clarke, J. Frederico, S. J. Gessner, S. Z. Green, M. J. Hogan, B. O'Shea, V. Yakimenko, W. An, C. E. Clayton, C. Joshi, K. A. Marsh, W. B. Mori, N. Vafaei-Najafabadi, M. D. Litos, E. Adli, C. A. Lindstrøm, W. Lu, "Acceleration of a trailing positron bunch in a plasma wakefield accelerator," Sci. Rep. **7**, 14180 (2017).

[12] D. Gamba, R. Corsini, S. Curt, S. Doebert, W. Farabolini, G. Mcmonagle, P. K. Skowronski, F. Tecker, S. Zeeshan, E. Adli, C. A. Lindstrøm, A. Ross and L. M. Wroe, "The CLEAR User Facility at CERN," Nucl. Instrum. Methods Phys. Res. A **909**, 480 (2018).

[13] R. Corsini, A. Curcio, S. Curt, S. Döbert, W. Farabolini, D. Gamba, R. Garcia Alia, T. Lefevre, G. McMonagle, P. K. Skowronski, M. Tali, F. Tecker, E. Adli, C. A. Lindstrøm, K. N. Sjobak, R. M. Jones and A. Lagzda, "First experiments at the CLEAR User Facility," *Proceedings of IPAC2018, Vancouver, BC, Canada* (JACoW, Geneva 2018), p. 4066.

[14] P. Muggli, O. Reimann, E. Adli, C. A. Lindstrøm, V. K. B. Olsen, J. Allen, S. J. Gessner, S. Z. Green, M. J. Hogan, M. D. Litos, B. D. O'Shea, V. Yakimenko, L. D. Amorim, G. Andonian, C. Joshi, K. A. Marsh, W. B. Mori, N. Vafaei-Najafabadi, O. Williams, N. C. Lopes, L. O. Silva, J. Vieira, "Measuring the self-modulation instability of electron and positron bunches in plasmas," *Proceedings of IPAC2015, Richmond, Virginia, USA* (JACoW, Geneva, 2015), p. 2506.

[15] E. Adli, V. K. Berglyd Olsen, C. A. Lindstrøm, P. Muggli, O. Reimann, J. M. Vieira, L. D. Amorim, C. I. Clarke, S. J. Gessner, S. Z. Green, M. J. Hogan, M. D. Litos, B. D. O'Shea, V. Yakimenko, C. Clayton, K. A. Marsh, W. B. Mori, C. Joshi, N. Vafaei-Najafabadi and O. Williams, "Progress of plasma wakefield self-modulation experiments at FACET," Nucl. Instrum. Methods Phys. Res. A **829**, 334 (2016).

[16] J. Pfingstner, E. Adli, C. A. Lindstrøm, E. Marín and D. Schulte, "Considerations for a drive beam scheme for a plasma wakefield linear collider," *Proceedings of IPAC2016, Busan, Korea* (JACoW, Geneva, 2016), p. 2565.

[17] E. Adli, C. A. Lindstrøm, J. Allen, C. I. Clarke, J. Frederico, S. J. Gessner, S. Z. Green, M. J. Hogan, M. D. Litos, B. O'Shea, V. Yakimenko, W. An, C. E. Clayton, K. A. Marsh, W. B. Mori, C. Joshi, N. Vafaei-Najafabadi, S. Corde and W. Lu, "Long-range attraction of an ultrarelativistic electron beam by a column of neutral plasma," New J. Phys. **18**, 103013 (2016).

[18] B. Hidding, A. Beaton, A. F. Habib, T. Heinemann, G. G. Manahan, P. Scherkl, A. Sutherland, D. Ullmann, E. Adli, C. A. Lindstrøm, S. J. Gessner, G. Andonian, A. Deng, J. B. Rosenzweig, D. L. Bruhwiler, J. R. Cary, C. I. Clarke, S. Z. Green, M. J. Hogan, B. D. O'Shea, V. Yakimenko, M. Downer, R. Zgadzaj, A. Knetsch, G. Wittig, O. S. Karger, M. D. Litos. J. D. A. Smith, "First measurements of Trojan Horse injection in a plasma wakefield accelerator," *Proceedings of IPAC2017, Copenhagen, Denmark* (JACoW, Geneva, 2017), p. 1252.

[19] Oscar Barbalat, "Applications of particle accelerators," *Proceedings of the 4th CERN Accelerator School, Jülich, Germany* (CERN, Geneva, 1990), p. 17.

[20] US Department of Energy, *Accelerators for America's Future* (US Department of Energy, Washington, DC, 2009).

[21] Joseph J. Thomson, "Cathode rays," Philos. Mag. **44**, 293 (1897).

[22] Ernest Rutherford, "The scattering of alpha and beta particles by matter and the structure of the atom," Philos. Mag. **21**, 669 (1911).

[23] James Chadwick, "The existence of a neutron," Proc. Royal Soc. Lond. A **136**, 692 (1932).

[24] Carl D. Anderson, "The positive electron," Phys. Rev. **43**, 491 (1933).

[25] O. Chamberlain, E. Segrè, C. Wiegand and T. Ypsilantis, "Observation of antiprotons," Phys. Rev. **100**, 947 (1955).

[26] C. L. Cowan, F. Reines, F. B. Harrison, H. W. Kruse and A. D. McGuire, "Detection of the free neutrino: a confirmation," Science **124**, 103 (1956).

[27] E. D. Bloom *et al.*, "High-energy inelastic $e-p$ scattering at 6° and 10°," Phys. Rev. Lett. **23**, 930 (1969).

[28] M. Breidenbach, J. I. Friedman, H. W. Kendall, E. D. Bloom, D. H. Coward, H. DeStaebler, J. Drees, L. W. Mo and R. E. Taylor, "Observed behavior of highly inelastic electron–proton scattering," Phys. Rev. Lett. **23**, 935 (1969).

[29] M. L. Perl *et al.*, "Evidence for anomalous lepton production in $e^+ - e^-$ annihilation," Phys. Rev. Lett. **35**, 1489 (1975).

[30] G. Arnison *et al.* (UA1 Collaboration), "Experimental observation of isolated large transverse energy electrons with associated missing energy at $s = 540$ GeV," Phys. Lett. B **122**, 103 (1983).

[31] P. Bagnaia *et al.* (UA2 Collaboration), "Evidence for $Z^0 \to e^+e^-$ at the CERN $\bar{p}p$ collider," Phys. Lett. B **129**, 130 (1983).

[32] F. Abe *et al.* (CDF Collaboration), "Observation of top quark production in $\bar{p}p$ collisions with the collider detector at Fermilab," Phys. Rev. Lett. **74**, 2626 (1995).

[33] G. Aad *et al.* (ATLAS Collaboration), "Observation of a new particle in the search for the Standard Model Higgs boson with the ATLAS detector at the LHC," Phys. Lett. B **716**, 1 (2012).

[34] S. Chatrchyan *et al.* (CMS Collaboration), "Observation of a new boson at a mass of 125 GeV with the CMS experiment at the LHC," Phys. Lett. B **716**, 30 (2012).

[35] Michael E. Peskin and Daniel V. Schroeder, *An Introduction to Quantum Field Theory* (Westview Press, Boulder, CO, 1995).

[36] B. Odom, D. Hanneke, B. D'Urso and G. Gabrielse, "New measurement of the electron magnetic moment using a one-electron quantum cyclotron," Phys. Rev. Lett. **97**, 030801 (2006).

[37] F. Archilli, M.-O. Bettler, P. Owen and K. A. Petridis, "Flavour-changing neutral currents making and breaking the Standard Model," Nature (London) **546**, 221 (2017).

[38] Hendrik A. Lorentz, *Versuch einer Theorie der electrischen und optischen Erscheinungen in bewegten Körpern* (E. J. Brill, Leiden, 1895).

[39] Gustaf Ising, "Prinzip einer Methode zur Herstellung von Kanalstrahlen höher Voltzahl," Ark. Mat. Astron. Fys. **18**, 1 (1924).

[40] Rolf Wideröe, "Über ein neues Prinzip zur Herstellung hoher Spannungen," R. Archiv f. Elektrotechnik **21**, 387 (1928).

[41] D. Tommasini *et al.*, "Status of the 16 T dipole development program for a future hadron collider," IEEE Trans. Appl. Supercond **28**, 1 (2018).

[42] O. S. Brüning, P. Collier, P. Lebrun, S. Myers, R. Ostojic, J. Poole and P. Proudlock (editors), *LHC Design Report* (CERN, Geneva, 2004).

[43] CERN, *LEP Design Report v.2: The LEP Main Ring* (CERN, Geneva, 1984).

[44] Joseph Larmor, "On the theory of the magnetic influence on spectra; and on the radiation from moving ions," Philos. Mag. **44**, 503 (1897).

[45] John D. Jackson, *Classical Electrodynamics, 3rd edition* (New York, NY, 1999).

[46] David d'Enterria, "Physics at the FCC-ee," *Particle Physics at the Year of Light* (World Scientific, Singapore, 2017), p. 182; arXiv:1601.06640.

[47] Vladimir Shiltsev, "The first colliders: AdA, VEP-1 and Princeton–Stanford," *Challenges and Goals for Accelerators in the XXI Century* (World Scientific, Singapore, 2016), p. 61; arXiv:1307.3116.

[48] T. Behnke (editor) *et al.*, *The International Linear Collider Technical Design Report*, (International Linear Collider, 2013).

[49] M. Aicheler (editor) *et al.*, *A Multi-TeV linear collider based on CLIC technology: CLIC Conceptual Design Report* (CERN, Geneva, 2013).

[50] M. J. Boland *et al.* (CLIC and CLICdp collaborations), "Updated baseline for a staged Compact Linear Collider," *CERN-2016-004* (CERN, Geneva, 2016).

[51] P. Royole-Degieux, R. Takahashi and B. Warmbein, "The ILC project keeps its momentum high," *CERN Courier* (15 Apr 2016).

[52] B. P. Abbott *et al.* (LIGO Scientific Collaboration and Virgo Collaboration), "Observation of gravitational waves from a binary black hole merger," Phys. Rev. Lett. **116**, 061102 (2016).

[53] A. Garner *et al.*, "Status and first results of the Canarias infrared camera experiment (CIRCE) for the Gran Telescopio Canarias," Proc. SPIE **9147**, 91474A (2014).

[54] P. J. Napier, D. S. Bagri, B. G. Clark, A. E. E. Rogers, J. D. Romney, A. R. Thompson and R. C. Walker, "The Very Long Baseline Array," Proceedings of the IEEE **82**, 658 (1994).

[55] John M. J. Madey, "Stimulated emission of bremsstrahlung in a periodic magnetic field," J. Appl. Phys. **42**, 1906 (1971).

[56] Louis de Broglie, "A tentative theory of light quanta," Philos. Mag. **47**, 446 (1924).

[57] Deborah D. Stine, *The Manhattan Project, the Apollo Program, and Federal Energy Technology R&D Programs: A Comparative Analysis* (Congressional Research Service, 2009).

[58] Michael Hiltzik, *Big Science: Ernest Lawrence and the Invention that Launched the Military-Industrial Complex* (Simon & Schuster, New York, NY, 2015).

[59] European Commission, "On the application of council regulation (EC) No 723/2009 of 25 June 2009 on the community legal framework for a European Research Infrastructure Consortium (ERIC)," *COM(2014) 460 final* (European Commission, Brussels, 2014).

[60] "U.S. to contribute $531 million to CERN's Large Hadron Collider project, *CERN Press Release* (8 Dec 1997).

[61] S. Peggs (editor) *et al.*, *ESS Technical Design Report* (ESS, Lund, 2013).

[62] Walter Wuensch, "High-gradient X-band technology: from TeV colliders to light sources and more," *CERN Courier* (23 Mar 2018).

[63] Alexander W. Chao and Weiren Chou (editors), *Reviews of Accelerator Science and Technology, Volume 2: Medical Applications of Accelerators* (World Scientific, Singapore, 2009).

[64] CERN, "Birth of the Web," https://home.cern/topics/birth-web.

[65] Liliana Teodorescu, "Artificial neural networks in high-energy physics," *Inverted CERN School of Computing, Geneva, Switzerland, (CERN, Geneva, 2005), p. 13*.

[66] "R&D pays: Economists suggest 20% return on public investment for research and innovation," *Science|Business Reporting* (Jun 2017).

[67] OECD, *Main Science and Technology Indicators, Vol. 2017 Issue 2* (OECD Publishing, Paris, 2018).

[68] Walter Wuensch, "CLIC accelerating structure development," *Proceedings of EPAC2008, Genoa, Italy* (JACoW, Geneva, 2008), p. 2922.

[69] A. Grudiev, S. Calatroni and W. Wuensch, "New local field quantity describing the high gradient limit of accelerating structures," Phys. Rev. ST Accel. Beams **12**, 102001 (2009).

[70] H. H. Braun, S. Döbert, I. Wilson and W. Wuensch, "Frequency and temperature dependence of electrical breakdown at 21, 30, and 39 GHz," Phys. Rev. Lett. **90**, 224801 (2003).

[71] Walter Wuensch, "Ultimate field gradient in metallic structures," *Proceedings of IPAC2017, Copenhagen, Denmark* (JACoW, Geneva, 2017), p. 24.

[72] G. L. Carr, M. C. Martin, W. R. McKinney, K. Jordan, G. R. Neil and G. P. Williams, "High-power terahertz radiation from relativistic electrons," Nature (London) **420**, 153 (2002).

[73] S. Bielawski *et al.*, "Tunable narrowband terahertz emission from mastered laser–electron beam interaction," Nat. Phys. **4**, 390 (2008).

[74] Donna Strickland and Gerard Mourou, "Compression of amplified chirped optical pulses," Opt. Commun. **56**, 219 (1985).

[75] E. Esarey, C. B. Schroeder and W. P. Leemans, "Physics of laser-driven plasma-based electron accelerators," Rev. Mod. Phys. **81**, 1229 (2009).

[76] Kazuhisa Nakajima, "Laser-driven plasma electron acceleration and radiation," Rev. Accel. Sci. Technol. **9**, 19 (2017).

[77] Mark J. Hogan, "Electron and positron beam-driven plasma acceleration," Rev. Accel. Sci. Technol. **9**, 63 (2017).

[78] Erik Adli and Patric Muggli, "Proton-beam-driven plasma acceleration," Rev. Accel. Sci. Technol. **9**, 85 (2017).

[79] Chunguang Jing, "Dielectric wakefield accelerators," Rev. Accel. Sci. Technol. **9**, 127 (2017).

[80] K. P. Wootton, J. McNeur and K. J. Leedle, "Dielectric laser accelerators: designs, experiments, and applications," Rev. Accel. Sci. Technol. **9**, 105 (2017).

[81] S. V. Bulanov, F. Pegoraro, A. M. Pukhov and A. S. Sakharov, "Transverse-wake wave breaking," Phys. Rev. Lett. **78**, 4205 (1997).

[82] A. Buck *et al.*, "Shock-front injector for high-quality laser-plasma acceleration," Phys. Rev. Lett. **110**, 185006 (2013).

[83] N. Vafaei-Najafabadi *et al.*, "Beam loading by distributed injection of electrons in a plasma wakefield accelerator," Phys. Rev. Lett. **112**, 025001 (2014).

[84] B. Hidding, G. Pretzler, J. B. Rosenzweig, T. Königstein, D. Schiller and D. L. Bruhwiler, "Ultracold electron bunch generation via plasma photocathode emission and acceleration in a beam-driven plasma blowout," Phys. Rev. Lett. **108**, 035001 (2012).

[85] E. L. Clark *et al.*, "Measurements of energetic proton transport through magnetized plasma from intense laser interactions with solids," Phys. Rev. Lett. **84**, 670 (2000).

[86] A. Maksimchuk, S. Gu, K. Flippo, D. Umstadter and V. Yu. Bychenkov, "Forward ion acceleration in thin films driven by a high-intensity laser," Phys. Rev. Lett. **84**, 4108 (2000).

[87] R. A. Snavely *et al.*, "Intense high-energy proton beams from petawatt-laser irradiation of solids," Phys. Rev. Lett. **85**, 2945 (2000).

[88] E. Brunetti *et al.*, "Low emittance, high brilliance relativistic electron beams from a laser-plasma accelerator," Phys. Rev. Lett. **105**, 215007 (2010).

[89] H. Braun, E. Boggasch, A. Tauschwitz and D. H. H. Hoffmann, "Application of plasma lenses in positron sources," *Proceedings of EPAC1992, Berlin, Germany* (Editions Frontièrs, Gif-sur-Yvette, 1992), p. 1650.

[90] D. K. Johnson *et al.*, "Positron source from X-rays emitted by plasma betatron motion," *Proceedings of LINAC2006, Knoxville, Tennessee, USA* (JACoW, Knoxville, TN, 2006), p. 94.

[91] R. Weingartner *et al.*, "Imaging laser-wakefield-accelerated electrons using miniature magnetic quadrupole lenses," Phys. Rev. ST Accel. Beams **14**, 052801 (2011).

[92] F. Marteau *et al.*, "Variable high gradient permanent magnet quadrupole (QUAPEVA)," Appl. Phys. Lett. **111**, 253503 (2017).

[93] J. Harrison, Y. Hwang, O. Paydar, J. Wu, E. Threlkeld, J. Rosenzweig, P. Musumeci and R. Candler, "High-gradient microelectromechanical system quadrupole electromagnets for particle beam focusing and steering," Phys. Rev. ST Accel. Beams **18**, 023501 (2015).

[94] J. van Tilborg *et al.*, "Active plasma lensing for relativistic laser-plasma-accelerated electron beams," Phys. Rev. Lett. **115**, 184802 (2015).

[95] Pisin Chen, "A possible final focusing mechanism for linear colliders," Part. Accel. **20**, 171 (1987).

[96] Daniel Schulte, "Application of advanced accelerator concepts for colliders," Rev. Accel. Sci. Technol. **9**, 209 (2017).

[97] S. M. Hooker, R. Bartolini, S. P. D. Mangles, A. Tünnermann, L. Corner, J. Limpert, A. Seryi and R. Walczak, "Multi-pulse laser wakefield acceleration: a new route to efficient, high-repetition-rate plasma accelerators and high flux radiation sources," J. Phys. B: At. Mol. Opt. Phys. **47**, 234003 (2014).

[98] Peter F. Moulton, "Spectroscopic and laser characteristics of Ti:Al_2O_3," J. Opt. Soc. Am. B **3**, 125 (1986).

[99] J. Cowley *et al.*, "Excitation and control of plasma wakefields by multiple laser pulses," Phys. Rev. Lett. **119**, 044802 (2017).

[100] T. Nubbemeyer *et al.*, "1 kW, 200 mJ picosecond thin-disk laser system," Opt. Lett. **42**, 1381 (2017).

[101] C. Jauregui, J. Limpert and A. Tünnermann, "High-power fibre lasers," Nat. Photonics **7**, 861 (2013).

[102] Toshiki Tajima and John M. Dawson, "Laser electron accelerator," Phys. Rev. Lett. **43**, 267 (1979).

[103] Gersh I. Budker, "Relativistic stabilized electron beam: I. Physical principles and theory," *Proceedings of the CERN Symposium on High Energy Accelerators and Pion Physics* (CERN, Geneva, 1956), p. 68.

[104] Vladimir I. Veksler, "Coherent principle of acceleration of charged particles," *Proceedings of the CERN Symposium on High Energy Accelerators and Pion Physics* (CERN, Geneva, 1956), p. 80.

[105] Yakov B. Fainberg, "The use of plasma waveguides as accelerating structures in linear accelerators," *Proceedings of the CERN Symposium on High Energy Accelerators and Pion Physics* (CERN, Geneva, 1956), p. 84.

[106] Hildred Blewett, "CERN Symposium on High-Energy Accelerators and Pion Physics," Physics Today **9**, 18 (1956).

[107] R. D. Ruth, A. W. Chao, P. L. Morton and P. B. Wilson, "A plasma wake field accelerator," Part. Accel. **17**, 171 (1985).

[108] Pisin Chen and John M. Dawson, "The plasma wake field accelerator," AIP Conf. Proc. **130**, 201 (1985).

[109] John M. Dawson, "Personal recollections on the development of plasma accelerators and light sources," AIP Conf. Proc. **569**, 3 (2001).

[110] Chandrashekhar J. Joshi, "John Dawson's advanced accelerator years," AIP Conf. Proc. **569**, 26 (2001).

[111] Chandrashekhar J. Joshi, "The development of laser- and beam-driven plasma accelerators as an experimental field," Phys. Plasmas **14**, 055501 (2007).

[112] Tom Katsouleas, "Physical mechanisms in the plasma wake-field accelerator," Phys. Rev. A **33**, 2056 (1986).

[113] J. B. Rosenzweig, D. B. Cline, B. Cole, H. Figueroa, W. Gai, R. Konecny, J. Norem, P. Schoessow and J. Simpson, "Experimental observation of plasma wake-field acceleration," Phys. Rev. Lett. **61**, 98 (1988).

[114] K. Nakajima, A. Enomoto, H. Kobayashi, H. Nakanishi, Y. Nishida, A. Ogata, S. Ohsawa, T. Oogoe, T. Shoji and T. Urano, "Plasma wake-field accelerator experiments at KEK," Nucl. Instrum. Methods Phys. Res. A **292**, 12 (1990).

[115] J. B. Rosenzweig, B. Breizman, T. Katsouleas and J. J. Su, "Acceleration and focusing of electrons in two-dimensional nonlinear plasma wake fields," Phys. Rev. A **44**, R6189 (1991).

[116] D. H. Whittum, W. M. Sharp, S. S. Yu, M. Lampe and G. Joyce, "Electron-hose instability in the ion-focused regime," Phys. Rev. Lett. **67**, 991 (1991).

[117] Konstantin Lotov, "Instability of long driving beams in plasma wakefield accelerators," *Proceedings of EPAC1998, Stockholm, Sweden* (IOP Publishing, Bristol, 1998), p. 806.

[118] N. Barov, J. B. and Rosenzweig, M. E. Conde, W. Gai and J. G. Power, "Observation of plasma wakefield acceleration in the underdense regime," Phys. Rev. ST Accel. Beams **3**, 011301 (2000).

[119] M. J. Hogan *et al.*, "Ultrarelativistic-positron-beam transport through meter-scale plasmas," Phys. Rev. Lett. **90**, 205002 (2003).

[120] B. E. Blue *et al.*, "Plasma-wakefield acceleration of an intense positron beam," Phys. Rev. Lett. **90**, 214801 (2003).

[121] P. Muggli *et al.*, "Meter-scale plasma-wakefield accelerator driven by a matched electron beam," Phys. Rev. Lett. **93**, 014802 (2004).

[122] M. J. Hogan *et al.*, "Multi-GeV energy gain in a plasma-wakefield accelerator," Phys. Rev. Lett. **95**, 054802 (2005).

[123] W. Lu, C. Huang, M. Zhou, W. B. Mori and T. Katsouleas, "Nonlinear theory for relativistic plasma wakefields in the blowout regime," Phys. Rev. Lett. **96**, 165002 (2006).

[124] W. Lu, C. Huang, M. Zhou, M. Tzoufras, F. S. Tsung, W. B. Mori and T. Katsouleas, "A nonlinear theory for multidimensional relativistic plasma wave wakefields," Phys. Plasmas. **13**, 056709 (2006).

[125] C. Huang *et al.*, "Hosing instability in the blow-out regime for plasma-wakefield acceleration," Phys. Rev. Lett. **99**, 255001 (2007).

[126] I. Blumenfeld *et al.*, "Energy doubling of 42 GeV electrons in a metre-scale plasma wakefield accelerator," Nature (London) **445**, 741 (2007).

[127] Ian Blumenfeld, "Scaling of the longitudinal electric fields and transformer ratio in a non-linear plasma wakefield accelerator," *Ph.D. thesis* (Stanford University, 2009).

[128] E. Kallos, T. Katsouleas, W. D. Kimura, K. Kusche, P. Muggli, I. Pavlishin, I. Pogorelsky, D. Stolyarov, V. Yakimenko, "High-gradient plasma-wakefield acceleration with two subpicosecond electron bunches," Phys. Rev. Lett. **100**, 074802 (2008).

[129] M. Litos *et al.*, "High-efficiency acceleration of an electron beam in a plasma wakefield accelerator," Nature (London) **515**, 92 (2014).

[130] S. Corde *et al.*, "Multi-gigaelectronvolt acceleration of positrons in a self-loaded plasma wakefield," Nature (London) **524**, 442 (2015).

[131] T. J. Mehrling, R. A. Fonseca, A. Martinez de la Ossa and J. Vieira, "Mitigation of the hose instability in plasma-wakefield accelerators," Phys. Rev. Lett. **118**, 174801 (2017).

[132] A. Aschikhin *et al.*, "The FLASHForward facility at DESY," Nucl. Instrum. Methods Phys. Res. A **806**, 175 (2016).

[133] M. Gross *et al.*, "Observation of the self-modulation instability via time-resolved measurements," Phys. Rev. Lett. **120**, 144802 (2018).

[134] G. Loisch *et al.*, "Observation of high transformer ratio plasma wakefield acceleration," Phys. Rev. Lett. **121**, 064801 (2018).

[135] E. Adli *et al.* (AWAKE Collaboration), "Experimental observation of proton bunch modulation in a plasma, at varying plasma densities," arXiv:1809.04478 (2018).

[136] E. Adli *et al.* (AWAKE Collaboration), "Acceleration of electrons in the plasma wakefield of a proton bunch," Nature (London) **561**, 363 (2018).

[137] E. Gschwendtner *et al.*, "AWAKE, The Advanced Proton Driven Plasma Wakefield Acceleration Experiment at CERN," Nucl. Instrum. Methods Phys. Res. A **829**, 76 (2016).

[138] C. Joshi *et al.*, "Plasma wakefield acceleration experiments at FACET II," Plasma Phys. Control. Fusion **60**, 034001 (2018).

[139] Chandrashekhar Joshi and Thomas Katsouleas, "Plasma accelerators at the energy frontier and on tabletops," Physics Today **56**, 47 (2003).

[140] E. Esarey, P. Sprangle, J. Krall and A. Ting, "Overview of plasma-based accelerator concepts," IEEE T. Plasma Sci. **24**, 252 (1996).

[141] P. H. Rebut, R. J. Bickerton and B. E. Keen, "The Joint European Torus: installation, first results and prospects," Nucl. Fusion **25**, 1011 (1985).

[142] Robert Aymar, "The ITER project," IEEE T. Plasma Sci. **25**, 1187 (1997); `https://www.iter.org`.

[143] Perry B. Wilson and James E. Griffin, "High energy electron linacs; application to storage ring RF systems and linear colliders," AIP Conf. Proc. **87**, 450 (1982).

[144] M. Litos *et al.*, "9 GeV energy gain in a beam-driven plasma wakefield accelerator," Plasma Phys. Control. Fusion **58**, 034017 (2016).

[145] Antoine Doche, "Particle acceleration with beam driven plasma wakefield," *Ph.D. thesis* (Université Paris-Saclay, 2018).

[146] Particle Physics Project Prioritization Panel (P5), *Building for Discovery — Strategic Plan for U.S. Particle Physics in the Global Context* (U.S. Department of Energy, Washington DC, 2014).

[147] L. K. Len *et al.*, *Advanced Accelerator Concepts Research Roadmap Workshop report* (U.S. Department of Energy, Washington DC, 2016).

[148] Eric R. Colby and L. K. Len, "Roadmap to the future," Rev. Accel. Sci. Technol. **9**, 1 (2016).

[149] Pushpalatha C. Bhat and Roy Rubinstein, "The International Committee for Future Accelerators (ICFA): history and the future," arXiv:1809.09718 (2018).

[150] Brigitte Cros and Patric Muggli, *Towards a Proposal for an Advanced Linear Collider, Report on the Advanced and Novel Accelerators for High Energy Physics Roadmap Workshop* (CERN, Geneva, 2017).

[151] Brigitte Cros and Patric Muggli, "Charting a course for advanced accelerators," CERN Courier **57**, 31 (2017).

[152] E. Adli, J.-P. Delahaye, S. J. Gessner, M. J. Hogan, T. O. Raubenheimer, W. An, C. Joshi and W. B. Mori, "A beam driven plasma-wakefield linear collider: from Higgs factory to multi-TeV," *Proceedings of the Snowmass Process CSS2013* (2013); arXiv:1308.1145.

[153] J. Rosenzweig, N. Barov, A. Murokh, E. Colby and P. Colestock, "Towards a plasma wake-field acceleration-based linear collider," Nucl. Instrum. Methods Phys. Res. A **410**, 532 (1998).

[154] A. Seryi, M. J. Hogan, S. Pei, T. O. Raubenheimer, P. Tenenbaum, T. Katsouleas, C. Huang, C. Joshi, W. B. Mori and P. Muggli, "A concept of plasma wake field acceleration linear collider (PWFA-LC)," *Proceedings of PAC2009, Vancouver, BC, Canada* (TRIUMF, Vancouver, 2010), p. 2688.

[155] C. B. Schroeder, E. Esarey, C. G. R. Geddes, C. Benedetti and W. P. Leemans, "Physics considerations for laser-plasma linear colliders," Phys. Rev. ST Accel. Beams **13**, 101301 (2010).

[156] R. J. England *et al.*, "Dielectric laser accelerators," Rev. Mod. Phys. **86**, 1337 (2014).

[157] C. Jing, S. Antipov, P. Schoessow, A. Kanareykin, J. G. Power, M. Conde and W. Gai "Argonne Flexible Linear Collider," *Proceedings of IPAC2013, Shanghai, China* (JACoW, Geneva, 2013), p. 1322.

[158] James Gillies, "Luminosity? Why don't we just say collision rate?" Quantum Diaries (2 Mar 2011).

[159] J. E. Augustin, N. Dikansky, Ya. Derbenev, J. Rees, B. Richter, A. Skrinsky, M. Tigner and H. Wiedemann, "Limitations on performance of e^+e^- storage rings and linear colliding beam systems at high energy," *Proceedings of the Workshop on Possibilities and Limitations of Accelerators and Detectors, Fermilab, Batavia, IL, USA* (Fermilab, Batavia, IL, 1979), p. 87.

[160] Alexander W. Chao, *Physics of Collective Beam Instabilities in High-Energy Accelerators* (Wiley, New York, NY, 1993).

[161] Ernest D. Courant and Hartland S. Snyder, "Theory of the alternating-gradient synchrotron," Ann. Phys. **3**, 1 (1958).

[162] Rhon Keinigs and Michael E. Jones, "Twodimensional dynamics of the plasma wakefield accelerator," Phys. Fluids **30**, 252 (1987).

[163] W. Lu, C. Huang, M. M. Zhou, W. B. Mori and T. Katsouleas, "Limits of linear plasma wakefield theory for electron or positron beams," Phys. Plasmas **12**, 063101 (2005).

[164] Aleksander I. Akhiezer and R. V. Polovin, "On the nonlinear theory of wave motions of electron plasma," J. Exp. Theor. Phys. **3**, 696; Zh. Eksp. Teor. Fiz. **30**, 915 (1956).

[165] John M. Dawson, "Nonlinear electron oscillations in a cold plasma," Phys. Rev. **113**, 383 (1959).

[166] Gennady Stupakov, "Short-range wakefields generated in the blowout regime of plasma-wakefield acceleration," Phys. Rev. Accel. Beams **21**, 041301 (2018).

[167] James Albritton and Paul Koch, "Cold plasma wavebreaking: production of energetic electrons," Phys. Fluids **18**, 1136 (1975).

[168] T. Mehrling, J. Grebenyuk, F. S. Tsung, K. Floettmann and J. Osterhoff, "Transverse emittance growth in staged laser-wakefield acceleration," Phys. Rev. ST Accel. Beams **15**, 111303 (2012).

[169] R. A. Fonseca *et al.*, "OSIRIS: a three-dimensional, fully relativistic particle in cell code for modeling plasma based accelerators," *Computational Science — ICCS 2002* (Springer, Berlin, Heidelberg, 2002), p. 342.

[170] Chet Nieter and John R. Cary, "VORPAL: a versatile plasma simulation code," J. Comput. Phys. **196**, 448 (2004).

[171] W. An, V. K. Decyk, W. B. Mori and T. M. Antonsen, "An improved iteration loop for the three dimensional quasi-static particle-in-cell algorithm: QuickPIC," J. Comput. Phys. **250**, 165 (2013).

[172] Jean-Luc Vay and Rémi Lehe, "Simulations for plasma and laser acceleration," Rev. Accel. Sci. Technol. **9**, 165 (2016).

[173] Nelson M. Blachman and Ernest D. Courant, "Scattering of particles by the gas in a synchrotron," Phys. Rev. **74**, 140 (1948).

[174] Hans A. Bethe, "Molière's theory of multiple scattering," Phys. Rev. **89**, 1256 (1953).

[175] Kohji Hirata and Kaoru Yokoya, "Nongaussian distribution of electron beams due to incoherent stochastic processes," Part. Accel. **39**, 147 (1992).

[176] Tor O. Raubenheimer, "Emittance growth due to beam gas scattering," *KEK-92-7* (KEK, Tsukuba, 1992).

[177] Bryan W. Montague, "Emittance growth from multiple scattering in the plasma beat-wave accelerator," *Proceedings of the CAS-ECFA-INFN Workshop: Generation of High Fields for Particle Acceleration to Very-high Energies* (CERN, Geneva, 1984), p. 208.

[178] N. Kirby, M. Berry, I. Blumenfeld, M. J. Hogan, R. Ischebeck and R. Siemann, "Emittance growth from multiple Coulomb scattering in a plasma wakefield accelerator," *Proceedings of PAC2007, Albuquerque, NM, USA* (IEEE, Piscataway, NJ, 2007), p. 3097.

[179] S. Lee and T. Katsouleas, "Wakefield accelerators in the blowout regime with mobile ions," AIP Conf. Proc. **472**, 524 (1999).

[180] J. B. Rosenzweig, A. M. Cook, A. Scott, M. C. Thompson and R. B. Yoder, "Effects of ion motion in intense beam-driven plasma wakefield accelerators," Phys. Rev. Lett. **95**, 195002 (2005).

[181] S. Lee *et al.*, "Energy doubler for a linear collider," Phys. Rev. ST Accel. Beams **5**, 011001 (2002).

[182] Tor O. Raubenheimer, "An afterburner at the ILC: the collider viewpoint," AIP Conf. Proc. **737**, 86 (2004).

[183] W. An, W. Lu, C. Huang, X. Xu, M. J. Hogan, C. Joshi and W. B. Mori, "Ion motion induced emittance growth of matched electron beams in plasma wakefields," Phys. Rev. Lett. **118**, 244801 (2017).

[184] C. Benedetti, C. B. Schroeder, E. Esarey and W. P. Leemans, "Emittance preservation in plasma-based accelerators with ion motion," Phys. Rev. Accel. Beams **20**, 111301 (2017).

[185] R. Gholizadeh, T. Katsouleas, P. Muggli, C. Huang and W. Mori, "Preservation of beam emittance in the presence of ion motion in future high-energy plasma-wakefield-based colliders," Phys. Rev. Lett. **104**, 155001 (2010).

[186] P. Muggli *et al.*, "Halo formation and emittance growth of positron beams in plasmas," Phys. Rev. Lett. **101**, 055001 (2008).

[187] Konstantin V. Lotov, "Radial equilibrium of relativistic particle bunches in plasma wakefield accelerators," Phys. Plasmas **24**, 023119 (2017).

[188] Jorge Vieira and J. T. Mendonça, "Nonlinear laser driven donut wakefields for positron and electron acceleration," Phys. Rev. Lett. **112**, 215001 (2014).

[189] N. Jain, T. M. Antonsen and J. P. Palastro, "Positron acceleration by plasma wakefields driven by a hollow electron beam," Phys. Rev. Lett. **115**, 195001 (2015).

[190] T. O. Raubenheimer, F.-J. Decker and J. T. Seeman, "Beam distribution function after filamentation," *Proceedings of PAC1995, Dallas, TX, USA* (IEEE, Piscataway, NJ, 1996), p. 3291.

[191] F.-J. Decker, C. Adolphsen, W. J. Corbett, P. Emma, I. Hsu, H. Moshammer, J. T. Seeman and W. L. Spence, "Dispersion and betatron matching into the linac," *Proceedings of PAC1991, San Francisco, CA, USA* (IEEE, New York, NY, 1991), p. 905.

[192] P. Michel, C. B. Schroeder, B. A. Shadwick, E. Esarey and W. P. Leemans, "Radiative damping and electron beam dynamics in plasma-based accelerators," Phys. Rev. E **74**, 026501 (2006).

[193] C. E. Clayton *et al.*, "Transverse envelope dynamics of a 28.5-GeV electron beam in a long plasma," Phys. Rev. Lett. **88**, 154801 (2002).

[194] C. E. Clayton *et al.*, "Self-mapping the longitudinal field structure of a non-linear plasma accelerator cavity," Nat. Commun. **7**, 12483 (2016).

[195] K. A. Marsh *et al.*, "Beam matching to a plasma wake field accelerator using a ramped density profile at the plasma boundary," *Proceedings of PAC2005, Knoxville, TN, USA* (JACoW, Geneva, 2005), p. 2702.

[196] I. Dornmair, K. Floettmann and A. R. Maier, "Emittance conservation by tailored focusing profiles in a plasma accelerator," Phys. Rev. ST Accel. Beams **18**, 041302 (2015).

[197] Klaus Floettmann, "Adiabatic matching section for plasma accelerated beams," Phys. Rev. ST Accel. Beams **17**, 054402 (2014).

[198] X. L. Xu *et al.*, "Physics of phase space matching for staging plasma and traditional accelerator components using longitudinally tailored plasma profiles," Phys. Rev. Lett. **116**, 124801 (2016).

[199] Ralph Assmann and Kaoru Yokoya, "Transverse beam dynamics in plasma-based linacs," Nucl. Instrum. Methods Phys. Res. A **410**, 544 (1998).

[200] S. Cheshkov, T. Tajima, W. Horton and K. Yokoya, "Particle dynamics in multistage wakefield collider," Phys. Rev. ST Accel. Beams **3**, 071301 (2000).

[201] C. Chiu, S. Cheshkov and T. Tajima, "High energy laser-wakefield collider with synchronous acceleration," Phys. Rev. ST Accel. Beams **3**, 101301 (2000).

[202] S. Cheshkov, T. Tajima, W. Horton and K. Yokoya, "Particle dynamics and its consequences in wakefield acceleration in a high energy collider," AIP Conf. Proc. **472**, 343 (1999).

[203] T. Tajima, S. Cheshkov, W. Horton and K. Yokoya, "A nonlinear particle dynamics map of wakefield acceleration in a linear collider," AIP Conf. Proc. **472**, 153 (1999).

[204] R. Akre *et al.*, "Beam stability studies in the LCLS linac," *Proceedings of FEL'08, Gyeongju, Korea* (JACoW, Geneva, 2009), p. 94.

[205] Yue Y. Lau, "Classification of beam breakup instabilities in linear accelerators," Phys. Rev. Lett. **63**, 1141 (1989).

[206] Karl L. F. Bane and Matthew Sands, "The short-range resistive wall wakefields," AIP Conf. Proc. **367**, 131 (1996).

[207] M. G. Kelliher and R. Beadle, "Pulse-shortening in electron linear accelerators," Nature (London) **187**, 1099 (1960).

[208] W. K. H. Panofsky and M. Bander, "Asymptotic theory of beam breakup in linear accelerators," Rev. Sci. Instrum. **39**, 206 (1968).

[209] V. E. Balakin, A. V. Novokhatsky and V. P. Smirnov, "VLEPP: transverse beam dynamics," *Proceedings of HEACC1983, Fermilab, Batavia, IL, USA* (Fermilab, Batavia, IL, 1983), p. 119.

[210] E. Adli *et al.*, "First results from the electron hose instability studies in FACET," *Proceedings of IPAC2012, New Orleans, LA, USA* (IEEE, Piscataway, 2012), p. 43.

[211] S. Deng *et al.*, "Hose instability and wake generation by an intense electron beam in a self-ionized gas," Phys. Rev. Lett. **96**, 045001 (2006).

[212] A. Burov, V. Lebedev and S. Nagaitsev, "Instability of a witness bunch in a plasma bubble," arXiv:1602.05260 (2016).

[213] V. Lebedev, A. Burov and S. Nagaitsev, "Efficiency versus instability in plasma accelerators," Phys. Rev. Accel. Beams **20**, 121301 (2017).

[214] A. Burov, S. Nagaitsev and V. Lebedev, "Beam breakup mitigation by ion mobility in plasma acceleration," arXiv:1808.03860 (2018).

[215] William A. Barletta, "Linear emittance damper with megagauss fields," *Proceedings of the Workshop on New Developments in Particle Acceleration Techniques, Orsay, France* (CERN, Geneva, 1987), p. 544.

[216] I. Yu. Kostyukov, E. N. Nerush and A. G. Litvak, "Radiative damping in plasma-based accelerators," Phys. Rev. ST Accel. Beams **15**, 111001 (2012).

[217] A. Deng, K. Nakajima, J. Liu, B. Shen, X. Zhang, Y. Yu, W. Li, R. Li and Z. Xu, "Electron beam dynamics and self-cooling up to PeV level due to betatron radiation in plasma-based accelerators," Phys. Rev. ST Accel. Beams **15**, 081303 (2012).

[218] Brian W. Montague, "Linear optics for improved chromaticity correction," *LEP Note 165* (CERN, Geneva, 1979).

[219] Pantaleo Raimondi and Andrei Seryi, "Novel final focus design for future linear colliders," Phys. Rev. Lett. **86**, 3779 (2001).

[220] Henri Zyngier, "Strategy for correcting for chromaticity" (in French), *LAL-77/35* (Laboratoire de l'Accélérateur Linéaire, Orsay, 1977).

[221] SLAC (edited by T. O. Raubenheimer), *Zeroth-order Design Report for the Next Linear Collider, Vol. 2* (SLAC, Menlo Park, 1996).

[222] F. C. Iselin, J. M. Jowett, J. Pancin and A. Adelmann, "MAD version 9," *Proceedings of EPAC2000, Vienna, Austria* (CERN, Geneva, 2000), p. 1042.

[223] Brian W. Montague and Francesco Ruggiero, "Apochromatic focusing for linear colliders," *CLIC Note 37* (CERN, Geneva, 1987).

[224] Andrzej Wolski, *Beam Dynamics in High Energy Particle Accelerators* (Imperial College Press, London, 2014).

[225] R. Lehe, C. B. Schroeder, J.-L. Vay, E. Esarey and W. P. Leemans, "Saturation of the hosing instability in quasilinear plasma accelerators," Phys. Rev. Lett. **119**, 244801 (2017).

[226] Toshiki Tajima, "Laser accelerator for ultrahigh energies," *Proceedings of HEACC1983, Fermilab, Batavia, IL, USA* (Fermilab, Batavia, IL, 1983), p. 470.

[227] T. Katsouleas, T. C. Chiou, C. Decker, W. B. Mori, J. S. Wurtele, G. Shvets and J. J. Su, "Laser wakefield acceleration & optical guiding in a hollow plasma channel," AIP Conf. Proc. **279**, 480 (1992).

[228] T. C. Chiou, T. Katsouleas, C. Decker, W. B. Mori, J. S. Wurtele, G. Shvets and J. J. Su, "Laser wakefield acceleration and optical guiding in a hollow plasma channel," Phys. Plasmas **2**, 310 (1995).

[229] T. C. Chiou and T. Katsouleas, "High beam quality and efficiency in plasma-based accelerators," Phys. Rev. Lett. **81**, 3411 (1998).

[230] C. B. Schroeder, D. H. Whittum and J. S. Wurtele, "Multimode analysis of the hollow plasma channel wakefield accelerator," Phys. Rev. Lett. **82**, 1177 (1999).

[231] S. Lee, T. Katsouleas, R. G. Hemker, E. S. Dodd and W. B. Mori, "Plasma-wakefield acceleration of a positron beam," Phys. Rev. E **64**, 045501 (2001).

[232] E. Zaidman, T. Tajima, D. Neuffer, K. Mima, T. Ohsuga and D. C. Barnes, "Study of the plasma fiber accelerator," IEEE T. Nucl. Sci. **32**, 3545 (1985).

[233] D. C. Barnes, T. Kurki-Suonio and T. Tajima, "Laser self-trapping for the plasma fiber accelerator," IEEE T. Plasma Sci. **15**, 154 (1987).

[234] T. C. Chiou, T. Katsouleas and W. B. Mori, "Stability of intense laser propagation in an underdense hollow channel plasma," Phys. Plasmas **3**, 1700 (1996).

[235] G. Shvets, J. S. Wurtele, T. C. Chiou and T. C. Katsouleas, "Excitation of accelerating wakefields in inhomogeneous plasmas," IEEE T. Plasma Sci. **24**, 351 (1996).

[236] Gennady Shvets, "Interaction of intense lasers with plasmas," *Ph.D. thesis* (Massachusetts Institute of Technology, 1995).

[237] J. Fan, E. Parra, I. Alexeev, K. Y. Kim, H. M. Milchberg, L. Ya. Margolin and L. N. Pyatnitskii, "Tubular plasma generation with a high-power hollow Bessel beam," Phys. Rev. E **62**, R7603 (2000).

[238] N. E. Andreev, S. S. Bychkov, V. V. Kotlyar, L. Ya. Margolin, L. N Pyatnitskii and P. G. Serafimovich, "Formation of high-power hollow Bessel light beams," Quantum Electron. **26**, 126 (1996).

[239] K. A. Marsh *et al.*, "Positron beam propagation in a meter long plasma channel," *Proceedings of PAC2003, Portland, OR, USA* (JACoW, Geneva, 2003), p. 731.

[240] N. Kirby, I. Blumenfeld, M. J. Hogan, R. H. Siemann, D. R. Walz, A. W. Davidson and C. Huang, "Investigation of a gas jet-produced hollow plasma wakefield accelerator," *Proceedings of PAC2009, Vancouver, BC, Canada* (TRIUMF, Vancouver, 2010), p. 4566.

[241] Neil Allen Kirby, "Properties of trapped electron bunches in a plasma wakefield accelerator," *Ph.D. thesis* (Stanford University, 2009).

[242] W. D. Kimura, H. M. Milchberg, P. Muggli, X. Li and W. B. Mori, "Hollow plasma channel for positron plasma wakefield acceleration," Phys. Rev. ST Accel. Beams **14**, 041301 (2011).

[243] C. B. Schroeder, E. Esarey, C. Benedetti and W. P. Leemans, "Control of focusing forces and emittances in plasma-based accelerators using near-hollow plasma channels," Phys. Plasmas **20**, 080701 (2013).

[244] C. B. Schroeder, C. Benedetti, E. Esarey and W. P. Leemans, "Beam loading in a laser-plasma accelerator using a near-hollow plasma channel," Phys. Plasmas **20**, 123115 (2013).

[245] L. Yi *et al.*, "Positron acceleration in a hollow plasma channel up to TeV regime," Sci. Rep. **4**, 4171 (2014).

[246] Y. Li, G. Xia, K. V. Lotov, A. P. Sosedkin, K. Hanahoe and O. Mete-Apsimon, "High-quality electron beam generation in a proton-driven hollow plasma wakefield accelerator," Phys. Rev. Accel. Beams **20**, 101301 (2017).

[247] Y. Li, G. Xia, K. V. Lotov, A. P. Sosedkin, K. Hanahoe and O. Mete-Apsimon, "Multi-proton bunch driven hollow plasma wakefield acceleration in the nonlinear regime," Phys. Plasmas **24**, 103114 (2017).

[248] C. B. Schroeder, C. Benedetti, E. Esarey and W. P. Leemans, "Laser-plasma-based linear collider using hollow plasma channels," Nucl. Instrum. Methods Phys. Res. A **829**, 113 (2016).

[249] L. D. Amorim, J. Vieira, R. A. Fonseca and L. O. Silva, "Positron plasma wakefield acceleration in a self-driven hollow channel," AIP Conf. Proc. **1777**, 070001 (2016).

[250] G. Penn, J.-L. Vay, R. Lehe, C. Schroeder and E. Esarey, "Beam breakup studies in a hollow plasma channel," AIP Conf. Proc. **1812**, 040009 (2017).

[251] Y. P. Wu *et al.*, "A near-ideal dechirper for plasma based electron and positron acceleration using a hollow channel plasma," arXiv:1805.07031 (2018).

[252] S. J. Gessner *et al.*, "Acceleration of positron beams in a hollow channel plasma" (to be published).

[253] Spencer J. Gessner, "Demonstration of the hollow channel plasma accelerator," *Ph.D. thesis* (Stanford University, 2016).

[254] B. D. O'Shea *et al.*, "Observation of acceleration and deceleration in gigaelectron-volt-per-metre gradient dielectric wakefield accelerators," Nat. Commun. **7**, 12763 (2016).

[255] Brendan D. O'Shea, "Gigavolt-per-meter wakefields in annular dielectric structures," *Ph.D. thesis* (University of California, Los Angeles, 2016).

[256] W. K. H. Panofsky and W. A. Wenzel, "Some considerations concerning the transverse deflection of charged particles in radiofrequency fields," Rev. Sci. Instrum. **27**, 967 (1956).

[257] M. J. Hogan *et al.*, "Plasma wakefield acceleration experiments at FACET," New J. Phys. **12**, 055030 (2010).

[258] Paul Emma, "First lasing of the LCLS X-Ray FEL at 1.5 Å," *Proceedings of PAC2009, Vancouver, BC, Canada* (TRIUMF, Vancouver, 2010), p. 3115.

[259] Stanford Linear Accelerator Center, *SLAC Linear Collider Conceptual Design Report, SLAC-Report-229* (Stanford University, Stanford, CA, 1980).

[260] John T. Seeman, *The Stanford Linear Collider* (Stanford University, Stanford, CA, 1991).

[261] Stanley D. Ecklund, "The Stanford Linear Collider positron source," *The Stanford Linear Collider positron source, SLAC-PUB-4437* (Stanford University, Stanford, CA, 1987).

[262] J. E. Clendenin *et al.*, "SLC positron source startup," *Proceedings of LINAC'88, Williamsburg, VA, USA* (CEBAF, Newport News, VA, 1989), p. 568.

[263] G. R. White, Y. Cai, R. O. Hettel, M. A. G. Johansson, V. Yakimenko and G. Yocky, "A compact 335 MeV positron damping ring design for FACET-II," *Proceedings of IPAC2017, Copenhagen, Denmark* (JACoW, Geneva, 2017), p. 3652.

[264] C. L. O'Connell *et al.*, "Plasma production via field ionization," Phys. Rev. ST Accel. Beams **9**, 101301 (2006).

[265] Caolionn L. O'Connell, "Plasma production via field ionization," *Ph.D. thesis* (Stanford University, 2005).

[266] P. Muggli, K. A. Marsh, S. Wang, C. E. Clayton, S. Lee, T. C. Katsouleas and C. Joshi, "Photo-ionized lithium source for plasma accelerator applications," IEEE T. Plasma Sci. **27**, 791 (1999).

[267] N. Vafaei-Najafabadi, J. L. Shaw, K. A. Marsh, C. Joshi and M. J. Hogan, "Meter scale plasma source for plasma wakefield experiments," AIP Conf. Proc. **1507**, 650 (2012).

[268] S. Z. Green *et al.*, "Laser ionized preformed plasma at FACET," Plasma Phys. Control. Fusion **56**, 084011 (2014).

[269] John H. McLeod, "The axicon: a new type of optical element," J. Opt. Soc. Am. **44**, 592 (1954).

[270] NIL Technology ApS (a nanoimprint lithography company), `https://www.nilt.com`.

[271] E. Adli, S. J. Gessner, S. Corde, M. J. Hogan and H. H. Bjerke, "Cherenkov light-based beam profiling for ultrarelativistic electron beams," Nucl. Instrum. Methods Phys. Res. A **783**, 35 (2015).

[272] M. D. Litos, M. R. Bionta, V. A. Dolgashev, R. J. England, D. Fritz, S. Gilevich, Ph. Hering and M. J. Hogan, "Evaluation of temporal diagnostic techniques for two-bunch FACET beam," *Proceedings of PAC2011, New York, NY, USA* (IEEE, New York, USA, 2011), p. 568.

[273] J. A. Valdmanis, G. Mourou and C. W. Gabel, "Picosecond electrooptic sampling system," Appl. Phys. Lett. **41**, 211 (1982).

[274] J. Shan, A. S. Weling, E. Knoesel, L. Bartels, M. Bonn, A. Nahata, G. A. Reider and T. F. Heinz, "Single-shot measurement of terahertz electromagnetic pulses by use of electro-optic sampling," Opt. Lett. **25**, 426 (2000).

[275] A. L. Cavalieri *et al.*, "Clocking femtosecond X rays," Phys. Rev. Lett. **94**, 114801 (2005).

[276] H. Zha, A. Latina, A. Grudiev, G. De Michele, A. Solodko, W. Wuensch, D. Schulte, E. Adli, N. Lipkowitz and G. S. Yocky, "Beam-based measurements of long-range transverse wakefields in the Compact Linear Collider main-linac accelerating structure," Phys. Rev. Accel. Beams **19**, 011001 (2016).

[277] Hao Zha and Alexej Grudiev, "Design of the Compact Linear Collider main linac accelerating structure made from two halves," Phys. Rev. Accel. Beams **20**, 042001 (2017).

[278] W. Gai, A. D. Kanareykin, A. L. Kustov and J. Simpson, "Numerical simulations of intense charged-particle beam propagation in a dielectric wake-field accelerator," Phys. Rev. E **55**, 3481 (1997).

[279] C. Li, W. Gai, C. Jing, J. G. Power, C. X. Tang and A. Zholents, "High gradient limits due to single bunch beam breakup in a collinear dielectric wakefield accelerator," Phys. Rev. ST Accel. Beams **17**, 091302 (2014).

[280] J. B. Rosenzweig, G. Andonian, M. Ferrario, P. Muggli, O. Williams, V. Yakimenko and K. Xuan, "Plasma wakefields in the quasinonlinear regime," AIP Conf. Proc. **1299**, 500 (2010).

[281] Denis G. Colombant and Yue Y. Lau, "Effects of frequency spreads on beam breakup instabilities in linear accelerators," Appl. Phys. Lett. **55**, 27 (1989).

[282] Dennis Gabor, "A space-charge lens for the focusing of ion beams," Nature (London) **160**, 89 (1947).

[283] Vladimir D. Shiltsev, *Electron Lenses for Super-Colliders* (Springer, New York, NY, 2016).

[284] Giulio Stancari, "Applications of electron lenses: scraping of high-power beams, beam-beam compensation, and nonlinear optics," AIP Conf. Proc. **1777**, 100007 (2016).

[285] V. Shiltsev, V. Danilov, D. Finley and A. Sery, "Considerations on compensation of beam-beam effects in the Tevatron with electron beams," Phys. Rev. ST Accel. Beams **2**, 071001 (1999).

[286] V. Shiltsev, Y. Alexahin, K. Bishofberger, V. Kamerdzhiev, G. Kuznetsov and X.-L. Zhang, "Experimental demonstration of colliding-beam-lifetime improvement by electron lenses," Phys. Rev. Lett. **99**, 244801 (2007).

[287] V. Shiltsev *et al.*, "Tevatron electron lenses: design and operation," Phys. Rev. ST Accel. Beams **11**, 103501 (2008).

[288] John B. Johnson, "A low voltage cathode ray oscillograph," J. Opt. Soc. Am. **6**, 701 (1922).

[289] Bodo von Borries and Ernst Ruska, "The short space-charge field of an auxiliary discharge as a collecting lens for cathode rays," Z. Phys. **76**, 649 (1932).

[290] Peter W. Hawkes, *Advances in Imaging and Electron Physics, Vol. 205* (Elsevier Science, 2018).

[291] Willard H. Bennett, "Magnetically self-focussing streams," Phys. Rev. **45**, 890 (1934).

[292] Willard H. Bennett, "Self-focusing streams," Phys. Rev. **98**, 1584 (1955).

[293] S. E. Graybill and S. V. Nablo, "Observations of magnetically self-focusing electron streams," Appl. Phys. Lett. **8**, 18 (1966).

[294] V. V. Zhukov, A. I. Morozov and G. Ya. Shepkin, "Experimental investigation of plasma focusing of ion beams," J. Exp. Theor. Phys. Lett. **9**, 14; Zh. Eksp. Teor. Fiz. Pis. Red. **9**, 24 (1969)

[295] R. Booth and H. W. Lefevre, "Space charge lens for high current ion beams," Nucl. Instrum. Methods **151**, 143 (1978).

[296] R. M. Mobley, G. Gammel and A. W. Maschke, "Gabor lenses," IEEE Trans. Nucl. Sci. **26**, 3112 (1979).

[297] Robert J. Adler, "Image field focusing of intense ultrarelativistic electron beams in vacuum," Part. Accel. **12**, 39 (1982).

[298] Robert B. Miller and Robert J. Adler, "A pinch effect for intense, magnetized, nonneutral electron beams," J. Appl. Phys. **53**, 6015 (1982).

[299] J. J. Su, T. Katsouleas, J. M. Dawson and R. Fedele, "Plasma lenses for focusing particle beams," Phys. Rev. A **41**, 3321 (1990).

[300] J. B. Rosenzweig, P. Schoessow, B. Cole, C. Ho, W. Gai, R. Konecny, S. Mtingwa, J. Norem, M. Rosing and J. Simpson, "Demonstration of electron beam selffocusing in plasma wake fields," Phys. Fluids B **2**, 1376 (1990).

[301] H. Nakanishi *et al.*, "Direct observation of plasma-lens effect," Phys. Rev. Lett. **66**, 1870 (1991).

[302] G. Hairapetian, P. Davis, C. E. Clayton, C. Joshi, S. C. Hartman, C. Pellegrini and T. Katsouleas, "Experimental demonstration of dynamic focusing of a relativistic electron bunch by an overdense plasma lens," Phys. Rev. Lett. **72**, 2403 (1994).

[303] R. Govil, W. P. Leemans, E. Yu. Backhaus and J. S. Wurtele, "Observation of return current effects in a passive plasma lens," Phys. Rev. Lett. **83**, 3202 (1999).

[304] J. S. T. Ng *et al.*, "Observation of plasma focusing of a 28.5 GeV positron beam," Phys. Rev. Lett. **87**, 244801 (2001).

[305] M. C. Thompson *et al.*, "Observations of low-aberration plasma lens focusing of relativistic electron beams at the underdense threshold," Phys. Plasmas **17**, 073105 (2010).

[306] C. Thaury *et al.*, "Demonstration of relativistic electron beam focusing by a laser-plasma lens," Nat. Commun. **6**, 6860 (2015).

[307] A. Marocchino *et al.*, "Experimental characterization of the effects induced by passive plasma lens on high brightness electron bunches," Appl. Phys. Lett. **111**, 184101 (2017).

[308] Wolfgang K. H. Panofsky and William R. Baker, "A focusing device for the external 350-Mev proton beam of the 184-inch cyclotron at Berkeley," Rev. Sci. Instrum. **21**, 445 (1950).

[309] E. B. Forsyth, L. M. Lederman and J. Sunderland, "The Brookhaven–Columbia plasma lens," IEEE Trans. Nucl. Sci. **12**, 872 (1965).

[310] J. Christiansen, K. Frank, H. Riege and R. Seeböck, "Studies of a plasma lens with pseudo-spark geometry for application in high energy particle accelerators," *CERN PS Note 84-10-AA* (CERN, Geneva, 1984).

[311] B. Autin, H. Riege, E. Boggasch, K. Frank, L. De Menna and G. Miano, "A z-pinch plasma lens for focusing high-energy particles in an accelerator," IEEE Trans. Nucl. Sci. **15**, 226 (1987).

[312] G. Le Dallic, M. L. di Scampamorte, R. Kowalewicz, S. Milner, H. Riege, J. Christiansen, K. Frank, M. Stetter and R. Tkotz, "First test results from the new CERN plasma lens," *CERN PS Note 90-30-AR* (CERN, Geneva, 1990).

[313] R. Kowalewicz, M. L. di Scampamorte, S. Milner, F. Pedersen, H. Riege, J. Christiansen, K. Frank, M. Stetter, R. Tkotz and E. Boggasch, "Performance of the CERN plasma lens in laboratory and beam tests at the antiproton source," *Proceedings of PAC1991, San Francisco, CA, USA* (IEEE, New York, NY, 1991), p. 2631.

[314] E. Boggasch, J. Jacoby, H. Wahl, K.-G. Dietrich, D. H. H. Hoffmann, W. Laux, M. Elfers, C. R. Haas, V. P. Dubenkov and A. A. Golubev, "z-pinch plasma lens focusing of a heavy-ion beam," Phys. Rev. Lett. **66**, 1705 (1991).

[315] E. Boggasch, A. Tauschwitz, H. Wahl, K.-G. Dietrich, D. H. H. Hoffmann, W. Laux, M. Stetter and R. Tkotz, "Plasma lens fine focusing of heavy-ion beams," Appl. Phys. Lett. **60**, 2475 (1992).

[316] M. Stetter, J. Christiansen, U. Neuner, S. Stöwe, R. Tkotz, T. Wagner, E. Boggasch, A. Tauschwitz, D. H. H. Hoffmann and P. Spiller, "Development of a plasma lens as a fine focusing lens for heavy-ion beams," Nuovo Cimento A **106**, 1725 (1993).

[317] N. A. Bobrova, A. A. Esaulov, J.-I. Sakai, P. V. Sasorov, D. J. Spence, A. Butler, S. M. Hooker and S. V. Bulanov, "Simulations of a hydrogen-filled capillary discharge waveguide," Phys. Rev. E **65**, 016407 (2001).

[318] B. H. P. Broks, K. Garloff and J. J. A. M. van der Mullen, "Nonlocal-thermal-equilibrium model of a pulsed capillary discharge waveguide," Phys. Rev. E **71**, 016401 (2005).

[319] A. J. Gonsalves, T. P. Rowlands-Rees, B. H. P. Broks, J. J. A. M. van der Mullen and S. M. Hooker, "Transverse interferometry of a hydrogen-filled capillary discharge waveguide," Phys. Rev. Lett. **98**, 025002 (2007).

[320] S. Steinke *et al.*, "Multistage coupling of independent laser-plasma accelerators," Nature (London) **530**, 190 (2016).

[321] J. van Tilborg *et al.*, "Nonuniform discharge currents in active plasma lenses," Phys. Rev. Accel. Beams **20**, 032803 (2017).

[322] R. Pompili *et al.*, "Experimental characterization of active plasma lensing for electron beams," Appl. Phys. Lett. **110**, 104101 (2017).

[323] J.-H. Röckemann *et al.*, "Direct measurement of focusing fields in active plasma lenses," Phys. Rev. Accel. Beams **21**, 122801 (2018).

[324] Thomas P. Wangler, *RF Linear Accelerators, 2nd edition* (Wiley, Weinheim, 2008), pp. 201–207.

[325] B. F. Bayanov, J. N. Petrov, G. I. Sil'vestrov, J. A. Maclachlan and G. L. Nicholls, "A lithium lens for axially symmetric focusing of high energy particle beams," Nucl. Instrum. Methods **190**, 9 (1981).

[326] B. F. Bayanov, A. D. Chernyakin, Yu. N. Petrov, G. I. Sil'vestrov, V. G. Volokhov, and T. A. Vsevolozhskaya and J. MacLachlan, "The proton beam lithium lens for the Fermilab anti-proton source," *Fermilab Note TM-1000* (Fermilab, Batavia, IL, 1980).

[327] P. Sievers, R. Bellone, A. Ijspeert and P. Zanasco, "Development of lithium lenses at CERN," IEEE Trans. Nucl. Sci. **32**, 3066 (1985).

[328] Alexander A. Mikhailichenko, "Lithium lens for positron production system," *Proceedings of EPAC2008, Genoa, Italy* (JACoW, Geneva, 2008), p. 2856.

[329] Alexander A. Mikhailichenko, "Lithium lens I.," *CBN-09-4* (Cornell University, Ithaca, NY, 2009).

[330] Gregory I. Silvestrov, "Lithium lenses for muon colliders," AIP Conf. Proc. **372**, 168 (1996).

[331] A. Hassanein *et al.*, "The design of a liquid lithium lens for a muon collider," *Proceedings of PAC1999, New York, NY, USA* (IEEE , Piscataway, NJ, 1999).

[332] Marshall N. Rosenbluth, "Infinite conductivity theory of the pinch," *Los Alamos Note LA-1850* (Los Alamos Scientific Laboratory, Los Alamos, NM, 1954).

[333] Francis Chen, *Introduction to Plasma Physics and Controlled Fusion, 3rd edition* (Springer, Berlin, Heidelberg, 2016).

[334] A. Mosnier *et al.*, "The probe beam linac in CTF3," *Proceedings of PAC2006, Edinburgh, UK* (CERN, Geneva, 2006), p. 679.

[335] Günther Geschonke and Andrea Ghigo, "CTF3 design report," *CERN PS Note 2002-008-RF* (CERN, Geneva, 2002).

[336] F. Toral *et al.*, "Design, manufacturing and tests of a micrometer precision mover for CTF3 quadrupoles," *Proceedings of EPAC2008, Genoa, Italy* (JACoW, Geneva, 2008), p. 1517.

[337] Friedrich Paschen, "On the potential difference required for spark initiation in air, hydrogen, and carbon dioxide at different pressures" (in German), Ann. Phys. (Berl.) **273**, 6975 (1889).

[338] O. Lishilin *et al.*, "First results of the plasma wakefield acceleration experiment at PITZ," Nucl. Instrum. Methods Phys. Res. Sec. A **829**, 37 (2016).

[339] J. van Tilborg, A. J. Gonsalves, E. H. Esarey, C. B. Schroeder and W. P. Leemans, "Density characterization of discharged gas-filled capillaries through common-path two-color spectral-domain interferometry," Opt. Lett. **43**, 2776 (2018).

[340] A. E. Dyson, C. Thornton and S. M. Hooker, "A compact, low cost Marx bank for generating capillary discharge plasmas," Rev. Sci. Instrum. **87**, 093302 (2016).

[341] P. Chen, S. Rajagopalan and J. Rosenzweig, "Final focusing and enhanced disruption from an underdense plasma lens in a linear collider," Phys. Rev. D **40**, 923 (1989).

[342] A. W. Weidemann, P. Chen and C.-K. Ng, "Plasma lens backgrounds at a future linear collider," Int. J. Mod. Phys. A **18**, 2857 (2003).

[343] Stefano Redaelli, "Stabilization of nanometre-size particle beams in the final focus system of the Compact Linear Collider (CLIC)," *Ph.D. thesis* (Lausanne University, 2003).

[344] V. Yakimenko *et al.*, "On the prospect of studying nonperturbative QED with beam-beam collisions," arXiv:1807.09271 (2018).

[345] I. F. Ginzburg, G. L. Kotkin, V. G. Serbo and V. I. Tel'nov, "Production of high-energy colliding $\gamma\gamma$ and γe beams with a high luminosity at VLEPP accelerators," J. Exp. Theor. Phys. Lett. **34**, 491; Pisma Zh. Eksp. Teor. Fiz. **34**, 514 (1981).

[346] Stan D. Ecklund, "Positrons for linear colliders," AIP Conf. Proc., **184**, 1592 (1989).

[347] Valery I. Telnov, "γ–γ, γ–electron colliders," *Proceedings of the International Conference on High-Energy Accelerators, Dubna, Russia* (JINR, Dubna, 1998), p. 88.

[348] D. Asner, H. Burkhardt, A. Roeck, J. De and Ellis, J. Gronberg, S. Heinemeyer, M. Schmitt, D. Schulte, M. Velasco and F. Zimmermann, "Higgs physics with a $\gamma\gamma$ collider based on CLIC 1," Eur. Phys. J. C **28**, 27 (2003).

[349] Kwang-Je Kim and Andrew M. Sessler, "$\gamma\gamma$ colliders," Beam Line **26**, 16 (1996).

[350] J. M. Cole *et al.*, "Experimental evidence of radiation reaction in the collision of a high-intensity laser pulse with a laser-wakefield accelerated electron beam," Phys. Rev. X **8**, 011020 (2018).

[351] K. Poder *et al.*, "Experimental signatures of the quantum nature of radiation reaction in the field of an ultraintense laser," Phys. Rev. X **8**, 031004 (2018).

[352] C. Bula *et al.*, "Observation of nonlinear effects in compton scattering," Phys. Rev. Lett. **76**, 3116 (1996).

[353] D. L. Burke *et al.*, "Positron production in multiphoton light-by-light scattering," Phys. Rev. Lett. **79**, 1626 (1997).

[354] Pisin Chen and Toshiki Tajima, "Testing Unruh radiation with ultraintense lasers," Phys. Rev. Lett. **83**, 256 (1999).

[355] R. Schützhold, G. Schaller and D. Habs, "Signatures of the Unruh effect from electrons accelerated by ultrastrong laser fields," Phys. Rev. Lett. **97**, 121302 (2006).

[356] William G. Unruh, "Notes on black-hole evaporation," Phys. Rev. D **14**, 870 (1976).

[357] Stephen W. Hawking, "Black hole explosions?" Nature (London) **248**, 30 (1974).

[358] Albert Einstein, *The Meaning of Relativity: Four Lectures Delivered at Princeton University, May, 1921* (Princeton University Press, Princeton, NJ, 1923).